Defluorinative Synthesis of Organophosphorus Compounds

有機リン化合物の脱フッ素的合成法

Zhensheng YOU

2023

Contents

Chapter 1

General Introduction

Overview

Organophosphorus compounds are organic molecules containing phosphorus, a group 15 element with atomic number 15.[1] Like other family members in the pnictogen, phosphorus contains five electrons in the outermost shell with a configuration of $3s^2 3p^3$ (Figure 1.1). Hence, it generally presents variable oxidation states including −3, 0, +3, and +5.[2]

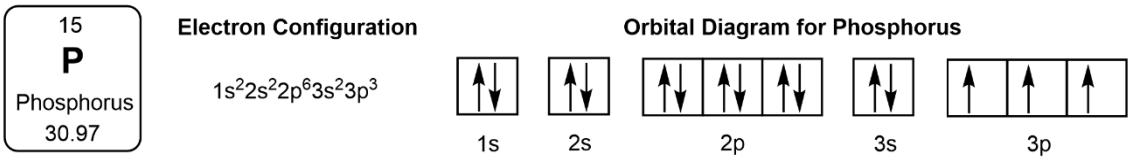

Figure 1.1. Electronic properties of phosphorus.

Organophosphorus compounds are typically classified as P(III) or P(V) based on the oxidation state of phosphorus. The nomenclature of organophosphorus compounds is complicated, as it relates to the oxidation state of phosphorus and the elements bonding to the phosphorus center.[3, 4] This thesis discusses organophosphorus compounds that contain the P–O functionality. Their basic nomenclature is illustrated in Figure 1.2.

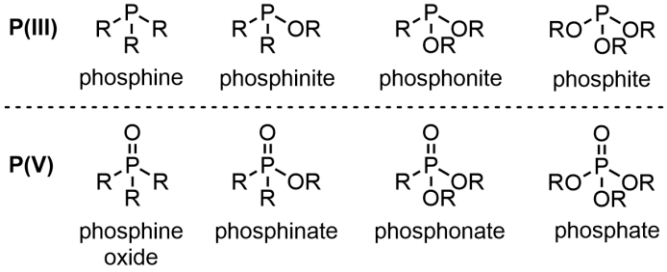

Figure 1.2. Typical organophosphorus compounds discussed in this thesis.

Organophosphorus compounds exist widely in pharmaceuticals, bioactive compounds, chemistry materials, and ligands for catalysis (Figure 1.3). Furthermore, aromatic building blocks serve vital roles in both academic and industrial chemistry.[5, 6] Hence, synthetic methodologies toward aryl organophosphorus compounds have attracted the interest of organic chemists for decades.

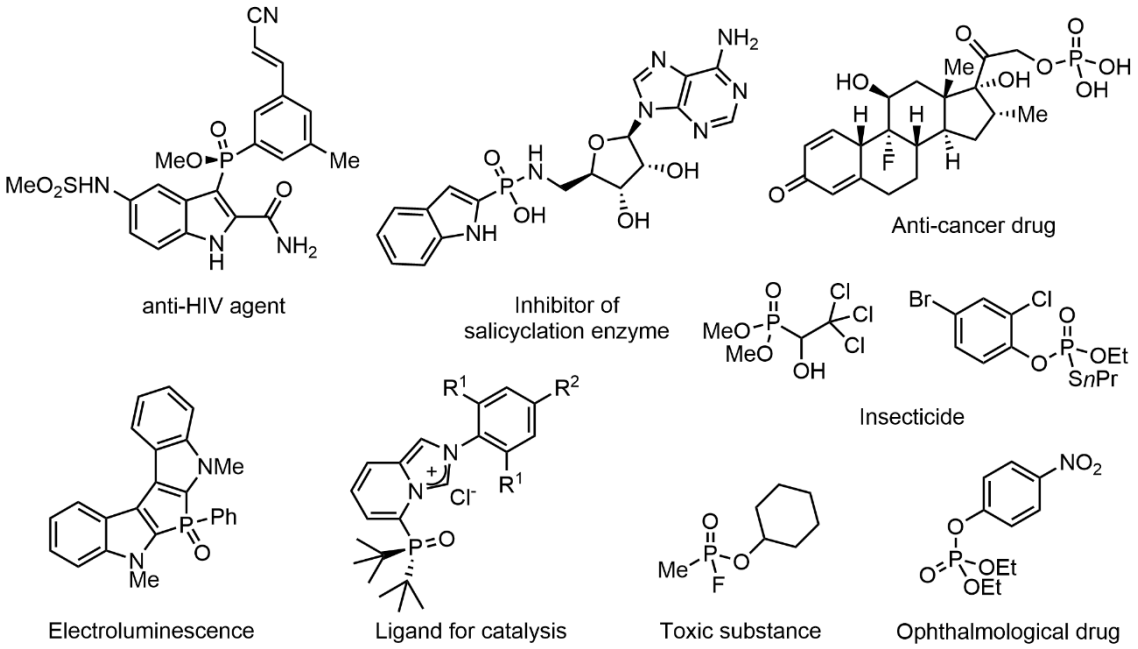

Figure 1.3. Examples of organophosphorus compounds containing a P=O moiety

However, the synthesis of organophosporus compounds from abundant aryl fluorides building blocks is still facing great challenge. It significantly limits the accessibility to complex organophosphorus compounds by direct late-stage functionalization. In this context, the thesis describes a series of convenient protocols for preparing various organophosphorus compounds from non-activated aryl fluorides through C(sp^2)–F cleavage.

In chapter 1, synthetic methodologies for C–P bond construction are summarized through a manner of different mechanisms, focusing on the role of organophosphorus compounds in those mechanism. A discussion is carried out to reveal the current challenge. Besides, C–F bond functionalization protocols are reviewed and discussed. In the end of this chapter, the major contents of this thesis are introduced.

1.1 C–P Bond Formation by Nucleophilic Substitution

1.1.1 Organophosphorus Compounds as Electrophiles

As a class of readily available reagents, chlorophosphines are widely utilized as electrophiles. One well-referenced example is the synthesis of bulky biaryl phosphine ligands, which are useful for palladium-catalyzed cross-coupling reactions.[7, 8] Their synthesis relies largely on the C–P bond formation between aryl organometallic nucleophiles and chlorophosphine electrophiles (Scheme 1.1a).[9 – 12] One significant drawback of this protocol is a tedious step-by-step synthetic procedure. A one-pot method was developed by generating biaryl organometallic nucleophile **8** from benzyne intermediate **7**. The improved process is less expensive and less time-consuming. Furthermore, it could be used to access ligands that were prepared by the previous protocol (Scheme 1.1b).[13]

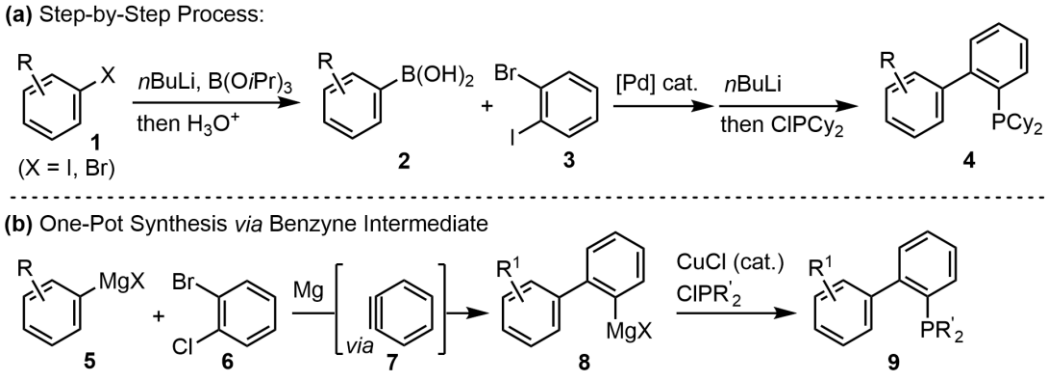

Scheme 1.1. Preparation of biaryl phosphine ligands.

Molecules with non-symmetrically substituted phosphorus atoms possess central chirality. Since the pioneering work of Knowles,[14] a huge library of *P*-chirogenic phosphines has been investigated.[15, 16] For example, an optically active menthyl group has been widely used as a chiral auxiliary for construction of *P*-chiral centers. Han and co-workers reported an efficient protocol for accessing *P*-chiral compounds that begins with the preparation of diastereomerically pure menthyl phosphine oxides (R_P)-**12** (Scheme 1.2a).[17] Nucleophilic substitution at the phosphorus center leads to inversion of the configuration, generating enantioenriched *P*-stereogenic phosphine oxides (S_P)-**13**.

Reduction of phosphine oxides to free phosphines often requires harsh conditions and causing the configuration inversion, which limits the application of the above-mentioned protocol.[18, 19] Giordano and Buono improved this procedure by stereo-retentive transformation of *sec*-phosphine oxides (S_P)-**13** to *sec*-phosphine–boranes (S_P)-**14**

through a deprotonation-protection-reduction strategy (Scheme 1.2b).[20] Zhao and co-workers developed a different approach by first stereospecifically chlorinating the *sec*-phosphine oxides (R_P/S_P)-**12** by oxalyl chloride. Subsequent nucleophilic attack by Grignard reagents delivers the corresponding tertiary phosphine–borane product **18**. Interestingly, in the last nucleophilic substitution step, aromatic Grignard reagents react in a stereo-retentive manner in contrast to aliphatic Grignard reagents that cause *P*-inversion (Scheme 1.2c).[21]

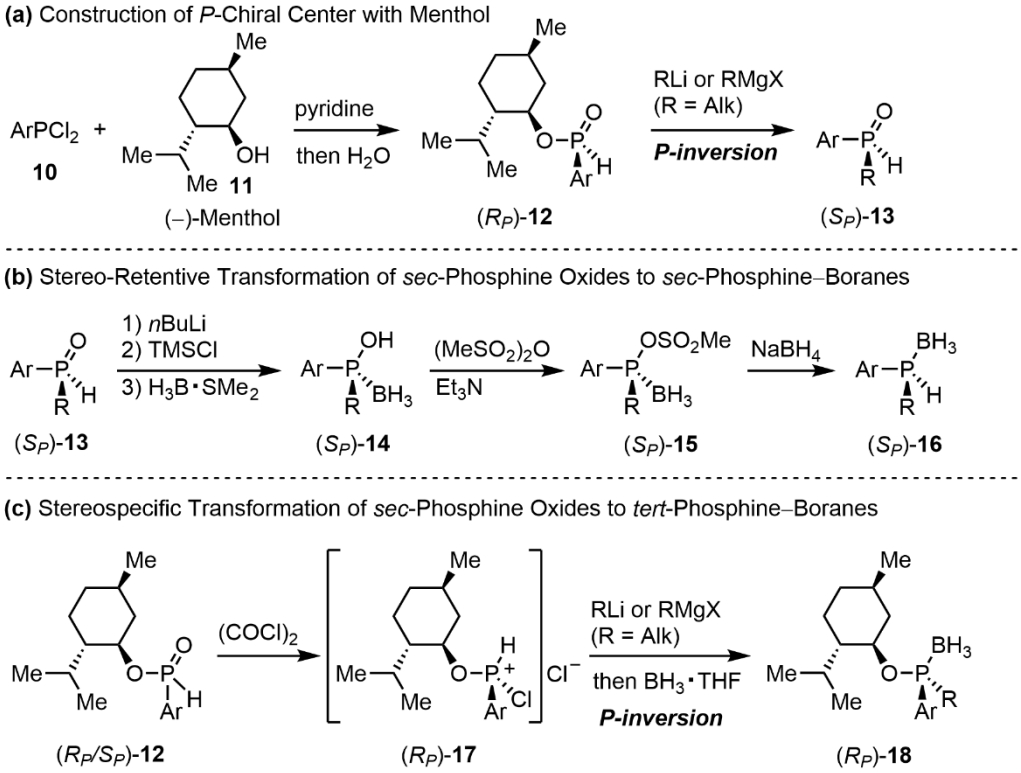

Scheme 1.2. Menthol in construction of *P*-chirogenic phosphorus centers.

Meanwhile, Jugé and co-workers reported a different approach, in which the *P*-chirogenic center was constructed using (+)-ephedrine as the chiral auxiliary.[22, 23] The resulting diastereomerically pure oxazaphospholidine–borane complexes (R_P)-**19** undergo a ring-opening process through nucleophilic substitution by organometallic reagents to give the corresponding aminophosphine–boranes **20**, which are transformed to tertiary phosphine boranes **22** through hydrolysis and substitution (Scheme 1.3a).

The above-mentioned method is useful in *P*-chirogenic phosphine ligand synthesis. In 2008, Kamer and co-workers reported the preparation and application of a polymer-supported *P*-chirogenic phosphinamine-phosphite ligand.[24] The phosphorus center of

(R_P)-**23** was attacked by lithiated polystyrene (PS) to deliver **24**, in which the hydroxy group was further functionalized by chlorophosphine. The borane moiety was removed by an amine to generate the desired phosphinamine-phosphite ligand **25**. The reported ligand was used in Rh-catalyzed asymmetric hydrogenation of alkenes. Despite the moderate enantioselectivity, the potential of the ephedrine chiral auxiliary was well-presented through this report (Scheme 1.3b).

XantPhos is a great example of privileged ligand design, which has been used for catalyzing a tremendous number of reactions. Hence, Holz and Börner chose XantPhos as a model and developed its *P*-chirogenic version (Scheme 1.3c).[25] The synthesis used Jugé's protocol to obtain chiral phosphine–borane (S_P)-**26**, which was then deprotected and nucleophilically attacked by deprotonated dimethyl xanthene to give the corresponding *P*-chirogenic bisphosphine (*S,S*)-**27**. The ligand performance was evaluated by Rh-catalyzed asymmetric hydrogenation of internal alkenes, and a high enantioselectivity was observed.

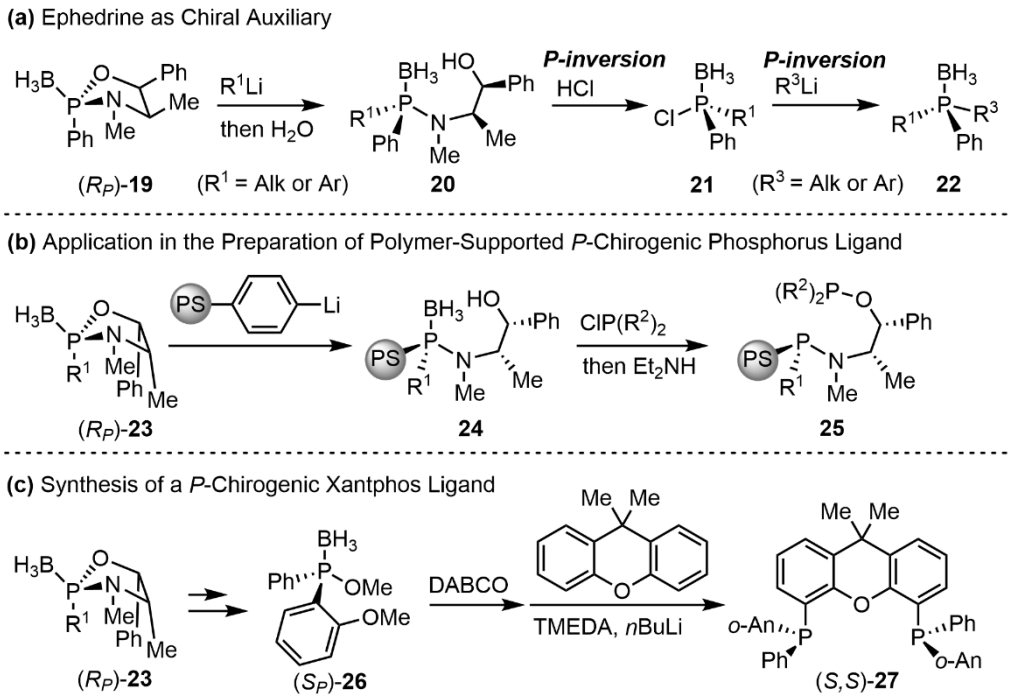

Scheme 1.3. Ephedrine as a chiral auxiliary for *P*-chirogenic compound synthesis.

Although Jugé's ephedrine method has been used for practical phosphine ligands synthesis,[26] the protocol suffers from the low reactivity of the P–N and P–O bonds in ephedrine, which limits its further application. To overcome those drawbacks, Han and co-workers activated the P–N bond in chiral amino alcohols with an arylsulfonyl group,

which significantly improved the reactivity of chiral template (R_P)-**29** (Scheme 1.4).[27] The well-designed benzoxazaphosphinine-2-oxide (R_P)-**29** exhibited good reactivity with various bulky organometallic nucleophiles and delivered the *P*-chiral phosphine oxides **31** in enantiomerically pure form. The protocol has been used for the preparation of *P*-chirogenic phosphine ligands such as **DIPAMP** and **MeO-BIBOP**.

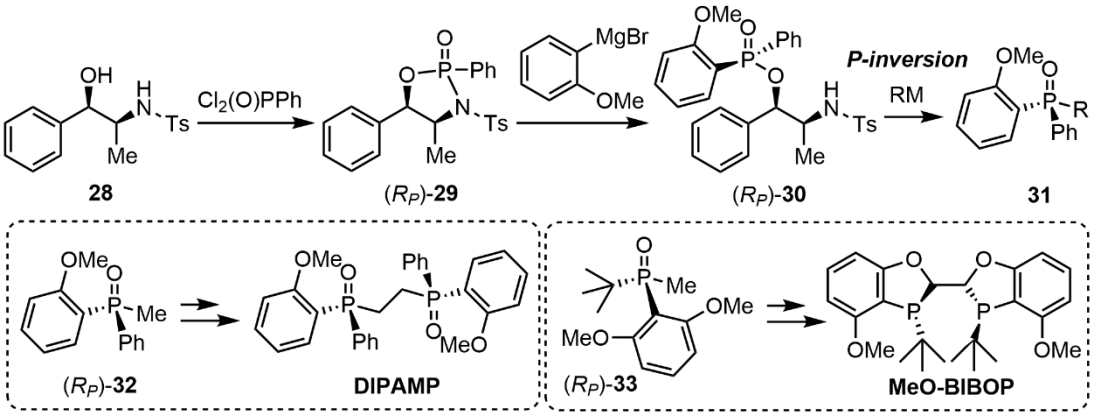

Scheme 1.4. Properly designed chiral auxiliary
for sterically hindered *P*-chiral phosphine oxide synthesis.

Verdaguer's group attempted to improve Jugé's strategy. [28] Initially, they selected *cis*-aminoindanol as a template for constructing a *P*-chiral center (Scheme 1.5a). Nucleophilic ring-opening of (R_P)-**34** would cause an inversion of the configuration at the *P*-chiral center. Methylation of the amine moiety led to no reaction. Upon switching the *tert*-butyl group to a phenyl group, ring-opening was possible under both conditions.[29] In contrast to free amine (R_P)-**39**, which followed a configurational inversion manner, ring-opening of methyl amine (R_P)-**41** occurred with a *P*-retention manner (Scheme 1.5b). The authors proposed the substituent on the amine moiety was the key for configuration control during the ring-opening process. A metal cation from the organometallic nucleophile, coordinates to the free amine before nucleophilic substitution. Methylation of the amine moiety would force nucleophilic substitution to occur at the frontside. Since *tert*-butyl is a bulky substituent, frontside S_N2 is inhibited. Meanwhile, phenyl is a relatively less bulky substituent, so the nucleophilic substitution at both sides of the phosphorus is possible. Computational studies revealed when nucleophilic substitution occurs from the frontside, the Li^+ cation is stabilized by H atoms from the BH_3 moiety. Such a stabilization effect fixed the location of the alkyl nucleophile to the frontside of the phosphorus. This mechanism facilitated ring-opening in a *P*-retention manner.

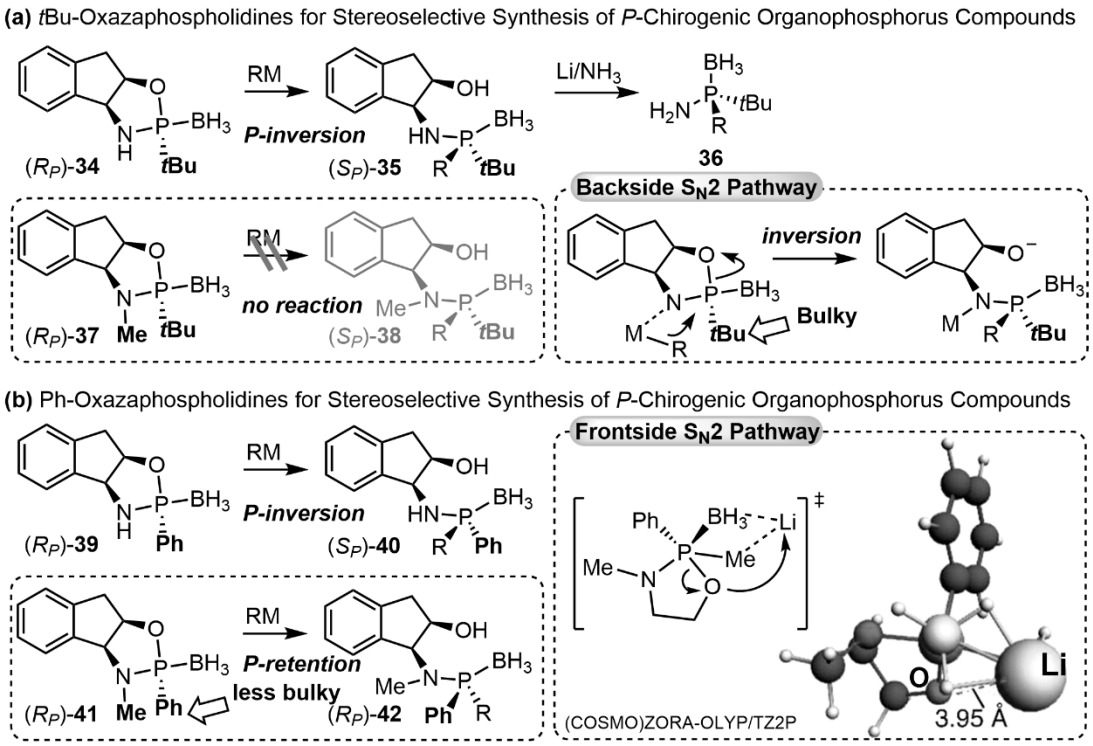

Scheme 1.5. Novel chiral oxazaphospholidine template design and mechanistic studies.

1.1.2 Organophosphorus Compounds as Nucleophiles

Since chlorophosphines are highly moisture-sensitive, switching the synthetic precursor to more easily handled phosphate would be more convenient in experimental synthesis. In 2014, Zheng and Fox reported an improved synthetic process (Scheme 1.6), in which the trichlorophosphine **43** was first transformed to di-*tert*-butyl phosphite **44**. Further esterification to **45** was performed after catalytic oxidation of phosphite **44**. The improved protocol gave an efficient approach to the precursor of phosphate pro-drugs.[30]

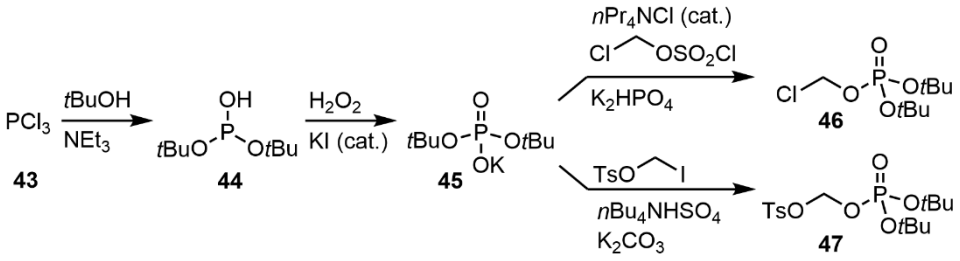

Scheme 1.6. Phosphate synthesis by using phosphite as a starting material.

Arylphosphine oxides are also potential pro-nucleophiles. Chiba and Takita reported a

dearylative nucleophilic substitution between arylphosphine oxides **48** and electrophiles in the presence of sodium hydride and lithium iodide (Scheme 1.7a).[31] The reaction specifically breaks the bond between phosphorus and the aryl group, and resulting nucleophile can attack several different classes of electrophiles. Computational studies suggested that the hydride species attacks the phosphorus center in an S_N2 *P*-inversion manner to generate the corresponding secondary phosphine oxide **53** (Scheme 1.7b). Next, **53** is deprotonated by the phenyl sodium species and reacts with electrophiles. It is noted that the sodium hydride-iodide composite has been used to reduce other species in a nucleophilic aromatic substitution (S_NAr) manner.[32] This is the first report of it being applied for the reduction of tertiary arylphosphine oxides to the corresponding secondary phosphine oxides.

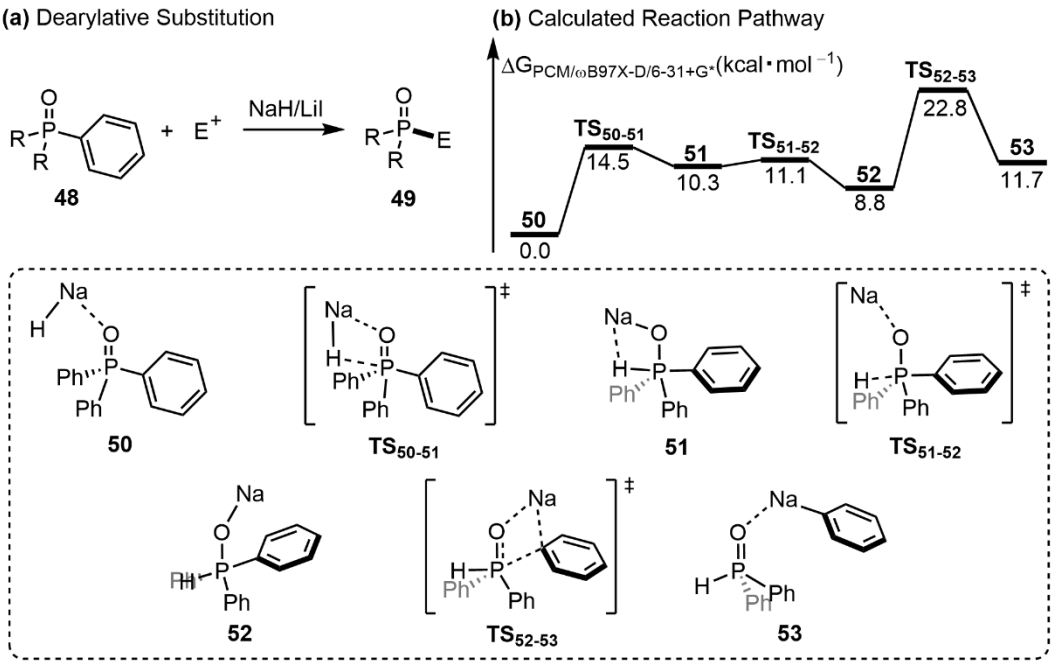

Scheme 1.7. Dearylation of phosphine oxides and sequential nucleophilic substitution.

The nucleophile of the above-mentioned reaction is generated from secondary phosphine oxides. In this context, secondary phosphine–boranes could also work as pro-nucleophiles. As a recent example, Jugé and co-workers reported a S_NAr-type reaction between secondary phosphine–boranes **54** and 1,2-dibromo- or 1,2-diiodobenzene **55** in the presence of *n*-butyllithium (Scheme 1.8).[33] Generally, neither bromide nor iodide are considered to be good leaving groups in S_NAr-type reactions.[34] In the current protocol, dihalobenzene **55** is activated by *n*-butyllithium through lithium-halogen exchange (**57**), followed by elimination to deliver aryne intermediate **59**. Meanwhile, secondary

phosphine–borane **54** is deprotonated (**58**) and undergoes SNAr with aryne intermediate **59** to deliver *o*-substituted phenyllithium intermediate **60**, in which lithium is replaced by bromide through lithium-halogen exchange with another equivalent of dihalobenzene **55**. Interestingly, the reaction proceeded in a *P*-retention manner.

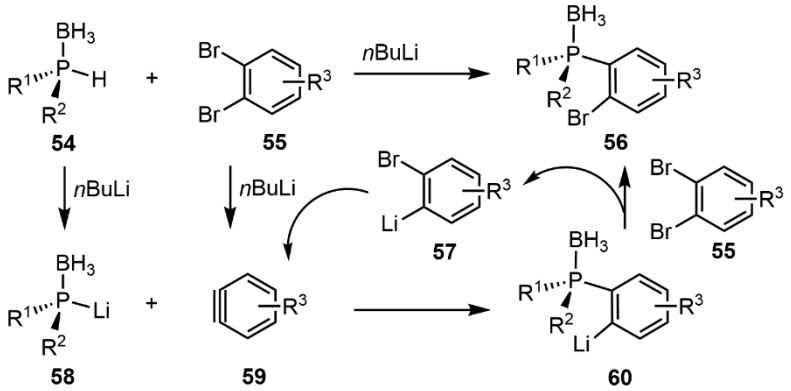

Scheme 1.8. Formation of (*o*-bromoaryl)phosphine–borane *via* aryne intermediate.

Kamer and co-workers reported an example of organophosphorus reagents as nucleophiles for the synthesis of solid-supported chiral bisphosphines (Scheme 1.9).[35] Commercially available resins were selected as the supports. Electrophilic **61** was substituted by nucleophilic lithium phosphide followed by borane protection to give phosphine–borane **62**. *In situ* lithiation and nucleophilic ring-opening proceeded with stereo-inversion to give the lithium salt **64**, which was attacked by lithium phosphide and protected by the borane moiety. Chiral bisphosphine ligands **65** exhibited good enantioselectivities in the Rh-catalyzed asymmetric hydrogenation of olefines.

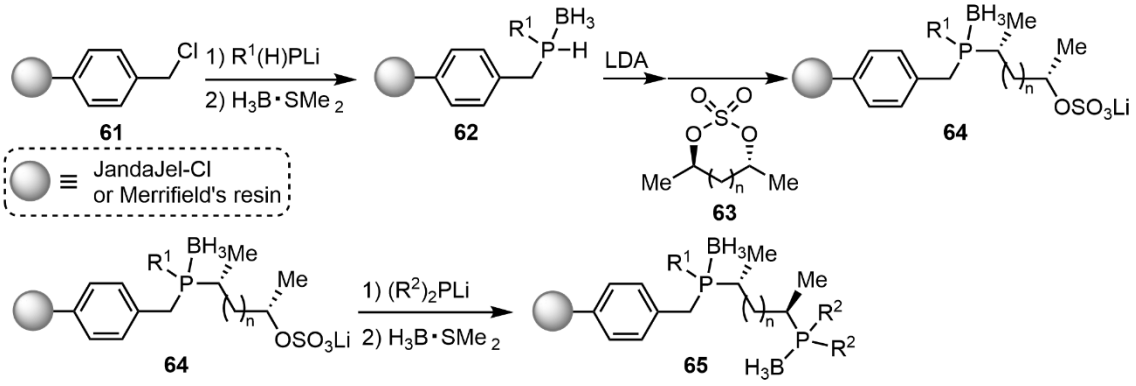

Scheme 1.9. Solid-supported bisphosphine synthesis.

As illustrated in Scheme 1.5b, the borane moiety of a phosphine–borane can interact with a lithium cation. The chiral surrounding of Li^+ might provide an opportunity to distinguish different configurations of the phosphorus center. Müller and co-workers mixed racemic secondary phosphine–borane (*rac*)-**66** with (–)-sparteine in the presence of *n*-butyllithium (Scheme 1.10a).[36] Interestingly, enantiopure **67** was obtained in dimeric form. Single-crystal X-ray analysis of **67** suggests two borane moieties from phosphides function as dimeric ligands of the lithium center. Such an interaction allows dynamic resolution of secondary phosphine–boranes. Livinghouse and co-workers prepared *P*-chirogenic ligands by adopting the dynamic resolution of phosphine–boranes (Scheme 1.10b). A series of bisphosphine borane backbones were obtained in an optically pure form with the assistance of (–)-sparteine.[37]

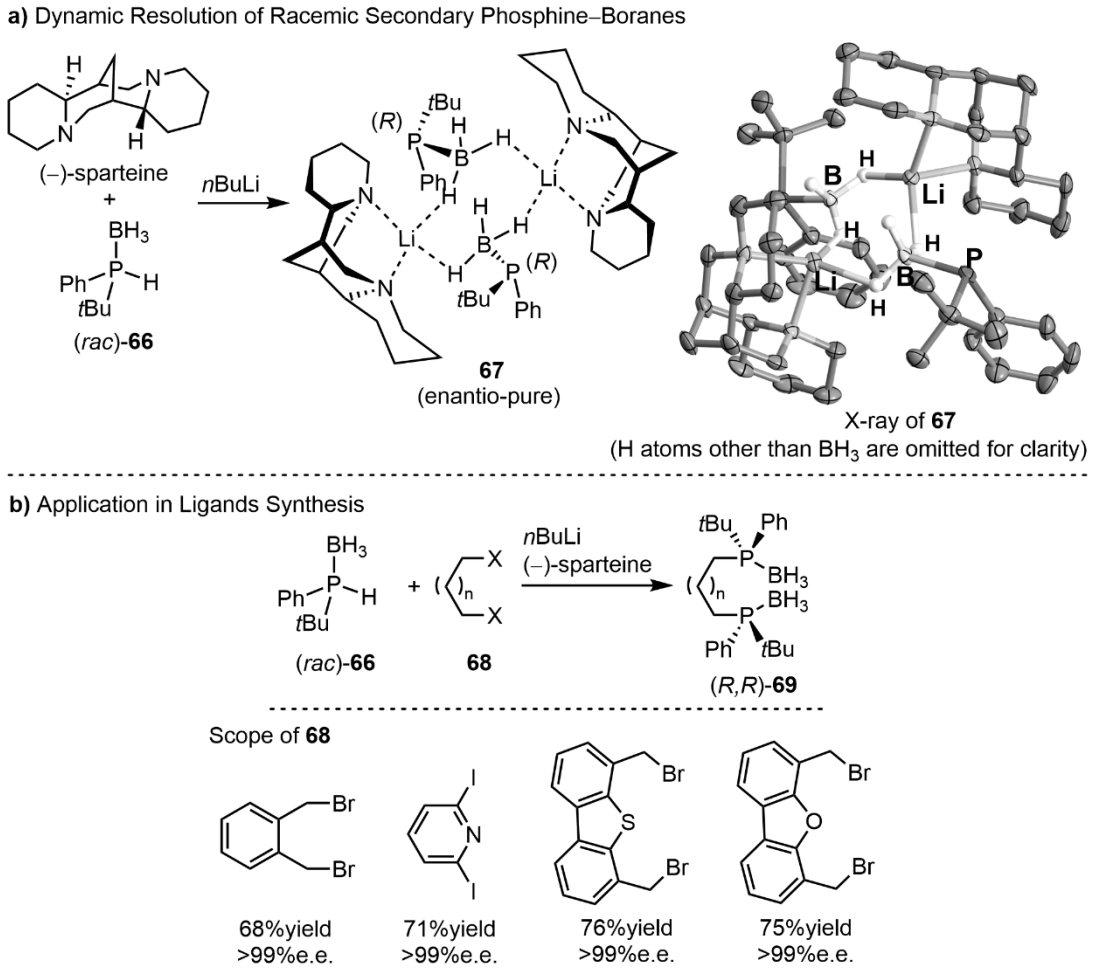

Scheme 1.10. Dynamic resolution of phosphine–boranes and their applications.

It is well known that nucleophilic substitution proceeds in a *P*-retention manner when

an organophosphorus reagent serves as a nucleophile.[38] Since the borane moiety could be removed by an amine under mild conditions through a completely *P*-retention manner,[39] using a phosphine–borane as a pro-nucleophile is an ideal protocol for preparing *P*-chirogenic phosphine ligands. Specifically, optically pure (*R*)-**70** was transformed to (*S*)-**71** through stereo-specific one-carbon degradation (Scheme 1.11a). Next, (*S*)-**71** was transformed to nucleophilic Li[**71**–H] and reacted with electrophilic (*R*)-**72**, which was derived from (*R*)-**70** by sulfonylation, to deliver (*R,R*)-**73** in a *P*-retentive manner.[40] As previously mentioned in Jugé's research (Scheme 1.8),[33] secondary phosphine boranes react with dibromobenzene in the presence of *n*BuLi through an aryne intermediate. This reaction proceeds with *P*-retention manner. Imamoto and co-workers applied the protocol to synthesize novel *P*-chirogenic bisphosphines.[41] *P*-Chiral monophosphine (*R*)-**75** was obtained through the above-mentioned protocol (Scheme 1.11b). The phosphorus center functions as a chiral auxiliary, which controls the absolute configuration of another phosphorus center in (*R,R*)-**77**.

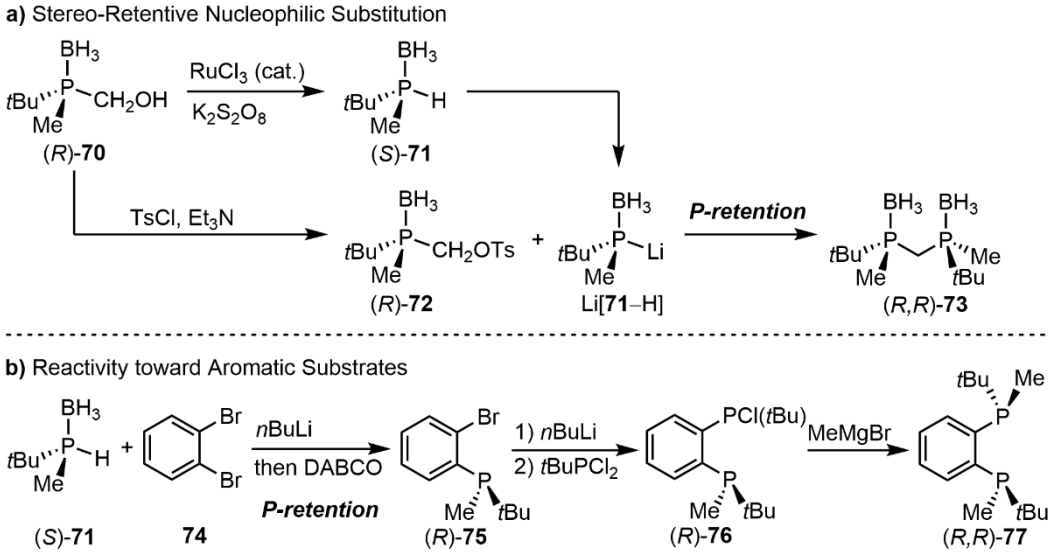

Scheme 1.11. Stereoretentive nucleophilic substitution with secondary phosphine–boranes as pro-nucleophiles.

The *o*-phenylene backbone in (*R,R*)-**77** is considered to provide a regulated environment during catalytic reactions. Imamoto and co-workers prepared the same compound through a different approach (Scheme 1.12).[42] First, optically active (*S*)-**71** was treated with iodine to deliver the corresponding phosphine–iodoborane (*S*)-**78**. Diphosphine–iodoborane **79** was obtained by reacting (*S*)-**78** with racemic **71**. Diastereomerically pure **79** was deprotonated and underwent SNAr with chromium

complex **80**. Interestingly, the absolute configuration of the phosphorus center was retained during the entire synthetic procedure.

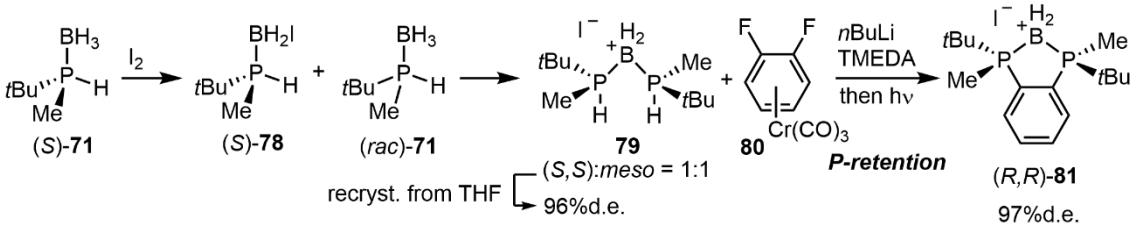

Scheme 1.12. Phosphine–borane salts as nucleophiles.

1.2 Hydrofunctionalization for Construction of C–P Bonds

One of the important challenges in catalytic hydrofunctionalization of alkynes for C–P bond formation is the regioselectivity. As illustrated in Scheme 1.13,[43] after coordination of a metal complex to alkynes, an unsaturated species inserts into the M–H bond followed by C–P reductive elimination to deliver the corresponding linear product. Alternatively, a branched product is obtained through M–P insertion followed by C–H reductive elimination.

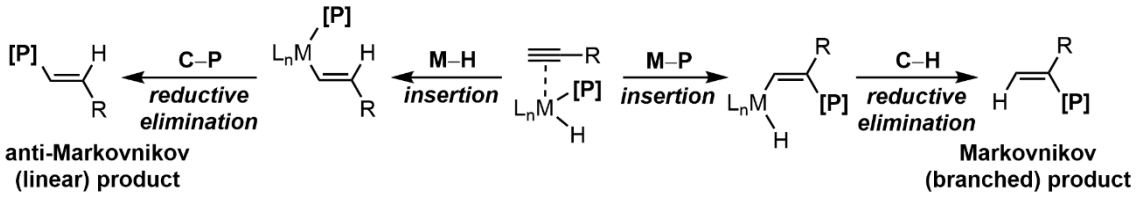

Scheme 1.13. Plausible mechanism of P−H bond addition to alkynes.

In this context, Beletskaya and co-workers reported a Pd-catalyzed hydrophosphonylation of terminal alkynes, in which the selectivity was controlled by well-designed ligands (Scheme 1.14).[44] Specifically, the reaction between alkyne **82** and *H*-phosphonate **83** in the presence of a palladium complex proceeded smoothly to give linear phosphonate product **85** with 2,4,6-trimethoxyphenyl phosphine (**84**) as a ligand. In contrast, when using 4-methoxyphenyl phosphine (**86**) as a ligand, branched phosphonate **87** was obtained as a product. The authors suggested that the *o*-methoxy group on **84** coordinates to the palladium center and restricts the rotation of the ligand. Hence, Pd–P insertion is preferred under such a condition. On the other hand, since

rotation of the ligand on **86** is not restricted, it possesses a larger steric hindrance, which promotes the pathway to branched products. As experimental evidence, the authors used both NMR and ESI-MS to confirm the potential intermediates.

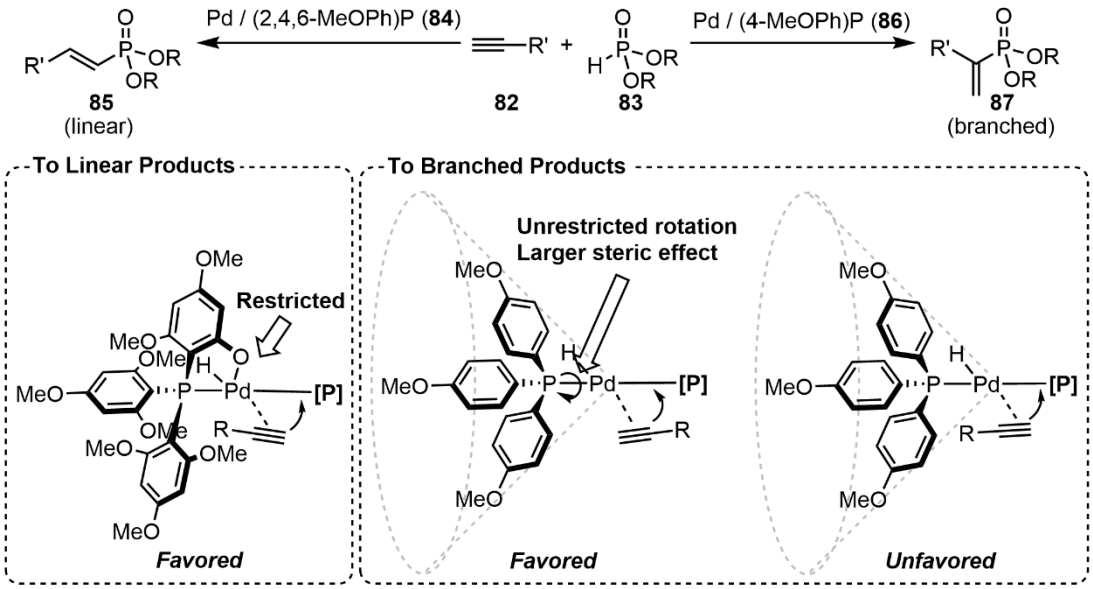

Scheme 1.14. Ligand-controlled selectivity between linear and branched hydrophosphonylation.

The selectivity between the two products is not only controlled by ligands but also by the valency of the metal center. Gaumont and co-workers reported an interesting reaction between diphenyl phosphine **88** and terminal alkenes **89** (Scheme 1.15).[45] When using Fe(II) salts as a catalysts, the reaction delivered linear hydrophosphination product **90**. However, only branched product **91** was obtained when using $FeCl_3$ as the catalyst. No by-products resulting from selectivity issue were obtained in either condition. The authors proposed that the Fe(II) salt might promote the reaction through a radical pathway in the presence of a trace amount of oxygen.

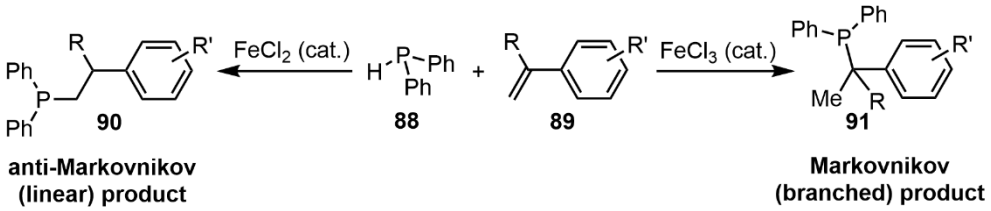

Scheme 1.15. Iron-enabled tunable selectivity in hydrophosphination.

Generally, hydrophosphination of terminal alkynes delivers the anti-Markovnikov product in *Z*-form.[46] Webster and co-workers reported a solvent-enabled tunable regioselective hydrophosphination between **88** and aryl/heteroaryl terminal alkynes **92** (Scheme 1.16).[47] When benzene was applied as the solvent, Markovnikov product **94** was obtained in the presence of an Fe(II) pre-catalyst **93**. In contrast, switching the solvent from benzene to dichloromethane delivered the *Z*-type anti-Markovnikov product **95**. The authors proposed that the reaction begins with the formation of an iron phosphide species **96**, and migratory insertion gives **97** after coordination to alkynes. The reaction between **97** and diphenylphosphine **88** delivers the Markovnikov products **94**. Alternatively, intermediate **97** might come from nucleophilic addition of **88** to Fe(II) complex **98**. Experimental evidence suggest dichloromethane oxidized the Fe(II) complex **93** to Fe(III) species, which promotes the reaction toward anti-Markovnikov products.

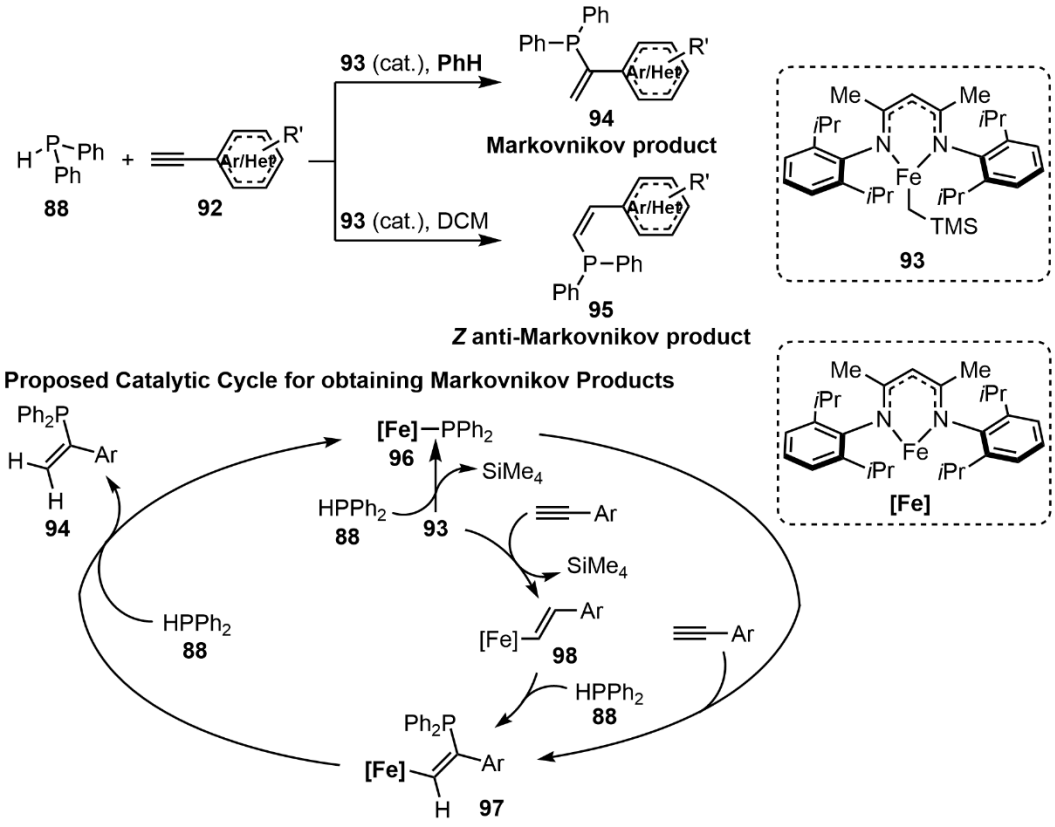

Scheme 1.16. Solvent-enabled tunable regioselective hydrophosphination.

1.3 C–P Bond Formation *via* Cross-Coupling Reactions

The Michaelis-Arbuzov reaction is a classical organic reaction that has been widely used for preparing alkyl phosphonates from alkyl halides **99** and phosphites **100** (Scheme 1.17a). However, aryl halides are not included in the reaction scope. Hirao and co-workers developed a palladium-catalyzed cross-coupling reaction between aryl halides **102** and *H*-phosphonates **103** in the presence of Pd(0) catalyst and triethyl amine base (Scheme 1.17b), affording the corresponding aryl phosphonates **104** in good yields.[48]

Kalek and Stawinski proposed a catalytic cycle for the above-mentioned Hirao coupling (Scheme 1.17c).[49] The Pd(0) complex is generated from the corresponding Pd source. After oxidative addition, *H*-phosphonate **103** coordinates to the Pd(II) center followed by deprotonation to deliver the Pd phosphonate complex **107**. Sequential reductive elimination generates the aryl phosphonate product **104** and completes the catalytic cycle. The reaction of *H*-phosphonate **103** was found to follow the first order kinetics, which suggested that the nucleophile coordination step was rate-determining in the catalytic cycle. Additionally, acetates, brought into the reaction by the Pd source in some cases, accelerated the reductive elimination step by generation of a highly reactive pentacoordinate Pd k^2-acetate species.

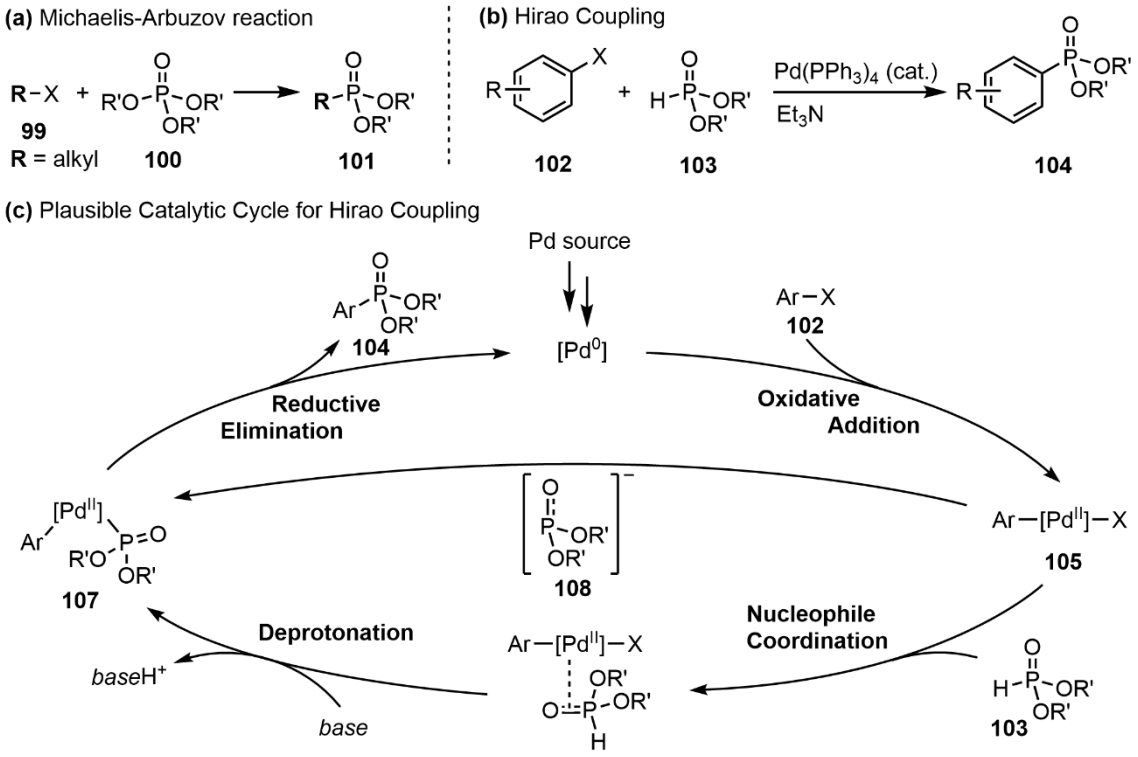

Scheme 1.17. Reaction between phosphonates and halide species.

Exploring the scope of the cross-coupling partner has been an important topic in the development of the Hirao coupling. Herzon and co-workers reported a cross-coupling reaction between secondary phosphine oxides **110** and aryl iodide **109** (Scheme 1.18a).[50] The reaction could proceed at room temperature. Interestingly, *P*-chirogenic secondary phosphine oxides were converted to the corresponding chiral aryl phosphine oxides in a *P*-retention manner.

Triphenylphosphine **112** is also an effective cross-coupling partner (Scheme 1.18b). Chan and co-workers found its reaction with aryl halide **102** could occur in the presence of Pd(0) catalysts and was further promoted by sodium iodide.[51] The authors proposed the key phosphonium intermediate **116** is generated from Pd(II) species **115** in the presence of an excess amount of **112**. Re-oxidative addition of **116** to Pd(0) complex **114** delivers a pentacoordinate Pd(II) species **117**, which gives arylphosphine **113** through ligand substitution and reductive elimination.

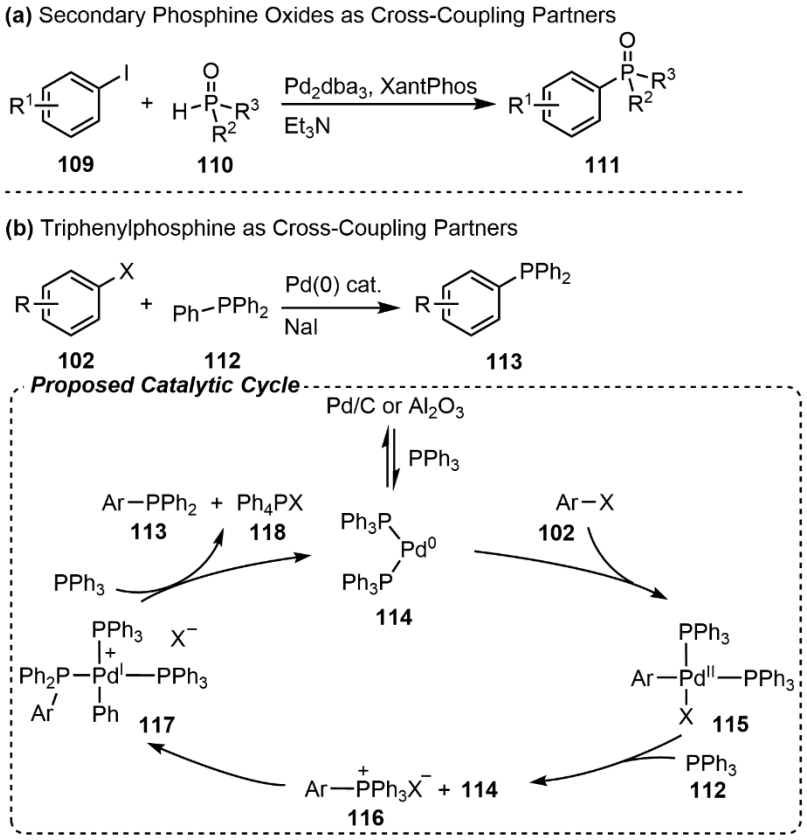

Scheme 1.18. Exploring other phosphorus cross-coupling partners.

The concept of using bench-stable phosphonium salts for cross-coupling has been further developed by Wang and Zhu (Scheme 1.19).[52] Different from *in situ* generation

of phosphonium, **120** was prepared stepwise and transformed to the corresponding alkyl diphenylphosphine **121** in the presence of a Pd(0) catalyst and a large excess of ammonium formate. Similar to Chan's work (Scheme 1.18b),[51] the reaction between phosphonium **120** and Pd(0) complex generates a phosphine-coordinated Pd(II) species **122**, which is further transformed to Pd–H species **123** in the presence of ammonium formate. Reductive elimination and ligand dissociation deliver **121** and hydrogenation product Ph–H. Their strategy is useful for not only alkylation of triphenylphosphine but also transfer hydrogenation of aromatic substituents on the phosphorus center.

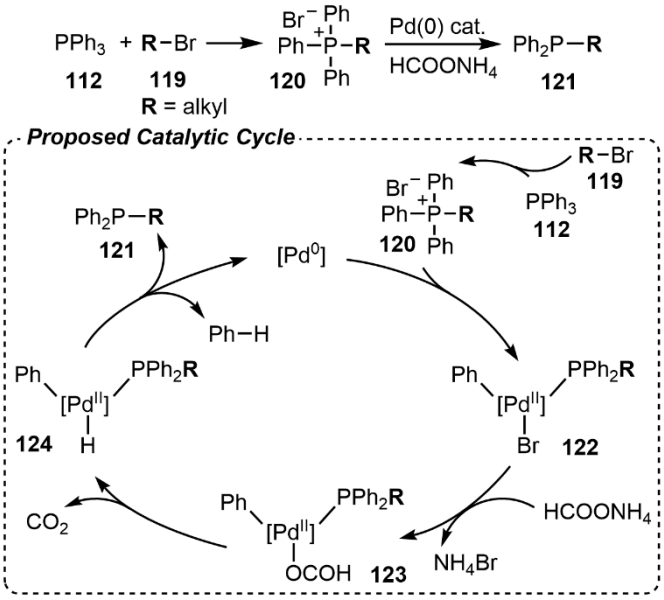

Scheme 1.19. Preparation of alkyl diphenylphosphines from phosphonium salts.

The use of more earth-abundant transition metals for C–P bond formation is also an important topic in the Hirao coupling strategy. Zhu and co-workers reported a Ni-catalyzed phosphinylation of aryl halides in water (Scheme 1.20).[53] The work presented a "green" reaction by using both earth-abundant nickel catalysts and water as a solvent.

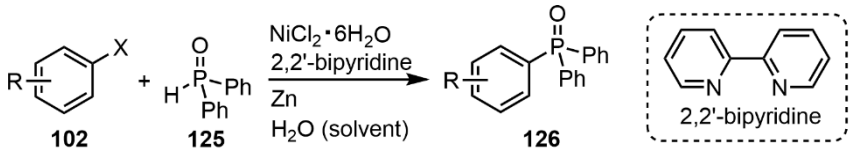

Scheme 1.20. Ni-catalyzed Hirao coupling in water.

Several groups confirmed that catalyst-free Hirao coupling occurred under photo-irradiation conditions.[54] Zeng and Li reported a photoinduced cross-coupling between aryl halides **102** and *H*-phosphonates **103** or secondary phosphine oxides **110** without catalysts and external photosensitizer (Scheme 1.21).[55] Photoinduced homolytic cleavage of phenyl bromide **127** generates phenyl radical **128**, which undergoes single electron transfer with sodium phosphite **130** to give phosphorus-centered radical **129**. Radical coupling between **129** and **128** delivers the corresponding aryl phosphonate **132**. Alternatively, phosphorus-centered radical **129** and phenyl radical **128** could be generated from a five-membered transition state $\mathbf{TS_{127\text{-}129}}$. Yu and Che previously reported a similar reaction using heteroaryl halides as cross-coupling partners.[56]

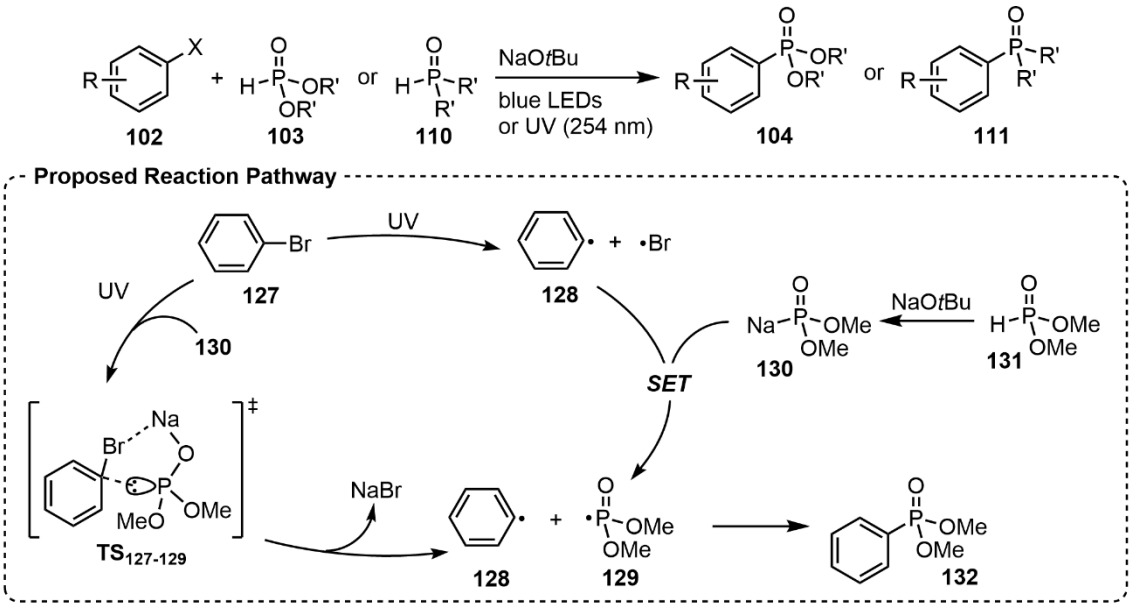

Scheme 1.21. Catalyst-free Hirao coupling enabled by photo-irradiation.

Asymmetric Hirao coupling is a convenient approach toward construction of *P*-chirogenic compounds from bench-stable secondary phosphine oxides. In this context, Cai and co-workers reported a palladium-catalyzed asymmetric cross-coupling between aminophenyl iodide **133** and racemic secondary phosphine oxides (*rac*)-**134** (Scheme 1.22).[57] However, the reaction scope was limited to diarylphosphine oxides, and only *o*-pivalamino phenyl iodide derivatives were effective cross-coupling partners.

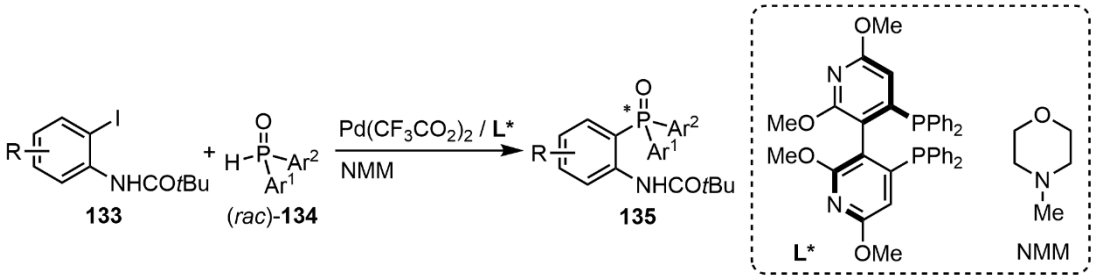

Scheme 1.22. Pd-catalyzed asymmetric cross-coupling between aminophenyl iodide and secondary phosphine oxides.

The strategy was further developed by Zhang and co-workers.[58] The reaction between alkyl aryl phosphine oxides and aryl bromide delivered the corresponding *P*-chirogenic tertiary phosphine oxides in both good yield and enantioselectivity in the presence of Pd(0)-XiaoPhos catalyst and cesium carbonate base (Scheme 1.23). The reaction begins with dynamic coordination of XiaoPhos to the Pd(0) center, which generates an active Pd(0) species **139** and an inactive dimer species [**139**]$_2$. Oxidative addition of phenyl bromide to **139** followed by transmetallation with the phosphorus reagent delivers intermediate **143**, which defines the absolute configuration of the phosphorus center. (*S*$_P$)-**143** is more favorable than (*R*$_P$)-**143** due to the steric effect between the XiaoPhos ligand and phosphorus reagent. Reductive elimination of favored (*S*$_P$)-**143** gives the desired *P*-chirogenic (*S*$_P$)-**145** and complete the catalytic cycle. Alternatively, the Pd(0) complex might first coordinate to **141,** which then undergoes oxidative addition to generate the intermediate **143**. Computational studies on **143** suggest the Gibbs free energy of (*S*$_P$)-**143** is 2.6 kcal·mol^{-1} lower than (*R*$_P$)-**143**, which is attributed to the stabilization effect from the N–H···O=P interaction.

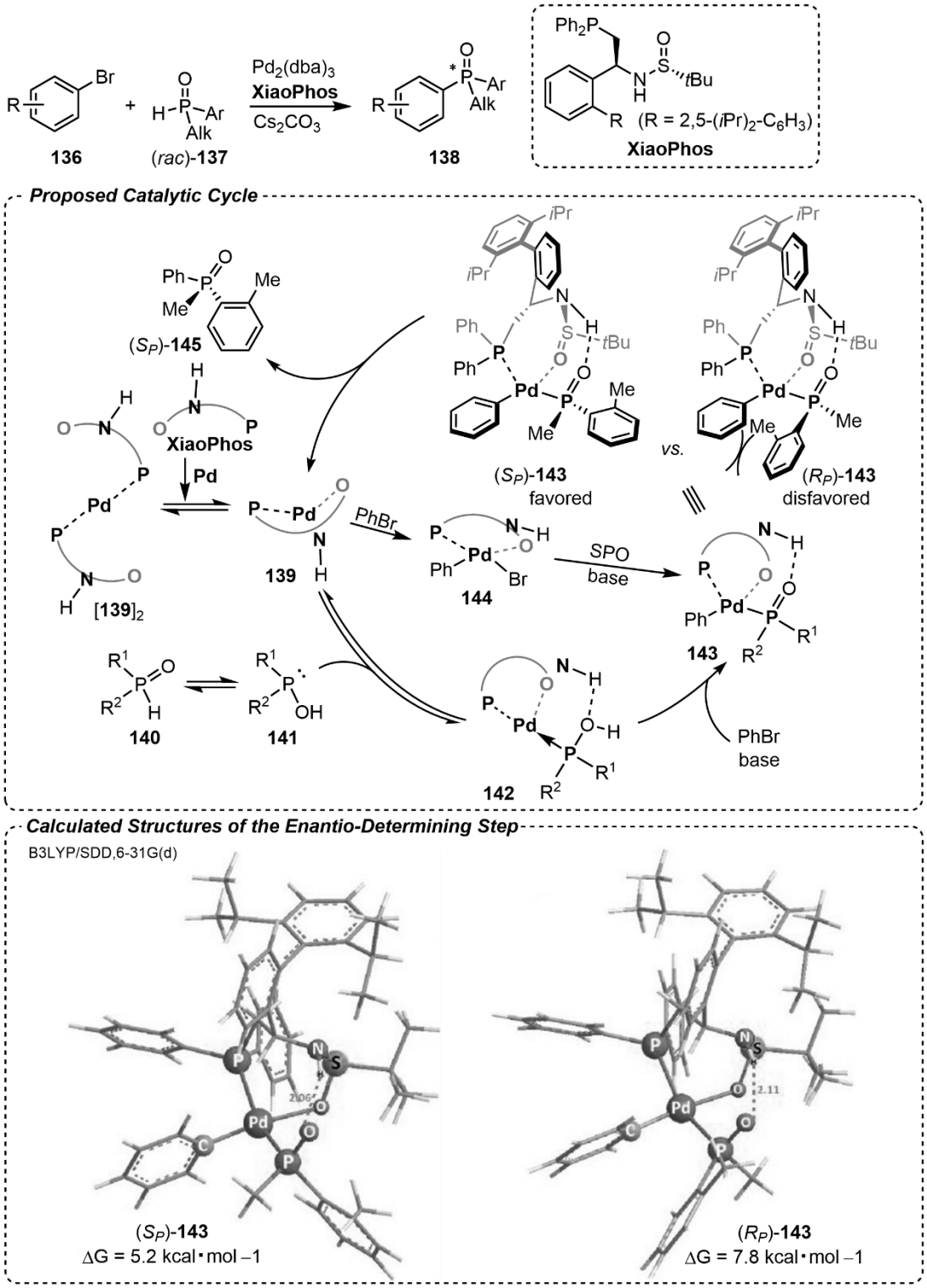

Scheme 1.23. XiaoPhos-enabled catalytic construction of *P*-chirogenic center by asymmetric Hirao coupling.

1.4 Discussion of the Current C–P Bond Formation Strategies

Strategies for constructing C–P bonds have been well-developed during the last few decades. Direct nucleophilic substitution is a convenient approach to access organophosphorus compounds. The protocols are useful for preparing *P*-chirogenic molecules by introducing chiral auxiliaries. Phosphorus reagents can act as either electrophiles or nucleophiles in these processes. Hydrofunctionalization is also an effective protocol for constructing C–P bonds through direct addition. In this context, several different methodologies have been developed for improving regioselectivity. Additionally, metal-catalyzed cross-coupling (Hirao coupling) is a powerful method for preparing organophosphorus compounds from commercially available building blocks. Recent developments have explored the usage of various metal catalysts, cross-coupling partners, or catalyst-free conditions. Several groups have prepared *P*-chirogenic molecules from racemic starting materials through catalytic asymmetric cross-coupling.

Despite the great progress that has been achieved in developing methodologies for C–P bond formation, preparation of complex organophosphorus compounds still faces great challenges. In this context, the direct derivation from existing backbones could be a convenient approach to complex organophosphorus compounds.

Due to increasing interest in the fluorine impact on pharmaceutical and chemical material performance,[59–61] aryl fluorides have been incorporated in a wide range of complex molecules. Indeed, aryl fluoride-containing drugs are the largest family in fluorine-pharmaceuticals (45.3%).[62] From the synthetic point of view, the C(sp^2)–F bond, which is the major moiety of aryl fluorides, is one of the strongest chemical bonds in nature,[63] remaining stable during general chemical transformations. Hence, the C(sp^2)–F bond is considered to be a suitable "detachable chemical handle" in late-stage functionalization of complex structures.[64–66] It would be convenient to prepare complex organophosphorus compounds through late-stage C(sp^2)–F cleavage. However, before the publication of chapter 2 of this thesis, only a few examples had been reported that used activated aryl fluorides as starting materials. Preparation of organophosphorus compounds from non-activated aryl fluorides is unknown.

In the next sections, representative protocols of C(sp^2)–F activation/functionalization will be reviewed. Examples of preparing organophosphorus compounds from aryl fluorides will be introduced.

1.5 Functionalization of Non-Activated Aryl Fluorides *via* C(sp^2)–F Cleavage

1.5.1 Transition-Metal-Catalyzed Cross-Coupling

Herrmann and co-workers proposed that the activation of C−F bonds requires an electron-rich metal center. It is known that a strong bond can be formed between magnesium and fluorine. Combining this hypothesis, they developed a Ni-catalyzed cross-coupling reaction between aryl fluorides **146** and aryl Grignard reagents **147** to prepare the corresponding biaryl products **148** (Scheme 1.24a). The electron-donating *N*-heterocyclic carbene (NHC) ligand was used for generating an electron-rich nickel center. The reaction could be used for functionalizing electron-neutral and -rich aryl fluorides.[67]

Organozinc reagents are also useful for this kind of transformation. Wang and co-workers reported the application of organozinc reagents **149** as cross-coupling partners in the Ni-catalyzed functionalization of aryl fluorides through C(sp^2)–F cleavage (Scheme 1.24b).[68] The scope of organozinc reagents includes both alkyl and aryl zinc substrates. The reaction could selectively cleave one C(sp^2)–F bond in polyfluorobenzene with the assistance of a carbonyl directing group. Organozinc reagents **149** not only serve as cross-coupling partners but also as reductants, reducing Ni(II) pre-catalysts to Ni(0) catalytic species **152** through an oxidative addition-reductive elimination process. After generation of catalytic species **152**, the reaction was proposed to proceed through a general cross-coupling cycle to deliver the corresponding product **150**.

Lee and co-workers developed a strategy to generate Grignard reagents *in situ* from aryl fluorides and use them for further reaction.[69] The reaction between non-activated aryl fluorides **146** and chlorosilanes **155** gave the corresponding defluorosilylation products **156** in the presence of a cobalt catalyst, 1,3-ketiminate ligand, and magnesium powder (Scheme 1.24c). Aryl fluorides **146** were proposed to be activated by 1,3-diketiminate-coordinated Co(I) complex **158**, generating an aryl Co(II) species **159**, which delivered the corresponding aryl Grignard reagents **161** in the presence of magnesium powder.

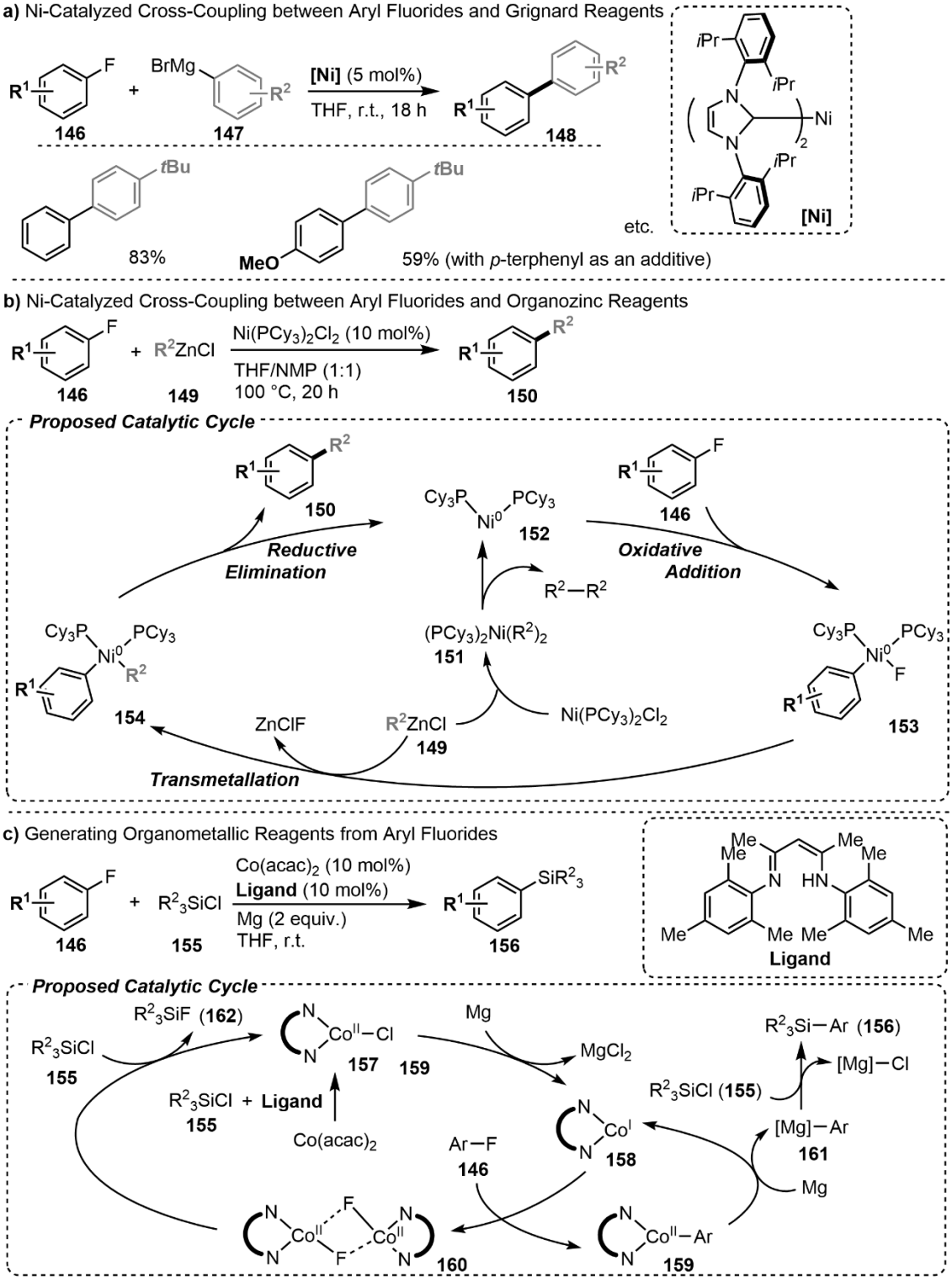

Scheme 1.24. Ni-catalyzed cross-coupling with organometallic reagents.

The usage of pyrophoric organometallic reagents is a major drawback of the above-mentioned protocols. Chatani and co-workers reported a Ni-catalyzed Suzuki-Miyaura cross-coupling between aryl fluorides and aryl boronic esters (Scheme 1.25).[70] The basic catalytic cycle follows the Ni(0)-Ni(II)-Ni(0) oxidative addition-reductive elimination manner. Cesium fluoride serves as a fluoride donor for the formation of boronate **163**. The addition of a catalytic amount of zirconium tetrafluoride largely enhanced the efficiency of the non-directed Suzuki-Miyaura coupling of aryl fluorides. Its role is considered to facilitate fluorine elimination during the oxidative addition or reductive elimination step.

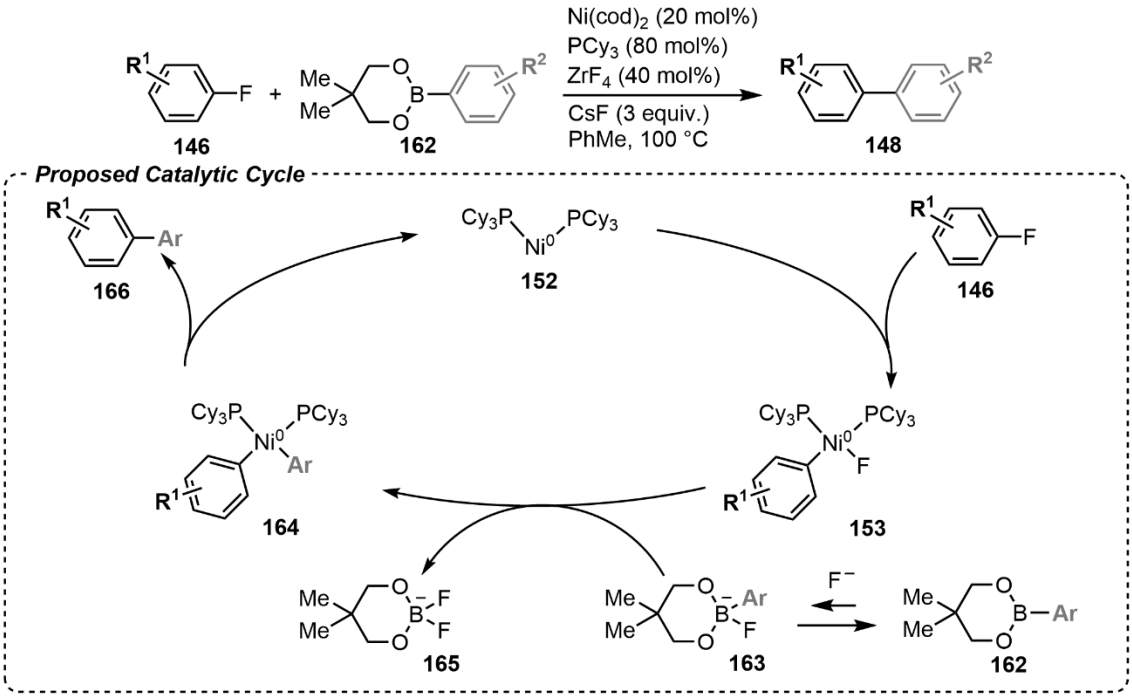

Scheme 1.25. Ni-catalyzed Suzuki-Miyaura cross-coupling with aryl fluorides.

The above-mentioned bimetallic catalysis system employs the cooperative action of Ni(0)-ZrF_4, Hosoya and Niwa also reported a Ni/Cu bimetallic catalysis system for defluoroborylation of non-activated aryl fluorides.[71] In the presence of Ni(0), Cu(I) catalyst, and stoichiometric cesium fluoride base, the reaction between aryl fluorides **146** and bis(pinacolato)diboron (B_2pin_2, **167**) delivered the corresponding arylboronic esters **168** in good yield (Scheme 1.26). The authors proposed that the reaction proceeded through a unique Ni(I) catalytic cycle. Ni(I) fluoride **169** is generated from the Ni(0) complex in the presence of copper iodide and cesium fluoride through single electron oxidation. Transmetallation between **169** and borylcopper **170** gives Ni(I) species **171**,

which cleaves the C(sp^2)–F bond of aryl fluorides **146**. Arylboronic ester **168** is obtained by borylation of Ni(I) complex **173**.

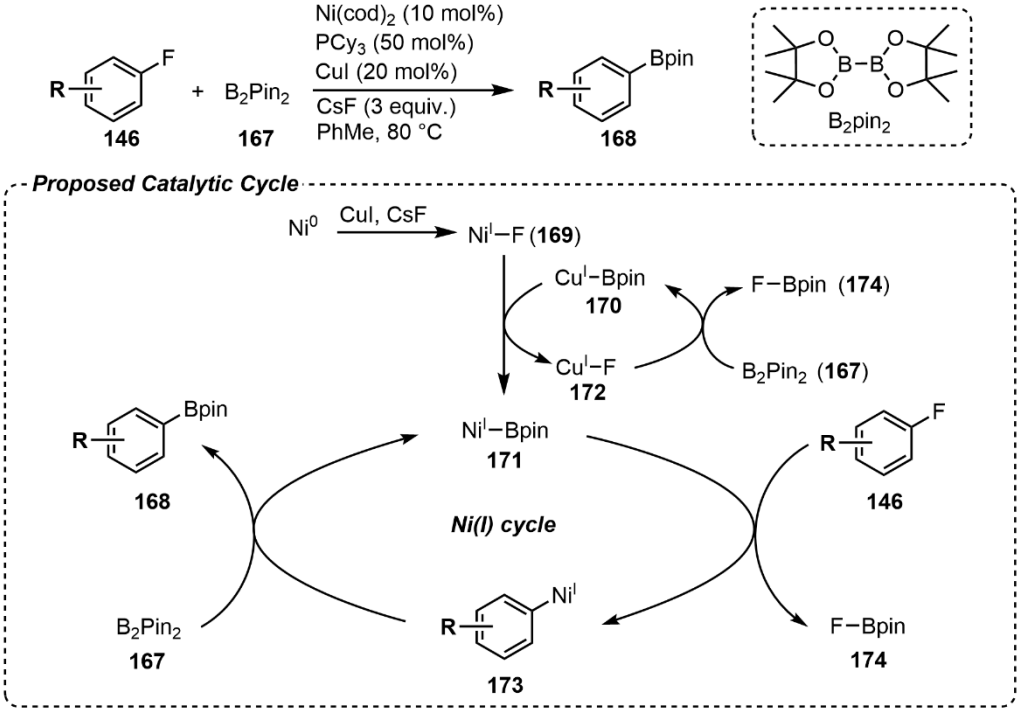

Scheme 1.26. Ni/Cu-catalyzed defluoroborylation of aryl fluorides.

The same reaction, but without the Cu(I) cocatalyst, was reported by Martin and co-workers (Scheme 1.27).[72] The authors proposed a Ni(0)-Ni(II)-Ni(0) oxidative addition-reductive elimination catalytic cycle for the reported reaction.

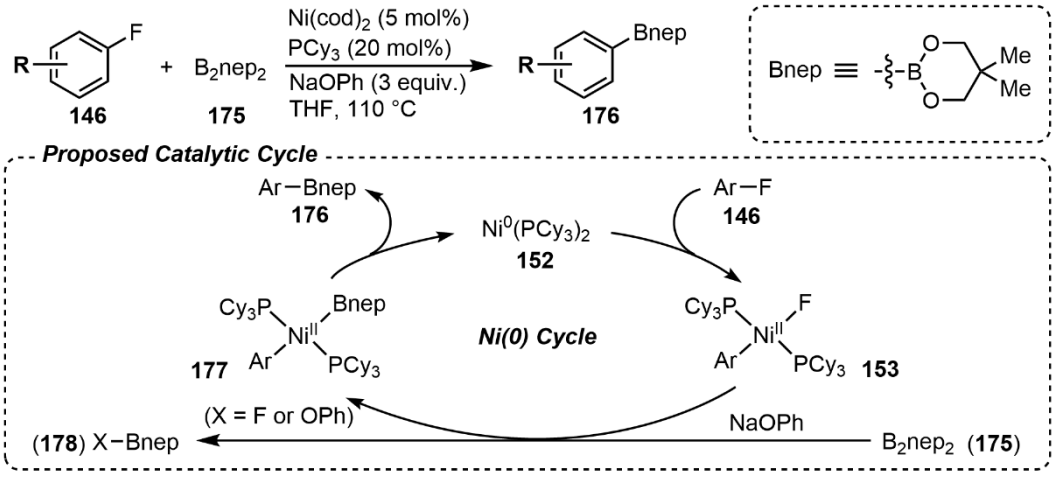

Scheme 1.27. Defluoroborylation of aryl fluorides with a Ni(0) catalytic cycle.

Electron-rich nickel complexes are widely used for other C(sp^2)–F functionalizations. For example, Wang and co-workers reported a nickel-catalyzed amination of aryl fluorides **146** with secondary amines **179** (Scheme 1.28a). The highly electron-donating NHC ligand was used for forming an electron-rich metal center.[73] In 2018, Iwai and Sawamura achieved the amination with primary amines **181** (Scheme 1.28b). An electron-donating bisphosphine ligand with a rigid *o*-phenylene backbone was proven to be effective for this class of transformation.[74]

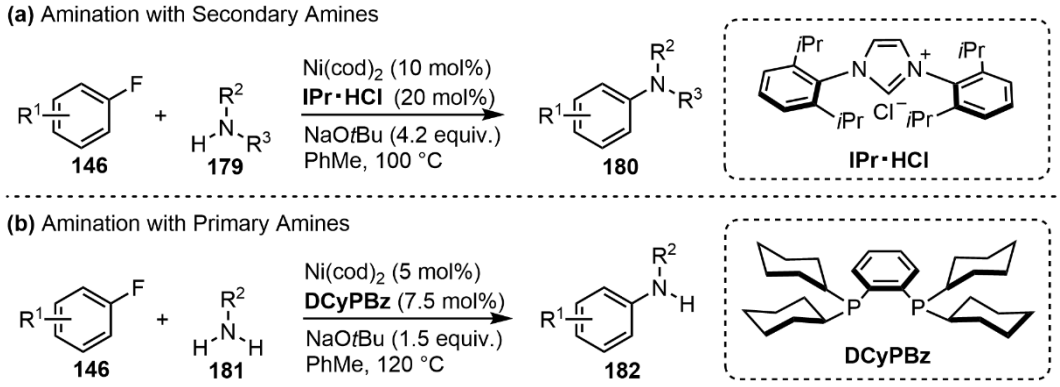

Scheme 1.28. Ni-catalyzed amination of aryl fluorides.

1.5.2 Nucleophilic Aromatic Substitution

Nucleophilic aromatic substitution (S_NAr) is a class of reaction in which a nucleophile displaces the leaving group on an aromatic compound.[75] It is one of the most used chemical reactions in pharmaceutical synthesis after the Suzuki-Miyaura cross-coupling and Buchwald-Hartwig amination.[76] Since fluoride is a good leaving group in S_NAr-type reactions,[75] it should be an efficient way for functionalizing aryl fluorides. However, traditional S_NAr requires electron-deficient aromatic rings, which limits the application of these methodologies. Recent studies suggested electron-neutral and -rich aromatic substrates also undergo S_NAr, but follow a concerted pathway (CS_NAr).[32, 77, 78] Hence, S_NAr has become a convenient approach for functionalizing non-activated aryl fluorides through C(sp^2)–F cleavage.

Caron and co-workers reported S_NAr between secondary nitriles **183** and non-activated aryl fluorides **146** (Scheme 1.29a). The authors suggested the reaction might pass through an intermediate in which the negative charge is stabilized by a potassium cation through coordination.[79] Organoborates are a class of pro-nucleophiles in S_NAr-type reactions.

Ohmiya and co-workers utilized benzyl borates **185** in the reaction with aryl fluorides **146** (Scheme 1.29b). All three examples, which were illustrated in the original paper, proceeded with moderate-to-good efficiency.[80] More recently, Chatani and co-workers developed the S_NAr reaction between aryl fluorides **146** and aliphatic amides **187** in the presence of stoichiometric NaHMDS base (HMDS = $–N(SiMe_3)_2$) (Scheme 1.29c). Computational studies revealed that the reaction passed through a concerted *ipso* substitution pathway.[81]

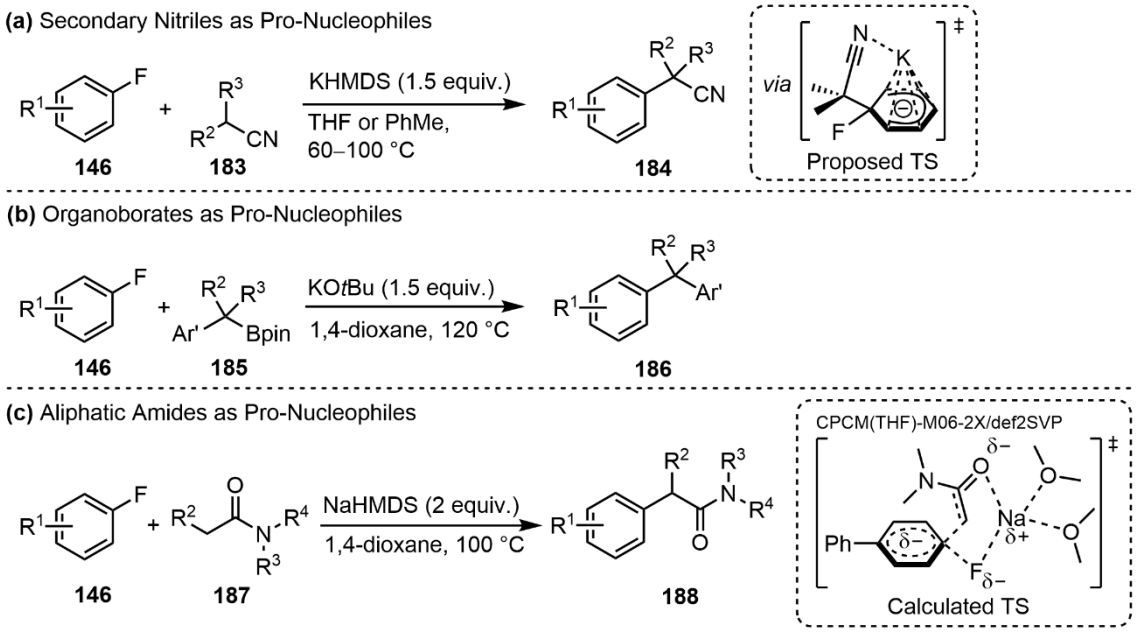

Scheme 1.29. S_NAr of non-activated aryl fluorides with carbon-centered nucleophiles.

Diness and Fairlie reported the *N*-arylation between diazoles **189** and aryl fluorides **146** (Scheme 1.30). Despite requiring harsh conditions for reaching high efficiency, the one-pot *N*-arylation followed by cross-coupling was achieved using 4-bromofluorobenzene as the starting material.[82]

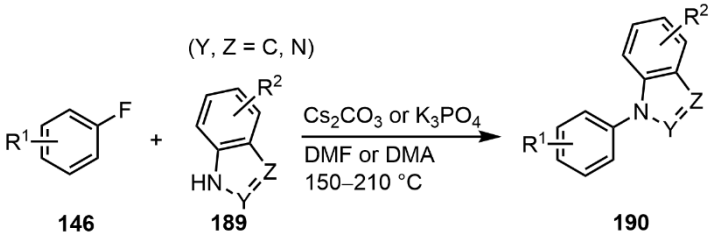

Scheme 1.30. *N*-Arylation with non-activated aryl fluorides.

In 2019, Studer[83] and Martin[84] respectively reported the defluorosilylation of non-activated aryl fluorides. Studer and co-workers reported the *ipso* substitution of aryl fluorides **146** with silyl lithium reagents **191** to deliver the corresponding tertiary silanes **192** (Scheme 1.31). Computational investigation on the reaction pathway suggested the reaction preferred the concerted mechanism which is mediated by a four-membered transition state $\mathbf{TS_{193\text{-}195}}$. In contrast, the pathway that generated a benzyne intermediate **199** not only possesses a high energy barrier but also is highly endothermic (22.9 kcal·mol^{-1}). The calculated energy barriers are in agreement with the employed reaction conditions. Hence, the reported defluorosilylation occurs through a CS_NAr pathway.

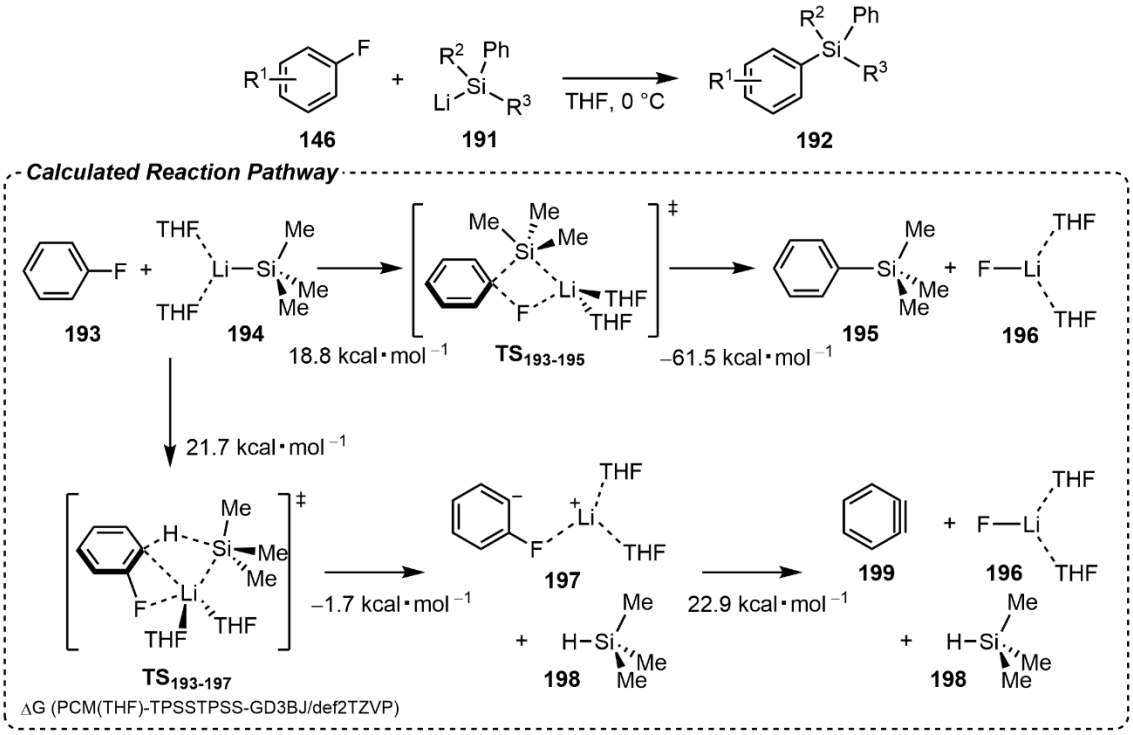

Scheme 1.31. Studer's work on the defluorosilylation of aryl fluorides.

Instead of directly using silyl lithium reagents as nucleophiles, Martin and co-workers applied silylboranes **201** as pro-nucleophiles for attacking aryl fluoride **146** or alkyl fluoride **200** to give the corresponding aryl silanes **192** or alkyl silanes **202** in the presence of LiHMDS base and 1,2-dimethoxyethane (DME) solvent (Scheme 1.32). Their computational studies suggested the current reaction prefers a concerted pathway. As experimental evidence, the authors performed an isotope-labeling experiment by applying deuterium-labeled alkyl fluorides **203** and **204**. The result showed the configuration of the *ipso* carbon was inverted after the substitution, which indicated that neither cationic

nor radical-type pathways were likely under the reported reaction conditions.

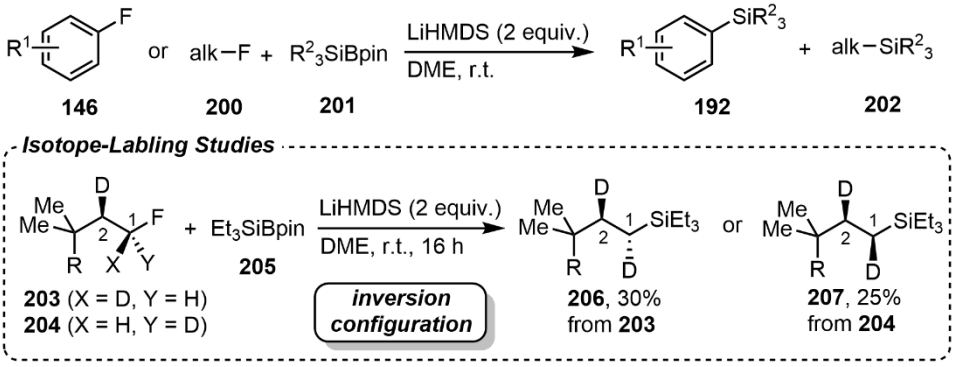

Scheme 1.32. Martin's work on the defluorosilylation of aryl fluorides.

Transition-metal-catalyzed SNAr faced great challenges due to the sluggish arene exchange steps. Shi and co-workers designed a novel hemilabile phosphine ligand for stabilizing the metal center during the arene dissociation step. They developed a Ru-catalyzed SNAr amination of aryl fluorides with primary or secondary amines (Scheme 1.33). NMR monitoring experiments suggested the designed methoxy site of the hemilabile ligand coordinated to and dissociated from the metal center during the reaction process. Such a hemilabile-ligand-design facilitated an efficient substrate association-dissociation process.[85]

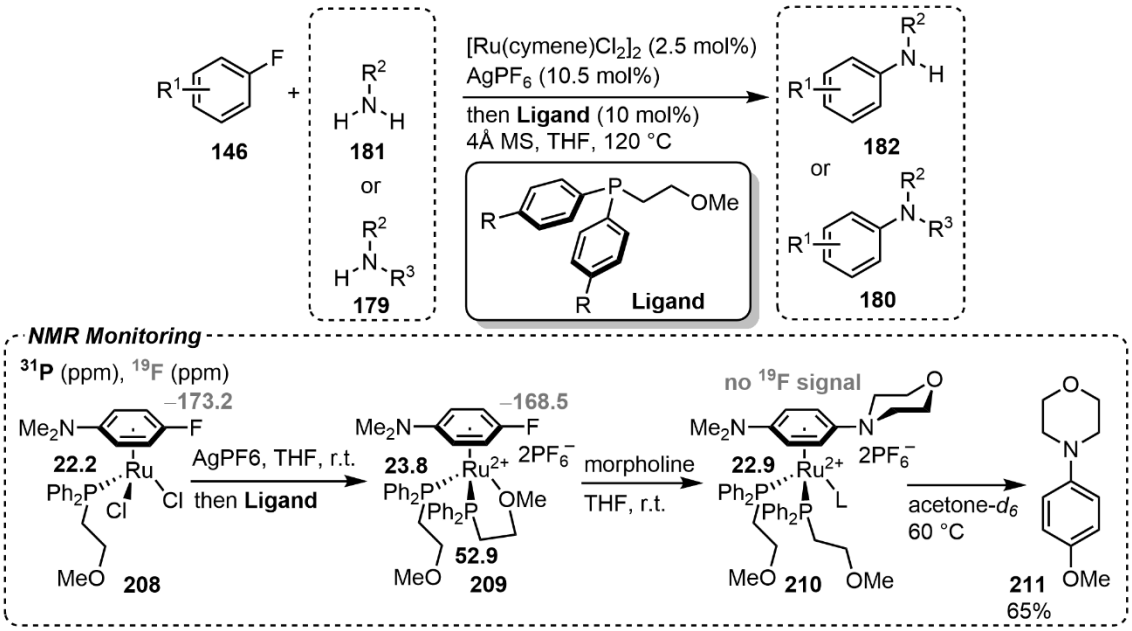

Scheme 1.33. Catalytic SNAr amination of aryl fluorides.

More recently, Shi and co-workers further developed a Rh-catalyzed hydroxylation and alkoxylation of aryl fluorides (Scheme 1.34). Since the electrophilicity of the fluoroarene complex was the key for the reactivity, the author replaced Ru complex with a Rh complex, which has a higher oxidation state. The catalytic cycle for the reported reaction involves S_NAr hydroxylation and arene exchange. They successfully isolated and characterized the important Meisenheimer intermediate **221**, which proved that the S_NAr step passed through a stepwise mechanism.[86]

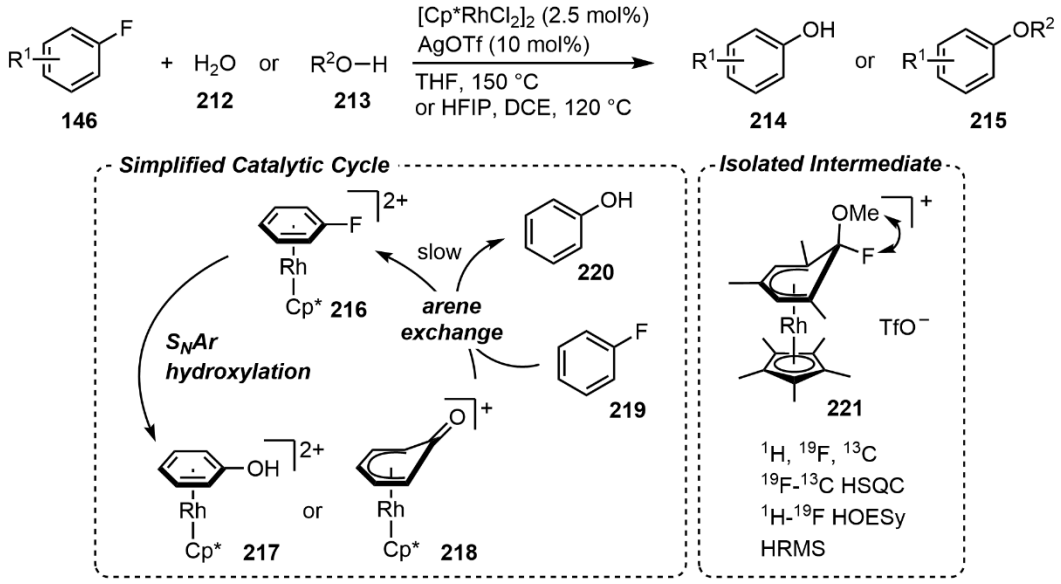

Scheme 1.34. Rh-catalyzed S_NAr hydroxylation and alkoxylation of aryl fluorides.

1.6 C(sp^2)–P Bond Formation *via* C(sp^2)–F Cleavage

As illustrated in the previous sections, construction of C–C, C–B, C–N, C–O, and C–Si bonds through C–F bond cleavage has been well studied. In contrast, methodologies for C–P bond formation remain less developed. C–P bonds (65 kcal · mol^{-1}) are significantly less stable than C–F bonds (116 kcal·mol^{-1}).[87] Hence, cleaving C–F bonds to construct C–P bonds should be thermodynamically unfavorable. Thus now, only few examples illustrating methodologies for preparing organophosphorus compounds from aryl fluorides have been reported.

Würthwein and co-workers reported a series of reactions between polyfluorobenzenes **222** (di- and tri-fluorobenzenes) and silyl phosphines **223** (Scheme 1.35).[88, 89] The reported protocol required harsh conditions, and the substrate scope was limited to

polyfluorobenzenes. Computational investigations suggested the reaction passed through a concerted S_NAr mechanism to generate a penta-coordinated phosphorus intermediate **226**, in which $FSiMe_3$ was dissociated by ligand-ligand coupling to deliver the corresponding phosphination product.

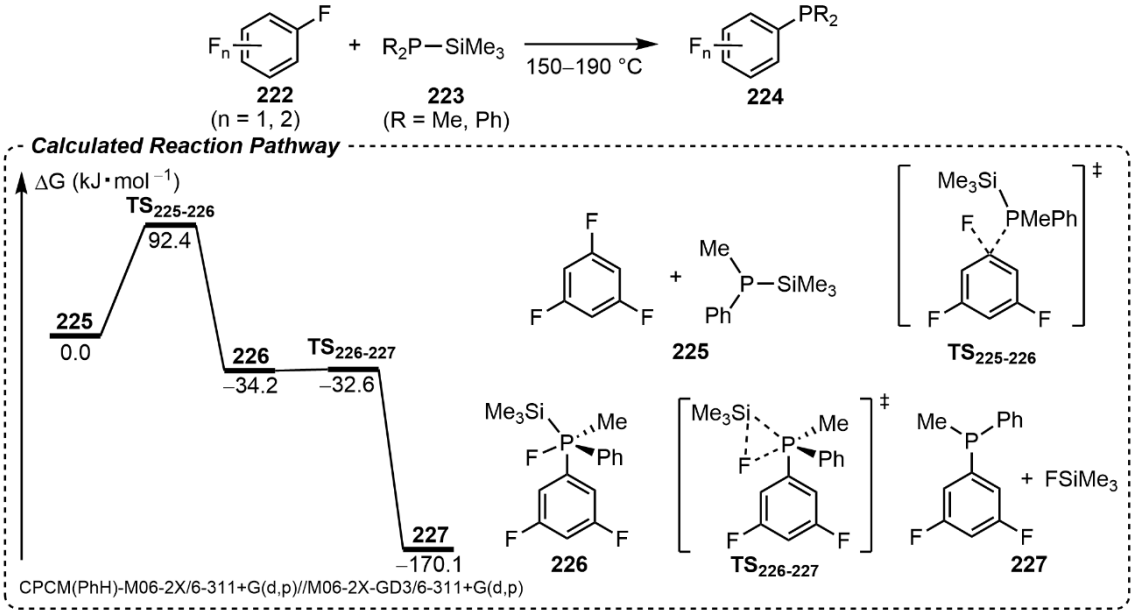

Scheme 1.35. Phosphination of polyfluorobenzenes with silylphosphines.

Thiel and co-workers reported an example of fluoride-catalyzed phosphination of aryl fluorides **228** with silylphosphines **223** (Scheme 1.36).[90] The protocol was limited to functionalizing electron-deficient aryl fluorides. The authors proposed fluoride catalysts activated silyl phosphine **223** to generate phosphide **231**, which attacked aryl fluorides **228** to deliver the corresponding phosphination products **229** and regenerated the catalyst.

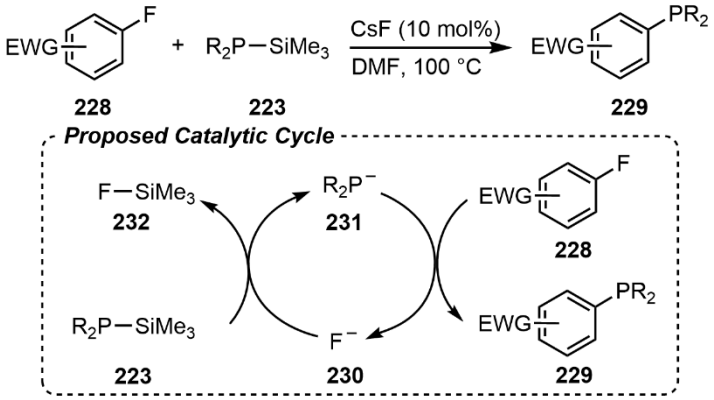

Scheme 1.36. Fluoride-catalyzed phosphination of aryl fluorides.

Recently, Zeng and Li reported a photoinduced phosphonylation protocol for non-activated aryl fluorides.[91] The reaction between aryl fluorides **146** and *H*-phosphonates **103** proceeded smoothly under UV irradiation in the presence of stoichiometric sodium hydride base to give the corresponding aryl phosphonates **104** (Scheme 1.37). The reaction was applied to a wide range of electron-deficient, -neutral, and -rich aryl fluorides. Similar to their previous work on aryl bromides (Scheme 1.21),[56] aryl fluorides were excited by UV light to generate phenyl radical **128** and a fluorine radical, which undergoes a single electron transfer (SET) with sodium phosphites **234** to give a phosphorus-centered radical **235**. Alternatively, **128** and **235** could be generated through a five-membered transition state under UV irradiation. Radical coupling between **128** and **235** delivered aryl phosphonates **236**. The authors conducted further computational investigations to confirm the proposed mechanism.

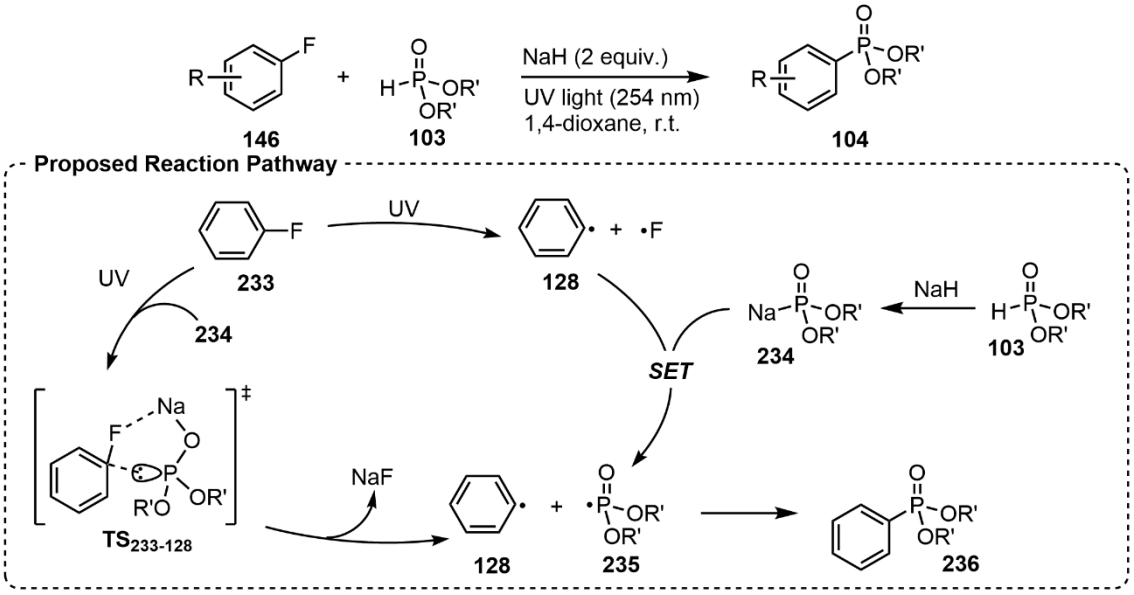

Scheme 1.37. Photoinduced phosphonylation of non-activated aryl fluorides.

1.7 Overview of This Thesis

The author has developed a series of protocols for preparing various organophosphorus compounds from non-activated aryl fluorides through C(sp^2)–F cleavage. In chapter 2, defluorinative phosphinylation through a nucleophile-dependent S_NAr mechanism is described. Chapter 3 illustrates defluorinative phosphonylation through nickel-catalysis.

1.7.1 Chapter 2: Defluorophosphinylation of Aryl Fluorides through Nucleophilic Aromatic Substitution

Non-activated aryl fluorides **146** reacted with secondary phosphine oxides **110** in the presence of a stoichiometric amount of KHMDS or KO*t*Bu base (Scheme 1.38). Notably, both electron-neutral and electron-rich aryl fluorides participated in the reaction with substantially stabilized anionic *P* nucleophiles to deliver the corresponding tertiary phosphine oxides **111**. Quantum chemical calculations suggested a nucleophile-dependent mechanism that involves both concerted and stepwise S_NAr reaction pathways.

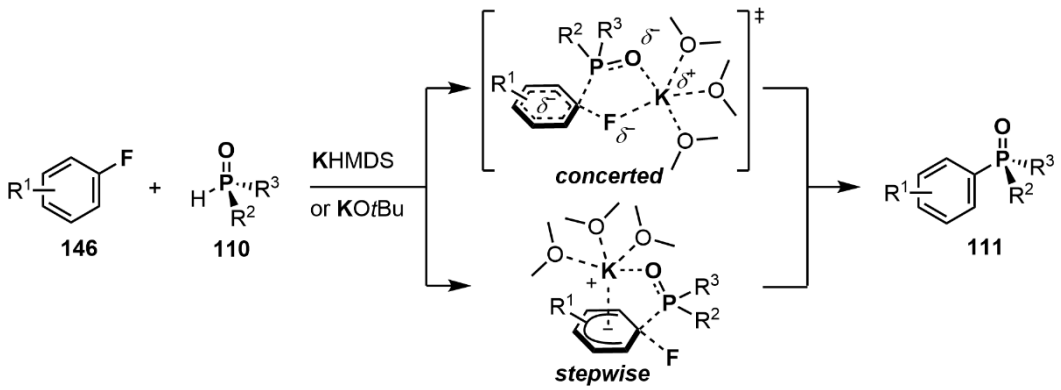

Scheme 1.38. S_NAr phosphinylation of non-activated aryl fluorides.

1.7.2 Chapter 3: Nickel-Catalyzed Defluorophosphonylation of Aryl Fluorides

A Ni-catalyzed cross-coupling between aryl fluorides **146** and di-*sec*-alkyl phosphonates **103** in the presence of stoichiometric KO*t*Bu base is described (Scheme 1.39). The reaction converted various aryl fluorides into the corresponding aryl phosphonates **104** even when electron-donating substituents were presented on the aromatic ring. The combined experimental and computational studies suggested Ni–K^+ cooperative action of a Ni(0) complex chelated with a strongly electron-donating ion-bridged dimeric phosphite ligand system $[(RO)_2PO^-K^+]_2$ that facilitates turnover-limiting

C–F bond oxidative addition of aryl fluorides.

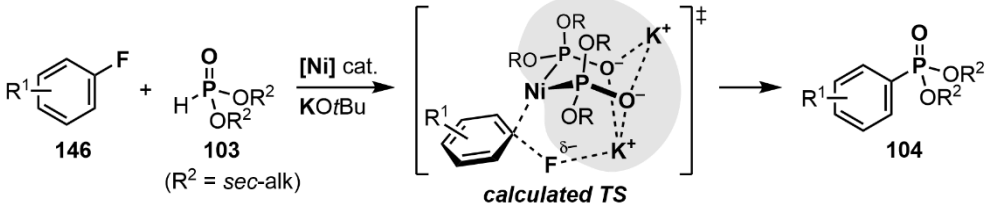

Scheme 1.39. Ni-catalyzed phosphonylation of aryl fluorides.

1.8 References

[1] Phosphorus. *CAS Common Chemistry*, American Chemical Society (the U.S.).

[2] M. Ooki, T. Oosawa, M. Tanaka, H. Chihara. Phosphorus. *Chemistry Dictionary*. 1994, Toukyou Kagaku Doujin, Tokyo (Japan). ISBN 4-8079-0411-6. p. 1531.

[3] P. J. Murphy. *Organophosphorus Reagents: A Practical Approach in Chemistry.* Ch.1-2 Nomenclature, 2004, Oxford University Press, Oxford (the U.K.). ISBN 0-1985-0262-1. p. 2.

[4] R. Okazaki. Nomenclature of Organophosphorus Compounds. *J. Synth. Org. Chem.* **1970**, *28*, 129−131.

[5] B. Thompson, M. Machas, D. R. Nielsen. Creating Pathways towards Aromatic Building blocks and Fine Chemicals. *Curr. Opin. Biotechnol.* **2015**, *36*, 1−7.

[6] R. L. Myers. *The 100 Most Important Chemical Compounds: A Reference Guide.* 2007, Greenwood Press, Westport (the U.S.). ISBN 0-313-33758-6.

[7] P. A. Forero-Cortéz, A. M. Haydl. The 25th Anniversary of the Buchwald-Hartwig Amination: Development, Applications, and Outlook. *Org. Process Res. Dev.* **2019**, *23*, 1478−1483.

[8] R. Martin, S. L. Buchwald. Palladium-Catalyzed Suzuki-Miyaura Cross-Coupling Reactions Employing Dialkylbiaryl Phosphine Ligands. *Acc. Chem. Res.* **2008**, *41*, 1461−1473.

[9] T. E. Barder, S. D. Walker, J. R. Martinelli, S. L. Buchwald. Catalysts for Suzuki-Miyaura Coupling Process: Scope and Studies of the Effect of Ligand Structure. *J. Am. Chem. Soc.* **2005**, *127*, 4685−4696.

[10] S. D. Walker, T. E. Barder, J. R. Martinelli, S. L. Buchwald. A Rationally Designed Universal Catalyst for Suzuki-Miyaura Coupling Process. *Angew. Chem. Int. Ed.*

2004, *43*, 1871−1876; *Angew. Chem.* **2004**, *116*, 1907−1912.

[11] J. Yin, M. P. Rainka, X.-X. Zhang, S. L. Buchwald. A Highly Active Suzuki Catalyst for the Synthesis of Sterically Hindered Biaryls: Novel Ligand Coordingation. *J. Am. Chem. Soc.* **2002**, *124*, 1162−1163.

[12] J. P. Wolfe, S. Wagaw, J.-F. Marcoux, S. L. Buchwald. Rational Development of Practical Catalysts for Aromatic Carbon−Nitrogen Bond Formation. *Acc. Chem. Res.* **1998**, *31*, 805−818.

[13] H. Tomori, J. M. Fox, S. L. Buchwald. An Improved Synthesis of Functionalized Biphenyl-Based Phosphine Ligands. *J. Org. Chem.* **2000**, *65*, 5334−5341.

[14] W. S. Knowles, M. J. Sabacky. Catalytic Asymmetric Hydrogenation Employing a Soluble, Optically Active, Rhodium Complex. *Chem. Commun. (London)* **1968**, 1445−1446.

[15] T. Imamoto. Synthesis and Applications of High-Performance *P*-Chiral Phosphine Ligands. *Proc. Jpn. Acad., Ser. B* **2021**, *97*, 520−542.

[16] M. Dutartre, J. Bayardon, S. Jugé. Application and Stereoselective Syntheses of *P*-Chirogenic Phosphorus Compounds. *Chem. Soc. Rev.* **2016**, *45*, 5771−5794.

[17] Q. Xu, C.-Q. Zhao, L.-B. Han. Stereospecific Nucleophilic Substitution of Optically Pure *H*-Phosphinates: A General Way for the Preparation of Chiral *P*-Stereogenic Phosphine Oxides. *J. Am. Chem. Soc.* **2008**, *130*, 12648−12655.

[18] E. Podyacheva, E Kuchuk, D. Chusov. Reduction of Phosphine Oxides to Phosphines. *Tetrahedron Lett.* **2019**, *60*, 575−582.

[19] D. Hérault, D. H. Nguyen, D. Nuel, G. Buono. Reduction of Secondary and Tertiary Phosphine Oxides to Phosphines. *Chem. Soc. Rev.* **2015**, *44*, 2508−2528.

[20] D. Gatineau, L. Giordano, G. Buono. Bulky, Optically Active *P*-Stereogenoic Phosphine-Boranes from Pure *H*-Menthylphosphinates. *J. Am. Chem. Soc.* **2011**, *133*, 10728−10731.

[21] J.-J. Ye, S.-Z. Nie, J.-P. Wang, J.-H. Wen, Y. Zhang, M.-R. Qiu, C.-Q. Zhang. Nucleophilic Substitution of *P*-Stereogenic Chiralphosphines: Mechanism, Stereochemistry, and Stereoselective Conversions of Diastereomeric Secondary Phosphine Oxides to Tertiary Phosphines. *Org. Lett.* **2017**, *19*, 5384−5387.

[22] A. Jaillet, C. Darcel, J. Bayardon, A. Schlachter, C. Salomon, Y. Rousselin, P. Harvey, S. Jugé. Design of *P*-Chirogenic Aminophosphine-Phosphite Ligands at Both Phosphorus Centers: Origin of Enantioselectivities in Pd-Catalyzed Allylic Reactions. *J. Org. Chem.* **2020**, *85*, 14391−14410.

[23] C. Bauduin, D. Moulin, E. B. Kaloun, C. Darcel, S. Jugé. Highly Enantiomerically Enriched Chlorophosphine Boranes: Synthesis and Applications as P-Chirogenic

Electrophilic Blocks. *J. Org. Chem.* **2003**, *68*, 4293−4301.

[24] R. den Heeten, B. H. G. Swennenhuis, P. W. N. M. van Leeuwen, J. G. de Vries, P. C. J. Kamer. Parallel Synthesis and Screening of Polymer-Supported Phosphorus-Stereogenic Aminophosphane-Phosphite and -Phosphinite Ligands. *Angew. Chem. Int. Ed.* **2008**, *47*, 6602−6605.

[25] J. Holz, K. Rumpel, A. Spannenberg, R. Paciello, H. Jiao, A. Börner. *P*-Chirogenic Xantphos Ligands and Related Ether Diphosphines: Synthesis and Application in Rhodium-Catalyzed Asymmetric Hydrogenation. *ACS Catal.* **2017**, *7*, 6162–6169.

[26] M. Biosca, P. de la Cruz-Sánchez, O. Pàmies, M. Diéguez. P-Stereogenic N-Phosphine-Phosphite Ligands for the Rh-Catalyzed Hydrogenation of Olefins. *J. Org. Chem.* **2020**, *85*, 4730–4739.

[27] Z. S. Han, N. Goyal, M. A. Herbage, J. D. Sieber, B. Qu, Y. Xu, Z. Li, J. T. Reeves, J.-N. Desrosiers, S. Ma, N. Grinberg, H. Lee, H. P. R. Mangunuru, Y. Zhang, D. Krishnamurthy, B. Z. Lu, J. J. Song, G. Wang, C. H. Senanayake. Efficient Asymmetric Synthesis of *P*-Chiral Phosphine Oxides *via* Properly Designed and Activated Benzoxazaphosphine-2-oxide Agents. *J. Am. Chem. Soc.* **2013**, *135*, 2474−2477.

[28] T. León, A. Riera, X. Verdaguer. Stereoselective Synthesis of *P*-Stereogenic Aminophosphines: Ring Opening of Bulky Oxzaphosphpolidines. *J. Am. Chem. Soc.* **2011**, *133*, 5740−5743.

[29] H. Zijlstra, T. León, A. de Cózar, C. F. Guerra, D. Byrom, A. Riera, X. Verdaguer, F. M. Bickelhaupt. Stereodivergent S_N2@P Reactions of Borane Oxazaphospholidines: Experimental and Theoretical Studies. *J. Am. Chem. Soc.* **2013**, *135*, 4483−4491.

[30] B. Zheng, R. J. Fox, M. Sugiyama, A. Fritz, M. D. Eastgate. Development of Efficient Process for the Preparation of Di-tert-Butyl Potassium Phosphate and Di-*tert*-Butyl (Chloromethyl) Phosphate. *Org. Process Res. Dev.* **2014**, *18*, 636−642.

[31] C. Tejo, J. H. Pang, D. Y. Ong, M. Oi, M. Uchiyama, R. Takita, S. Chiba. Dearylation of Arylphosphine Oxides Using a Sodium Hydride-Iodide Composite. *Chem. Commun.* **2018**, *54*, 1782−1785.

[32] S. Rohrbach, A. J. Smith, J. H. Pang, D. L. Poole, T. Tuttle, S. Chiba, J. A. Murphy. Concerted Nucleophilic Aromatic Substitution Reactions. *Angew. Chem. Int. Ed.* **2019**, *58*, 16368−16388; *Angew. Chem.* **2019**, *131*, 16518−16540.

[33] J. Bayardon, H. Laureano, V. Diemer, M. Dutartre, U. Das, Y. Rousselin, J.-C. Henry, F. Colobert, F. R. Leroux, S. Jugé. Stereoselective Synthesis of *o*-Bromo (or Iodo)aryl *P*-Chirogenic Phosphines Based on Aryne Chemistry. *J. Org. Chem.* **2012**, *77*, 5759−5769.

[34] N. A. Senger, B. Bo, Q. Cheng, J. R. Keeffe, S. Gronert, W. Wu. The Element Effect Revisited: Factors Determining Leaving Group Ability in Activated Nucleophilic Aromatic Substitution Reactions. *J. Org. Chem.* **2012**, *77*, 9535−9540.

[35] F. J. L. Heutz, M. C. Samuels, P. C. J. Kamer. Solid-Phase Synthesis of Recyclable Diphosphine Ligands. *Catal. Sci. Technol.* **2015**, *5*, 3296−3301.

[36] G. Müller, J. Brand. Mono(borane)phosphides as Ligands to Lithium and Aluminum. *Organometallics* **2003**, *22*, 1463−1467.

[37] B. Wolfe, T. Livinghouse. A Direct Synthesis of P-Chiral Phosphine−Borane *via* Dynamic Resolution of Lithiated Racemic *tert*-Butylphenylphosphine−Borane with (−)-Sparteine. *J. Am. Chem. Soc.* **1998**, *120*, 5116−5117.

[38] T. Miura, H. Yamada, S.-I. Kikuchi, T. Imamoto. Synthesis and Reactions of Optically Active Secondary Dialkylphosphine-Boranes. *J. Org. Chem.* **2000**, *65*, 1877−1880.

[39] T. Imamoto. Synthesis and Reactions of Phosphine-Boranes. *J. Synth. Org. Chem. Jpn.* **1993**, *51*, 223−231.

[40] T. Imamoto, K. Tamura, T. Ogura, Y. Ikematsu, D. Mayama, M. Sugiya. Improved Synthetic Routes to Methylene-Bridged *P*-Chiral Diphosphine Ligands via Secondary Phosphine−Boranes. *Tetrahedron Asmmetry* **2010**, *21*, 1522−1528.

[41] T. Imamoto, K. Tamura, Z. Zhang, Y. Horiuchi, M. Sugiya, K. Yoshida, A. Yanagisawa, I. D. Gridnev. Rigid *P*-Chiral Phosphine Ligands with *tert*-Butylmethylphosphino Groups for Rhodium-Catalyzed Asymmetric Hydrogenation of Functionalized Alkenes. *J. Am. Chem. Soc.* **2012**, *134*, 1754−1769.

[42] Y. Yamamoto, T. Koizumi, K. Katagiri, Y. Furuya, H. Danjo, T. Imamoto, K. Yamaguchi. Facile Synthesis of Highly Congested 1,2-Diphosphinobenzenes from Bis(phosphine)boronium Salts. *Org. Lett.* **2006**, *8*, 6103–6106.

[43] V. P. Ananikov, A. V. Makarov, I. P. Beletskaya. Catalytic Hydrofunctionalization of Alkynes through P−H Bond Addition: The Unique Role of Orientation and Properties of the Phosphorus Group in the Insertion Step. *Chem. Eur. J.* **2011**, *17*, 12623−12630.

[44] V. P. Ananikov, J. V. Ivanova, L. L. Khemchyan, I. P. Beletskaya. Unusual Control of Reaction Selectivity through a Subtle Change in the Ligand: Proof of Concept and Application in Pd-Catalyzed C−P Bond Formation. *Eur. J. Org. Chem.* **2012**, 3830−3840.

[45] L. Routaboul, F. Toulgoat, J. Gatignol, J.-F. Lohier, B. Norah, O. Delacroix, C. Alayrac, M. Taillefer, A.-C. Gaumont. Iron-Salt-Promoted Highly Regioselective α and β Hydrophosphination of Alkenyl Arenes. *Chem. Eur. J.* **2013**, *19*, 8760–8764.

[46] C. A. Bange, R. Waterman. Challenges in Catalytic Hydrophosphination. *Chem. Eur.*

J. **2016**, *22*, 12598−12605.

[47] A. K. King, K. J. Gallagher, M. F. Mahon, R. L. Webster. Markovnikov versus *anti*-Markovnikov Hydrophosphination: Divergent Reactivity Using an Iron(II) β-diketminate Pre-Catalyst. *Chem. Eur. J.* **2017**, *23*, 9039−9043.

[48] T. Hirao, T. Masunaga, Y. Oshiro, T. Agawa. A Novel Synthesis of Dialkyl Arenephosphonates. *Synthesis* **1981**, *13*, 56−57.

[49] M. Kalek, J. Stawinski. Palladium-Catalyzed C−P Bond Formation: Mechanistic Studies on the Ligand Substitution and the Reductive Elimination. An Intramolecular Catalysis by the Acetate Group in Pd^{II} Complexes. *Organometallics* **2008**, *27*, 5876−5888.

[50] A. J. Bloomfield, S. B. Herzon. Room Temperature, Palladium-Mediated *P*−Arylation of Secondary Phosphine Oxides. *Org. Lett.* **2012**, *14*, 4370−4373.

[51] Y. Wang, C. W. Lai, F. Y. Kwong, W. Jia, K. S. Chan. Synthesis of Aryl Phosphines *via* Phosphination with Triphenylphosphine by Supported Palladium Catalysts. *Tetrahedron* **2004**, *60*, 9433−9439.

[52] M. Lei, X. Chen, Y. Wang, L. Zhang, H. Zhu, Z. Wang. Homogeneous and Heterogeneous Pd-Catalyzed Selective C−P Activation and Transfer Hydrogenation for "Group-Substitution" Synthesis of Trivalent Phosphines. *Org. Lett.* **2022**, *24*, 2868−2872.

[53] X. Zhang, H. Liu, X. Hu, G. Tang, J. Zhu, Y. Zhao. Ni(II)/Zn Catalyzed Reductive Coupling of Aryl Halides with Diphenylphosphine Oxide in Water. *Org. Lett.* **2011**, *13*, 3478−3481.

[54] Q. Dou, L. Geng, B. Cheng, C.-J. Li, H. Zeng. Photoinduced Transition-Metal and External Photosensitizer Free Cross-Coupling of Aryl Triflates with Trialkyl Phosphites. *Chem. Commun.* **2021**, *57*, 8429−8432.

[55] H. Zeng, Q. Dou, C.-J. Li. Photoinduced Transition-Metal-Free Cross-Coupling of Aryl Halides with *H*-Phosphonates. *Org. Lett.* **2019**, *21*, 1301−1305.

[56] J. Yuan, W.-P. To, Z.-Y. Zhang, C.-D. Yue, S. Meng, J. Chen, Y. Liu, G.-A. Yu, C.-M. Che. Visible-Light-Promoted Transition-Metal-Free Phosphinylation of Heteroaryl Halides in the Presence of Potassium *tert*-Butoxide. *Org. Lett.* **2018**, *20*, 7816−7820.

[57] Y. Zhang, H. He, Q. Wang, Q. Cai. Asymmetric Synthesis of Chiral P-Stereogenic Triaryl Phosphine Oxides *via* Pd-Catalyzed Kinetic Arylation of Diaryl Phosphine Oxides. *Tetrahedron Lett.* **2016**, *57*, 5308−5311.

[58] Q. Dai, W. Li, Z. Li, J. Zhang. *P*-Chiral Phosphines Enabled by Palladium/Xiao-Phos-Catalyzed Asymmetric P−C Cross-Coupling of Secondary Phosphine Oxides and Aryl Bromides. *J. Am. Chem. Soc.* **2019**, *141*, 20556−20564.

[59] Y. Zhou, J. Wang, Z. Gu, S. Wang, W. Zhu, J. L. Aceña, V. A. Soloshonok, K. Izawa, H. Liu. Next Generation of Fluorine-Containing Pharmaceuticals, Compounds Currently in Phase II−III Clinical Trials of Major Pharmaceutical Companies: New Structual Trends and Therapeutic Areas. *Chem. Rev.* **2016**, *116*, 422−518.

[60] J. Wang, M. Sánchez-Roselló, J. L. Aceña, C. del Pozo, A. E. Sorochinsky, S. Fustero, V. A. Soloshonok, H. Liu. Fluorine in Pharmaceutical Industry: Fluorine-Containing Drugs Introduced to the Market in the Last Decade (2001−2011). *Chem. Rev.* **2014**, *114*, 2432−2506.

[61] R. Berger, G. Resnati, P. Metrangolo, E. Weber, J. Hulliger. Organic Fluorine Compounds: A Great Opportunity for Enhanced Materials Properties. *Chem. Soc. Rev.* **2011**, *40*, 3496−3508.

[62] M. Inoue, Y. Sumii, N. Shibata. Contribution of Organofluorine Compounds to Pharmaceuticals. *ACS Omega* **2020**, *5*, 10633−10640.

[63] K. Daasbireg. Estimation of Bond Dissociation Gibbs Energies for Carbon−Halogen Bonds in Anion Radicals of Some Aryl Halides and Substituted Benzyl Halides. *J. Chem. Soc., Perkin Trans. 2* **1994**, 1275−1277.

[64] D. Ge, X.-Q. Chu. Multiple-Fold C−F Bond Functionalization for the Synthesis of (Hetero)cyclic Compounds: Fluorine as a Detachable Chemical Handle. *Org. Chem. Front.* **2022**, *9*, 2013−2055.

[65] L. Fu, Q. Chen, Y. Nishihara. Recent Advances in Transition-Metal-Catalyzed C−C Bond Formation *via* C(sp^2)−F Cleavage. *Chem. Rec.* **2021**, *21*, 3394−3410.

[66] H. Amii, K. Uneyama. C−F Bond Activation in Organic Synthesis. *Chem. Rev.* **2009**, *109*, 2119−2183.

[67] V. P. W. Böhm, C. W. K. Gstöttmayr, T. Weskamp, W. A. Herrmann. Catalytic C−C Bond Formation through Selective Activation of C−F Bonds. *Angew. Chem. Int. Ed.* **2001**, *40*, 3387−3389.

[68] F. Zhu, Z.-X. Wang. Nickel-Catalyzed Cross-Coupling of Aryl Fluorides and Organozinc Reagents. *J. Org. Chem.* **2014**, *79*, 4285−4292.

[69] S. Lim, H. Cho, J. Jeong, M. Jang, H. Kim, S. H. Cho, E. Lee. Cobalt-Catalyzed Defluorosilylation of Aryl Fluorides *via* Grinard Reagent Formation. *Org. Lett.* **2020**, *22*, 7387–7392.

[70] M. Tobisu, T. Xu, T. Shimasaki, N. Chatani. Nickel-Catalyzed Suzuki-Miyaura Reaction of Aryl Fluorides. *J. Am. Chem. Soc.* **2011**, *133*, 19505−19511.

[71] T. Niwa, H. Ochiai, Y. Watanabe, T. Hosoya. Ni/Cu-Catalyzed Defluoroborylation of Fluoroarenes for Diverse C−F Bond Functionalizations. *J. Am. Chem. Soc.* **2015**, *137*, 14313−14318.

[72] X.-W. Liu, J. Echavarren, C. Zarate, R. Martin. Ni-Catalyzed Borylation of Aryl Fluorides *via* C–F Cleavage. *J. Am. Chem. Soc.* **2015**, *137*, 12470−12473.

[73] F. Zhu, Z.-X. Wang. Nickel-Catalyzed Coupling of Fluoroarenes and Amines. *Adv. Synth. Catal.* **2013**, *355*, 3694−3702.

[74] T. Harada, Y. Ueda, T. Iwai, M. Sawamura. Nickel-Catalyzed Amination of Aryl Fluorides with Primary Amines. *Chem. Commun.* **2018**, *54*, 1718−1721.

[75] P. Y. Bruice. *Organic Chemistry, 6th Edition.* 2007, Prentice Hall, New Jersey (the U.S.). ISBN 0-321-69768-5. p. 690.

[76] D. G. Brown, J. Boström. Analysis of Past and Present Synthetic Methodologies on Medicinal Chemistry: Where Have All the New Reactions Gone? *J. Med. Chem.* **2016**, *59*, 4443–4458.

[77] A. J. J. Lennox. Meisenheimer Complexes in S_NAr Reactions: Intermediates or Transition States? *Angew. Chem. Int. Ed.* **2018**, *57*, 14686–14688; *Angew. Chem.* **2018**, *130*, 14898–14900.

[78] C. N. Neumann, T. Ritter. Facile C – F Bond Formation through a Concerted Nucleophilic Aromatic Substitution Mediated by the PhenoFluor Reagent. *Acc. Chem. Res.* **2017**, *50*, 2822–2833.

[79] S. Caron, E. Vazquez, J. M. Wojcik. Preparation of Tertiary Benzylic Nitriles from Aryl Fluordies. *J. Am. Chem. Soc.* **2000**, *122*, 712–713.

[80] M. Takeda, K. Nagao, H. Ohmiya. Transition-Metal-Free Cross-Coupling by Using Tertiary Benzylic Organoborates. *Angew. Chem. Int. Ed.* **2020**, *59*, 22460–22464; *Angew. Chem.* **2020**, *132*, 22646–22650.

[81] A. Matsuura, Y. Ano, N. Chatani. Nucleophilic Aromatic Substitution of Non-Activated Aryl Fluorides with Aliphatic Amides. *Chem. Commun.* **2022**, *58*, 9898–9901.

[82] F. Diness, D. P. Fairlie. Catalyst-Free *N*-Arylation Using Unactivated Fluorobenzenes. *Angew. Chem. Int. Ed.* **2012**, *51*, 8012–8016; *Angew. Chem.* **2012**, *124*, 8136–8140.

[83] S. Mallick, P. Xu, E.-U. Würthwein, A. Studer. Silyldefluorination of Fluoroarenes by Concerted Nucleophilic Aromatic Substitution. *Angew. Chem. Int. Ed.* **2019**, *58*, 283–287; *Angew. Chem.* **2019**, *131*, 289–293.

[84] X.-W. Liu, C. Zarate, R. Martin. Base-Mediated Defluorosilylation of $C(sp^2)$–F and $C(sp^3)$–F Bonds. *Angew. Chem. Int. Ed.* **2019**, *58*, 2064–2068; *Angew. Chem.* **2019**, *131*, 2086–2090.

[85] Q.-K. Kang, Y. Lin, Y. Li, H. Shi. Ru(II)-Catalyzed Amination of Aryl Fluorides *via* η^6-Coordination. *J. Am. Chem. Soc.* **2020**, *142*, 3706–3711.

[86] Q.-K. Kang, Y. Lin, Y. Li, L. Xu, K. Li, H. Shi. Catalytic S_NAr Hydroxylation and Alkoxylation of Aryl Fluorides. *Angew. Chem. Int. Ed.* **2021**, *60*, 20391–20399; *Angew. Chem.* **2021**, *133*, 20554–20562.

[87] P. Flowers, K. Theopold, R. Langley, W. R. Robinson. *Ch. 7.5 Strength of Ionic and Covalent Bonds, Chemistry 2e (Digital Edition).* 2019, OpenStax, Rice University, Texas (the U.S.). ISBN 1-947172-61-1. Url: https://openstax.org/books/chemistry-2e/pages/7-5-strengths-of-ionic-and-covalent-bonds.

[88] S. I. Zhivetyeva, L. I. Goryunov, I. Yu. Bagryanskaya, J. Grobe, V. D. Shteingarts, E.-U. Würthwein. Phosphinodefluorination of Polyfluorobenzenes by Silylphosphines $Ph(R)PSiMe_3$ (R = Me, Ph): Further Experimental and Computational Evidences for the Concerted A_ND_N Mechanism of Aromatic Nucleophilic Substitution. *J. Fluor. Chem.* **2014**, *164*, 58−69.

[89] L. I. Goryunov, J. Grobe, D. Le Van, V. D. Shteingarts, R. Mews, E. Lork, E.-U. Würthwein. Di- and Trifluorobenzenes in Reactions with Me_2EM (E = P, N; M = $SiMe_3$, $SnMe_3$, Li) Reagents: Evidence for a Concerted Mechanism of Aromatic Nucleophilic Substitution. *Eur. J. Org. Chem.* **2010**, 1111−1123.

[90] A. Reis, D. Dehe, S. Farsadpour, I. Munstein, Y. Sun, W. R. Thiel. Fluoride Catalyzed P–Aryl-Coupling—a Mild Approach to Functionalized Arylphosphines. *New J. Chem.* **2011**, *35*, 2488−2495.

[91] Q. Dou, Y. Lang, H. Zeng, C.-J. Li. Photoinduced Transition-Metal and External Photosensitizer Free Phosphonation of Unactivated $C(sp^2)$−F Bond *via* SET Process Under Mild Conditions. *Fundam. Res.* **2021**, *1*, 742−746.

Chapter 2

Phosphinylation of Aryl Fluorides through Nucleophilic Aromatic Substitution

2.1 Introduction

Nucleophilic aromatic substitution (S_NAr) is a classical and fundamental chemical reaction.[1] The S_NAr occurs most commonly between highly nucleophilic reagents and aryl halides with strongly electron-withdrawing substituents, proceeding through a widely accepted stepwise manner mediated by Meisenheimer complexes (Scheme 2.1a).[2, 3] Meanwhile, a series of reports have recently described that electron-neutral or electron-rich aryl electrophiles prefer concerted reaction mechanisms without intermediates. This class of reactions is denoted as CS_NAr (Scheme 2.1b).[4–6] Generally, reaction mechanisms in S_NAr are dominated by electronic properties of aryl electrophiles rather than nucleophiles.[7–9]

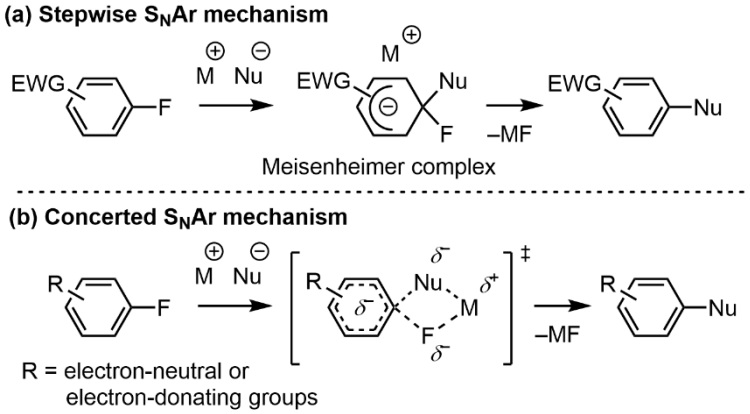

Scheme 2.1. S_NAr reactions of aryl fluorides.

Herein, the author describes his finding that S_NAr reactions of non-activated or even electron-rich aryl fluorides occurred efficiently with potassium diorganophosphinites despite their substantial stability as anionic species (Scheme 2.2).[10] This S_NAr reaction produced a variety of tertiary phosphine oxides, including a blue OLED molecule obtained through the reaction of an electron-rich *p*-fluoroaniline derivative, and enantioenriched *P*-chiral tertiary phosphine oxides obtained through a stereoretentive reaction with *P*-chiral secondary phosphine oxides. Quantum chemical calculations suggested unusual nucleophile-dependent mechanistic features of this S_NAr reaction, showing that both concerted and stepwise S_NAr reaction pathways are feasible. This is due to non-covalent interactions and ambiphilic nature of the potassium diorganophosphinite nucleophiles.

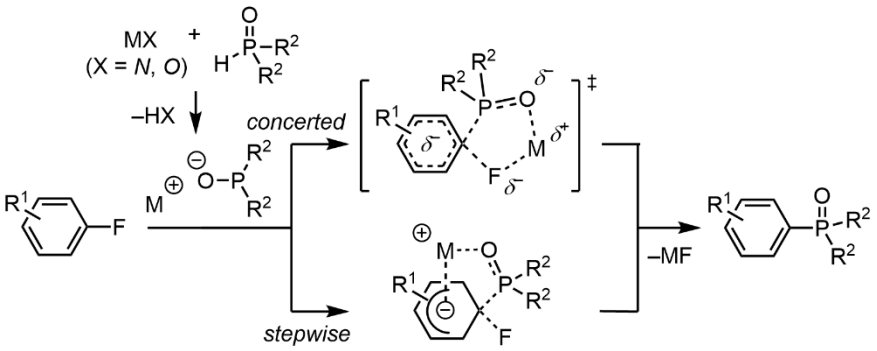

Scheme 2.2. Phosphinylation of non-activated aryl fluorides.

2.2 Results and Discussion

Specifically, heating and stirring a mixture of 4-fluorobiphenyl (**1a**, 0.125 mmol), dicyclohexylphosphine oxide (**2a**, 0.25 mmol), KHMDS (potassium hexamethyldisilazide, 0.25 mmol) as a base, and CPME (cyclopentyl methyl ether, 0.5 mL) as a solvent at 120 °C over 7 h led to the clean formation of the *ipso*-substitution product (4-biphenyl)dicyclohexylphosphine oxide (**3a**) in 99% isolated yield (Table 2.1, entry 1) (see Experimental Section for optimization of the reaction conditions and for the procedure of 2.5 mmol-scale reaction). No *meta*-phosphinylation product **3b** was detected in the crude mixture, excluding the possibility that the reaction proceeds through the aryne intermediate.[11] The reaction occurred efficiently even with equimolar amounts of **2a** and KHMDS relative to **1a**, giving **3a** in 88% yield with an extended reaction time (24 h, entry 2).

Fluoride is essential as a leaving group. The corresponding chlorobiphenyl gave a mixture of **3a** and **3b** (2.2:1 ratio; Table 2.1, entry 3), indicating the formation of aryne intermediates. The reaction of the bromide and iodide gave the dehaloprotonation product (biphenyl) as the major product without forming **3a** or **3b** in a meaningful amount.

Table 2.1. Dehalophosphinylation of 4-halobiphenyls[a]

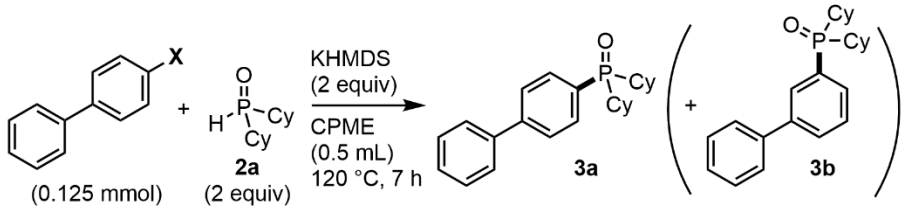

Entry	**X**	Yield of **3a**[b]
1	F (**1a**)	99%
2[c]	F (**1a**)	88%
3	Cl	44% (**3a**/**3b**, 2.2:1)
4[d,e]	Br	0%
5[d]	I	0%

[a] Conditions: Aryl halides (0.125 mmol), **2a** (0.25 mmol), KHMDS (0.25 mmol), CPME (0.5 mL), 120 °C, 7 h. [b] Isolated yield. [c] **2a** (0.125 mmol), KHMDS (0.125 mmol), 24 h. [d] ArX was fully consumed, and biphenyl (~65%) was formed. [e] A trace amount of **3a** was detected by ^{31}P NMR analysis in the crude mixture.

KHMDS appeared to be the most effective base for the reaction between **1a** and **2a**. NaHMDS decreased the yield (50%), while no reaction occurred with LiHMDS (0%), indicating the importance of the potassium cation. While KO*t*Bu was less effective (82%), the yield could be improved with an extended reaction time (24 h, 96%). KH was as effective as KOtBu (84%). Weaker potassium bases such as KOMe, K_3PO_4 and K_2CO_3 exhibited much less or no reactivity. An organic base 1,8-diazabicyclo[5.4.0]undec-7-ene (DBU) did not induce the reaction (see Experimental Section for optimization).

Having the optimal reaction conditions in hand, the scope of aryl fluorides was investigated with **2a** (Scheme 2.3). 3- and 2-Fluorobiphenyls were efficiently converted to the corresponding aryl phosphine oxides **3b** and **3c**, respectively. Electron-donating (OMe and NMe_2) and electron-withdrawing (CF_3) substituents were tolerated (**3d**–**3f**). While relatively bulky 1-naphthyl fluoride was a suitable substrate (**3g**), 4'-fluoro-2,4,6-triisopropyl-1,1'-biphenyl having bulky *i*Pr substituents at the distal benzene ring was much less reactive (**3h**, 12%).[12] Pyridine-based aryl fluorides such as 2-(4-fluorophenyl)pyridine and 3-fluoropyridine participated in the reaction (**3i** and **3j**). Fluoroferrocene was less reactive but gave **3k** in 42% yield with an extended reaction time (24 h).

Simple monocyclic aryl fluorides showed a significant decrease in reactivity. Most typically, electron-neutral and electron-rich aryl fluorides such as fluorobenzene and 4-

fluoro-*N*,*N*-dimethylaniline were not reactive (**3l** and **3m**). An electron-deficient aryl fluoride, 1-fluoro-4-(trifluoromethyl)benzene, was a suitable substrate, giving **3n** in 65% yield. Interestingly, there was an apparent tendency for π-extended aryl fluorides to show relatively high reactivities. Thus, when the *N*,*N*-dimethylamino group of 4-fluoro-*N*,*N*-dimethylaniline was changed to the *N*,*N*-diphenylamino or *N*-carbazolyl group, the reaction proceeded smoothly to give the corresponding defluorophosphinylation products **3o** or **3p**, respectively. Furthermore, the reaction between 9-(4-fluorophenyl)-*9H*-carbazole and diphenylphosphine oxide (**2d**) with KO*t*Bu as a base allowed straightforward synthesis of the blue OLED compound **3q**, which was previously accessed through multi-step synthesis.[13, 14]

1,2-Difluorobenzene underwent double defluorophosphinylation with **2a** and KHMDS (4 equiv) at 120 °C over 20 h, giving *o*-phenylene-bridged bisphosphine dioxide **4a** in 71% yield (Scheme 2.3). The molecular structure of **4a** was confirmed by X-ray crystallographic analysis (CCDC 2008761, see Experimental Section for details).

Next, the scope of secondary phosphine oxides was examined in the defluorophosphinylation of 4- and 2-fluorobiphenyls (Scheme 2.3). Dibutylphosphine oxide (**2b**) participated in the reactions to give **3r** and **3u** in 85% and 96% yields, respectively. Sterically demanding di-*tert*-butylphosphine oxide (**2c**) served as a suitable phosphinylation agent (**3s** and **3v**). Diphenylphosphine oxide (**2d**) was successfully utilized for this protocol with KO*t*Bu as a base (**3t** and **3w**). With **2d**, KO*t*Bu was more effective base than KHMDS in the reaction of **1a** (27% vs 4%, 7 h) or **1c** (56% vs 40%, 7 h).

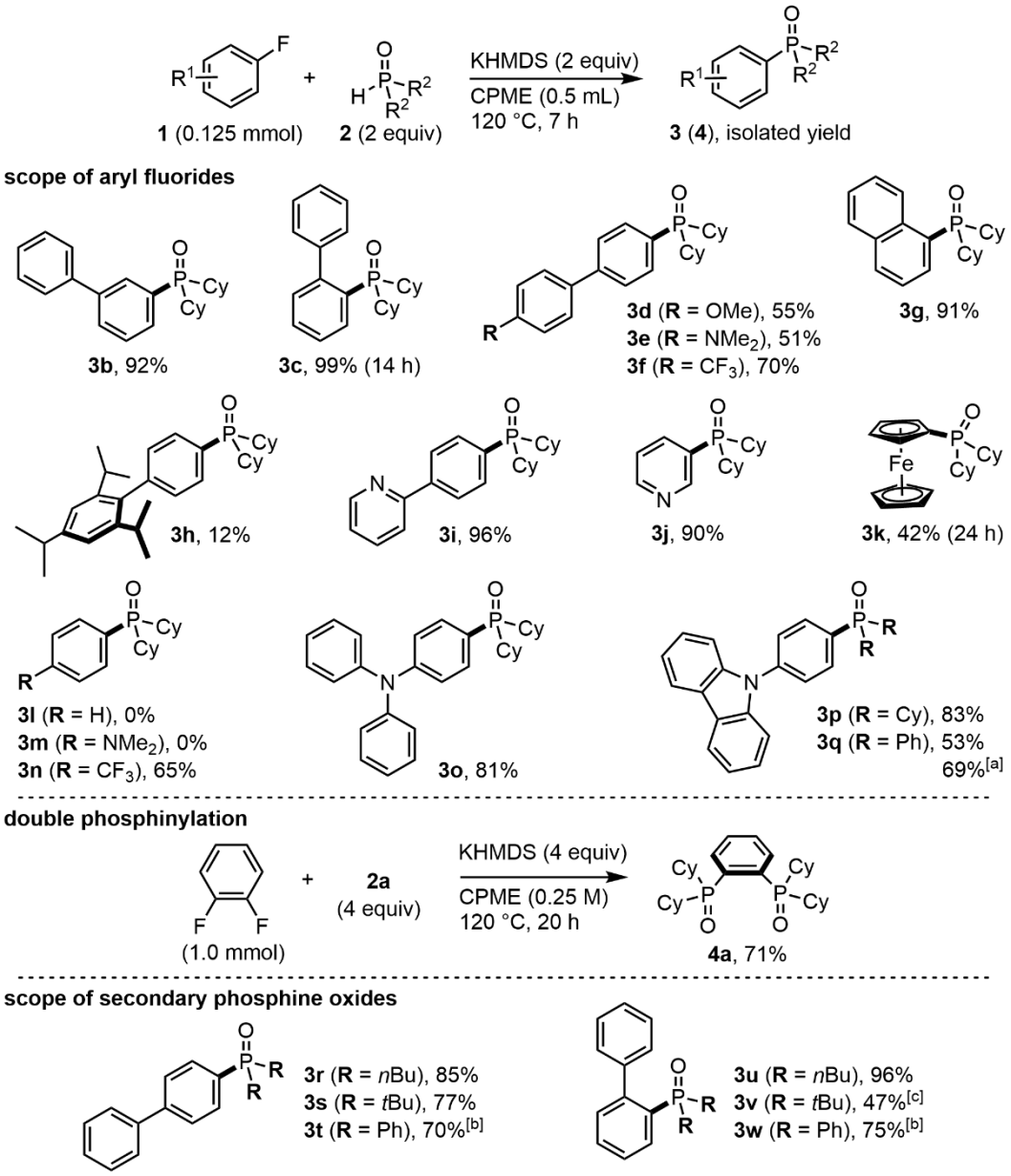

Scheme 2.3. Scope of aryl fluorides and secondary phosphine oxides. Reaction conditions: **1** (0.125 mmol), **2** (0.25 mmol), KHMDS (0.25 mmol), CPME (0.5 mL), 120 °C, 7 h. Isolated yields are shown. [a] KO*t*Bu as a base (0.25 mmol), 14 h. [b] KO*t*Bu as a base (0.25 mmol), 24 h. [c] **1c** (0.125 mmol), **2c** (0.125 mmol), KHMDS (0.125 mmol), CPME (0.5 mL), 120 °C, 48 h.

The present protocol is applicable to the synthesis of *P*-chirogenic tertiary phosphine oxides. The reaction between 1-naphthyl fluoride and enantioenriched secondary phosphine oxide (*S*)-**2e** with *t*Bu and Ph substituents at the P atom proceeded smoothly to afford (*S*)-**3x** without erosion of the enantiomeric purity (Scheme 2.4a). Its molecular

structure and absolute configuration were confirmed by single-crystal X-ray diffraction analysis (CCDC 2008762, see Experimental Section for details). Therefore, it is concluded that the defluorophosphinylation proceeded in a stereoretentive manner. The reaction between 1,2-difluorobenzene and (*S*)-**2e** proceeded in THF at 50 °C, affording *P*-chirogenic bisphosphine dioxide (*S*,*S*)-**4b** in 97% yield (Scheme 2.4b, absolute configuration were confirmed by single-crystal X-ray diffraction analysis, CCDC 2008763, see Experimental Section for details). Furthermore, unsymmetrical bisphosphine dioxide (*S*)-**4d** was synthesized from 1,2-difluorobenzene by stepwise twofold defluorophosphinylation with **2c** and (*S*)-**2e** (Scheme 2.4c). In the initial step using **2c**, selective mono defluorophosphinylation occurred to give **3y** as the sole product (**4c** was not formed). While (*S*,*S*)-**4b** and (*S*)-**4d** could be regarded as potential precursors of *o*-phenylene-bridged chiral bisphosphines, which are expected to be useful chiral ligands in asymmetric catalysis,[15, 16] attempts at stereospecific reduction have been unsuccessful so far. The P=O reduction of (*S*,*S*)-**4b** proceeded with Ti(O*i*Pr)$_4$ and (EtO)$_2$MeSiH in C_6D_6/toluene (1:1) in 120 °C for 0.5 h. However, after treatment with S_8, a 1:1 mixture of the racemic and meso phosphine sulfides was obtained (see Experimental Section for details).

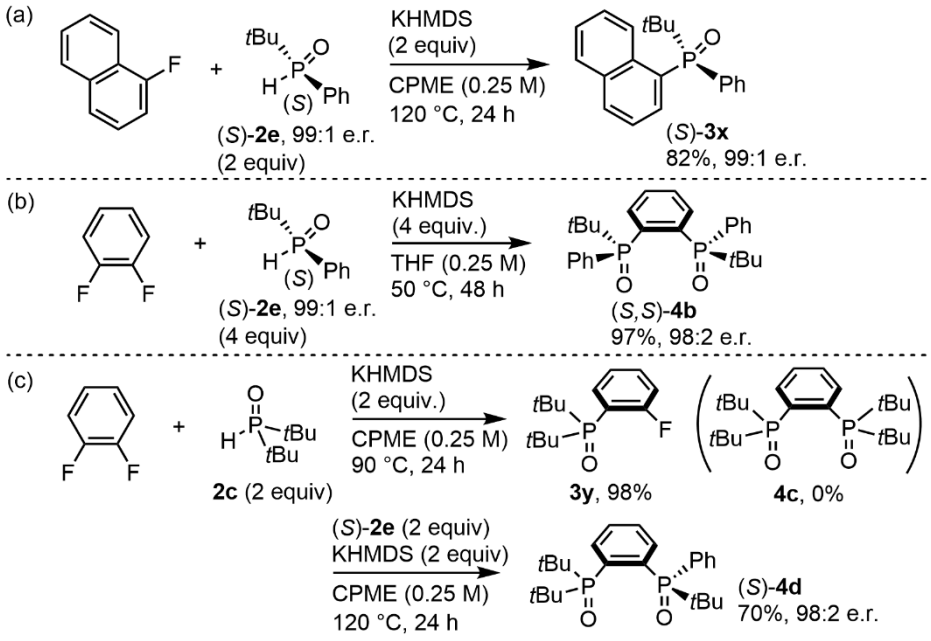

Scheme 2.4. Synthesis of *P*-chiral tertiary phosphine oxides.

To gain insight into the mechanism, the reaction between **1a** and **2a** with KHMDS as a base in CPME/C_6D_6 was monitored by ^{31}P NMR spectroscopy (Scheme 2.5). The

treatment of **2a** (45 ppm) with KHMDS at 120 °C caused the formation of white precipitates (see Experimental Section for details). The ^{31}P NMR analysis of the suspension was indicative of the formation of potassium phosphinite K[**2a**–H] (114 ppm).[17] Subsequent addition of **1a** (120 °C, 17 h) caused gradual conversion of K[**2a**–H] to the phosphinylation product **3a** (42 ppm), leading to 70% yield of **3a**. Thus, deprotonation of **2a** by KHMDS to produce K[**2a**–H] is the initial step of the defluorophosphinylation and the potassium phosphinite K[**2a**–H] is the nucleophile that attacks the aryl fluoride (**1a**).[18]

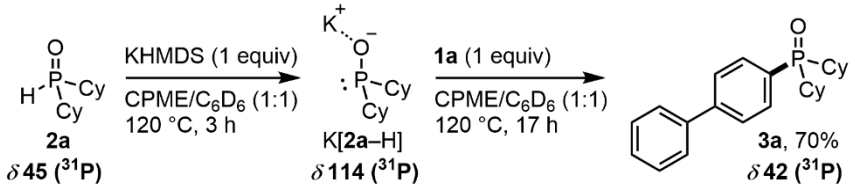

Scheme 2.5. Stepwise phosphinylation monitored by ^{31}P NMR.

The significance of fluoride as the leaving group is strongly supportive of an S_NAr reaction pathway. Based on this assumption, DFT calculations were performed for the reaction of **1a** and K[**2a**–H] solvated by three dimethyl ether molecules [CPCM(THF)-M06-2X/def2TZVPD//CPCM(THF)-M06-2X/def2SVP].[19-22] The calculation including dispersion corrections and diffuse functions provided two reasonable reaction pathways, one concerted (CS_NAr) and the other stepwise as shown in Figure 2.1.

The concerted S_NAr pathway (path a) is initiated by a coordination of the fluorine atom of **1a** to K^+ of K[**2a**–H] to form **Int1**. The concerted *ipso*-substitution of the fluoride anion with the phosphinite anion through a five-centered transition state (**TS1**, $\Delta G^‡$ = 16.8 kcal·mol^{-1}) affords **Pro1** with simultaneous formation of the $KF(OMe_2)_3$ fragment coordinated with the oxygen atom of the phosphine oxide. The stepwise S_NAr pathway (path b) starts from a π-complex (**Int2**) with η^6-coordination of the aromatic ring of **1a** to K^+. The approach of the P atom to the *ipso* carbon (C1) proceeds through **TS2** ($\Delta G^‡$ = 15.8 kcal·mol^{-1}) with the potassium cation remaining bound to the dearomatizing ring at C4, stabilizing the developing negative charge, and leading to a Meisenheimer-type short-lived intermediate (**Int3**). The reaction temperature (120 °C) of the optimal conditions is much higher than that expected from the calculated energy barriers for **TS1** and **TS2**. This should be due to the existence of K[**2a**–H] in a less reactive aggregated form. In fact, the reaction proceeds even at r.t., while it is too slow to reach to completion with a reasonable reaction time (8%, 72 h, see Experimental Section for details). It should be noted that a partial negative charge at the leaving fluoride atom seems to be substantially stabilized

by one or more C–H···F interactions donated by the *P*-cyclohexyl groups as observed in both **TS2** and **Int3** (see Experimental Section for details). The subsequent rearomatizing C–F bond cleavage proceeds through **TS3** to produce structurally interesting fluorine-bound five-coordinate phosphorus species **Pro2**, which would undergo facile elimination of KF via an aggregative salt metathesis to afford the tertiary phosphine oxide **3a**. Based on these computational results, the unusual tolerance of this S_NAr reaction toward electron-neutral or electron-rich aryl fluorides can be attributed to the electron-withdrawing nature of the phosphinyl group and the well-defined geometrical arrangement of the potassium cation so as to stabilize the negative charges in the fluoride leaving group (in path a) and the benzene ring (in path b). In the case of the stepwise pathway (path b), additional stabilization of the negative charge at the leaving fluoride atom may be caused not only by the F···P interaction leading to the formation of the pentacoordinate P center but also by the C–H···F interactions donated by the C–H bonds in the *P*-cyclohexyl groups.

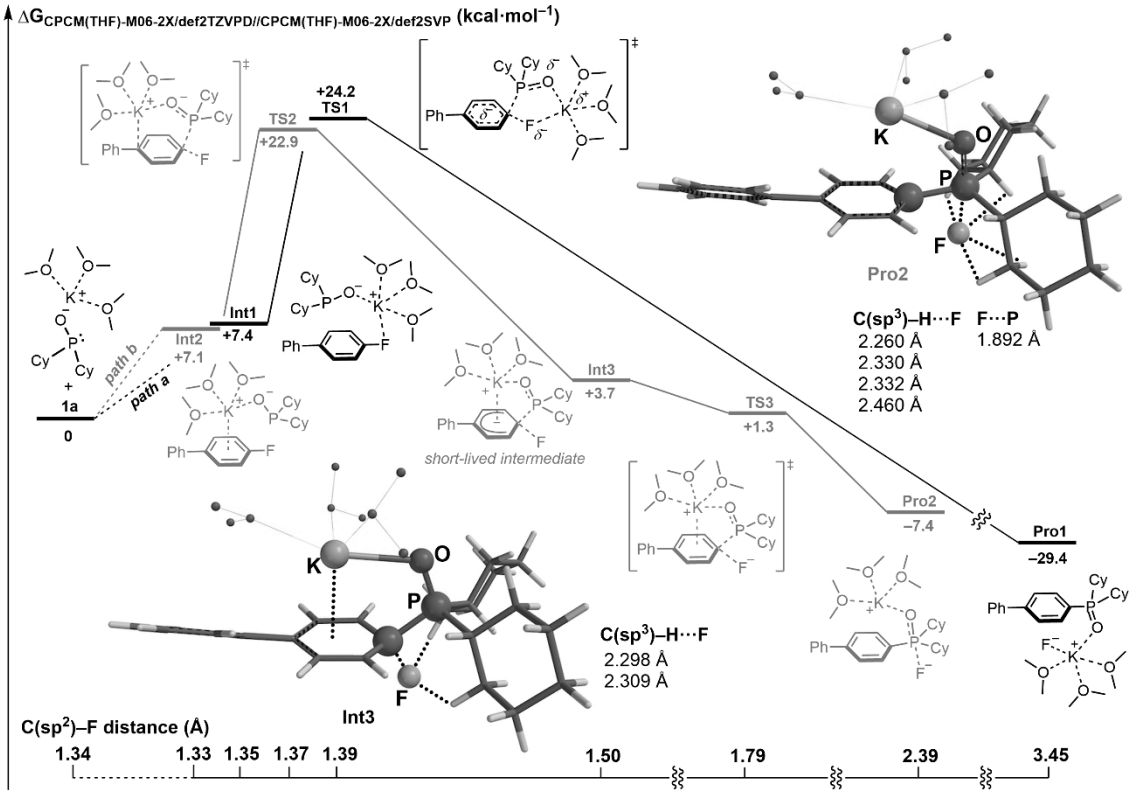

Figure 2.1. Energy profiles for the reaction of **1a** and K[**2a**–H] [CPCM(THF)-M06-2X/def2TZVPD//CPCM(THF)-M06-2X/def2SVP]. Solid or dashed lines in the profiles indicate that the connectivity between the two states was confirmed or not by the IRC (intrinsic reaction coordinate) analysis, respectively.

2.3 Conclusions

In summary, the author has developed a new S_NAr reaction. Non-activated aryl fluorides reacted with potassium diorganophosphinites that were prepared *in situ* from secondary phosphine oxide and potassium bases such as KHMDS and KO*t*Bu. A variety of aryl fluorides, including strongly electron-rich *p*-fluoroaniline derivatives, participated in the reaction with the substantially stabilized anionic *P*-nucleophiles, thus forming the corresponding tertiary phosphine oxides. The present protocol allows stereospecific synthesis of *P*-chiral tertiary phosphine oxides from enantioenriched secondary phosphine oxides. Quantum chemical calculations showed a nucleophile-dependent mechanism, which involves both stepwise and concerted S_NAr reaction pathways.

2.4 Experimental Section

2.4.1 Instrumentation and Chemicals

Nuclear magnetic resonance (NMR) spectra were recorded on a JEOL JNM-ECXII spectrometer, operating at 400, 100.5 and 161.8 MHz for ^{1}H, ^{13}C and ^{31}P NMR, respectively. Chemical shift values for ^{1}H, ^{13}C and ^{31}P NMR are referenced to Me_4Si (0 ppm), $CDCl_3$ (77.0 ppm) and H_3PO_4 (0 ppm), respectively. Chemical shifts are reported in δ ppm. High-resolution mass spectra were recorded at the GC-MS & NMR Laboratory, Research Faculty of Agriculture, Hokkaido University (JEOL JMS-T100GCv for FD-MS). HPLC analyses were conducted on a HITACHI ELITE Lunchroom system with a HITACHI L-2455 diode array detector. Optical rotations were measured on a JASCO P-2200. IR spectra were measured with a PerkinElmer Frontier instrument. TLC analyses and PTLC separation were performed on commercial glass plates bearing 0.25-mm layer of Merck Silica gel $60F_{254}$. Silica gel (Kanto Chemical Co., Silica gel 60 N, spherical, neutral) was used for column chromatography. Automatic flash chromatography was performed with Biotage® Isolera™ Prime.

All reactions were carried out under nitrogen or argon atmosphere. The defluorophosphinylation reactions were conducted with ChemiStation™ Personal Organic Synthesizer PPM-5512 (EYELA). Materials were obtained from commercial suppliers or prepared according to standard procedures unless otherwise noted. Cyclopentyl methyl ether (CPME, dehydrated) was purchased from Fujifilm Wako Pure Chemicals Co., Ltd. and purified by passage through activated alumina under positive argon pressure followed by freeze-pump-thaw degassing. Tetrahydrofuran (THF,

dehydrated stabilizer free) was purchased from Kanto Chemical Co., Inc. and dried and deoxidized by passage through packed columns of neutral alumina and copper(II) oxide under positive argon pressure (Grubbs solvent system). Potassium hexamethyldisilazide (KHMDS, 95%) and potassium *tert*-butoxide (KO*t*Bu, >97%) were purchased from Sigma-Aldrich Co. and Tokyo Chemical Industry Co., Ltd., respectively, and used as received. All bases and solvents were stored inside a nitrogen-filled glove box.

2.4.2 Preparation of Substrates

1a was purchased from Sigma-Aldrich Co. and used as received. **1c**, **1g**, **1j**, **1l**–**1n**, **1q** were purchased from Tokyo Chemical Industry Co., Ltd. and used as received. **1b, 1d**–**1f**, **1h**–**1i** were prepared by Pd-catalyzed cross-coupling reaction between 3- or 4-fluorophenylboronic acid and corresponding iodo- or bromobenzene. **1o**–**1p** were prepared by Pd-catalyzed amination of 4-bromofluorobenzne. **1k** was prepared following the reported procedure.[23]

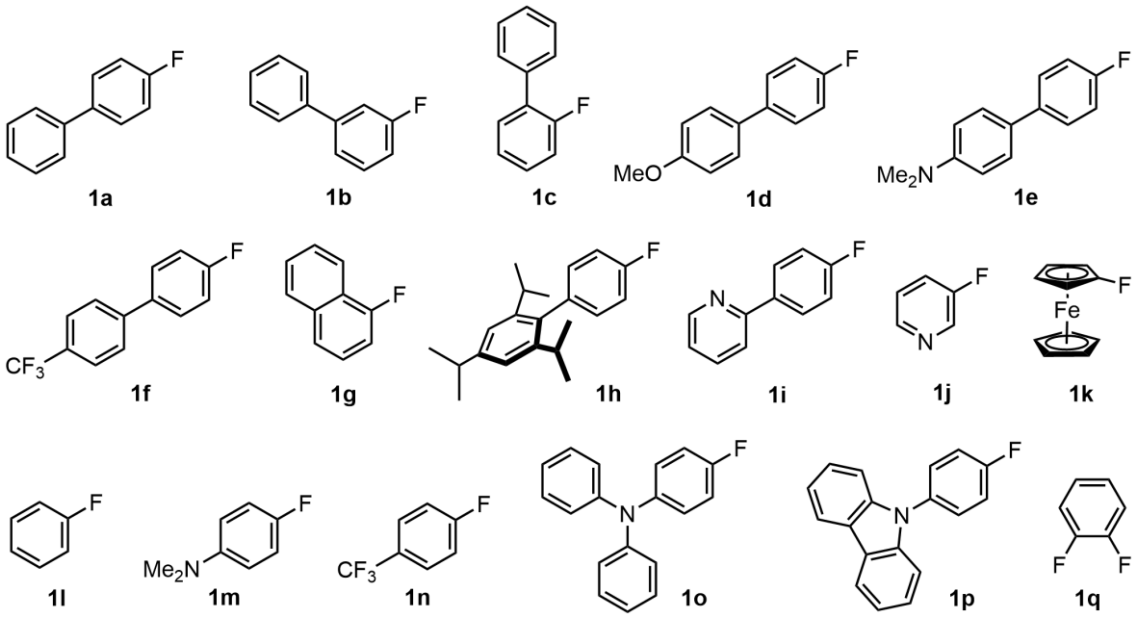

Figure 2.2. Aryl fluorides used in this work.

Secondary phosphine oxide **2a**,[24] **2c**[25] were synthesized through the reaction between PCl_3 and the corresponding Grignard reagent followed by hydrolysis. **2b** was prepared through the reaction between $H(O)P(OEt)_2$ and *n*-BuMgCl by following the reported procedure with slightly modifications.[26] **2d** was purchased from Tokyo

Chemical Industry Co., Ltd. and used as received. (±)-**2e**[27] was prepared through the reaction between $PPhCl_2$ and *t*-BuMgCl followed by hydrolysis. Enantioenriched *P*-chirogenic secondary phosphine oxide (*S*)-**2e** (99:1 e.r.) was obtained through chiral resolution of (±)-**2e** according to the reported procedure.[28]

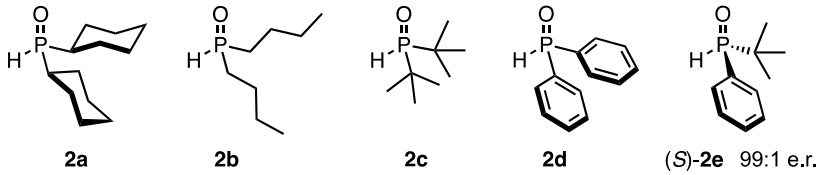

Figure 2.3. Secondary phosphine oxide used in this work.

2.4.3 Experimental Procedures

General Procedure for Defluorophosphinylation of Aryl Fluorides

In a N_2-filled glove box, **1a** (21.5 mg, 0.125 mmol, 1 equiv.), **2a** (53.6 mg, 0.25 mmol, 2 equiv.) and CPME (0.3 mL) were placed in a 10 mL glass tube containing a magnetic stirring bar. The mixture was stirred for approx. 5 min. Next, KHMDS (49.9 mg, 0.25 mmol, 2 equiv.) and CPME (0.2 mL) were added to the tube without further stirring. The glass tube was sealed with a screw cap and was removed from the glove box. The mixture was stirred at 120 °C for 7 h. After cooling to room temperature, the reaction mixture was passed through a short plug of Celite and washed with CH_2Cl_2. Volatiles were removed by evaporation under reduced pressure. Full conversion of **1a** was confirmed by ^{19}F NMR analysis using benzotrifluoride as an internal standard. The crude product was purified by flash chromatography on silica gel with slow gradient elution (CH_2Cl_2/MeOH, 100:0-to-97:3) followed by preparative thin layer chromatography (CH_2Cl_2/MeOH, 93:7) to give **3a** as a white solid (45.5 mg, 99% yield).

Preparation of 3a (2.5 mmol scale without a glove box)

A flame-dried 100 mL two-necked round-bottom flask equipped with a condenser and a magnetic stir bar was vacuumed and filled with Ar. **1a** (430 mg, 2.5 mmol, 1 equiv.), **2a** (1072 mg, 5.0 mmol, 2 equiv.) and dry CPME (5 mL) were placed in the flask, and the mixture was stirred at room temperature for approx. 5 min. Next, KHMDS (998 mg, 5.0 mmol, 2.0 equiv., weighted quickly under air) and dry CPME (5 mL) were added to the flask. The flask was connected to an Ar-filling balloon and heated at 120 °C for 24 h. After cooling to room temperature, deionized water (10 mL) was added to the reaction

mixture. The organic layer was extracted with CH_2Cl_2, dried over $MgSO_4$ and filtered. Volatiles were removed by evaporation under reduced pressure. The crude product was purified by flash chromatography on silica gel with slow gradient elution (CH_2Cl_2/MeOH, 100:0-to-95:5) to give **3a** as a white solid (861 mg, 94% yield).

Figure 2.4. Photographic images of the reaction setup and the isolated product.

Preparation of 4a (1.0 mmol scale)

In a N_2-filled glove box, **1q** (98.4 µl, 1.0 mmol, 1 equiv.), **2a** (857.6 mg, 4.0 mmol, 4 equiv.) and CPME (3 mL) were placed in a 50 mL glass tube containing a magnetic stirring bar. The mixture was stirred for approx. 5 min. Next, KHMDS (798.4 mg, 4.0 mmol, 4 equiv.) and CPME (1 mL) were added to the tube without further stirring. The glass tube was sealed with a screw cap and was removed from the glove box. The mixture was stirred at 120 °C for 20 h. After cooling to room temperature, the reaction mixture was passed through a short plug of Celite and washed by CH_2Cl_2. Volatiles were removed by evaporation under reduced pressure. The residue was purified by flash chromatography on silica gel with slow gradient elution (CH_2Cl_2/MeOH 100:0-to-96:4) followed by recrystallization from hot EtOAc/hexane to give **4a** as white crystals (359.0 mg, 71% yield).

Preparation of (*S*,*S*)-4b

In a N_2-filled glove box, **1q** (12.3 µl, 0.125 mmol, 1 equiv.), (*S*)-**2e** (99:1 e.r., 91.1 mg,

0.50 mmol, 4 equiv.) and THF (0.3 mL) were placed in a 10-mL glass tube containing a magnetic stirring bar. The mixture was stirred for approx. 5 min. Next, KHMDS (99.8 mg, 0.50 mmol, 4 equiv.) and THF (0.2 mL) were added to the tube without further stirring. The glass tube was sealed with a screw cap and was removed from the glove box. The mixture was stirred at 50 °C for 48 h. After cooling to room temperature, the reaction mixture was passed through a short plug of Celite and washed with CH_2Cl_2. Volatiles were removed by evaporation under reduced pressure. The residue was purified by flash chromatography on silica gel with slow gradient elution (CH_2Cl_2/MeOH, 100:0-to-93:7) to give (*S*,*S*)-**4b** as a white solid (53.2 mg, 97% yield, 98:2 e.r.). The enantiomeric ratio was determined by chiral HPLC. In the crude ^{1}H NMR spectrum, a small amount of minor product (~67:1) was detected. Although this product has not been fully characterized, this ratio likely corresponds to the diastereomeric ratio of the product.

Preparation of (*S*)-4d

In a N_2-filled glove box, **1q** (98.4 µl, 1.0 mmol, 1 equiv.), **2c** (324.8 mg, 2.0 mmol, 2 equiv.) and CPME (2 mL) were placed in a 50 mL glass tube containing a magnetic stirring bar. The mixture was stirred for approx. 5 min. Next, KHMDS (399.2 mg, 2.0 mmol, 2 equiv.) and CPME (2 mL) were added to the tube without further stirring. The glass tube was sealed with a screw cap and was removed from the glove box. The mixture was stirred at 90 °C for 24 h. After cooling to room temperature, the reaction mixture was passed through a short plug of Celite and washed by CH_2Cl_2. Volatiles were removed by evaporation under reduced pressure. The residue was purified by flash chromatography on silica gel with gradient elution (CH_2Cl_2/MeOH 100:0-to-95:5) to give **3y** as light-yellowish oil (249.9 mg, 98% yield).

Next, in a N_2-filled glove box, (*S*)-**2e** (99:1 e.r., 45.6 mg, 0.25 mmol, 2 equiv.), **3y** (32.0 mg, 0.125 mmol, 1 equiv.) in CPME (0.3 mL) were placed in a 10-mL glass tube containing a magnetic stirring bar. The mixture was stirred for approx. 5 min. Next, KHMDS (49.9 mg, 0.25 mmol, 2.0 equiv.) and CPME (0.2 mL) were added to the tube without further stirring. The glass tube was sealed with a screw cap and was removed from the glove box. The mixture was stirred at 120 °C for 24 h. After cooling to room temperature, the reaction mixture was passed through a short plug of Celite and washed with CH_2Cl_2. Volatiles were removed by evaporation under reduced pressure. The residue was purified by automatic flash chromatography on RediSep® flashcolumn 12 g silica-gel with slow gradient elution ($CHCl_3$/MeOH, 100:0-to-90:10) followed by preparative thin layer chromatography (CH_2Cl_2/MeOH, 92:8) to give to give (*S*)-**4d** as a white foam (36.6 mg, 70% yield, 98:2 e.r.). The enantiomeric ratio was determined by chiral HPLC.

2.4.4 Reaction Optimization

Table 2.2. Base effects on the reaction of **1a** and **2a**

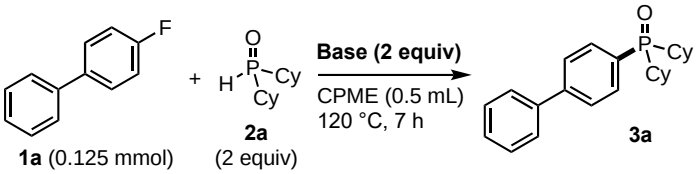

1a (0.125 mmol) **2a** (2 equiv) **3a**

Entry	Base	Isolated yield of **3a** [%]
1	**KHMDS**	**99** (88)[a,b]
2	NaHMDS	50
3	LiHMDS	0
4	KO*t*Bu	82 (96)[b]
5	NaO*t*Bu	65
6	LiO*t*Bu	12
7	KH	84
8	KOMe	37
9	K_3PO_4	0
10	K_2CO_3	0
11	DBU	0

[a] 1 equiv. of **2a** and base. [b] 24 h.

Table 2.3. Solvent effects on the reaction of **1a** and **2a**

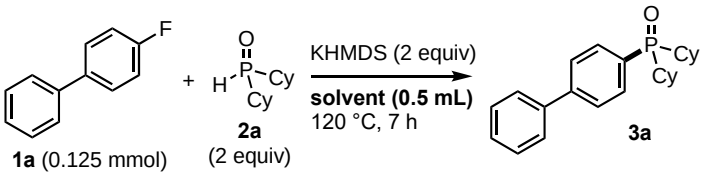

1a (0.125 mmol) **2a** (2 equiv) **3a**

Entry	Solvent	Isolated yield of **3a** [%]
1	**CPME**	**99**
2	toluene	75
3	*N,N*-dimethylacetamide	51

Table 2.4. Temperature effects on the reaction of **1a** and **2a**

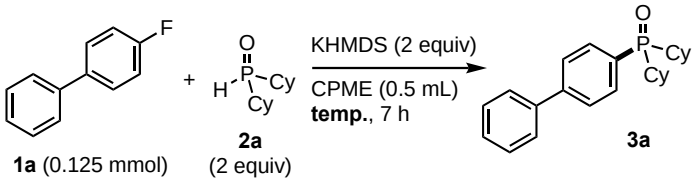

1a (0.125 mmol) **2a** (2 equiv) **3a**

Entry	Temperature	Isolated yield of **3a** [%]
1	**120**	**99**
2	100	74
3	80	29

2.4.5 Reduction of Bisphosphine Dioxide

The P=O reduction of (*S*,*S*)-**4b** proceeded by treatment with $Ti(OiPr)_4$ and $(EtO)_2MeSiH$, giving **5** (Figure 2.5). The subsequent reation with excess sulfer gave the corresponding bisphosphine disulfide **6** (*rac*/*meso* ~1:1). The ^1H NMR spectra of the crude products in the reduction and sulfidation are shown in Figure 2.6 and 2.7, respectively. The structure of *rac*-**6** was confirmed by comparison with an authentic sample.

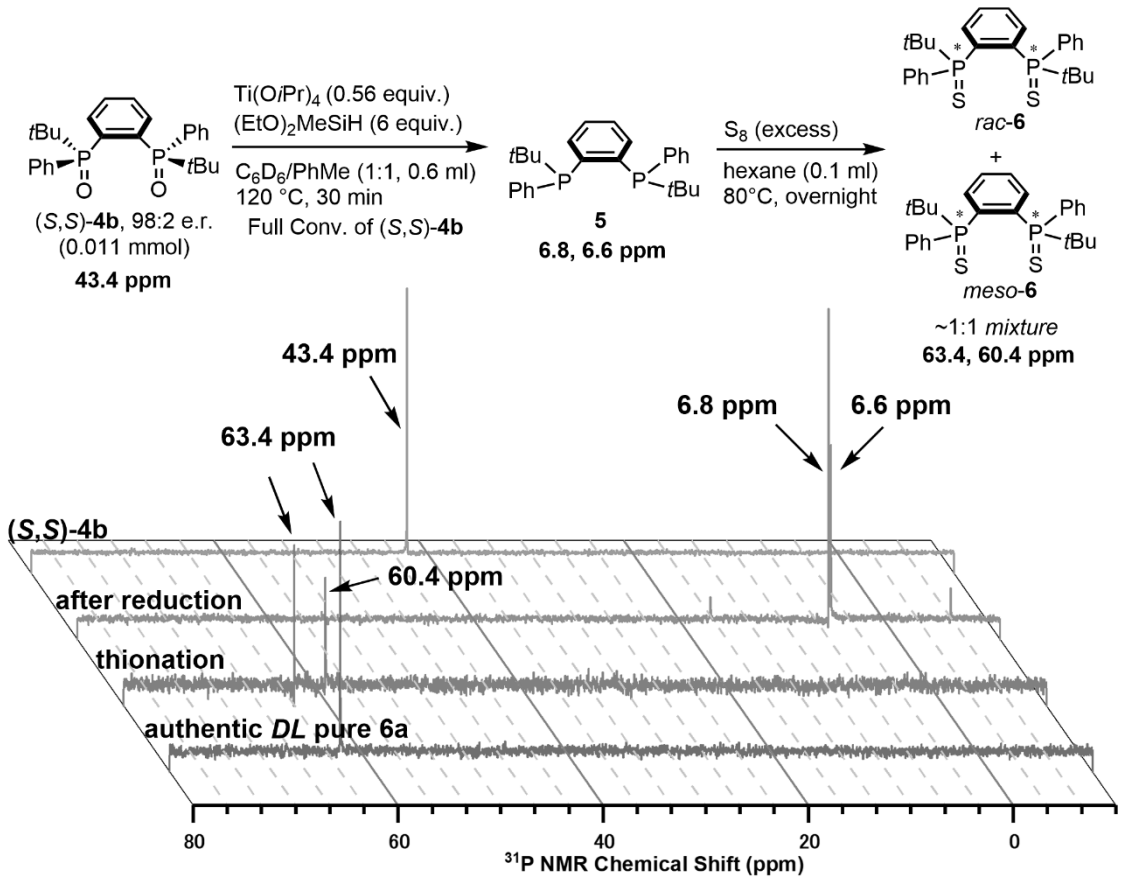

Figure 2.5. Rceduction of (*S*,*S*)-**4b** followed by sulfidation

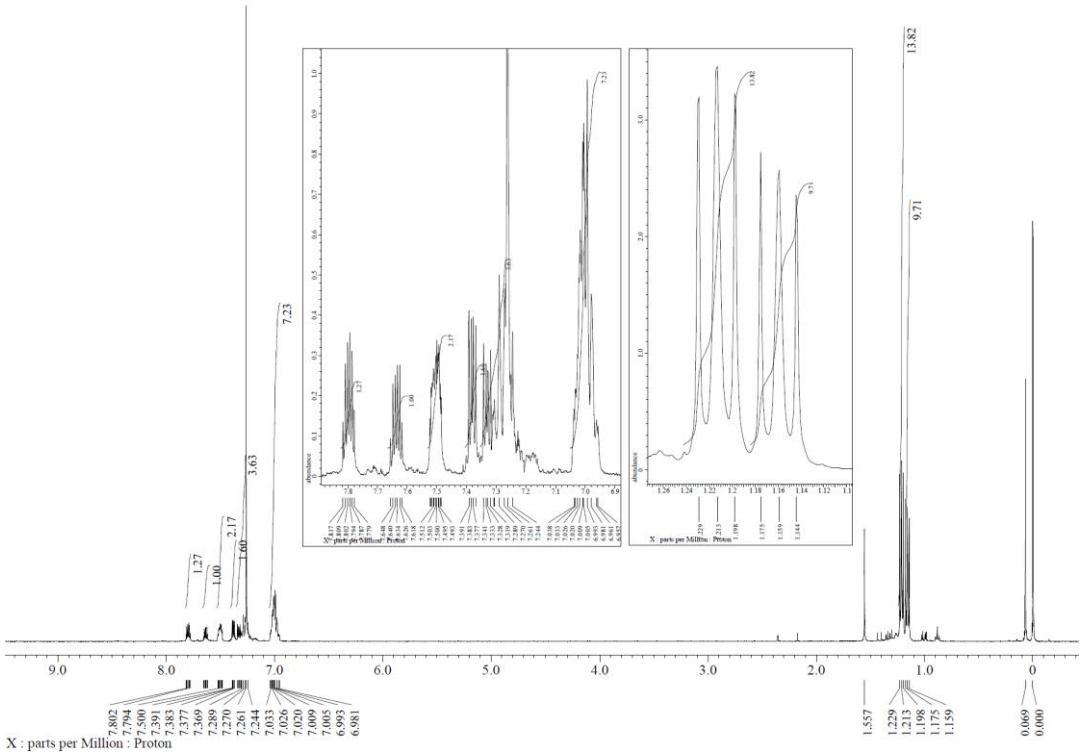

Figure 2.6. ^{1}H NMR spectrum of the crude product **5** after P=O reduction (400 MHz).

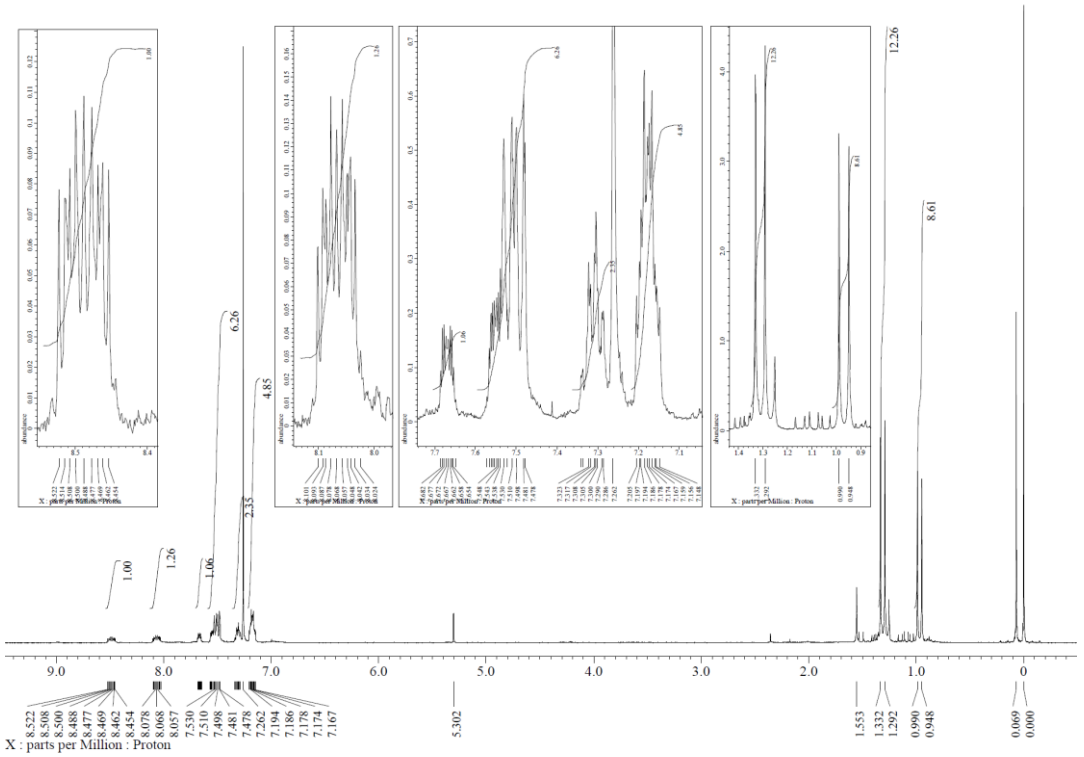

Figure 2.7. ^{1}H NMR spectrum of the crude product **6** after sulfidation (400 MHz).

Preparation of *rac*-6

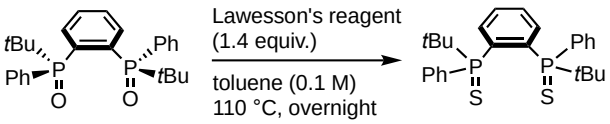

(*S*,*S*)-**4b**, >99:1 e.r.
(0.084 mmol)

rac-**6**
53% yield

In a N_2-filled glove box, (*S*,*S*)-**4b** (36.8 mg, 0.084 mmol, 1 equiv.), Lawesson's reagent (47.5 mg, 0.117 mmol, 1.4 equiv.) and toluene (0.84 mL) were placed in a 10-mL glass tube containing a magnetic stirring bar. Next, the glass tube was sealed with a screw cap and was removed from the glove box. The mixture was stirred at 110 °C for overnight. After cooling to room temperature, the reaction was quenched by treatment with aqueous saturated Na_2CO_3. The organic layer was passed through a short plug of $MgSO_4$/Celite/$MgSO_4$ and washed with EtOAc. Volatiles were removed by evaporation under reduced pressure. The residue was purified by chromatography on silica gel with gradient elution (Hexane/EtOAc 100:0-to-85:15) to give *rac*-**6** as a white powder (21.1 mg, 53%).

M.p.: 216.7–220.4 °C. **^{1}H NMR** (400 MHz, $CDCl_3$): δ 8.54–8.43 (m, 2H), 7.71–7.63 (m, 2H), 7.51 (dd, J = 12.4, 7.2 Hz, 4H), 7.32 (t, J = 6.6 Hz, 2H), 7.18 (td, J = 7.2, 3.2 Hz, 4H), 0.97 (d, J = 16.0 Hz, 18H). **^{13}C NMR** (100.5 MHz, $CDCl_3$): δ 136.5 (dd, J_{C-P} = 70.9, 5.7 Hz, 2C), 135.5 (dd, J_{C-P} = 9.5, 9.5 Hz, 2C), 132.6–132.2 (m, 4C), 130.4 (2C), 129.7–129.3 (m, 2C), 128.1–127.7 (m, 4C), 127.8 (d, J_{C-P} = 75.7 Hz, 2C), 40.3 (d, J_{C-P} = 51.8 Hz, 2C), 26.8 (6C). **^{31}P NMR** (161.8 MHz, $CDCl_3$): δ 63.4. **IR** (ATR): 1478, 1436, 1392, 1361, 1314, 1175, 1098, 1019, 803, 748, 732, 713, 668 cm^{-1}. **HRMS-FD** (*m/z*): $[M]^+$ Cacld for $C_{26}H_{32}P_2S_2$, 470.1421; found, 470.1436.

An equimolar mixture (1:1) of the two enantiomers was confirmed by chiral HPLC analysis [2 × CHIRALCEL® OD-H column, 4.6 mmφ × 250 mmL, Daicel Chemical Industries], hexane/*i*PrOH = 99:1, 1.0 mL/min, 40 °C, 250 nm UV detector, retention time = 22.77 min, 25.01 min.

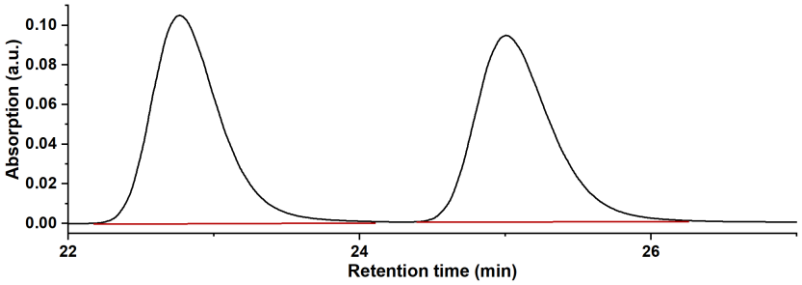

Retention time (min)	Area	Area%
22.77	1725437	50.18
25.01	1712868	49.82

2.4.6 NMR Studies

The reaction of **1a** and **2a** with KHMDS in CPME/C_6D_6 was monitoired by ^{31}P NMR spectroscopy (Figure 2.8). The treatment of **2a** (45 ppm) with KHMDS at 120 °C caused the formation of white precipitates. The ^{31}P NMR analysis of the suspension was clearly indicative of the formation of potassium phosphinite K[**2a**–H] (114 ppm).[17] Subsequent addition of **1a** (120 °C, 17 h) gave the phosphinylation product **3a** in 70% isolated yield (42 ppm). Thus, deprotonation of **2a** by KHMDS to produce K[**2a**–H] is an initial step in the defluorophosphinylation.

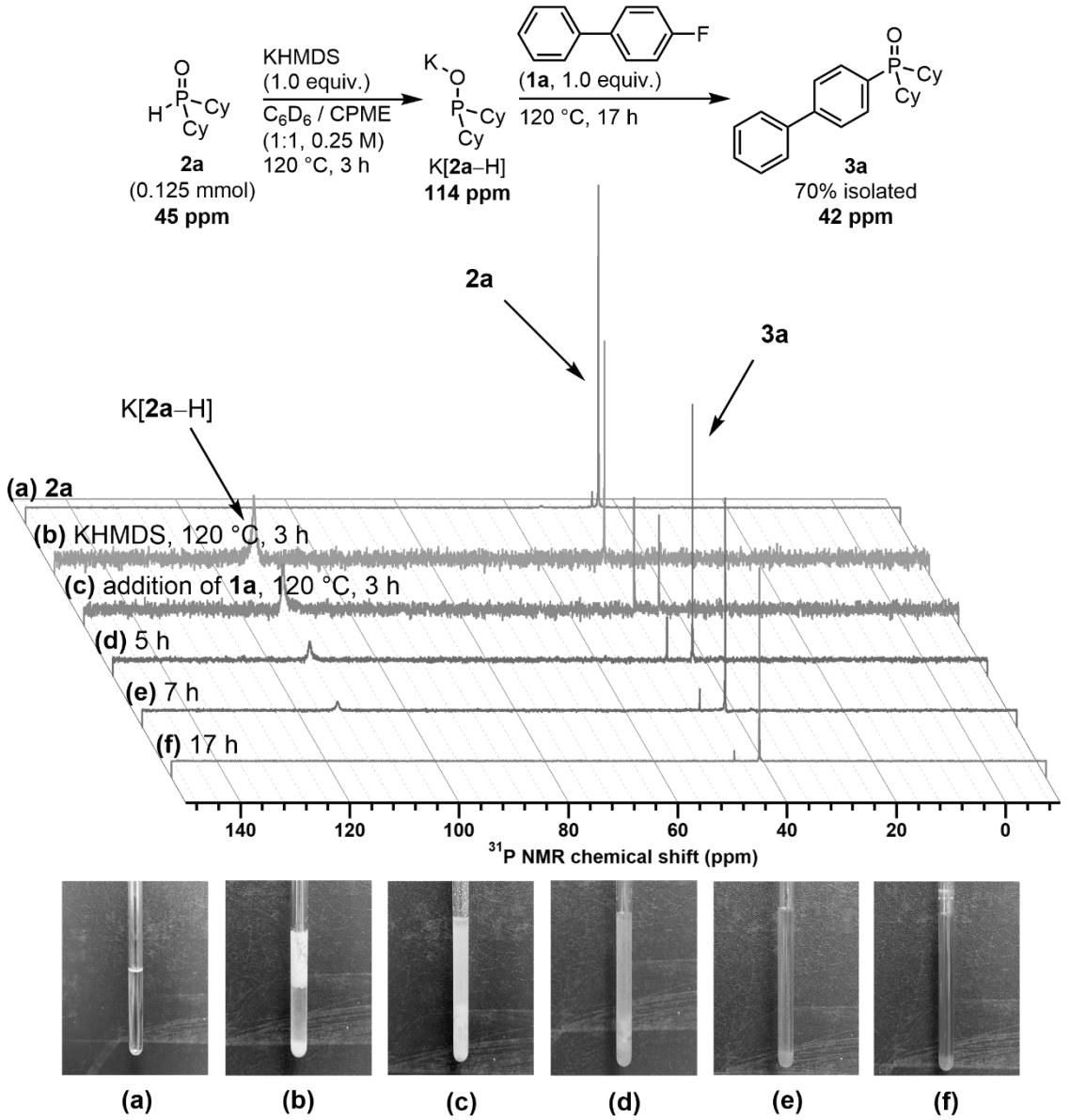

Figure 2.8. Monitoring defluorophosphinylation by ^{31}P NMR spectroscopy.

2.4.7 Computational Studies

General Information

All calculations of the geometory optimizations were performed by Gaussian 16 package.[8] The geometory optimizations and frequency calculations of all structures were conducted at the M06-2X functional [19] in conjunction with the def2SVP basis set [21, 22] in the presence of three Me_2O models. The self-consistent reaction field (SCRF) method based on conductor-like polarizable continuum model (CPCM)[29, 30] was adopted to evaluate the effects of solvent (THF). All the transition states were traced with intrinsic reaction coordinate (IRC) analyses by the use of Global Reaction Route Mapping (GRRM) program[31] to describe the reaction pathway. This level is denoted as CPCM(THF)-M06-2X/def2SVP. For describing energy diagram, the relative energies were corrected for the thermal free energies and given in kcal·mol^{-1}. The structures of intermediates and transition states were described by GaussView 6.0 package.[32]

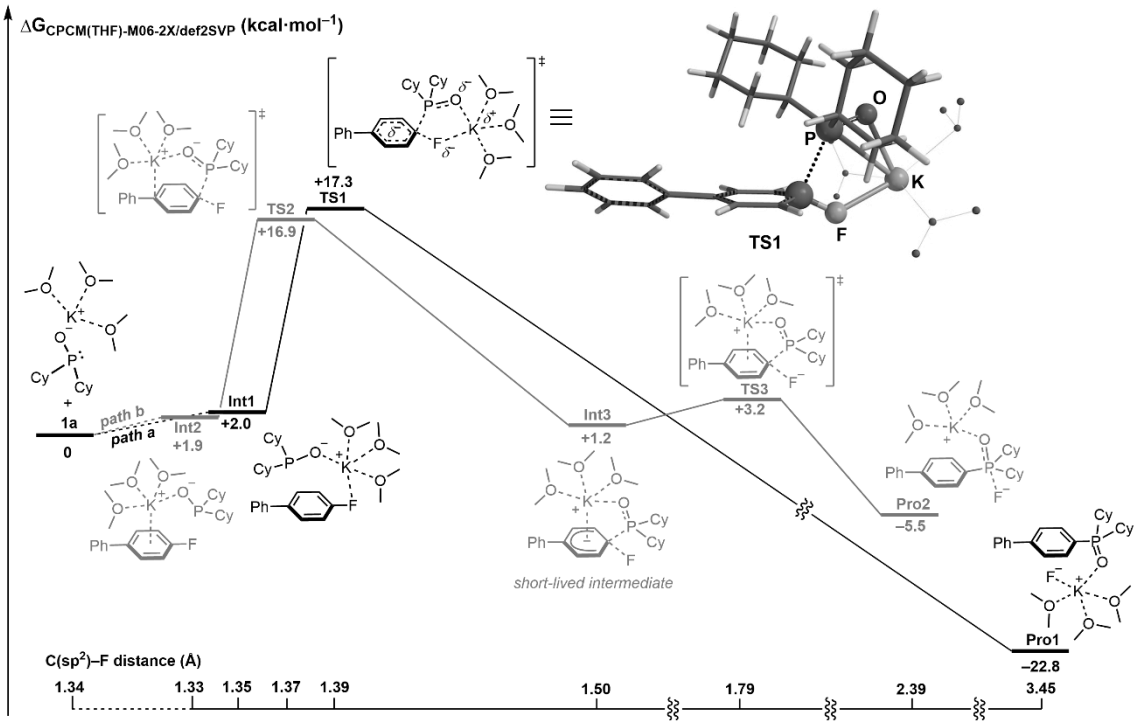

Figure 2.9. Energy diagram of the reaction pathway at CPCM(THF)-M06-2X/def2SVP level of theory.

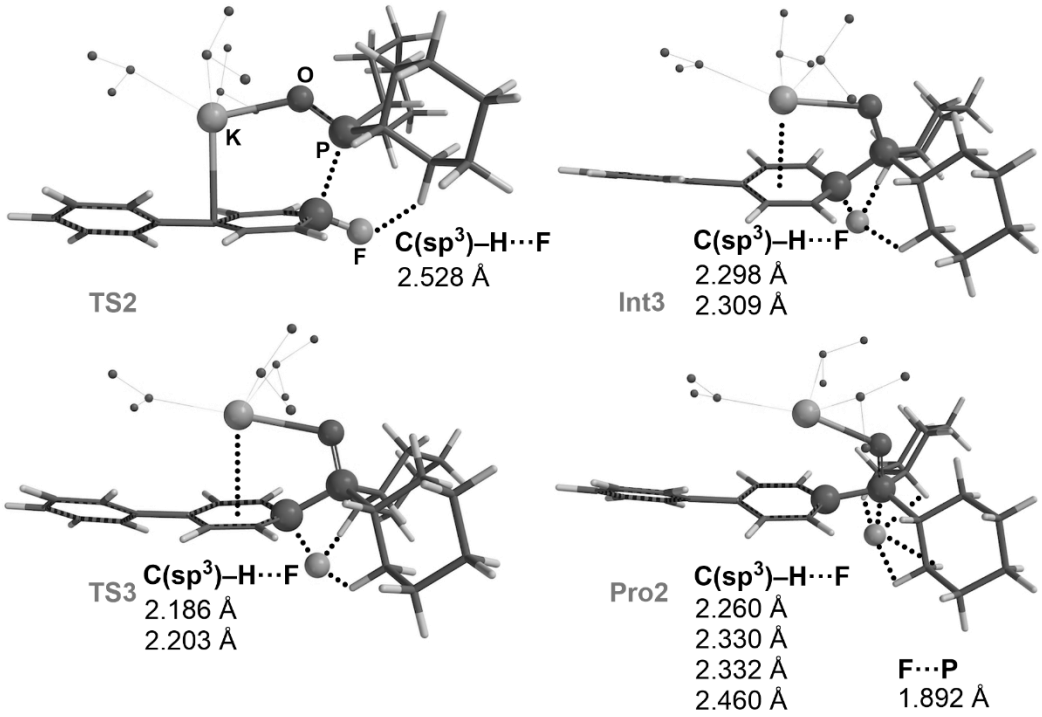

Figure 2.10. Non-covalent interactions in key geometries.

For better consideration of properties of the fluoride anion in DFT calculations, additional single point calculations with diffuse functions at CPCM(THF)-M06-2X/def2TZVPD[20,33] level of theory was carried out based on geometries obtained through the method described as above (Figure 2.9). Each transition state had a single imaginary frequency. This method is denoted as CPCM(THF)-M06-2X/def2TZVPD//CPCM(THF)-M06-2X/def2SVP. The result is shown in Figure 2.1. The relative energies were corrected for the thermal free energies and given in kcal·mol^{-1}. Transformation from **Int3** to **Pro2** is an essentially barrierless process similar to that with CPCM(THF)-M06-2X/def2SVP level of theory.

Recently, Fleurat-Lessard and co-workers disclosed an unexpected failure of B3LYP functional for an intramolecular nucleophilic aromatic substitution.[34] In the current research, Meisenheimer-type complex was missing when adopting B3LYP functional in the calculation. Thus, the M06-2X functional was adopted for the DFT calculations.

$KOPPh_2$ as Starting Material

Additional theoretical investigation using K[**2d**–H] as a P source was performed for the stepwise reaction pathway through a Meisenheimer-type complex (Figure 2.11). The energy barrier (16.0 kcal·mol^{-1}) is slightly higher than that with K[**2a**–H] (15.0 kcal·mol^{-1}) at CPCM(THF)-M06-2X/def2SVP level of theory, which is consistent with the experimental results.

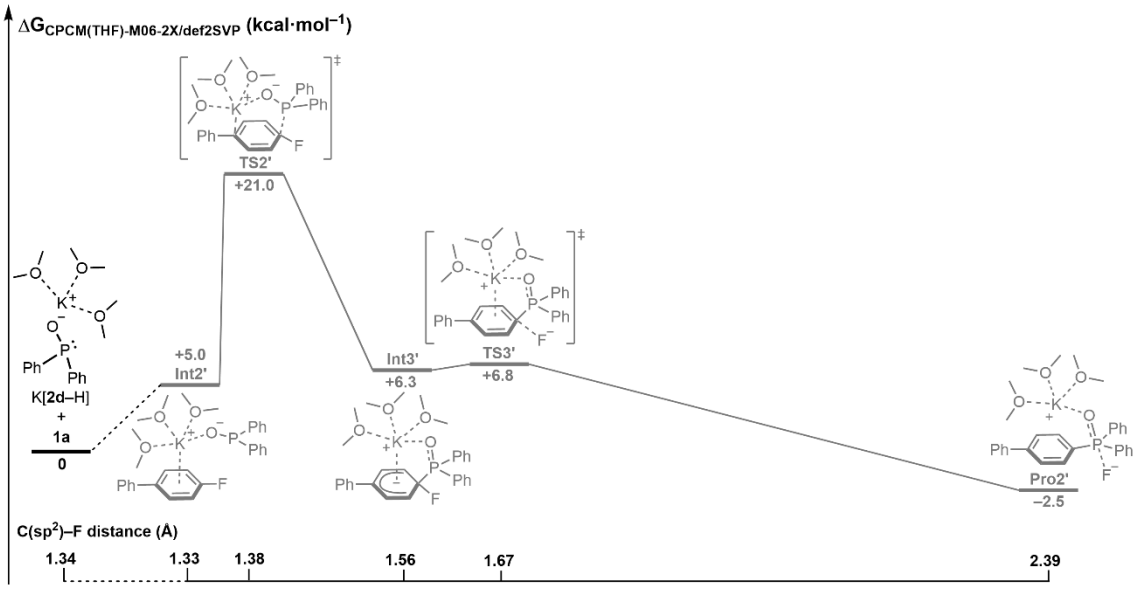

Figure 2.11. Energy diagram of the reaction pathway with K[**2d**–H].

Energies of Each Geometry

Energy (Hartree) = Electronic Energy (EE) + Thermal Free Energy Correction

Table 2.5. Energies of each geometry

	Level of Theory	
Geometry Name	CPCM(THF)-M06-2X/def2SVP	CPCM(THF)-M06/def2TZVPD //CPCM(THF)-M06-2X/def2SVP
K[2a–H]·3Me$_2$O	–1950.289019	–1951.645921
K[2d–H]·3Me$_2$O	–1943.234154	-
1a	–561.760178	–562.387571
Int1	–2512.045942	–2514.021632
TS1	–2512.021648	–2513.994961
Pro1	–2512.085520	–2514.080268
Int2	–2512.046159	–2514.022130
TS2	–2512.022199	–2513.997027
Int3	–2512.047229	–2514.027636
TS3	–2512.044144	–2514.031440
Pro2	–2512.058014	–2514.045329
Int2′	–2504.986291	-
TS2′	–2504.960931	-
Int3′	–2504.984258	-
TS3′	–2504.983549	-
Pro2′	–2504.998310	-

2.4.8 X-ray Crystallographic Study

Data were collected on a Rigaku XtaLAB Synergy (Cu-*K*α radiation, λ = 1.5418 Å). The diffraction data were processed using CrysAlisPro software.[35] The structure was solved by ShelXT,[36] and refined by least squares method on F^2 by. ShelXL progaram.[37] Non-hydrogen atoms were refined anisotropically. All hydrogen atoms were located on the calculated positions and refined using a riding model. All calculations were performed using the Olex2 program.[38] The supplementary crystallographic data for this research can be obtained free of charge from the Cambridge Crystallographic Data Centre *via* https://www.ccdc.cam.ac.uk/structures/.

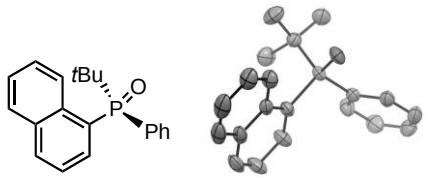

Crystal data for (*S*)-**3x** (CCDC 2008762; recrystallization from EtOAc/hexane). $C_{20}H_{21}OP$, M = 308.34, orthorhombic, space group $P2_12_12_1$ (#19), a = 8.80440(10) Å, b = 9.41040(10) Å, c = 20.1299(2) Å, α = 90°, β = 90°, g = 90°, V = 1667.82(3) Å^3, T = 200 K, Z = 4, density (calc.) = 1.228 g/cm^3, total reflections collected = 8221, independent reflections = 3329 (R_{int} = 0.0243), $R1$ (I>2σ(I)) = 0.0329, $wR2$ (all data) = 0.0872, GOF = 1.059. Flack parameter = –0.009(9).

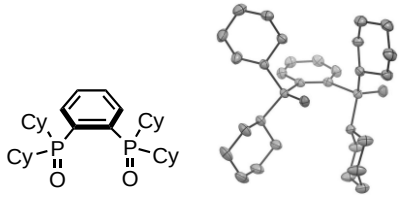

Crystal data for **4a** (CCDC 2008761; recrystallization from EtOAc/hexane). $C_{30}H_{48}O_2P_2$, M = 502.62, triclinic, space group P-1 (#2), a = 10.0665(3) Å, b = 11.1573(5) Å, c = 14.7623(4) Å, α = 68.752(4)°, β = 84.469(2)°, γ = 64.698(4)°, V = 1393.70(10) Å^3, T = 200 K, Z = 2, density (calc.) = 1.198 g/cm^3, total reflections collected = 15001, independent reflections = 5595 (R_{int} = 0.0256), $R1$ (I>2σ(I)) = 0.0379, $wR2$ (all data) = 0.1061, GOF = 1.064.

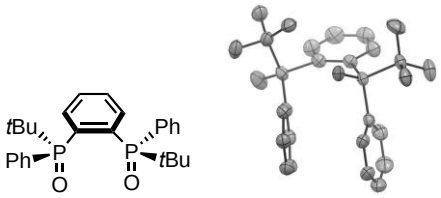

Crystal data for (*S*,*S*)-**4b** (CCDC 2008763; recrystallization from EtOAc/hexane). $C_{26}H_{32}O_{2.5}P_2$, M = 446.45, orthorhombic, space group $C222_1$ (#20), a = 10.86500(10) Å, b = 17.10400(10) Å, c = 26.9063(2) Å, α = 90°, β = 90°, γ = 90°, V = 5000.13(7) Å^3, T = 200 K, Z = 8, density (calc.) = 1.186 g/cm^3, total reflections collected = 13125, independent reflections = 5027 (R_{int} = 0.0208), $R1$ (I>2σ(I)) = 0.0300, $wR2$ (all data) = 0.0821, GOF = 1.046, Flack parameter = 0.002(6).

2.4.9 Compound Characterization Data

[1,1'-Biphenyl]-4-yldicyclohexylphosphine Oxide (3a)

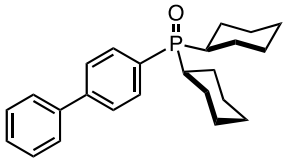

The product **3a** was isolated by flash chromatography on silica gel with slow gradient elution (CH_2Cl_2/MeOH 100:0-to-97:3) followed by preparative thin-layer chromatography (CH_2Cl_2/MeOH, 93:7) as a white solid (45.5 mg, 99% yield). **M.p.**: 195.7–196.3 °C. **^{1}H NMR** (400 MHz, $CDCl_3$): δ 7.76–7.67 (m, 4H), 7.66–7.61 (m, 2H), 7.47 (dd, J = 7.2, 7.2 Hz, 2H), 7.39 (tt, J = 7.6, 1.2 Hz, 1H), 2.15–2.00 (br, 4H), 1.90–1.62 (m, 8H), 1.42–1.09 (m, 10H). **^{13}C NMR** (100.5 MHz, $CDCl_3$): δ 143.9, 140.1, 132.0 (d, $J_{C–P}$ = 7.0 Hz, 2C), 128.9 (2C), 128.4 (d, $J_{C–P}$ = 86.4 Hz), 128.0, 127.2 (2C), 126.9 (d, $J_{C–P}$ = 10.6 Hz, 2C), 35.2 (d, $J_{C–P}$ = 67.1 Hz, 2C), 26.5 (d, $J_{C–P}$ = 12.5 Hz, 2C), 26.4 (d, $J_{C–P}$ = 11.5 Hz, 2C), 25.9 (2C), 25.6 (2C), 24.6 (d, $J_{C–P}$ = 2.9 Hz, 2C). **^{31}P NMR** (161.8 MHz, $CDCl_3$): δ 45.8. **IR** (ATR): 2929, 2853, 1443, 1399, 1330, 1320, 1208, 1165, 1131, 1101, 1062, 1017, 896, 854, 840, 824, 782, 747, 700, 604 cm^{-1}. **HRMS-FD** (*m/z*): $[M]^+$ Cacld for $C_{24}H_{31}OP$, 366.2113; found, 366.2128.

[1,1'-Biphenyl]-3-yldicyclohexylphosphine Oxide (3b)

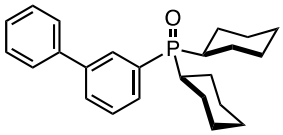

The product **3b** was isolated by flash chromatography on silica gel with slow gradient elution (CH_2Cl_2/MeOH, 100:0-to-97:3) followed by preparative thin-layer chromatography (CH_2Cl_2/MeOH, 95:5) as a colorless oil contaminated with small amount of impurities (42.0 mg, 92% yield). **^{1}H NMR** (400 MHz, $CDCl_3$): δ 7.90 (d, J = 10.3 Hz, 1H), 7.74 (dd, J = 8.0, 1.6 Hz, 1H), 7.67–7.58 (m, 3H), 7.55 (td, J = 7.8, 1.6 Hz, 1H), 7.47 (t, J = 7.6 Hz, 2H), 7.39 (tt, J = 7.2, 1.2 Hz, 1H), 2.20–2.00 (m, 4H), 1.95–1.55 (m, 8H), 1.44–1.08 (m, 10H). **^{13}C NMR** (100.5 MHz, $CDCl_3$): δ 141.2 (d, $J_{C–P}$ = 10.5 Hz), 140.2, 130.7 (d, $J_{C–P}$ = 82.4 Hz), 130.2–129.8 (m, 3C), 128.8 (2C), 128.6 (d, $J_{C–P}$ = 11.5 Hz), 127.7, 127.2 (2C), 35.1 (d, $J_{C–P}$ = 67.0 Hz, 2C), 26.4 (d, $J_{C–P}$ = 13.4 Hz, 2C), 26.3 (d, $J_{C–P}$ = 12.5 Hz, 2C), 25.8 (2C), 25.5 (d, $J_{C–P}$ = 1.9 Hz, 2C), 24.6 (d, $J_{C–P}$ = 2.9 Hz, 2C). **^{31}P NMR** (161.8 MHz, $CDCl_3$): δ 45.9. **IR** (ATR): 2928, 2853, 2209, 1448, 1398, 1275, 1210, 1164, 1113, 1077, 908, 891, 853, 823, 800, 755, 725, 700, 641, 615 cm^{-1}. **HRMS-FD** (*m/z*): $[M]^+$ Cacld for $C_{24}H_{31}OP$, 366.2113; found, 366.2130.

[1,1'-Biphenyl]-2-yldicyclohexylphosphine Oxide (3c)

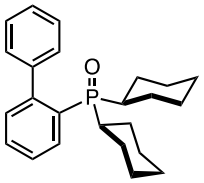

[Reaction time 14 h] The product **3c** was isolated by flash chromatography on silica gel with slow gradient elution (CH_2Cl_2/MeOH, 100:0-to-97:3) as a white solid (45.2 mg, 99% yield). **M.p.**: 113.8–116.2 °C. **^{1}H NMR** (400 MHz, $CDCl_3$): δ 8.17–8.08 (m, 1H), 7.52–7.47 (m, 2H), 7.45–7.39 (m, 3H), 7.26–7.18 (m, 3H), 1.87–1.78 (m, 2H), 1.78–1.64 (m, 4H), 1.61–1.48 (m, 4H), 1.44–1.26 (m, 6H), 1.22–0.99 (m, 6H). **^{13}C NMR** (100.5 MHz, $CDCl_3$): δ 143.8 (d, $J_{C–P}$ = 8.6 Hz), 142.0, 133.9 (d, $J_{C–P}$ = 5.7 Hz), 130.9 (d, $J_{C–P}$ = 9.7 Hz), 130.4, 129.7 (a part of doublet signal, overlapping), 128.8 (2C), 127.8 (2C), 127.2 (d, $J_{C–P}$ = 9.7 Hz), 38.1 (d, $J_{C–P}$ = 66.0 Hz, 2C), 26.6–26.2 (m, 8C), 25.6 (2C). One carbon is missing due to overlapping. **^{31}P NMR** (161.8 MHz, $CDCl_3$): δ 48.9. **IR** (ATR): 2926, 2847, 1442, 1426, 1177, 1151, 1126, 1077, 1035, 1006, 917, 880, 847, 814, 778, 761, 731, 706, 677, 617 cm^{-1}. Spectral data match those reported in the literature.[39]

Dicyclohexyl(4'-methoxy-[1,1'-biphenyl]-4-yl)phosphine Oxide (3d)

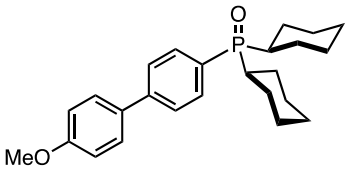

The product **3d** was isolated by flash chromatography on silica gel with slow gradient elution (CH_2Cl_2/MeOH, 100:0-to-97:3) as a white solid (28.6 mg, 55% yield). **M.p.**: 165.3–167.1 °C. **^{1}H NMR** (400 MHz, $CDCl_3$): δ 7.74–7.62 (m, 4H), 7.58 (d, J = 8.8 Hz, 2H), 7.00 (d, J = 9.2 Hz, 2H), 3.86 (s, 3H), 2.15–1.98 (m, 4H), 1.91–1.59 (m, 8H), 1.42–1.07 (m, 10H). **^{13}C NMR** (100.5 MHz, $CDCl_3$): δ 159.6, 143.4, 132.4, 131.9 (d, $J_{C–P}$ = 7.6 Hz, 2C), 128.2 (2C), 127.7 (d, $J_{C–P}$ = 87.2 Hz), 126.3 (d, $J_{C–P}$ = 10.1 Hz, 2C), 114.3 (2C), 55.3, 35.2 (d, $J_{C–P}$ = 67.3 Hz, 2C), 26.5 (d, $J_{C–P}$ = 12.5 Hz, 2C), 26.3 (d, $J_{C–P}$ = 12.4 Hz, 2C), 25.8 (2C), 25.5 (2C), 24.6 (2C). **^{31}P NMR** (161.8 MHz, $CDCl_3$): δ 45.9. **IR** (ATR): 2928, 2852, 1608, 1598, 1579, 1522, 1492, 1463, 1446, 1391, 1318, 1292, 1257, 1205, 1180, 1162, 1114, 1072,1037, 999, 920, 899, 888, 853, 813, 758, 744, 727, 715 cm^{-1}. **HRMS-FD** (*m/z*): $[M]^+$ Cacld for $C_{25}H_{33}O_2P$, 396.2218; found, 396.2212.

Dicyclohexyl(4'-(dimethylamino)-[1,1'-biphenyl]-4-yl)phosphine Oxide (3e)

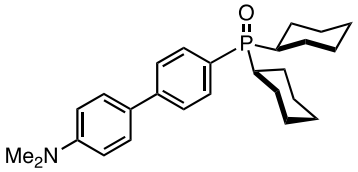

The product **3e** was isolated by flash chromatography on silica gel with slow gradient elution (CH_2Cl_2/MeOH, 100:0-to-97:3) to yield a white solid (26.1 mg, 51% yield). **M.p.**: ~230 °C (decomp.). **^{1}H NMR** (400 MHz, $CDCl_3$): δ 7.70–7.62 (m, 4H), 7.55 (d, J = 12.0 Hz, 2H), 6.81 (d, J = 12.0 Hz, 2H), 3.01 (s, 6H), 2.13–1.97 (m, 4H), 1.93–1.61 (m, 8H), 1.41–1.08 (m, 10H). **^{13}C NMR** (100.5 MHz, $CDCl_3$): δ 150.3, 143.8, 131.9 (d, J_{C-P} = 8.0 Hz, 2C), 127.8 (2C), 127.5, 126.6 (d, J_{C-P} = 88.2 Hz), 125.7 (d, J_{C-P} = 10.1 Hz, 2C), 112.6 (2C), 40.4 (2C), 35.2 (d, J_{C-P} = 68.0 Hz, 2C), 26.5 (d, J_{C-P} = 12.4 Hz, 2C), 26.4 (d, J_{C-P} = 11.6 Hz, 2C), 25.8 (2C), 25.5 (2C), 24.6 (d, J_{C-P} = 3.0 Hz, 2C). **^{31}P NMR** (161.8 MHz, $CDCl_3$): δ 45.9. **IR** (ATR): 2922, 2851, 1611, 1595, 1534, 1496, 1445, 1364, 1207, 1161, 1109, 898, 854, 805, 755 cm^{-1}. **HRMS-FD** (*m/z*): $[M]^+$ Cacld for $C_{26}H_{36}NOP$, 409.2535; found, 409.2522.

Dicyclohexyl(4'-(trifluoromethyl)-[1,1'-biphenyl]-4-yl)phosphine Oxide (3f)

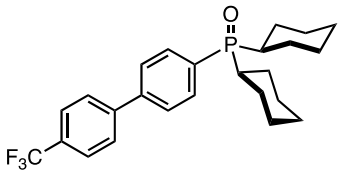

The product **3f** was isolated by flash chromatography on silica gel with slow gradient elution (CH_2Cl_2/MeOH, 100:0-to-97:3) as a white solid (38.2 mg, 70% yield). **M.p.**: 196.2–197.3 °C. **^{1}H NMR** (400 MHz, $CDCl_3$): δ 7.82–7.67 (m, 8H), 2.21–1.97 (m, 4H), 1.94–1.57 (m, 8H), 1.42–1.08 (m, 10H). **^{13}C NMR** (100.5 MHz, $CDCl_3$): δ 143.6, 142.3, 132.1 (d, J_{C-P} = 8.0 Hz, 2C), 129.9 (d, J_{C-P} = 84.3 Hz), 129.9 (q, J_{C-F} = 31.7 Hz), 127.5 (2C), 127.0 (d, J_{C-P} = 10.6 Hz, 2C), 125.8 (d, J_{C-P} = 3.8 Hz, 2C), 124.1 (q, J_{C-F} = 272.2 Hz), 35.2 (d, J_{C-P} = 67.1 Hz, 2C), 26.4 (d, J_{C-P} = 12.5 Hz, 2C), 26.3 (d, J_{C-P} = 12.5 Hz, 2C), 25.8 (2C), 25.5 (d, J_{C-P} = 1.9 Hz, 2C), 24.6 (d, J_{C-P} = 2.8 Hz, 2C). **^{31}P NMR** (161.8 MHz, $CDCl_3$): δ 45.7. **IR** (ATR): 2931, 2853, 1617, 1449, 1390, 1323, 1208, 1164, 1120, 1069, 1017, 1005, 890, 854, 819, 790, 760, 726, 674, 642 cm^{-1}. **HRMS-FD** (*m/z*): $[M]^+$ Cacld for $C_{25}H_{30}F_3OP$, 434.1986; found, 434.1993.

Dicyclohexyl(naphthalen-1-yl)phosphine Oxide (3g)

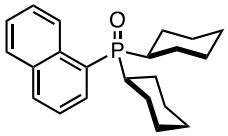

The product **3g** was isolated by flash chromatography on silica gel with slow gradient elution (CH_2Cl_2/MeOH, 100:0-to-97:3) as a white solid (38.8 mg, 91% yield). **M.p.**: 68.5–69.2 °C. **^{1}H NMR** (400 MHz, $CDCl_3$): δ 8.97 (br, 1H), 7.98 (d, J = 7.6 Hz, 1H), 7.88 (d, J = 8.4 Hz, 1H), 7.79 (br, 1H), 7.61–7.48 (m, 3H), 2.40–2.11 (m, 4H), 1.88–1.77 (m, 2H), 1.75–1.53 (m, 6H), 1.53–1.04 (m, 10H). **^{13}C NMR** (100.5 MHz, $CDCl_3$): δ 135.1 (br), 133.8 (d, $J_{C–P}$ = 8.6 Hz), 132.3 (d, $J_{C–P}$ = 1.9 Hz), 132.0 (br), 128.8, 127.0, 126.9, 126.3 (d, $J_{C–P}$ = 81.4 Hz), 126.1, 124.1 (d, $J_{C–P}$ = 12.5 Hz), 37.1 (d, $J_{C–P}$ = 66.0 Hz, 2C), 26.45 (d, $J_{C–P}$ = 13.4 Hz, 2C), 26.42 (d, $J_{C–P}$ = 11.5 Hz, 2C), 25.7 (2C), 25.6 (d, $J_{C–P}$ = 1.9 Hz, 2C), 25.4 (2C). **^{31}P NMR** (161.8 MHz, $CDCl_3$): δ 50.8 (br). **IR** (ATR): 2932, 2850, 1591, 1504, 1448, 1326, 1280, 1211, 1170, 1150, 1115, 1023, 1007, 977, 926, 892, 853, 823, 810, 803, 777, 720, 664, 640 cm^{-1}. Spectral data match those reported in the literature.[40]

Dicyclohexyl(2',4',6'-triisopropyl-[1,1'-biphenyl]-4-yl)phosphine Oxide (3h)

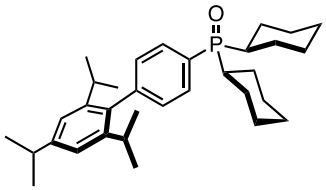

The product **3h** was isolated by flash chromatography on silica gel with slow gradient elution (CH_2Cl_2/MeOH, 100:0-to-97:3) as a white solid (7.2 mg, 12% yield). **M.p.**: 179.9–181.6 °C. **^{1}H NMR** (400 MHz, $CDCl_3$): δ 7.68 (dd, J = 9.6, 8.4 Hz, 2H), 7.30 (dd, J = 8.4, 2.4 Hz, 2H), 7.07 (s, 2H), 2.95 (quin, J = 6.8 Hz, 1H), 2.52 (quin, J = 7.2 Hz, 2H), 2.14–2.01 (m, 4H), 1.90–1.76 (m, 6H), 1.76–1.66 (m, 4H), 1.40–1.15 (m, 14H), 1.08 (d, J = 6.8 Hz, 12H). **^{13}C NMR** (100.5 MHz, $CDCl_3$): δ 148.3, 146.2 (2C), 144.2, 136.1, 131.0 (d, $J_{C–P}$ = 7.6 Hz, 2C), 129.8 (d, $J_{C–P}$ = 10.6 Hz, 2C), 127.7 (d, $J_{C–P}$ = 86.2 Hz), 120.6 (2C), 35.1 (d, $J_{C–P}$ = 67.0 Hz, 2C), 34.3, 30.3 (2C), 26.5 (d, $J_{C–P}$ = 10.6 Hz, 2C), 26.4 (d, $J_{C–P}$ = 12.5 Hz, 2C), 26.0 (2C), 25.5 (2C), 24.7 (d, $J_{C–P}$ = 2.9 Hz, 2C), 24.1 (4C), 24.0 (2C). **^{31}P NMR** (161.8 MHz, $CDCl_3$): δ 46.1. **IR** (ATR): 2930, 2854, 1609, 1449, 1383, 1350, 1276, 1210, 1164, 1098, 1003, 920, 879, 852, 842, 823, 762, 725, 528, 518 cm^{-1}. **HRMS-FD** (*m/z*): $[M]^+$ Cacld for $C_{33}H_{49}OP$, 492.3521; found, 492.3541.

Dicyclohexyl(4-(pyridin-2-yl)phenyl)phosphine Oxide (3i)

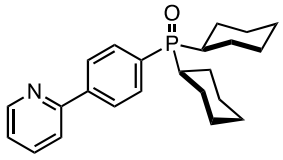

The product **3i** was isolated by flash chromatography on silica gel with slow gradient elution (CH_2Cl_2/MeOH, 100:0-to-96:4) followed by preparative thin-layer chromatography (CH_2Cl_2/MeOH, 95:5) as a white solid (44.0 mg, 96% yield). **M.p.**: 177.6–178.3 °C. **^{1}H NMR** (400 MHz, $CDCl_3$): δ 8.74–8.68 (m, 1H), 8.09 (d, J = 8.4 Hz, 2H), 7.85–7.73 (m, 4H), 7.33–7.24 (m, 1H), 2.15–1.98 (m, 4H), 1.96–1.57 (m, 8H), 1.42–1.06 (m, 10H). **^{13}C NMR** (100.5 MHz, $CDCl_3$): δ 156.4, 149.8 (dd, $J_{C–P}$ = 16.3, 2.9 Hz), 142.1 (d, $J_{C–P}$ = 1.9 Hz), 136.9, 131.9 (d, $J_{C–P}$ = 7.6 Hz, 2C), 130.5 (d, $J_{C–P}$ = 85.3 Hz), 126.8–126.4 (m, 2C), 122.7 (d, $J_{C–P}$ = 27.8 Hz), 120.9 (d, $J_{C–P}$ = 3.9 Hz), 35.1 (d, $J_{C–P}$ = 67.0 Hz, 2C), 26.7–25.1 (m, 8C), 24.5 (2C). **^{31}P NMR** (161.8 MHz, $CDCl_3$): δ 45.8. **IR** (ATR): 2925, 2851, 1588, 1575, 1553, 1466, 1451, 1434, 1391, 1293, 1265, 1207, 1163, 1118, 1107, 1096, 1071, 1007, 989, 921, 899, 850, 826, 775, 752, 741, 723, 676, 636, 618 cm^{-1}. **HRMS-FD** (*m/z*): $[M]^+$ Cacld for $C_{23}H_{30}NOP$, 367.2065; found, 367.2064.

Dicyclohexyl(pyridin-3-yl)phosphine Oxide (3j)

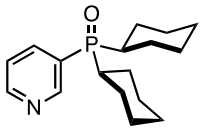

The product **3j** was isolated by flash chromatography on silica gel with slow gradient elution (CH_2Cl_2/MeOH, 100:0-to-95:5) followed by preparative thin-layer chromatography (CH_2Cl_2/MeOH, 93:7) as a white solid contaminated with small amount of impurities (32.8 mg, 90% yield). **M.p.**: 156.7–158.9 °C. **^{1}H NMR** (400 MHz, $CDCl_3$): δ 8.82–8.71 (m, 2H), 8.09 (ddd, J = 8.0, 8.0, 2.0 Hz, 1H), 7.45 (dd, J = 6.0, 5.2 Hz, 1H), 2.14–1.96 (m, 4H), 1.94–1.56 (m, 8H), 1.38–1.07 (m, 10H). **^{13}C NMR** (100.5 MHz, $CDCl_3$): δ 152.0, 151.3 (d, $J_{C–P}$ = 9.6 Hz), 140.11 (d, $J_{C–P}$ = 5.7 Hz), 126.3 (d, $J_{C–P}$ = 80.5 Hz), 123.5 (d, $J_{C–P}$ = 7.6 Hz), 35.2 (d, $J_{C–P}$ = 68.0 Hz, 2C), 26.2 (d, $J_{C–P}$ = 13.5 Hz, 2C), 26.1 (d, $J_{C–P}$ = 12.5 Hz, 2C), 25.7 (2C), 25.4 (d, $J_{C–P}$ = 1.9 Hz, 2C), 24.4 (d, $J_{C–P}$ = 2.8 Hz, 2C). **^{31}P NMR** (161.8 MHz, $CDCl_3$): δ 44.4. **IR** (ATR): 2923, 2851, 1578, 1562, 1467, 1449, 1407, 1382, 1295, 1267, 1207, 1166, 1116, 1073, 1045, 1027, 1007, 918, 899, 852, 825, 808, 760, 748, 713, 620, 570, 542, 531 cm^{-1}. **HRMS-FD** (*m/z*): $[M]^+$ Cacld for $C_{17}H_{26}NOP$, 291.1752; found, 291.1748.

Ferrocenyl-2-yldicyclohexylphosphine Oxide (3k)

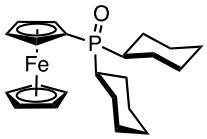

[Raction time 24 h] The product **3k** was isolated by flash chromatography on silica gel with slow gradient elution (CH_2Cl_2/MeOH, 100:0-to-97:3) followed by preparative thin-layer chromatography (CH_2Cl_2/MeOH, 95:5) as a bright-brown solid (21.0 mg, 42% yield). **M.p.**: 182 °C (decomp.). **^{1}H NMR** (400 MHz, $CDCl_3$): δ 4.42 (d, J = 1.6 Hz, 2H), 4.37 (d, J = 1.2 Hz, 2H), 4.32 (s, 5H), 2.04–1.63 (m, 12H), 1.50–1.37 (m, 2H), 1.35–1.10 (m, 8H). **^{13}C NMR** (100.5 MHz, $CDCl_3$): δ 72.2 (d, $J_{C–P}$ = 95.8 Hz), 71.4 (d, $J_{C–P}$ = 10.6 Hz, 2C), 70.4 (d, $J_{C–P}$ = 9.6 Hz, 2C), 69.6 (5C), 37.0 (d, $J_{C–P}$ = 69.0 Hz, 2C), 26.7 (d, $J_{C–P}$ = 12.5 Hz, 2C+2C, overlapping), 26.3 (d, $J_{C–P}$ = 1.9 Hz, 2C), 25.9 (2C), 25.4 (d, $J_{C–P}$ = 2.9 Hz, 2C). **^{31}P NMR** (161.8 MHz, $CDCl_3$): δ 46.3. **IR** (ATR): 2929, 1450, 1209, 1174, 1154, 1035, 818, 752, 740, 628 cm^{-1}. **HRMS-FD** (*m/z*): $[M]^+$ Cacld for $C_{22}H_{31}FeOP$, 398.1462; found, 398.1463. Spectral data match those reported in the literature.[41]

Dicyclohexyl(4-(trifluoromethyl)phenyl)phosphine Oxide (3n)

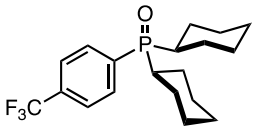

The product **3n** was isolated by flash chromatography on silica gel with slow gradient elution (CH_2Cl_2/MeOH, 100:0-to-95:5) as a white solid (29.3 mg, 65% yield). **M.p.**: 174.7–176.3 °C. **^{1}H NMR** (400 MHz, $CDCl_3$): δ 7.81 (dd, J = 8.4, 8.4 Hz, 2H), 7.74 (d, J = 6.8 Hz, 2H), 2.14–2.00 (m, 4H), 1.90–1.64 (m, 6H), 1.64–1.53 (m, 2H), 1.37–1.09 (m, 10H). **^{13}C NMR** (100.5 MHz, $CDCl_3$): δ 134.8 (d, $J_{C–P}$ = 80.5 Hz), 133.1 (q, $J_{C–F}$ = 34.5 Hz), 132.0 (d, $J_{C–P}$ = 7.6 Hz, 2C), 125.2–124.8 (m, 2C), 123.7 (q, $J_{C–F}$ = 272.6 Hz), 35.1 (d, $J_{C–P}$ = 67.0 Hz, 2C), 26.3 (d, J = 11.5 Hz, 2C), 26.2 (d, J = 12.5 Hz, 2C), 25.7 (2C), 25.5 (d, J = 2.9 Hz, 2C), 24.5 (d, J = 2.9 Hz, 2C). **^{31}P NMR** (161.8 MHz, $CDCl_3$): δ 45.5. **IR** (ATR): 2929, 2853, 1443, 1399, 1330, 1320, 1208, 1165, 1131, 1101, 1062, 1017, 896, 854, 840, 824, 782, 747, 700, 604 cm^{-1}. Spectral data match those reported in the literature.[40]

Dicyclohexyl(4-(diphenylamino)phenyl)phosphine Oxide (3o)

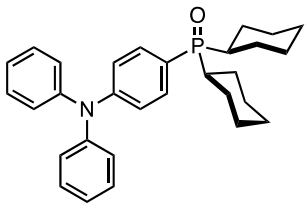

The product **3o** was isolated by flash chromatography on silica gel with slow gradient elution (CH_2Cl_2/MeOH, 100:0-to-97:3) followed by preparative thin-layer chromatography (CH_2Cl_2/MeOH, 93:7) as a white foam contaminated with small amount of impurities (46.2 mg, 81% yield). **M.p.**: 180.9–181.1 °C. **^{1}H NMR** (400 MHz, $CDCl_3$): δ 7.43 (t, J = 8.8 Hz, 2H), 7.31 (t, J = 7.2 Hz, 4H), 7.50 (d, J = 8.8 Hz, 4H), 7.11 (t, J = 7.2 Hz, 2H), 7.05 (dd, J = 8.8, 2.0 Hz, 2H), 2.11–1.91 (m, 4H), 1.91–1.55 (m, 8H), 1.40–1.08 (m, 10H). **^{13}C NMR** (100.5 MHz, $CDCl_3$): δ 150.3 (d, $J_{C–P}$ = 2.8 Hz), 146.8 (2C), 132.4 (d, $J_{C–P}$ = 8.6 Hz, 2C), 129.5 (4C), 125.7 (4C), 124.1 (2C), 120.8 (d, $J_{C–P}$ = 91.1 Hz), 120.2 (d, $J_{C–P}$ = 10.6 Hz, 2C), 35.2 (d, $J_{C–P}$ = 68.0 Hz, 2C), 26.5 (d, $J_{C–P}$ = 13.5 Hz, 2C), 26.4 (d, $J_{C–P}$ = 12.5 Hz, 2C), 25.9 (2C), 25.5 (2C), 24.6 (d, $J_{C–P}$ = 2.9 Hz, 2C). **^{31}P NMR** (161.8 MHz, $CDCl_3$): δ 45.7. **IR** (ATR): 2928, 2853, 1586, 1491, 1449, 1329, 1270, 1209, 1162, 1110, 1076, 891, 852, 822, 756, 726, 696, 660, 639, 623 cm^{-1}. **HRMS-FD** (*m/z*): $[M]^+$ Cacld for $C_{30}H_{36}NOP$, 457.2535; found, 457.2527.

(4-(9*H*-Carbazol-9-yl)phenyl)dicyclohexylphosphine Oxide (3p)

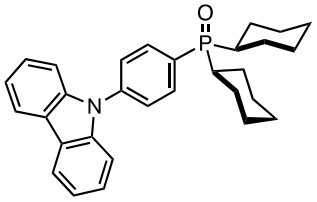

The product **3p** was isolated by flash chromatography on silica gel with slow gradient elution (CH_2Cl_2/MeOH, 100:0-to-97:3) followed by preparative thin-layer chromatography (CH_2Cl_2/MeOH, 95:5) as a white foam contaminated with small amount of impurities (47.2 mg, 83% yield). **M.p.**: 227.3–229.9 °C. **^{1}H NMR** (400 MHz, $CDCl_3$): δ 8.14 (d, J = 7.2 Hz, 2H), 7.90 (t, J = 8.8 Hz, 2H), 7.71 (dd, J = 8.4, 2.0 Hz, 2H), 7.50 (d, J = 8.4 Hz, 2H), 7.43 (t, J = 7.4, Hz, 2H), 7.31 (t, J = 7.2 Hz, 2H), 2.23–2.03 (m, 4H), 1.95–1.67 (m, 8H), 1.48–1.15 (m, 10H). **^{13}C NMR** (100.5 MHz, $CDCl_3$): δ 140.5 (d, $J_{C–P}$ = 2.9 Hz), 140.2 (2C), 133.1 (d, $J_{C–P}$ = 7.7 Hz, 2C), 128.8 (d, $J_{C–P}$ = 84.3 Hz), 126.2 (d, $J_{C–P}$ = 10.6 Hz, 2C), 126.0 (2C), 123.6 (2C), 120.37 (2C), 120.35 (2C), 109.7 (2C), 35.2 (d, $J_{C–P}$ = 68.0 Hz, 2C), 26.4 (d, $J_{C–P}$ = 12.5 Hz, 2C), 26.3 (d, $J_{C–P}$ = 11.6 Hz, 2C), 25.8

(2C), 25.5 (d, J = 1.9 Hz, 2C), 24.6 (d, J = 3.8 Hz, 2C). **^{31}P NMR** (161.8 MHz, $CDCl_3$): δ 45.6. **IR** (ATR): 2927, 2853, 1597, 1505, 1479, 1451, 1364, 1336, 1317, 1277, 1230, 1211, 1164, 1099, 1078, 916, 893, 852, 824, 759, 724, 674, 641, 625 cm^{-1}. **HRMS-FD** (*m/z*): $[M]^+$ Cacld for $C_{30}H_{34}NOP$, 455.2378; found, 455.2365.

(4-(9*H*-Carbazol-9-yl)phenyl)diphenylphosphine Oxide (3q)

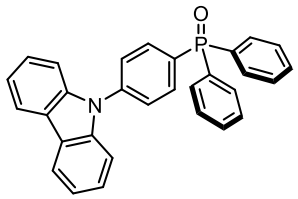

[KO*t*Bu as a base, 14 h] The product **3q** was isolated by automatic flash chromatography (RediSep® FlashColumn 4g, Hexane/EtOAc 100:0-to-0:100) as a white foam (38.4 mg, 69% yield). **M.p.**: 180.9–181.1 °C. **^{1}H NMR** (400 MHz, $CDCl_3$): δ 8.12 (d, J = 7.6 Hz, 2H), 7.90 (dd, J = 11.2, 8.0 Hz, 2H), 7.84–7.75 (m, 4H), 7.70 (dd, J = 8.0, 2.4 Hz, 2H), 7.63–7.56 (m, 2H), 7.56–7.49 (m, 4H), 7.49–7.45 (m, 2H), 7.41 (td, J = 8.0, 1.2 Hz, 2H), 7.30 (t, J = 7.6 Hz, 2H). **^{13}C NMR** (100.5 MHz, $CDCl_3$): δ 141.1 (d, $J_{C–P}$ = 2.9 Hz), 140.1 (2C), 133.8 (d, $J_{C–P}$ = 10.6 Hz, 2C), 132.1 (d, $J_{C–P}$ = 105.4 Hz, 2C), 132.1 (2C, overlapping), 132.1 (d, $J_{C–P}$ = 9.5 Hz, 4C, overlapping), 131.3 (d, $J_{C–P}$ = 100.8 Hz), 128.6 (d, $J_{C–P}$ = 12.5 Hz, 4C), 126.4 (d, $J_{C–P}$ = 13.4 Hz, 2C), 126.1 (2C), 123.7 (2C), 120.5 (2C), 120.4 (2C), 109.6 (2C). **^{31}P NMR** (161.8 MHz, $CDCl_3$): δ 29.2. **IR** (ATR): 3055, 2989, 1595, 1502, 1479, 1462, 1450, 1437, 1403, 1335, 1317, 1227, 1191, 1174, 1118, 1072, 1028, 1017, 998, 915, 831, 769, 749, 731, 719, 693, 673, 641, 624 cm^{-1}. Spectral data match those reported in the literature.[13]

[1,1'Biphenyl]-4-yldibutylphosphine Oxide (3r)

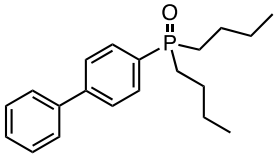

The product **3r** was isolated by flash chromatography on silica gel with slow gradient elution (CH_2Cl_2/MeOH, 100:0-to-97:3) followed by preparative thin-layer chromatography (CH_2Cl_2/MeOH, 96:4) as a white solid (33.3 mg, 85% yield). **M.p.**: 111.0–111.8 °C. **^{1}H NMR** (400 MHz, $CDCl_3$): δ 7.81–7.67 (m, 4H), 7.62 (d, J = 8.4 Hz, 2H), 7.46 (t, J = 7.2 Hz, 2H), 7.39 (t, J = 6.8 Hz, 1H), 2.09–1.81 (m, 4H), 1.72–1.56 (m, 2H), 1.54–1.32 (m, 6H), 0.89 (t, J = 7.2 Hz, 6H). **^{13}C NMR** (100.5 MHz, $CDCl_3$): δ 144.1

(d, $J_{C–P}$ = 1.9 Hz), 139.9, 131.7 (a part of doublet signals, $J_{C–P}$ ≈ 90 Hz), 130.9 (d, $J_{C–P}$ = 8.6 Hz, 2C), 128.8 (2C), 128.0, 127.2 (d, $J_{C–P}$ = 11.6 Hz, 2C), 127.1 (2C), 29.7 (d, $J_{C–P}$ = 68.0 Hz, 2C), 24.1 (d, $J_{C–P}$ = 14.4 Hz, 2C), 23.5 (d, $J_{C–P}$ = 3.8 Hz, 2C), 13.5 (2C). **^{31}P NMR** (161.8 MHz, $CDCl_3$): δ 41.0. **IR** (ATR): 2949, 1465, 1169, 1116, 902, 833, 790, 752, 726, 694 cm^{-1}. **HRMS-FD** (*m/z*): $[M]^+$ Cacld for $C_{20}H_{27}OP$, 314.1800; found, 314.1797.

[1,1'-Biphenyl]-4-yldi-*tert*-butylphosphine Oxide (3s)

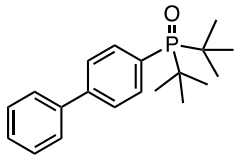

The product **3s** was isolated by flash chromatography on silica gel with slow gradient elution (CH_2Cl_2/MeOH, 100:0-to-95:5) as a white solid (30.4 mg, 77% yield). **M.p.**: 149.0–155.3 °C. **^{1}H NMR** (400 MHz, $CDCl_3$): δ 7.93 (br, 2H), 7.73–7.58 (m, 4H), 7.47 (t, J = 7.2 Hz, 2H), 7.39 (t, J = 7.2 Hz, 1H), 1.31 (d, J = 14.0 Hz, 18H). **^{13}C NMR** (100.5 MHz, $CDCl_3$): δ 143.5 (d, $J_{C–P}$ = 2.9 Hz), 140.0, 132.9 (br, 2C), 129.9 (d, $J_{C–P}$ = 78.4 Hz), 128.9 (2C), 127.9, 127.2 (2C), 126.4 (br, 2C), 35.8 (d, $J_{C–P}$ = 60.3 Hz, 2C), 27.1 (6C). **^{31}P NMR** (161.8 MHz, $CDCl_3$): δ 52.7. **IR** (ATR): 3039, 2968, 1600, 1475, 1389, 1366, 1191, 1119, 1154, 1101, 1021, 1007, 980, 956, 925, 844, 814, 769, 729, 701, 656, 650 cm^{-1}. **HRMS-FD** (*m/z*): $[M]^+$ Cacld for $C_{20}H_{27}OP$, 314.1800; found, 314.1795.

[1,1'-Biphenyl]-4-yldiphenylphosphine Oxide (3t)

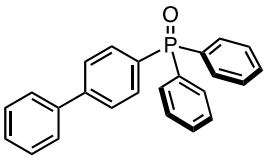

[KO*t*Bu as a base, 24 h] The product **3t** was purified by automatic flash chromatography (Biotage® Sfar Duo 5g, Hexane/EtOAc, 98:2-to-0:100) as a white solid (30.8 mg, 70% yield). **M.p.**: 122.9–124.3 °C. **^{1}H NMR** (400 MHz, $CDCl_3$): δ 7.79–7.64 (m, 9H), 7.63–7.53 (m, 4H), 7.52–7.43 (m, 5H), 7.39 (tt, J = 7.2, 1.2 Hz, 1H). **^{13}C NMR** (100.5 MHz, $CDCl_3$): δ 144.7 (d, $J_{C–P}$ = 2.9 Hz), 139.9, 133.0 (a part of doublet signals, 2C), 132.6 (d, $J_{C–P}$ = 10.6 Hz, 2C), 132.1 (d, $J_{C–P}$ = 10.6 Hz, 4C), 131.9 (d, $J_{C–P}$ = 2.8 Hz, 2C), 131.0 (d, $J_{C–P}$ = 105.4 Hz), 128.9 (2C), 128.5 (d, $J_{C–P}$ = 12.5 Hz, 4C), 128.1, 127.2 (2C), 127.9 (a part of doublet signals, 2C). **^{31}P NMR** (161.8 MHz, $CDCl_3$): δ 29.7. **IR** (ATR): 3057, 1599, 1552, 1483, 1437, 1391, 1180, 1116, 1074, 1006, 835, 752, 726, 695, 657 cm^{-1}.

Spectral data match those reported in the literature.[42]

[1,1'-Biphenyl]-2-yldibutylphosphine Oxide (3u)

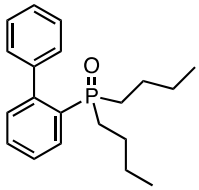

The product **3u** was isolated by flash chromatography on silica gel with slow gradient elution (CH_2Cl_2/MeOH, 100:0-to-97:3) followed by preparative thin-layer chromatography (CH_2Cl_2/MeOH, 96:4) as a whitish oil (37.8 mg, 96% yield). **^{1}H NMR** (400 MHz, $CDCl_3$): δ 8.27–8.18 (m, 1H), 7.52 (t, J = 3.6 Hz, 2H), 7.44–7.37 (m, 3H), 7.29–7.20 (m, 3H), 1.68–1.43 (m, 4H), 1.43–1.18 (m, 8H), 0.82 (t, J = 7.2 Hz, 6H). **^{13}C NMR** (100.5 MHz, $CDCl_3$): δ 143.9 (d, $J_{C–P}$ = 9.6 Hz), 141.4 (d, $J_{C–P}$ = 2.8 Hz), 134.0 (d, $J_{C–P}$ = 5.7 Hz), 130.9, 130.7 (d, $J_{C–P}$ = 9.5 Hz), 130.0 (a part of doublet signals, $J_{C–P} \approx 100$ Hz), 129.0 (2C), 128.0, 127.8 (2C), 127.4 (d, $J_{C–P}$ = 9.6 Hz), 30.1 (d, $J_{C–P}$ = 69.0 Hz, 2C), 23.9 (d, $J_{C–P}$ = 15.3 Hz, 2C), 23.4 (d, $J_{C–P}$ = 4.8 Hz, 2C), 13.5 (2C). **^{31}P NMR** (161.8 MHz, $CDCl_3$): δ 42.6. **IR** (ATR): 2958, 2925, 2871, 1587, 1562, 1462, 1440, 1378, 1343, 1279, 1217, 1176, 1150, 1125, 1081, 1053, 1008, 970, 905, 866, 792, 777, 762, 721, 708, 667 cm^{-1}. **HRMS-FD** (*m/z*): $[M]^+$ Cacld for $C_{20}H_{27}OP$, 314.1800; found, 314.1809.

[1,1'-Biphenyl]-2-yldi-*tert*-butylphosphine Oxide (3v)

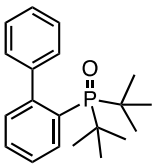

[**1c** (0.125 mmol), **2c** (0.125 mmol), KHMDS (0.125 mmol), CPME, 120 °C, 48 h] The product **3v** was isolated by flash chromatography on silica gel with slow gradient elution (CH_2Cl_2/MeOH, 100:0-to-95:5) followed by preparative thin-layer chromatography (CH_2Cl_2/MeOH, 95:5) as a white solid (18.6 mg, 47% yield). **M.p.**: 129.7–132.2 °C. **^{1}H NMR** (400 MHz, $CDCl_3$): δ 7.64 (t, J = 8.8 Hz, 1H), 7.47 (tt, J = 7.6, 1.2 Hz, 1H), 7.40–7.33 (m, 1H), 7.32–7.19 (m, 6H), 1.25 (d, J = 13.6 Hz, 18H). **^{13}C NMR** (100.5 MHz, $CDCl_3$): δ 149.7 (d, $J_{C–P}$ = 3.9 Hz), 142.3 (d, $J_{C–P}$ = 1.9 Hz), 133.1 (d, $J_{C–P}$ = 9.6 Hz), 131.1 (d, $J_{C–P}$ = 11.6 Hz), 129.9 (d, $J_{C–P}$ = 2.8 Hz), 128.9 (2C), 128.7 (d, $J_{C–P}$ = 74.8 Hz), 126.6, 126.2 (2C), 125.2 (d, $J_{C–P}$ = 11.6 Hz), 36.9 (d, $J_{C–P}$ = 59.4 Hz, 2C), 27.5 (6C). **^{31}P NMR** (161.8 MHz, $CDCl_3$): δ 53.1. **IR** (ATR): 3057, 2971, 2854, 1587, 1558, 1474, 1443, 1425, 1390, 1357, 1196, 1170, 1160, 1120, 1085, 1007, 996, 933, 904, 880, 813, 778, 757,

698, 666, 645, 616 cm^{-1}. Spectral data match those reported in the literature.[43]

[1,1'-Biphenyl]-2-yldiphenylphosphine Oxide (3w)

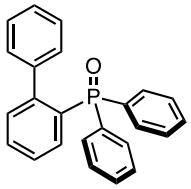

[KO*t*Bu as a base, 24 h] The product **3w** was purified by automatic flash chromatography (Biotage® Sfar Duo 5 g, Hexane:EtOAc 98:2-to-0:100) as a white solid (33.4 mg, 75% yield). **M.p.**: 148.3–150.4 °C. **^{1}H NMR** (400 MHz, $CDCl_3$): δ 7.62–7.52 (m, 5H), 7.46–7.27 (m, 9H), 7.24–7.17 (m, 2H), 7.10–7.00 (m, 3H). **^{13}C NMR** (100.5 MHz, $CDCl_3$): δ 147.7 (d, $J_{C–P}$ = 8.6 Hz), 140.3 (d, $J_{C–P}$ = 3.8 Hz), 134.0 (d, $J_{C–P}$ = 11.6 Hz), 133.0 (d, $J_{C–P}$ = 104.4 Hz, 2C), 131.9 (d, $J_{C–P}$ = 9.6 Hz), 131.71 (d, $J_{C–P}$ = 1.9 Hz), 131.68 (d, $J_{C–P}$ = 101.6 Hz), 131.6 (d, $J_{C–P}$ = 8.6 Hz, 4C), 131.1 (d, $J_{C–P}$ = 1.9 Hz, 2C), 130.1 (2C), 128.1 (d, $J_{C–P}$ = 12.5 Hz, 4C), 127.14 (2C), 127.08, 126.5 (d, $J_{C–P}$ = 12.5 Hz). **^{31}P NMR** (161.8 MHz, $CDCl_3$): δ 28.3. **IR** (ATR): 3054, 1585, 1559, 1481, 1467, 1448, 1437, 1306, 1190, 1138, 1106, 1070, 1029, 998, 968, 920, 854, 786, 766, 757, 750, 736, 718, 704, 693, 615 cm^{-1}. Spectral data match those reported in the literature.[44]

(*S*)-*tert*-Butyl(naphthalen-1-yl)phenylphosphine Oxide [(*S*)-3x]

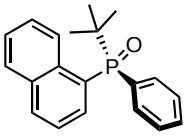

99:1 e.r.

[24 h] The product **(*S*)-3x** was isolated by automatic flash chromatography (Biotage® Sfar Duo 5 g, Hexane/EtOAc, 98:2-to-40:60) as a white powder (31.5 mg, 82% yield, 99:1 e.r.). **M.p.**: 155.3–157.7 °C. **^{1}H NMR** (400 MHz, $CDCl_3$): δ 9.02–8.94 (m, 1H), 8.02–7.78 (m, 5H), 7.53–7.37 (m, 6H), 1.39 (d, J = 14.4 Hz, 9H). **^{13}C NMR** (100.5 MHz, $CDCl_3$): δ 134.8 (d, $J_{C–P}$ = 7.7 Hz), 134.2 (d, $J_{C–P}$ = 8.6 Hz), 132.9 (d, $J_{C–P}$ = 89.1 Hz), 132.7 (d, $J_{C–P}$ = 2.8 Hz), 132.33 (d, overlapping), 132.25 (d, $J_{C–P}$ = 7.6 Hz, 2C), 131.3 (d, $J_{C–P}$ = 2.9 Hz), 128.4 (d, $J_{C–P}$ = 38.4 Hz, 2C), 128.2 (d, overlapping), 128.1, 127.3 (d, $J_{C–P}$ = 88.1 Hz), 126.9, 126.2, 123.5 (d, $J_{C–P}$ = 13.4 Hz), 34.9 (d, $J_{C–P}$ = 70.0 Hz), 26.1 (3C). **^{31}P NMR** (161.8 MHz, $CDCl_3$): δ 44.9. **IR** (ATR): 2965, 1501, 1471, 1440, 1393, 1364, 1326, 1202, 1174, 1156, 1102, 1024, 980, 817, 804, 776, 754, 704, 669, 636, 613 cm^{-1}. $[\alpha]_D^{27}$ = +72.43 (c = 1.00, $CHCl_3$). Spectral data match those reported in the literature.[45]

Di-*tert*-butyl(2-fluorophenyl)phosphine Oxide (3y)

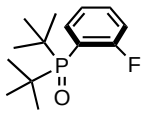

[1.0 mmol scale, CPME, 90 °C, 24 h] The product **3y** was isolated by flash chromatography on silica gel with slow gradient elution (CH_2Cl_2/MeOH 100:0-to-95:5) as a light-yellowish oil (249.9 mg, 98% yield). **^{1}H NMR** (400 MHz, $CDCl_3$): δ 8.19–8.05 (m, 1H), 7.57–7.47 (m, 1H), 7.32 (dd, J = 7.2, 7.2 Hz, 1H), 7.14–7.03 (m, 1H), 1.27 (d, J = 14.8 Hz, 18H). **^{13}C NMR** (100.5 MHz, $CDCl_3$): δ 161.2 (dd, $J_{C–F,\ C–P}$ = 246.3, 3.8 Hz), 137.0 (dd, J = 5.8, 1.9 Hz), 133.5 (dd, J = 7.7, 1.9 Hz), 124.4 (dd, J = 7.6, 1.9 Hz), 118.6 (dd, $J_{C–P,\ C–F}$ = 71.9, 23.9 Hz), 115.2 (dd, J = 24.9, 4.8 Hz), 36.1 (d, $J_{C–P}$ = 61.4 Hz, 2C), 26.5 (d, $J_{C–P}$ = 3.8 Hz, 6C). **^{31}P NMR** (161.8 MHz, $CDCl_3$): δ 59.1 (d, $J_{P–F}$ = 8.6 Hz). **IR** (ATR): 2955, 2903, 2871, 1603, 1570, 1472, 1438, 1392, 1368, 1292, 1256, 1206, 1154, 1119, 1073, 1014, 934, 824, 814, 764, 721, 677, 648 cm^{-1}. **HRMS-FD** (*m/z*): $[M]^+$ Cacld for $C_{14}H_{22}FOP$, 256.1392; found, 256.1384.

1,2-Bis(dicyclohexylphosphinoyl)benzene (4a)

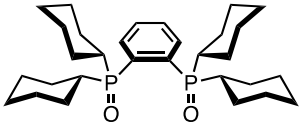

[**1q** (1.0 mmol), **2a** (4 equiv), KHMDS (4 equiv), CPME, 120 °C (0.25 M), 20 h] The product **4a** was isolated by flash chromatography on silica gel with slow gradient elution (CH_2Cl_2/MeOH, 100:0-to-96:4) followed by recrystallization from hot EtOAc/hexane as white crystals (359 mg, 71% yield). **M.p.**: 228.1–230.5 °C. **^{1}H NMR** (400 MHz, $CDCl_3$): δ 8.61 (dd, J = 8.4, 8.4 Hz, 1H), 7.64 (dd, J = 7.2, 7.2 Hz, 1H), 7.51 (dd, J = 7.6, 7.6 Hz, 1H), 7.45–7.32 (m, 1H), 3.17–3.02 (m, 2H), 2.27–2.14 (m, 2H), 2.14–1.94 (m, 4H), 1.94–1.53 (m, 16H), 1.53–1.02 (m, 20H). **^{13}C NMR** (100.5 MHz, $CDCl_3$): δ 139.27 (dd, $J_{C–P}$ = 71.9, 6.6 Hz), 137.4 (dd, $J_{C–P}$ = 8.6, 5.7 Hz), 133.5 (dd, $J_{C–P}$ = 82.4, 7.7 Hz), 130.8–130.1 (m, 2C), 129.3 (d, J = 11.7 Hz), 38.6 (d, $J_{C–P}$ = 65.1 Hz, 2C), 38.3 (d, $J_{C–P}$ = 66.1 Hz, 2C), 27.2–25.6 (m, 20C). **^{31}P NMR** (161.8 MHz, $CDCl_3$): δ 52.7, 48.8. **IR** (ATR): 2989, 2932, 1394, 1250, 1066, 1057, 892 cm^{-1}. **HRMS-FD** (*m/z*): $[M]^+$ Cacld for $C_{30}H_{48}O_2P_2$, 502.3130; found, 502.3120.

(*S*,*S*)-1,2-Bis(*tert*-butylphenylphosphinoyl)benzene [(*S*,*S*)-4b]

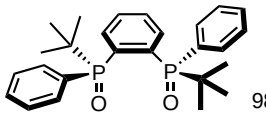

98:2 e.r.

[**1q** (0.125 mmol), (*S*)-**2e** (4 equiv), KHMDS (4 equiv), THF (0.25 M), 50 °C, 48 h] The product (*S*,*S*)-**4b** was isolated by flash chromatography on silica gel with slow gradient elution (CH_2Cl_2/MeOH, 100:0-to-93:7) as a white powder (53.2 mg, 97% yield, 98:2 e.r.). **M.p.**: 310 °C (decomp.). **^{1}H NMR** (400 MHz, $CDCl_3$): δ 8.51–8.41 (m, 2H), 7.77–7.67 (m, 2H), 7.25–7.15 (m, 6H), 7.00 (td, J = 7.4, 2.4 Hz, 4H), 1.32 (d, J = 14.4 Hz, 18H). **^{13}C NMR** (100.5 MHz, $CDCl_3$): δ 136.6 (dd, $J_{C–P}$ = 84.3, 7.6 Hz, 2C), 135.3 (t, $J_{C–P}$ = 9.6 Hz, 2C), 132.4 (d, $J_{C–P}$ = 93.9 Hz, 2C), 131.7–131.3 (m, 4C), 130.3 (2C), 129.9 (dd, $J_{C–P}$ = 12.5, 4.8 Hz, 2C), 127.3–127.0 (m, 4C), 35.8 (d, $J_{C–P}$ = 69.9 Hz, 2C), 26.9 (6C). **^{31}P NlMR** (161.8 MHz, $CDCl_3$): δ 43.4. **IR** (ATR): 2963, 1476, 1436, 1180, 1152, 1099, 813, 765, 743, 729, 716, 705, 692, 615 cm^{-1}. **HRMS-FD** (*m/z*): $[M+H]^+$ Cacld for $C_{26}H_{33}O_2P_2$, 439.1956; found, 439.1964. $[\alpha]_D^{27}$ = –39.39 (*c* = 1.10, $CHCl_3$).

(*S*)-Di-*tert*-butyl(2-(*tert*-butyl(phenyl)phosphinoyl)phenyl)phosphine Oxide [(*S*)-4d]

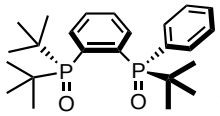

98:2 e.r.

[0.125 mmol scale, CPME, 120 °C, 24 h] The product (*S*)-**4d** was purified by automatic flash chromatography (RediSep® FlashColumn 12 g, $CHCl_3$/MeOH 100:0-to-90:10) followed by preparative thin-layer chromatography (CH_2Cl_2/MeOH, 92:8) as white foam (36.6 mg, 70% yield, 98:2 e.r.). **^{1}H NMR** (400 MHz, $CDCl_3$): δ 8.46 (t, J = 9.2 Hz, 1H), 7.73 (td, J = 9.2, 2.0 Hz, 1H), 7.68–7.50 (m, 4H), 7.39–7.29 (m, 3H), 1.39 (d, J = 13.6 Hz, 9H), 1.17 (d, J = 13.6 Hz, 9H), 1.01 (d, J = 13.2 Hz, 9H). **^{13}C NMR** (100.5 MHz, $CDCl_3$): δ 138.7 (d, $J_{C–P}$ = 81.5 Hz), 136.8 (d, $J_{C–P}$ = 74.8 Hz), 134.6–134.2 (m), 133.6–133.0 (m), 132.2 (d, $J_{C–P}$ = 9.6 Hz, 2C), 129.7, 129.3 (d, $J_{C–P}$ = 10.6 Hz), 128.6 (d, $J_{C–P}$ = 9.7 Hz), 126.6 (d, $J_{C–P}$ = 12.5 Hz, 2C), 37.8 (d, $J_{C–P}$ = 73.8 Hz), 37.2 (d, $J_{C–P}$ = 72.9 Hz), 35.8 (d, $J_{C–P}$ = 71.9 Hz), 28.1 (3C), 27.4 (3C), 27.0 (3C). One carbon is missing due to overlapping. **^{31}P NMR** (161.8 MHz, $CDCl_3$): δ 54.7, 42.6. **IR** (ATR): 3047, 2964, 2900, 1474, 1439, 1394, 1369, 1216, 1197, 1173, 1132, 1116, 1070, 1056, 1020, 935, 812, 785, 752, 734, 708, 700, 667, 640, 609, 591, 529, 517 cm^{-1}. **HRMS-FD** (*m/z*): $[M+H]^+$ Cacld for $C_{24}H_{37}O_2P_2$, 419.2269; found, 419.2253. $[\alpha]_D^{27}$ = +3.50 (*c* = 1.00, $CHCl_3$).

2.4.10 HPLC Charts

(*S*)-**3x**

The e.r. value (99:1) was determined by chiral HPLC analysis [CHIRALCEL® IG-3 column, 4.6 mmφ × 250 mmL, Daicel Chemical Industries], hexane/*i*PrOH = 92:8, 1.0 mL/min, 25 °C, 220 nm UV detector, retention time = 62.95 min (major), 68.01 min (minor).

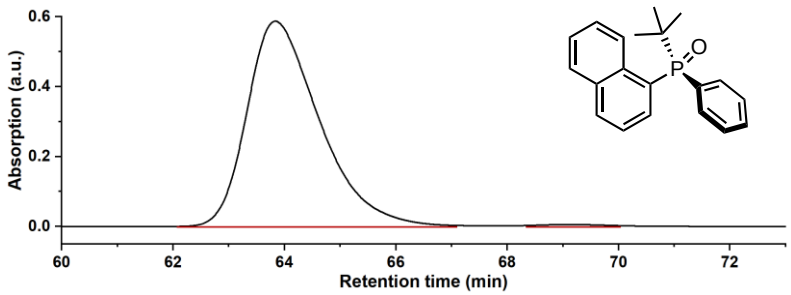

Retention time (min)	Area	Area%
63.84	26587089	99.35
69.07	172477	0.65

rac-**3x**

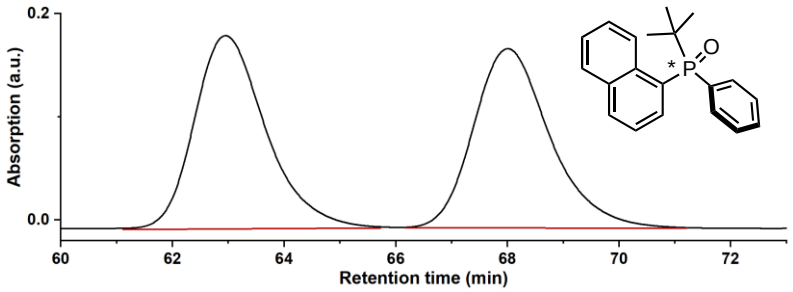

Retention time (min)	Area	Area%
62.95	8282362	50.04
68.01	8267999	49.96

(*S*,*S*)-**4b**

The e.r. value (98:2) was determined by chiral HPLC analysis [CHIRALCEL® OZ-H column, 4.6 mmφ×250 mmL, Daicel Chemical Industries], hexane/*i*PrOH = 80:20, 1.0 mL/min, 40 °C, 220 nm UV detector, retention time = 7.88 min (minor), 8.81 min (meso), 9.67 min (major).

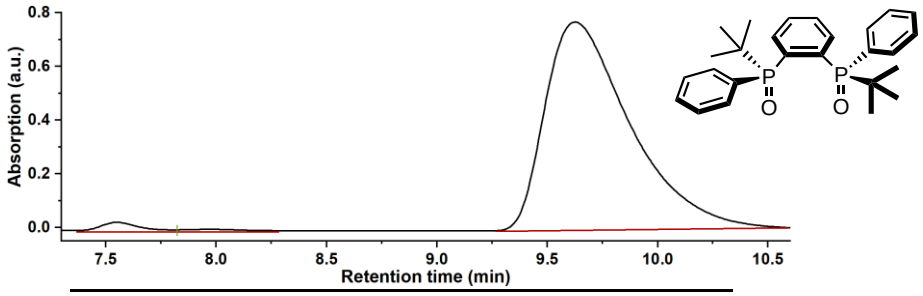

Retention time (min)	Area	Area%
7.55	176709	1.62
9.63	10736762	98.38

rac-**4b**

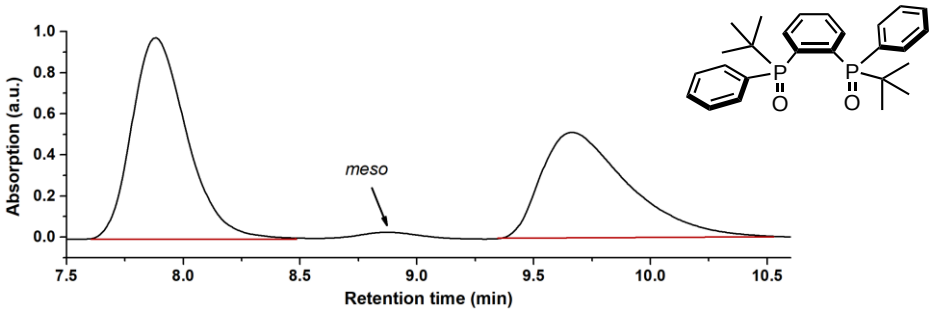

Retention time (min)	Area	Area%
7.88	8012808	52.99
9.67	7108439	47.01

(*S*)-**4d**

The e.r. value (98:2) was determined by chiral HPLC analysis [CHIRALCEL® OZ-H column, 4.6 mmφ×250 mmL, Daicel Chemical Industries], hexane/*i*PrOH = 96:4, 2.0 mL/min, 40 °C, 220 nm UV detector, retention time = 23.41 min (major), 35.87 min (minor).

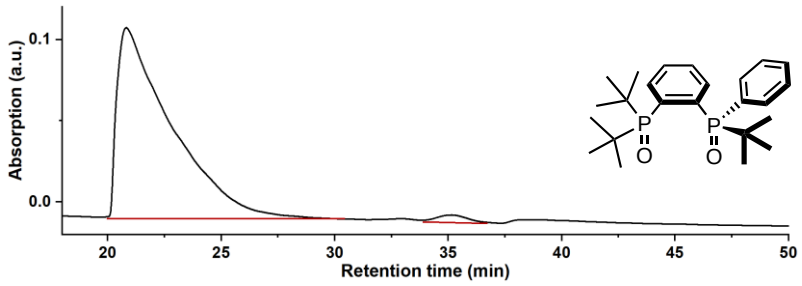

Retention time (min)	Area	Area%
20.81	9744444	98.49
35.15	149165	1.51

rac-**4d**

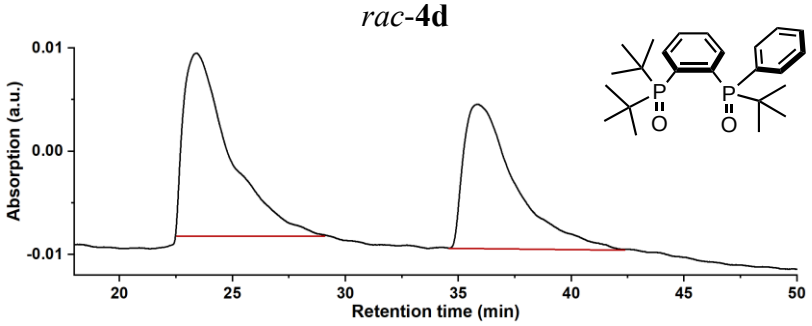

Retention time (min)	Area	Area%
23.41	1301790	53.01
35.87	1154197	46.99

2.5 References

[1] J. F. Bunnett, R. E. Zahler. Aromatic Nucleophilic Substitution Reactions. *Chem. Rev.* **1951**, *49*, 273–412.

[2] F. Terrier. Rate and Equilibrium Studies in Jackson-Meisenheimer Complexes. *Chem. Rev.* **1982**, *82*, 77–152.

[3] V. M. Vlasov. Fluoride Ion as a Nucleophile and a Leaving Group in Aromatic Nucleophilic Substitution Reactions. *J. Fluor. Chem.* **1993**, *61*, 193–216.

[4] S. Rohrbach, A. J. Smith, J. H. Pang, D. L. Poole, T. Tuttle, S. Chiba, J. A. Murphy. Concerted Nucleophilic Aromatic Substitution Reactions. *Angew. Chem. Int. Ed.* **2019**, *58*, 16368–16388; *Angew. Chem.* **2019**, *131*, 16518–16540.

[5] A. J. J. Lennox. Meisenheimer Complexes in S_NAr Reactions: Intermediates or Transition States? *Angew. Chem. Int. Ed.* **2018**, *57*, 14686–14688; *Angew. Chem.* **2018**, *130*, 14898–14900.

[6] C. N. Neumann, T. Ritter. Facile C–F Bond Formation through a Concerted Nucleophilic Aromatic Substitution Mediated by the PhenoFluor Reagent. *Acc. Chem. Res.* **2017**, *50*, 2822–2833.

[7] S. Rohrbach, J. A. Murphy, T. Tuttle. Computational Study on the Boundary Between the Concerted and Stepwise Mechanism of Bimolecular S_NAr Reactions. *J. Am. Chem. Soc.* **2020**, *142*, 14871–14876.

[8] E. E. Kwan, Y. Zeng, H. A. Besser, E. N. Jacobsen. Concerted Nucleophilic Aromatic Substitutions. *Nat. Chem.* **2018**, *10*, 917–923

[9] C. N. Neumann, J. M. Hooker, T. Ritter. Concerted Nucleophilic Aromatic Substitution with $^{19}F^-$ and $^{18}F^-$. *Nature* **2016**, *534*, 369–373.

[10] For the S_NAr reaction of aryl fluorosulfonates with tetramethylammonium fluoride, which does not require an electron-withdrawing substituent at the aromatic ring, see: S. D. Schimler, M. A. Cismesia, P. S. Hanley, R. D. J. Froese, M. J. Jansma, D. C. Bland, M. S. Sanford. Nucleophilic Deoxyfluorination of Phenols *via* Aryl Fluorosufonate Intermediates. *J. Am. Chem. Soc.* **2017**, *139*, 1452–1455.

[11] A. Bhunia, S. R. Yetra, A. T. Biju. Recent Advances in Transition-Metal-Free Carbon-Carbon and Carbon-Heteroatom Bond-Forming Reactions Using Arynes. *Chem. Soc. Rev.* **2012**, *41*, 3140–3152.

[12] In the defluorosilylation of aryl fluorides with silyl lithium reagents, 4'-fluoro-2,4,6-trimethyl-1,1'-biphenyl with a large torsion angle was an unfavorable substrate for the concerted *ipso* substitution. See: S. Mallick, P. Xu, E.-U. Würthwein, A. Studer. Silyldefluorination of Fluoroarenes by Concerted Nucleophilic Aromatic

Substitution. *Angew. Chem. Int. Ed.* **2019**, *58*, 283–287; *Angew. Chem.* **2019**, *131*, 289–293.

[13] H. Xu, K. Yin, W. Huang. Highly Improved Electroluminescence from a Series of Novel Eu^{III} Complexes with Functional Single-Coordinate Phosphine Oxide Ligands: Tuning the Intramolecular Energy Transfer, Morphology, and Carrier Injection Ability of the Complexes. *Chem. Eur. J.* **2007**, *13*, 10281–10293.

[14] D. Kim, L. Zhu, J.-L. Brédas. Electronic Structure of Carbazole-Based Phosphine Oxides as Ambipolar Host Materials for Deep Blue Electrophosphorescence: A Density Functional Theory Study. *Chem. Mater.* **2012**, *24*, 2604–2610.

[15] K. Tamura, M. Sugiya, K. Yoshida, A. Yanagisawa, T. Imamoto. Enantiopure 1,2-Bis(*tert*-butylmethylphosphino)benzene as a Highly Efficient Ligand in Rhodium-Catalyzed Asymmetric Hydrogenation. *Org. Lett.* **2010**, *12*, 4400–4403.

[16] T. Imamoto, K. Tamura, Z. Zhang, Y. Horiuchi, M. Sugiya, K. Yoshida, A. Yanagisawa, I. D. Gridnev. Rigid *P*-Chiral Phosphine Ligands with *tert*-Butylmethylphosphino Groups for Rhodium-Catalyzed Asymmetric Hydrogenation of Functionalized Alkenes. *J. Am. Chem. Soc.* **2012**, *134*, 1754–1769.

[17] A. J. Kendall, D. T. Seidenkranz, D. R. Tyler. Improved Synthetic Route to Heteroleptic Alkylphosphine Oxides. *Organometallics* **2017**, *36*, 2412–2417.

[18] For theoretically calculated pK_a values of organophosphorus compounds, including secondary phosphine oxides, in DMSO, see: J.-N. Li, L. Liu, Y. Fu, Q.-X. Guo. What are the Pk_a Values of Organophosphorus Compounds? *Tetrahedron* **2006**, *62*, 4453–4462.

[19] Y. Zhao, D. G. Truhlar. The M06 Suite of Density Functionals for Main Group Thermochemistry, Thermochemical Kinetics, Noncovalent Interactions, Excited States, and Transition Elements: Two New Functionals and Systematic Testing of Four M06-Class Functionals and 12 Other Functionals. *Theor. Chem. Acc.* **2008**, *120*, 215–241.

[20] A. Hellweg, D. Rappoport. Development of New Auxiliary Basis Functions of the Karlsruhe Segmented Contracted Basis Sets Including Diffuse Basis Functions (def2-SVPD, def2-TZVPPD, and def2-QVPPD) for RI-MP2 and RI-CC Calculations. *Phys. Chem. Chem. Phys.* **2015**, *17*, 1010–1017.

[21] F. Weigend, R. Ahlrichs. Balanced Basis Sets of Split Valence, Triple Zeta Valence and Quadruple Zeta Valence Quality for H to Rn: Design and Assessment of Accuracy. *Phys. Chem. Chem. Phys.* **2005**, *7*, 3297–3305.

[22] F. Weigend. Accurate Coulomb-Fitting Basis Sets for H to Rn. *Phys. Chem. Chem. Phys.* **2006**, 1057–1065.

[23] K. Sünkel, S. Weigand, A. Hoffmann, S. Blomeyer, C. G. Reuter, Y. V. Vishnevskiy, N. W. Mitzel. Synthesis and Characterization of 1,2,3,4,5-Pentafluoroferrocene. *J. Am. Chem. Soc.* **2015**, *137*, 126–129.

[24] S. Montel, T. Jia, P. J. Walsh. Palladium-Catalyzed α-Arylation of Benzylic Phosphine Oxides. *Org. Lett.* **2014**, *16*, 130–133.

[25] K. A. Smoll, W. Kaminsky, K. I. Goldberg. Photolysis of Pincer-Ligated Pd^{II}–Me Complexes in the Presence of Molecular Oxygen. *Organometallics* **2017**, *36*, 1213–1216.

[26] C. A. Busacca, J. C. Lorenz, N. Grinberg, N. Haddad, M. Hrapchak, B. Latli, H. Lee, P. Sabila, A. Saha, M. Sarvestani, S. Shen, R. Varsolona, X. Wei, C. H. Senanayake. A Superior Method for the Reduction of Secondary Phosphine Oxides. *Org. Lett.* **2005**, *7*, 4277–4280.

[27] R. Beaud, R. J. Phipps, M. J. Gaunt. Enantioselective Cu-Catalyzed Arylation of Secondary Phosphine Oxides with Diaryliodonium Salts toward the Synthesis of *P*-Chiral Phosphines. *J. Am. Chem. Soc.* **2016**, *138*, 13183–13186.

[28] J. Drabowicz, P. Łyżwa, J. Omelańczuk, K. M. Pietrusiewicz, M. Mikołajczyk. New Procedure for the Resolution of Chiral *tert*-Butylphenylphosphine Oxide and Some of Its Reactions. *Tetrahedron: Asymmetry* **1999**, *10*, 2757–2763.

[29] V. Barone, M. Cossi. Quantum Calculation of Molecular Energies and Energy Gradients in Solution by a Conductor Solvent Moedel. *J. Phys. Chem. A* **1998**, *102*, 1995–2001.

[30] M. Cossi, N. Rega, G. Scalmani, V. Barone. Energies, Structures, and Electronic Properties of Molecules in Solution with the C-PCM Solation Model. *J. Comput. Chem.* **2003**, *24*, 669–681.

[31] Global Reaction Route Mapping (GRRM) program, Version 17-A01, S. Maeda, Y. Harabuchi, Y. Sumiya, M. Takagi, K. Suzuki, K. Sugiyama, Y. Ono, M. Hatanaka, Y. Osada, T. Taketsugu, K. Morokuma, K. Ohno, **2017**.

[32] GaussView, Version 6.1, R. Dennington, T. A. Keith, J. M. Millam, Semichem Inc., Shawnee Mission, KS, **2016**.

[33] Information of def2TZVPD basis set was obtained from the following URL site, *Basis Set Exchange* (https://www.basissetexchange.org). For more details, See: B. P. Pritchard, D. Altarawy, B. Didier, T. D. Gibson, T. L. Windus. New Basis Set Exchange: An Open, Up-to-Date Resource for the Molecular Sciences Community. *J. Chem. Inf. Model.* **2019**, *59*, 4814–4820.

[34] N. Chéron, D. Jacquemin, P. Fleurat-Lessard. A Qualitative Failure of B3LYP for Textbook Organic Reactions. *Phys. Chem. Chem. Phys.* **2012**, *14*, 7170–7175.

[35] *CrysAlisPro*, version 1.171.39.45h; Rigaku Corporation, Oxford,UK, **2018**.

[36] G. M. Sheldrick. *SHELXT* - Integrated Space-Group and Crystal-Structure Determination. *Acta Crystallogr.* **2015**, *A71*, 3–8.

[37] G. M. Sheldrick. A Short History of *SHELX Acta Crystallogr. Sect. A: Found. Crystallogr.* **2008**, *A64*, 112−122.

[38] O. V. Dolomanov, L. J. Bourhis, R. J. Gildea, J. A. K. Howard, H. Pushmann. *OLEX2*: A Complete Structure Solution, Refinement and Analysis Program. *J. Appl. Crystallogr.* **2009**, *42*, 339−341.

[39] C. A. Busacca, R. Raju, N. Grinberg, N. Haddad, P. Jame-Jones, H. Lee, J. C. Lorenz, A. Saha, C. H. Senanayake. Reduction of Tertiary Phosphine Oxides with DIBAL-H. *J. Org. Chem.* **2008**, *73*, 1524–1531.

[40] R. Yu, X. Chen, Z. Wang. Palladium-Catalyzed C−P(III) Bond Formation Reaction with Acylphosphines as Phosphorus Source. *Tetrahedron Lett.* **2016**, *57*, 3404–3406.

[41] C. Bailie, L. Zhang, J. Xiao. Ferrocenyl Monophosphine Ligands: Synthesis and Applications in the Suzuki-Miyaura Coupling of Aryl Chlorides. *J. Org. Chem.* **2004**, *69*, 7779–7782.

[42] J.-S. Zhang, T. Chen, L.-B. Han. Palladium-Catalyzed Direct Decarbonylative Phosphorylation of Benzoic Acids with P(O)–H Compounds. *Eur. J. Org. Chem.* **2020**, 1148–1153.

[43] D. Zhang, J. A. Celaje, A. Agua, C. Doan, T. Steward, R. Bau, M. Selke. Photooxidation of Mixed Aryl and Biarylphosphines. *Org. Lett.* **2010**, *12*, 3100–3103.

[44] C. Baillie, J. Xiao. Palladium-Catalyzed Synthesis of Biaryl Phosphines. *Tetrahedron* **2004**, *60*, 4159–4168.

[45] J. Chrzanowski, D. Krasowska, M. Urbaniak, L. Sieroń, P. Pokora-Sobczak, O. M. Demchuk, J. Drabowicz. Synthesis of Enantioenriched Aryl-*tert*-Butylphenylphosphine Oxides *via* Cross-Coupling Reactions of *tert*-Butylphenylphosphine Oxide with Aryl Halides. *Eur. J. Org. Chem.* **2018**, 4614–4627.

Chapter 3

Nickel-Catalyzed Defluorophosphonylation of Aryl Fluorides

3.1 Introduction

The classical approach to C–F to C–P bond transformation involves a S_NAr-type reaction with phosphorus pro-nucleophiles, which are limited to secondary phosphines and phosphine oxides, and the use of more electron-deficient phosphonic acid diesters [$HP(O)(OR)_2$] has not been reported. Organophosphonic acids [$RP(O)(OH)_2$] and their derivatives are widely used as drugs or pro-drugs,[1, 2] chelators of metallic salts,[3, 4] surface modifiers,[5] and phosphoantigens.[6] Thus, the development of a phosphonylation reaction of aryl fluorides is demanded. However, the literature contains only one example of $C(sp^2)$–F bond phosphonylation, which was achieved *via* a photoinduced SET process that required photo-irradiation with ultraviolet light (λ = 254 nm).[7]

In chapter 2, a nucleophile-dependent S_NAr reaction of non-activated aryl fluorides with potassium diorganophosphinites ($R_2PO^-K^+$) has been introduced. In this reaction, the K^+ cation plays a critical role, stabilizing the negative charge of the leaving F^- anion. With this knowledge, the author hypothesized combining the K^+ cation with the well-established ability of a Ni catalyst to activate C–F bonds and thereby achieve phosphonylation of aryl fluorides.

In this chapter, the author reports a Ni-catalyzed cross-coupling reaction between aryl fluorides and dialkyl phosphonates [$HP(O)(OR)_2$] in the presence of KO*t*Bu as a stoichiometric base. The reaction uses commercially available Ni complexes as catalyst precursors and requires no exogeneous ligands. A wide range of aryl fluorides were successfully converted into the corresponding aryl phosphonates. Interestingly, the reaction proceeds specifically with di-*sec*-alkyl phosphonates. Mechanistic studies suggested that the catalytic cycle involves turnover-limiting oxidative addition of the aryl fluoride to a Ni(0) complex coordinated with potassium dialkyl phosphites [$(RO)_2PO^-K^+$] through cooperative action of a Ni(0)–K^+ bimetallic system.

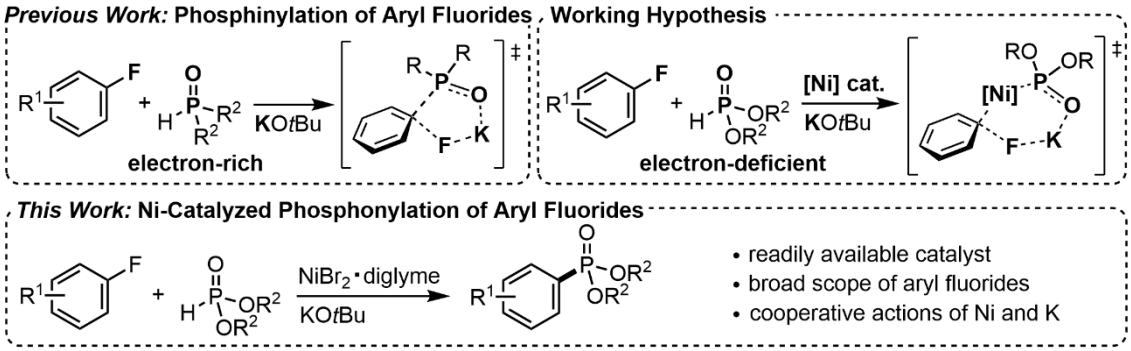

Figure 3.1. Defluorinative C–P bond formation.

3.2 Results and Discussion

To begin with, the reaction between 4-fluorobiphenyl (**1a**, 0.125 mmol) and dicyclohexyl phosphonate (**2a**, 0.25 mmol) in the presence of $NiBr_2$·diglyme (5 mol%, 0.00625 mmol) and KO*t*Bu (0.25 mmol) in toluene (0.5 mL) at 120 °C led to the clean and complete conversion of **2a** to the corresponding defluorinative phosphonylation product (**3a**) in quantitative yield (99% based on ^{1}H NMR spectroscopy) (Table 3.1, entry 1). When the amount of KO*t*Bu was decreased to 0.125 mmol (1 equiv to **1a**, 0.5 equiv to **2a**), product **3a** was not obtained, suggesting the formation of an inactive Ni species through the direct reaction of a Ni species with nondeprotonated dialkyl phosphonate **2a** (entry 2). NiI_2 exhibited a catalytic performance similar to that of $NiBr_2$·diglyme (entry 3), whereas other Ni(II) complexes such as $NiCl_2$ and $Ni(acac)_2$ (acac = acetylacetonate) gave **3a** in moderate yields (entries 4–6). Notably, the Ni(0) complex, $Ni(cod)_2$ (cod = 1,5-cyclooctadiene) also catalyzed the present reaction, suggesting that Ni(0) is an active species in the catalytic process (entry 7). No reaction occurred in the absence of a Ni catalyst (entry 8). The base strongly influenced the reaction efficiency. Specifically, the use of bases that have smaller cations (e.g., NaO*t*Bu and LiO*t*Bu) in place of KO*t*Bu in entry 1 resulted in a substantial decrease in the product yield (entries 9 and 10). The phosphonylation product **3a** was not obtained at all with less basic potassium salts such as K_2CO_3 and K_3PO_4 (entries 11 and 12). The addition of exogeneous ligands did not substantially affect the product yield (see Experimental Section for details).

Table 3.1. Ni-catalyzed phosphonylation of 4-fluorobiphenyl (**1a**) with dicyclohexyl phosphonate (**2a**)[a]

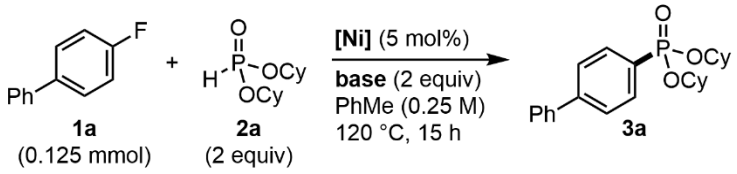

Entry	[Ni]	Base	Yield of **3a**[b]
1	$NiBr_2$·diglyme	KO*t*Bu	99%
2[c]	$NiBr_2$·diglyme	KO*t*Bu	0%
3	NiI_2	KO*t*Bu	99%
4	$NiBr_2$	KO*t*Bu	55%
5	$NiCl_2$	KO*t*Bu	62%
6	$Ni(acac)_2$	KO*t*Bu	77%
7	$Ni(cod)_2$	KO*t*Bu	70%
8	None	KO*t*Bu	0%
9	$NiBr_2$·diglyme	NaO*t*Bu	33%
10	$NiBr_2$·diglyme	LiO*t*Bu	2%
11	$NiBr_2$·diglyme	K_2CO_3	0%
12	$NiBr_2$·diglyme	K_3PO4	0%

[a] Reaction conditions: **1a** (0.125 mmol), **2a** (0.25 mmol), Ni complexes (0.00625 mmol, 5 mol% to 1a), base (0.25 mmol), toluene (0.5 mL), 120 °C, 15 h. [b] ^{1}H NMR yield obtained using 1,3,5-trimethoxybenzene as an internal standard. [c] 0.125 mmol of base. acac = acetylacetonate, cod = 1,5-cyclooctadiene, HMDS = hexamethyldisilazide.

With the optimal conditions in hand, the substrate scope was investigated (Scheme 3.1). Aryl fluorides possessing electron-donating substituents such as methoxy (OMe), dimethylamino (NMe_2), diphenylamino (NPh_2), and methyl (Me) groups participated in the phosphonylation reaction to afford the corresponding aryl phosphonates in good yields (**3b**–**3e**). Simple fluorobenzene also exhibited excellent reactivity, forming **3f** in 90% yield. Electron-withdrawing amide groups were tolerated on the aromatic ring, and the corresponding products **3g** and **3h** were obtained in 86% and 74% yields, respectively. However, the aryl fluoride with a highly electron-withdrawing trifluoromethyl group resulted in a low yield of **3i** (15% yield). π-Extended aryl fluorides were suitable substrates for the present phosphonylation reaction, and the corresponding products were obtained in excellent yields (**3j**–**3l**). However, 2-fluorobiphenyl and 1-fluoro-2,6-dimethylbenzene did not give products **3m** and **3n**. Heteroaryl fluorides were successfully

converted to the corresponding phosphonates (**3o** and **3p**). For the synthesis of **3b**,**3d**, **3k**, the reaction was conducted with $Ni(cod)_2$ and potassium hexamethyldisilazide (KHMDS) because the protocol with $NiBr_2$·diglyme and KO*t*Bu produced small amounts of phosphorus-containing byproducts, which hampered the isolation of the pure products.

Next, the scope of dialkyl phosphonates was examined. Diisopropyl phosphite (**2b**) afforded the corresponding phosphonate **3q** in 84% yield, whereas dialkyl phosphonates with tertiary (**2c**) or primary (**2d**) *O*-alkyl groups failed to give the products (**3r**, **3s**). Diphenyl phosphonate (**2e**) also exhibited no reactivity. Thus, the present reaction was specifically possible with phosphonates with two secondary *O*-alkyl groups. Racemic phosphinate **3u** was obtained in 53% yield from 4-fluorobiphenyl and cyclohexyl phenylphosphinate (**2f**) under slightly modified reaction conditions.

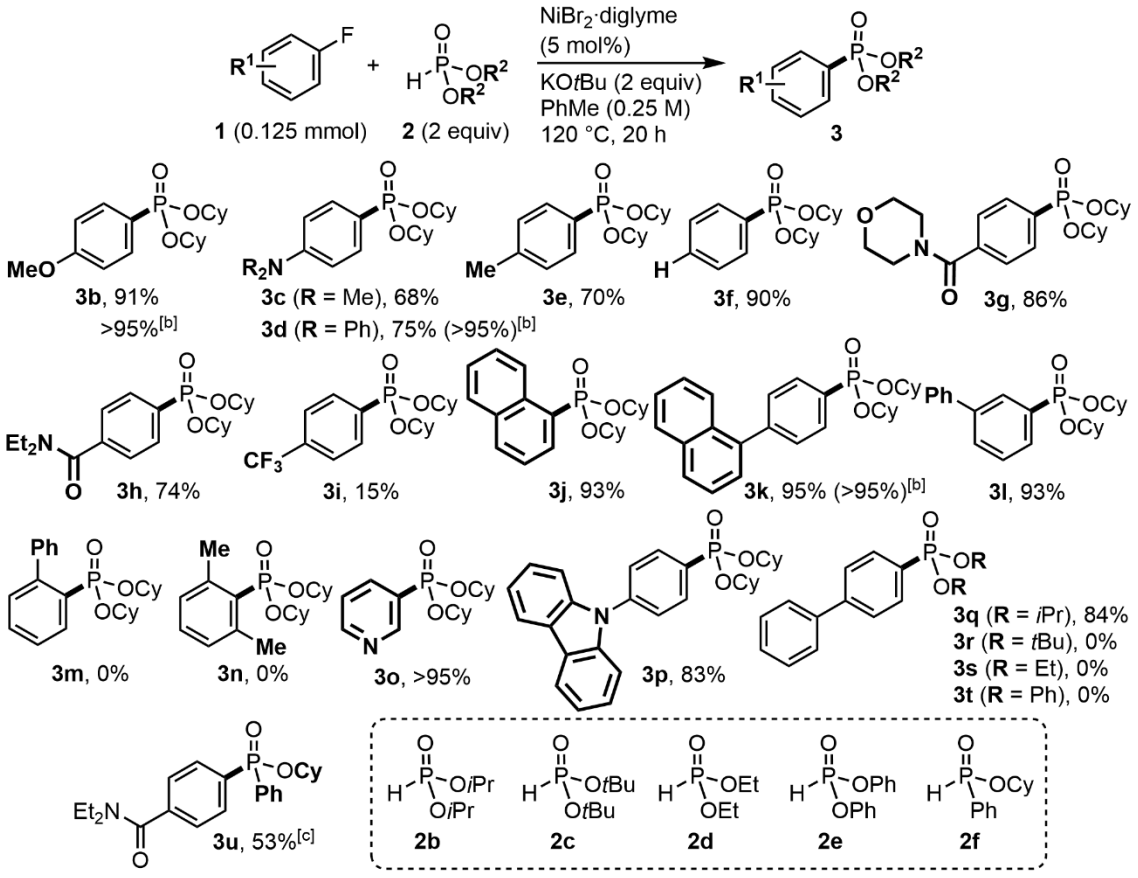

Scheme 3.1. Scope of aryl fluorides and dialkyphosphonates.[a]

[a] Reaction conditions: **1** (0.125 mmol), **2** (0.25 mmol), $NiBr_2$·diglyme (0.00625 mmol, 5 mol% to **1**), KO*t*Bu (0.25 mmol), PhMe (0.5 mL), 120 °C, 20 h. Yields of isolated products are shown. [b] $Ni(cod)_2$ (0.00625 mmol) as catalyst, KHMDS (0.25 mmol) as base. [c] THF as a solvent, 80 °C, 20 h.

The reaction was applicable for a gram-scale synthesis. When the reaction of aryl fluoride **1b** with phosphonate **2b** was carried out on a 5.0 mmol scale, 1.1 g of arylphosphonate **3v** was isolated (84% yield, Scheme 3.2a). Defluorinative phosphonylation of *N*-methyl paroxetine, an antidepressant, afforded the corresponding arylphosphonate **3w** in 50% yield, demonstrating the potential of the present protocol for the synthesis of structurally complicated organophosphorus compounds using scaffolds of biologically functional molecules (Scheme 3.2b). Twofold defluorophosphonylation occurred with 1,4-difluorobenzene **4** under slightly modified reaction conditions, affording the corresponding *p*-phenylenediphosphonic acid ester **5** in 63% yield (Scheme 3.2c).

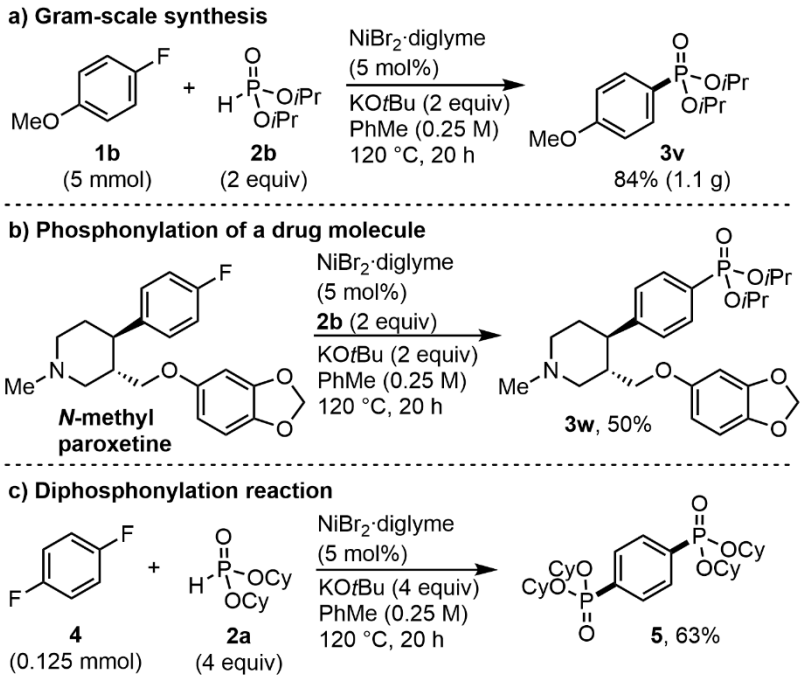

Scheme 3.2. Synthetic applications.

To gain insights into the reaction mechanism, a series of control experiments were performed. Under the standard conditions, the reaction between **1a** and **2a** delivered the corresponding aryl phosphonate **3a** in 99% yield (Table 3.2, entry 1). The addition of 18-crown-6 (2 equiv) inhibited the reaction completely, suggesting direct participation of a potassium cation in the catalysis (entry 2). Although KHMDS is sufficiently basic to deprotonate dialkyl phosphonaets. Using KHMDS with $NiBr_2$·diglyme catalysts failed to give **3a** (entry 3). By contrast, the use of KHMDS with $Ni(cod)_2$ instead of $NiBr_2$·diglyme afforded **3a** in a quantitative yield (entry 4), suggesting that catalytically active nickel

species were generated from the reduction of a Ni(II) pre-catalyst with potassium *tert*-butoxide but not with KHMDS.

Table 3.2. Control experiments[a]

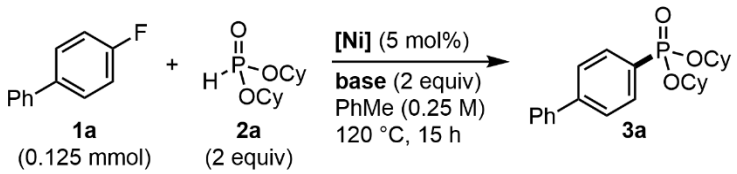

Entry	[Ni]	Base	Yield of **3a**[b]
1	$NiBr_2$·diglyme	KO*t*Bu	99%
2[c]	$NiBr_2$·diglyme	KO*t*Bu	0%
3	$NiBr_2$·diglyme	KHMDS	0%
4	$Ni(cod)_2$	KHMDS	99%

[a] Reaction conditions: **1a** (0.125 mmol), **2a** (0.25 mmol), Ni complexes (0.00625 mmol, 5 mol% to 1a), base (0.25 mmol), toluene (0.5 mL), 120 °C, 15 h. [b] ^{1}H NMR yield obtained using 1,3,5-trimethoxybenzene as an internal standard. [c] 18-Crown-6 (0.25 mmol, 2 equiv) was added.

Stoichiometric experiments with *H*-phosphonates [H(O)P(OR)$_2$] and potassium tert-butoxide (see Experimental Section for details) indicated the generation of potassium phosphite [KOP(OR)$_2$], which participated in the current defluorinative phosphonylation instead of *H*-phosphonates [H(O)P(OR)$_2$]. For gaining the further information about the *in situ* generated nickel species, a titration experiment between K[**2b**–H] and $Ni(cod)_2$ was carried out and monitored by ^{1}H NMR spectroscopy. As illustrated in Figure 3.2, when the increasing amount of K[**2b**–H] was added to $Ni(cod)_2$, the dissociation of cod from the nickel center and the formation of free cod were detected by ^{1}H NMR spectroscopy. Besides, ^{31}P{^{1}H} NMR analysis also confirmed the formation of phosphite-ligated Ni complex (see Experimental Section for details). After totally 5 equiv. of K[**2b**–H] had been added into a solution of $Ni(cod)_2$ in toluene-d_8, 1 equiv. of aryl fluoride **2b** was added into the reaction mixture, which was further heated at 120 °C for 15 h, resulting in the corresponding aryl phosphonate **3v** with an 84% yield. The experiment suggested the Ni species, which is generated from Ni(0) species and potassium phosphites [KOP(OR)$_2$], was plausible active species for the current defluorophosphonylation.

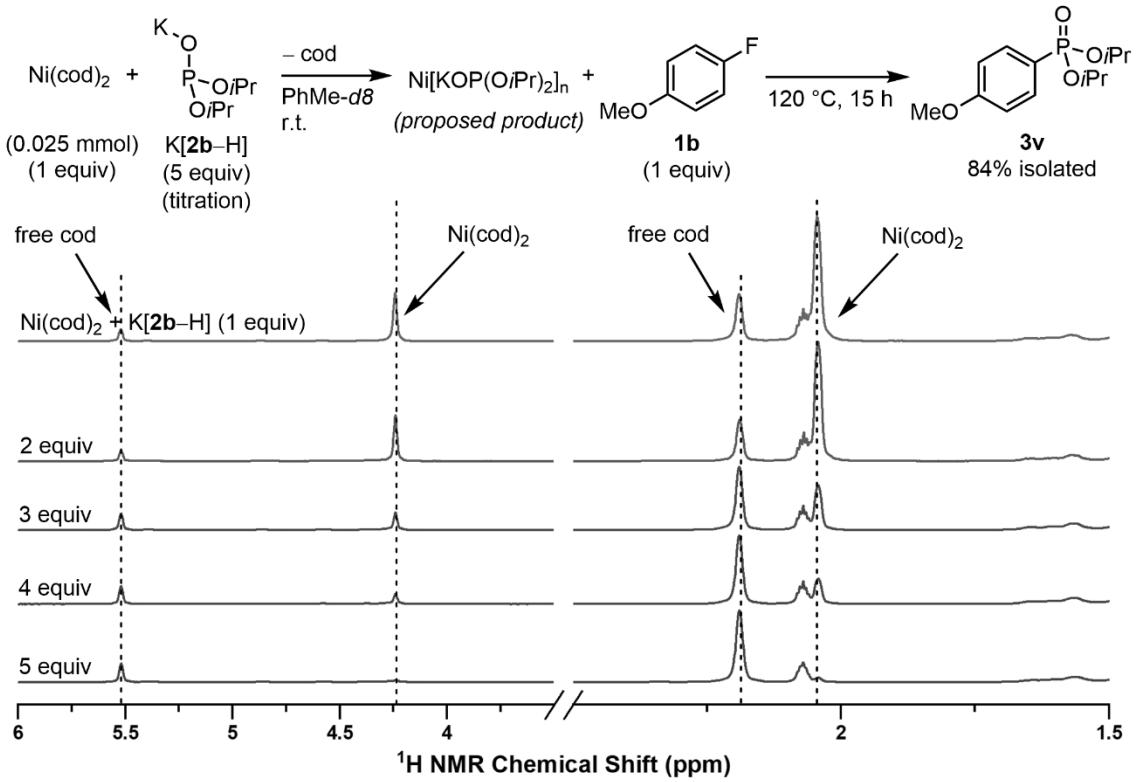

Figure 3.2. Complexation experiment and stoichiometric reaction.

To explain the specific reactivity of di-*sec*-alkyl phosphonates, we conducted reactions with a mixture of phosphonates with different *O*-alkyl groups (Scheme 3.3). When aryl fluoride **1b** was treated with a 1:1 mixture of diisopropyl and diethyl phosphonates (**1b** : **2b** : **2d** = 1:1:1) in the presence of $NiBr_2$·diglyme (5 mol%) and KO*t*Bu (2 equiv), no C–P coupling product was obtained, indicating that diethyl phosphonate (**2d**) inhibited the reaction of diisopropyl phosphonate (**2b**). Thus, the irreversible formation of a catalytically inactive species from **2d** and $NiBr_2$·diglyme is strongly suggested.

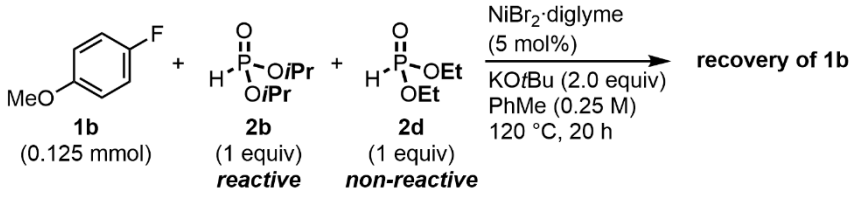

Scheme 3.3. Reactions with a mixture of phosphites.

To further investigate the reaction pathway of Ni complex, kinetic studies were carried out by *in situ* infrared (IR) spectroscopy for the reaction of potassium salt K[**2a**–H], which was formed in situ from *H*-phosphonate **2a** and KO*t*Bu base, with 4-methoxylphenyl fluoride (**1b**) promoted by $Ni(cod)_2$ in toluene at 120 °C (Scheme 3.4). The rate was found to be first order in both **1b** and $Ni(cod)_2$, suggesting that a reaction of the aryl fluoride with a monomeric Ni complex would be a turnover-limiting step. However, we failed to determine the reaction order for K[**2a**–H] because of its low solubility (see Experimental Section for details).

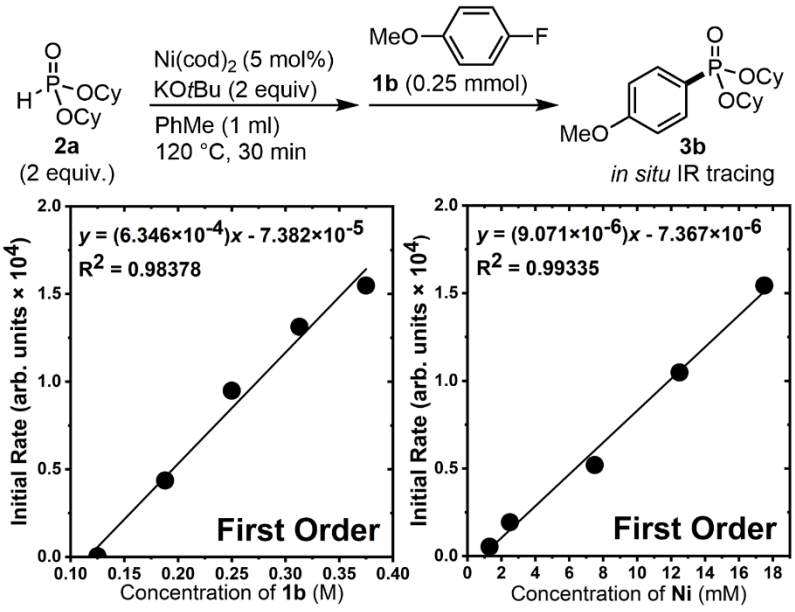

Scheme 3.4. Kinetic experiments.

For computational investigations, the author assumes metal chelation by ion-bridged dimers of the potassium dialkyl phosphites $\{M[P(OR)_2O^-K^+]_2\}$ on the basis of analogy with the chelation by hydrogen-bonded phosphorus dimers $[(RO)_2POH\cdots{}^-OP(OR)_2]$ reported in the literature.[8] Calculations were performed at the M06/SDD,6-311+G(d,p)/SMD//M06/lanl2dz,6-31G(d) level of theory using the Gaussian 16 package. To include solvent effects, the explicit coordination of a toluene molecule to each K^+ cation was considered in all the calculations. Energy profiles are given in Figure 3.3 for the oxidative addition of fluorobenzene (**1f**) to the Ni(0) complex $\{Ni^0[P(OiPr)_2OK]_2\cdot(toluene)_2\}$ coordinated with two $P(OiPr)_2OK$ ligands (Figure 3.3a) and for reductive elimination of the arylphosphonates $[PhP(O)(OiPr)_2]$ from Ni(II) complexes $\{[P(OiPr)_2OK]_2Ni^{II}(Ph)[P(O)(OiPr)_2]\cdot(toluene)_2\}$ (Figure 3.3b).

As shown in Figure 3.3a, the C–F bond oxidative addition of fluorobenzene to the Ni

center of Ni(0) intermediate **Int-1a** (R = *i*Pr) to produce the corresponding pseudo-square-planar Ni(II) intermediate (**Int-2a**) occurs with Lewis acidic direct participation of one of the K^+ cations, as indicated by the increase of the K···F interaction (from 2.76 Å to 2.46 Å) as the reaction proceeds from **Int-1a** to transition state $\mathbf{TS_{1a–2a}}$. This process is 10.9 kcal·mol^{-1} exergonic with a barrier of 14.1 kcal·mol^{-1}, altering the P–Ni–P bite angle from 105° (for **Int-1a**) to 96° (for **Int-2a**). We reason that not only the push–pull effect of the Ni–K^+ bimetallic system but also strong electron donation by the two anionic phosphorus ligands [P(O*i*Pr)$_2$O$^-$] facilitate the C–F bond oxidative addition.

Next, the author attempted to identify a transition state for the direct reductive elimination of PhP(O)(O*i*Pr)$_2$ from **Int-2a**; however, a reasonable transition-state structure was not found. This failure prompted us to investigate reductive elimination after ligand exchange at the Ni(II) center from the F^- anion to P(O*i*Pr)$_2$O$^-$. The geometry-optimized Ni(II) complex (**Int-3a**) with three anionic P ligands adopts a pseudo-square-planar geometry. The P–Ni–P bite angle (96°) with the original two P ligands is unchanged upon this ligand exchange. The computational estimation of the relative energy between **Int-2a** and **Int-3a** is too challenging because of the insoluble natures of KF and P(O*i*Pr)$_2$OK in the reaction system and was therefore not pursued in the present study. Reductive elimination from **Int-3a** proceeds through $\mathbf{TS_{3a-4a}}$ with an energy barrier (10.9 kcal·mol^{-1}) much lower than that for the oxidative addition process (14.1 kcal·mol^{-1}) to afford **Int-4a** with an η^2-coordinated phosphonylbenzene *via* a 7.2 kcal·mol^{-1} exergonic process.

We also conducted a computational study for the less favorable reaction with the bulkier phosphorus agent di-*tert*-butyl phosphonate (R = *t*Bu). The corresponding energy diagrams are given in Figure 3.3b. As in the case with diisopropyl phosphonate (R = *i*Pr), the C–F bond oxidative addition (**Int-1b**–$\mathbf{TS_{1b-2b}}$–**Int-2b**) proceeds with Lewis acidic participation of the K^+ cation, with an energy barrier of 15.8 kcal·mol^{-1}, which is only 1.7 kcal·mol^{-1} larger than that for the reaction with diisopropyl phosphate (R = iPr). Thus, the oxidative addition step is likely not responsible for the lower reactivity of di-*tert*-butyl phosphonate compared with that of diisopropyl phosphate. By contrast, the change of the phosphonate alkyl groups from *i*Pr ($\mathbf{TS_{3a-4a}}$) to *t*Bu ($\mathbf{TS_{3b-4b}}$) strongly influenced the ease of reductive elimination, increasing the energy barrier to 20.1 kcal·mol^{-1}. The energy barrier of $\mathbf{TS_{3b-4b}}$ is 9.2 kcal·mol^{-1} higher in energy than that for the reaction with the diisopropyl phosphonate, which is thereby deduced to be a reason for the experimentally observed inertness of H(O)P(O*t*Bu)$_2$ (**2c**). Steric congestion in $\mathbf{TS_{3b-4b}}$ is likely responsible for the increased energy barrier (see Experimental Section for further discussions).

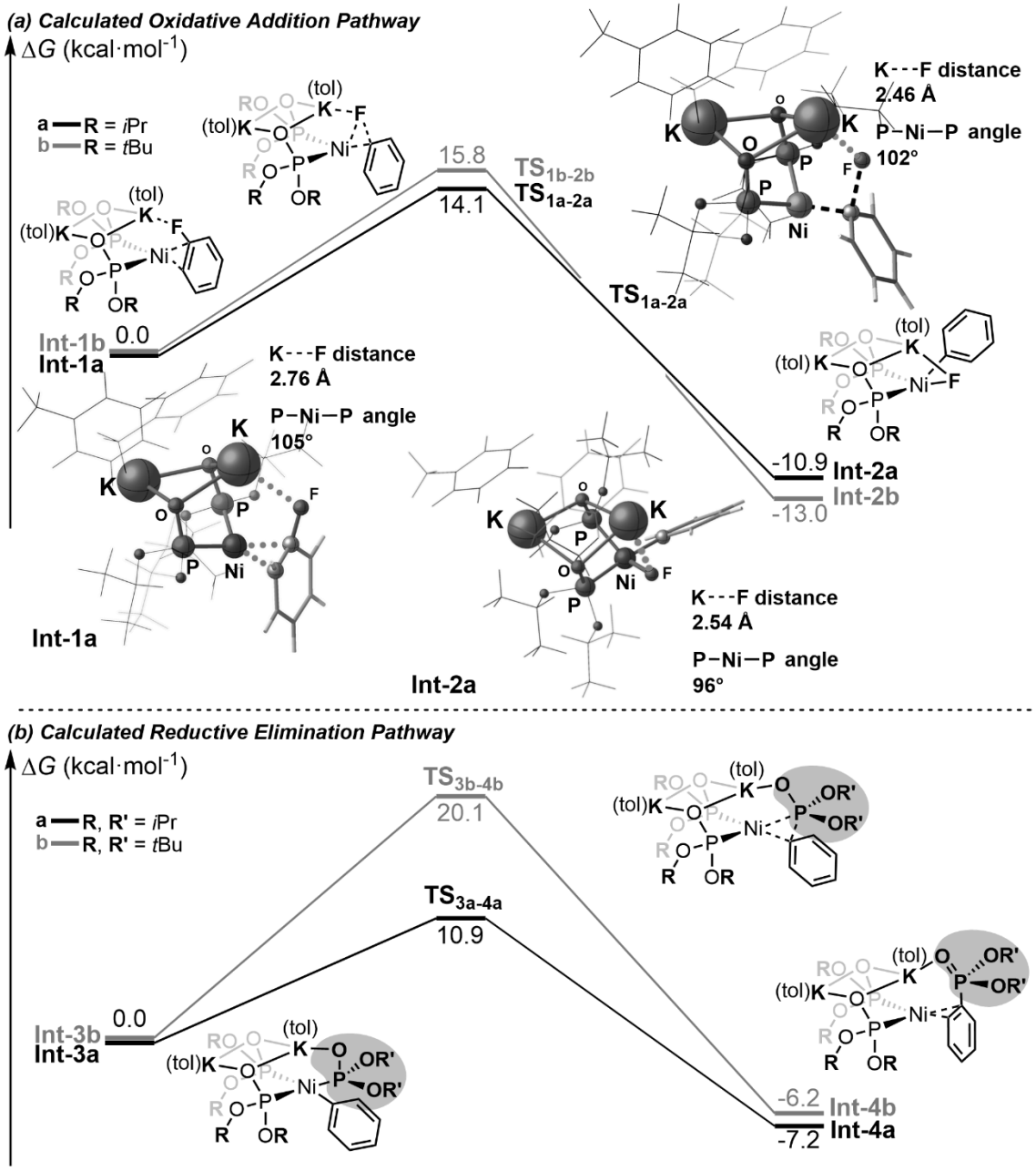

Figure 3.3. Energy profile of oxidative addition and reductive elimination steps calculated at [M06/SDD,6-311+G(d,p)/SMD//M06/lanl2dz,6-31G(d)] level of theory.

On the basis of the results of the experimental and theoretical studies, a proposed reaction mechanism is illustrated in Scheme 3.5. The catalyst precursor $NiBr_2$·diglyme is activated by $(OR)_2PO^-K^+$ (K[**2**–H]) generated by deprotonation of di-alkyl phosphonate **2** with KO*t*Bu to afford Ni(0) complexes $\{Ni[P(OR)_2OK]_n$ (n = 3, 4)$\}$ that chelated with a strongly electron-donating ion-bridged dimeric phosphite ligand system $[P(OR)_2O^-K^+]_2$ (for DFT calculation of Ni(II) reduction process, see Experimental Section). Ligand

exchange between one or two molecules of K[**2**–H] and aryl fluoride **1** gives a Ni(0) complex (**A**) η^2-coordinated with the aryl fluoride. The pronounced inhibitory effect by diethyl phosphonate **2d** is deduced to be attributable to the inertness of $Ni^0[P(OEt)_2OK]_n$ (n = 3, 4) toward ligand dissociation. Then, turnover-limiting oxidative addition of aryl fluoride **1** to the Ni center of **A** gives an aryl nickel(II) fluoride (**B**). Next, replacement of the F^- anion on the Ni center with a phosphonate anion $[\mathbf{2a}–H]^-$ forms aryl(phosphonyl)nickel(II) complex **C**. Finally, reductive elimination of arylphosphonate **3** from **C** and re-coordination of aryl fluoride **1** regenerates Ni(0) complex **A** to complete the catalytic cycle.

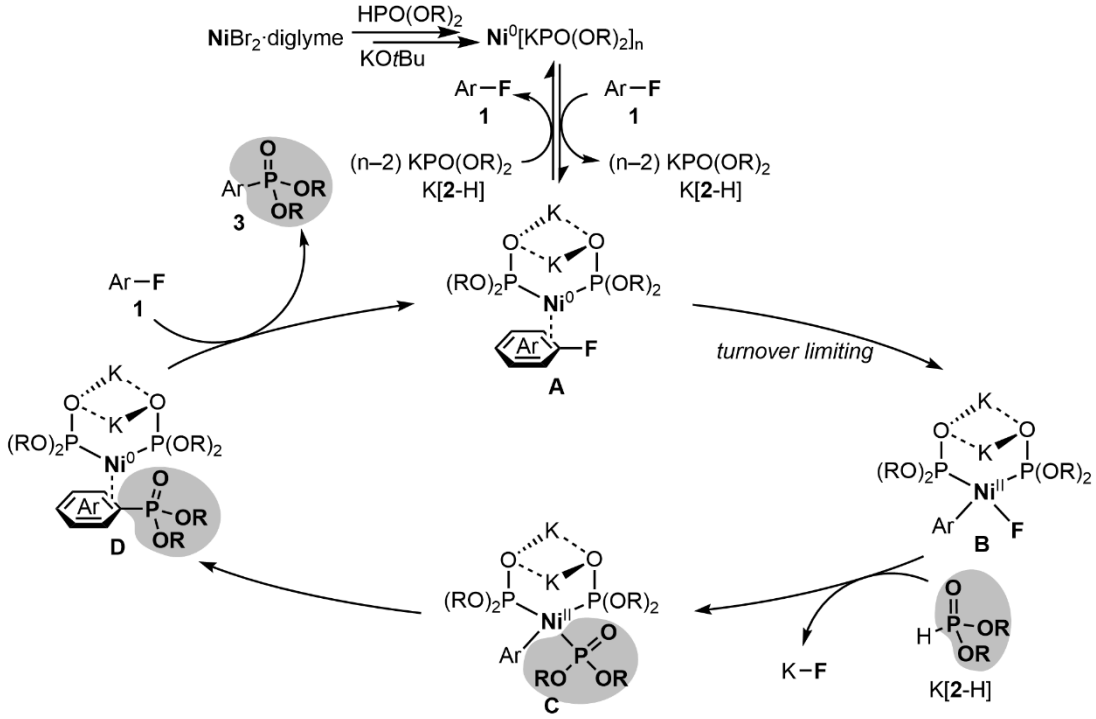

Scheme 3.5. A proposed catalytic cycle.

3.3 Conclusions

In summary, Ni-catalyzed defluorinative phosphonylations of aryl fluorides with dialkyl phosphonates [HP(O)(OR)2] have been achieved using KO*t*Bu as a base. The reaction required no exogeneous ligands, and commercially available and bench-stable Ni(II) complexes exhibited high catalytic activities. Various aryl fluorides were successfully converted to the corresponding arylphosphonates irrespective of their electronic natures. The reaction proceeded specifically with di-*sec*-alkyl phosphonates.

Experimental and computational mechanistic investigations suggested that Ni–K^+ cooperative action of a Ni(0) complex chelated with a strongly electron-donating ion-bridged dimeric phosphite ligand $[P(OR)_2O^-K^+]_2$ facilitates turnover-limiting C–F bond oxidative addition of aryl fluorides.

3.4 Experimental Section

3.4.1 Instrumentation and Chemicals

Nuclear magnetic resonance (NMR) spectra were recorded on a JEOL JNM-ECXII spectrometer, operating at 400, 100.5 and 161.8 MHz for ^{1}H, ^{13}C{^{1}H} and ^{31}P{^{1}H} NMR, respectively. Chemical shift values for ^{1}H, ^{13}C{^{1}H} and ^{31}P{^{1}H} NMR are referenced to Me_4Si (0 ppm), $CDCl_3$ (77.0 ppm) and H_3PO_4 (0 ppm), respectively. For PhMe-*d*$_8$ solutions, the chemical shifts are referenced to the residue protium of the solvents δ Ar–H (7.00 ppm). Chemical shifts are reported in δ ppm. High-resolution mass spectra were recorded at the Instrumental Analysis Division, Global Facility Center, Creative Research Institution, Hokkaido University (Thermo Fisher Scientific Exactive or JEOL JMS-T100LP for ESI-MS). IR spectra were measured with a PerkinElmer Frontier instrument. *In situ* FT-IR tracing was performed with a Mettler Toledo ReactIR 15 equipped with a silicon ATR probe (SiComp). Thin layer chromatography (TLC) analyses and preparative thin layer chromatography (PTLC) separation were performed on commercial glass plates bearing 0.25-mm layer of Merck Silica gel 60 F_{254}. Silica gel (Kanto Chemical Co., Silica gel 60 N, spherical, neutral) was used for column chromatography.

All reactions were carried out under nitrogen or argon atmosphere. The defluorophosphonylation reactions were conducted with ChemiStation™ Personal Organic Synthesizer PPM-5512 (EYELA) or oil bath for maintaining internal temperature. Materials were obtained from commercial suppliers or prepared according to standard procedures unless otherwise noted. PhMe (Toluene, dehydrated) was purchased from Kanto Chemical Co., Inc. and dried and deoxidized by passage through packed columns of neutral alumina and copper(II) oxide under positive argon pressure (Grubbs solvent system, purchased from NIKKO HANSEN Co., Ltd.).[9] Toluene (deoxidized) were purchased from Fujifilm Wako Pure Chemicals Co., Ltd and used as received. PhMe-*d*$_8$ was purchased from Kanto Chemical Co., Inc. and degassed by freeze-pump-thaw cycle. Nickel(II) bromide ethylene glycol dimethyl ether complex ($NiBr_2 \cdot$ diglyme) and bis(cyclooctadiene)Nickel(0) complex $[Ni(cod)_2]$ were purchased from Sigma-Aldrich Co. and Kanto Chemical Co., Inc., respectively, and used as received. Potassium *tert*-butoxide (KO*t*Bu, >97%) were purchased from Tokyo Chemical Industry Co., Ltd. and

used as received. All metal complexes, bases and solvents were stored inside a nitrogen-filled glove box.

3.4.2 Preparation of Substrates

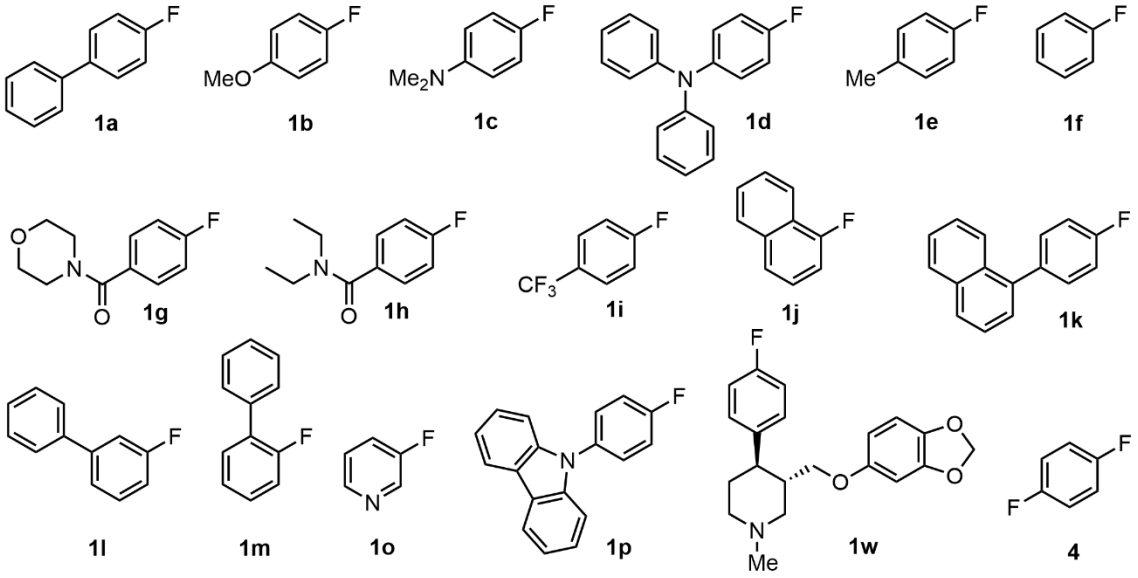

Figure 3.4. Aryl fluorides used in this work.

1a was purchased from Sigma-Aldrich Co. and used as received. **1b**, **1c**, **1e**, **1f**, **1i**, **1j**, **1l**–**1o**, **1w**, **4** were purchased from Tokyo Chemical Industry Co., Ltd. and used as received. **1g** was prepared through the reported procedure with slight modifications.[10] **1d** and **1p** were prepared by Pd-catalyzed amination of 4-bromofluorobenzene. **1k** was prepared by Pd-catalyzed cross-coupling between 4-fluorophenylboronic acid and the corresponding 2-bromonapthalene. **1h** is a known compound.[11]

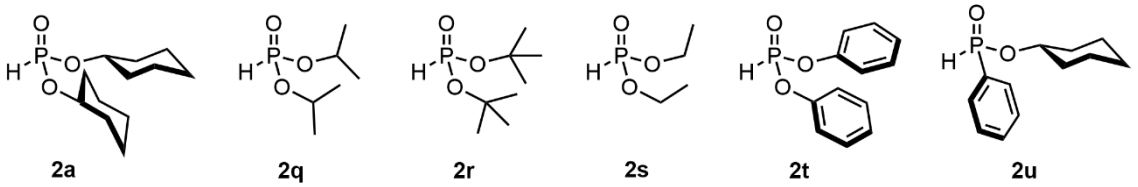

Figure 3.5. *H*-phosphonates and phosphinic acids used in this work.

2a[12] and **2f**[13] were prepared according to the reported procedure with slight modifications. **2c**[14] was prepared through the reaction between phosphorous trichloride and *tert*-butyl alcohol in the presence of pyridine. **2b** was purchased from Tokyo Chemical Industry Co., Ltd. and used as received. **2d** and **2e** were purchased from Tokyo

Chemical Industry Co., Ltd. and freshly distilled before use.

3.4.3 Experimental Procedures

Typical Procedures for Ni-Catalyzed Defluorophosphonylation of Aryl Fluorides [Procedure A]

In a nitrogen-filled glove box, $NiBr_2$·diglyme (2.2 mg, 0.00625 mmol, 5 mol% to Ar–F) and PhMe (0.1 mL) were placed in a flame-dried 10 mL glass tube containing a magnetic stirring bar. Next, **1a** (21.5 mg, 0.125 mmol, 1 equiv), **2a** (61.6 mg, 0.25 mmol, 2 equiv) and PhMe (0.2 mL) were added to the mixture. After stirring for 5 min, KO*t*Bu (28.1 mg, 0.25 mmol, 2 equiv) and PhMe (0.2 mL) were added, and the mixture turns into orange upon stirring. The glass tube was sealed with a screw cap and was removed from the glove box. The mixture was stirred at 120 °C for 20 h. After cooling to room temperature, the dark-red reaction mixture was passed through a short plug of silica gel with eluent (CH_2Cl_2/MeOH, 90:10). Volatiles were removed by evaporation under reduced pressure. In order to remove recovered dialkylphosphonates, the reaction crude was heated to 90 °C under high vacuum (140 Pa) for 12 h. After returning to room temperature, the crude product was purified by flash chromatography on silica gel with slow gradient elution (CH_2Cl_2/MeOH, 100:0-to-98:2) followed by preparative thin layer chromatography (CH_2Cl_2/MeOH, 98:2) to give **3a** as a light-brownish oil (48.4 mg, 0.12 mmol, 97% yield) containing a trace amount of non-isolable tricyclohexyl phosphate ($^{31}P\{^1H\}$ NMR: –2.4 ppm).[15]

[Procedure B]

As showing above, the usage of $NiBr_2$·diglyme would give the isolated product containing a trace amount of non-isolable tricyclohexyl phosphate. Hence, the catalyst was switched from $NiBr_2$·diglyme to $Ni(cod)_2$ to avoid unexpected contamination in some examples.

Specifically, in a nitrogen-filled glove box, $Ni(cod)_2$ (1.7 mg, 0.00625 mmol, 5 mol% to Ar–F) and PhMe (0.1 mL) were placed in a flame-dried 10 mL glass tube containing a magnetic stirring bar. Next, **1a** (21.5 mg, 0.125 mmol, 1 equiv), **2a** (61.6 mg, 0.25 mmol, 2 equiv) and PhMe (0.2 mL) were added to the mixture. After stirring for 5 min, KHMDS (49.9 mg, 0.25 mmol, 2 equiv.) and PhMe (0.2 mL) were added, and the mixture turns into orange upon stirring. The glass tube was sealed with a screw cap and was removed from the glove box. The mixture was stirred at 120 °C for 20 h. After cooling to room temperature, the dark-red reaction mixture was passed through a short plug of silica gel

with eluent (CH_2Cl_2/MeOH, 90:10). Volatiles were removed by evaporation under reduced pressure. In order to remove recovered dialkylphosphonates, the reaction crude was heated to 90 °C under high vacuum (140 Pa) for 12 h. After returning to room temperature, the crude product was purified by flash chromatography on silica gel with slow gradient elution (CH_2Cl_2/MeOH 100:0-to-97:3) followed by preparative thin layer chromatography (CH_2Cl_2/MeOH, 98:2) to give **3a** as a whitish oil (49.4 mg, 0.124 mmol, 99% yield).

Preparation of 3v (5.0 mmol scale without a glove box)

An flame-dried 100 mL two-necked round-bottom flask equipped with a condenser and a magnetic stir bar was vacuumed and filled with Ar. $NiBr_2$·diglyme (88.2 mg, 0.25 mmol, 5 mol% to Ar–F), **1b** (0.57 mL, 5.0 mmol, 1 equiv), **2b** (1.63 mL, 10.0 mmol, 2 equiv) and PhMe (10 mL) were placed in the flask, and the mixture was stirred at room temperature for approx. 5 min. Next, KO*t*Bu (1.1221 g, 10.0 mmol, 2 equiv) and PhMe (10 mL) were added to the flask. The flask was connected to an Ar-filling balloon and heated at 120 °C for 20 h. After cooling to room temperature, the organic layer was extracted by EtOAc, washed by deionized water and brine, dried over $MgSO_4$ and filtered. Volatiles were removed by evaporation under reduced pressure. the crude product was purified by flash chromatography on silica gel with slow gradient elution (CH_2Cl_2/MeOH, 100:0-to-97:3) to give **3v** as a whitish oil (1.14 g, 4.2 mmol, 84% yield).

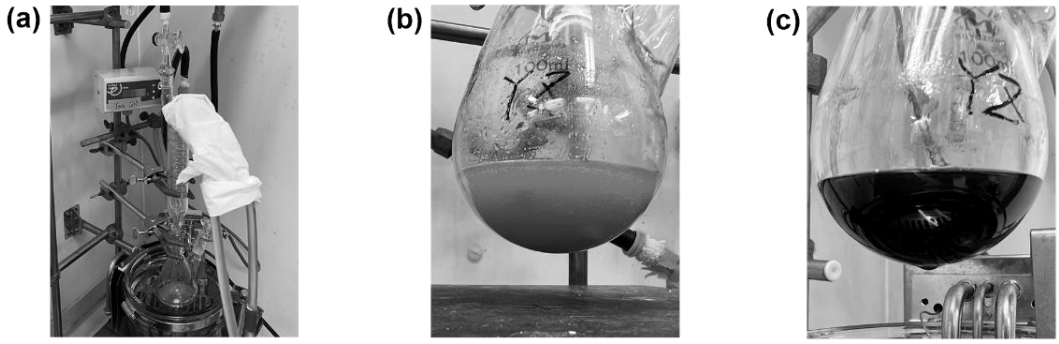

Figure 3.6. Photographic images of gram-scale reaction. (a) Reaction setup. The reaction mixture (a) before and (b) after the reaction.

3.4.4 Reaction Optimization

Table 3.3. Catalyst effects on the reaction of **1a** and **2a**

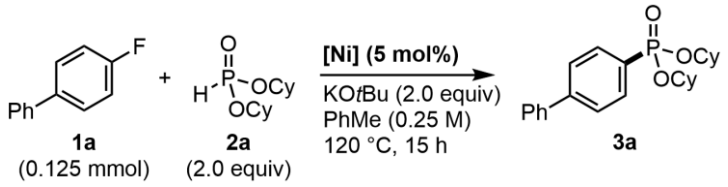

Entry	[Ni]	^{1}H NMR yield of **3a** [%][a]
1	**$NiBr_2$·diglyme**	**>99**
2	$NiBr_2$·diglyme	99[b]
3	$NiBr_2$·DME	83
4	NiI_2	>99
5	$NiBr_2$	55
6	$NiCl_2$	62
7	$Ni(acac)_2$	77
8	$Ni(cod)_2$	70
9	None	0

[a] Determined by ^{1}H NMR by using 1,3,5-trimethoxybenzene as an internal standard.
[b] The reaction was carried out in the dark.

Table 3.4. Solvent effects on the reaction of **1a** and **2a**

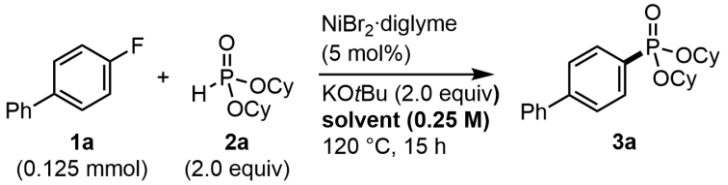

Entry	Solvent	^{1}H NMR yield of **3a** [%][a]
1	**PhMe**	**>99**
2	CPME	81
3	Bu_2O	32
5	mesitylene	97

[a] Determined by ^{1}H NMR by using 1,3,5-trimethoxybenzene as an internal standard.

Table 3.5. Base effects on the reaction of **1a** and **2a**

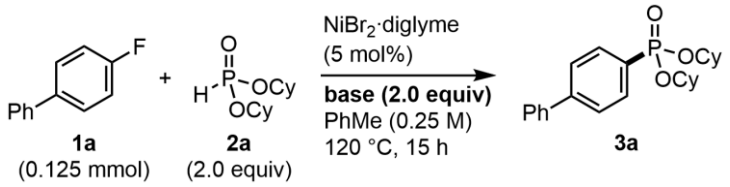

Entry	Base	^{1}H NMR yield of **3a** [%][a]
1	**KO*t*Bu**	**>99**
2	NaO*t*Bu	33
3	LiO*t*Bu	2
4	KHMDS	0
5	NaHMDS	11
6	LiHMDS	0
7	KH	7
8	K_2CO_3	0
9	K_3PO_4	0
10	KOAc	0
11	KOMe	0
12	DBU	0

[a] Determined by ^{1}H NMR by using 1,3,5-trimethoxybenzene as an internal standard.

Table 3.6. Temperature effects on the reaction of **1a** and **2a**

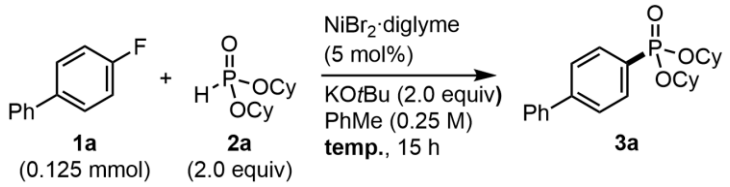

Entry	Temperature (°C)	^{1}H NMR yield of **3a** [%][a]
1	**120**	**>99**
2	100	>99
3	80	2
4	25	4[b]

[a] Determined by ^{1}H NMR by using 1,3,5-trimethoxybenzene as an internal standard.
[b] reaction time = 72 h.

Table 3.7. Stoichiometric effects on the reaction of **1a** and **2a**

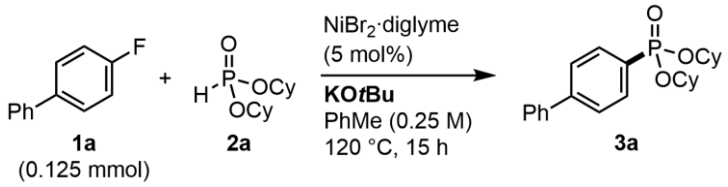

Entry	Amount of **2a**	Amount of KO*t*Bu	^{1}H NMR yield of **3a** [%][a]
1	**2.0 equiv**	**2.0 equiv**	**>99**
2	2.0 equiv	1.0 equiv	0
3	2.0 equiv	3.0 equiv	49
4	1.0 equiv	2.0 equiv	48
5	3.0 equiv	2.0 equiv	9

[a] Determined by ^{1}H NMR by using 1,3,5-trimethoxybenzene as an internal standard.

Table 3.8. Effects on the reaction of base and catalysts

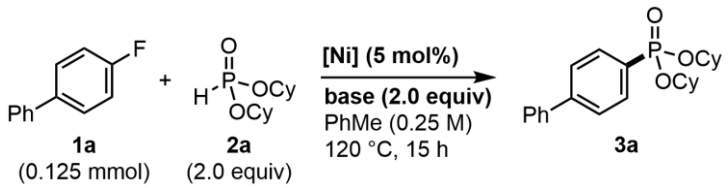

Entry	Ni complex	Base	^{1}H NMR yield of **3a** [%][a]
1	**NiBr$_2$·diglyme**	**KO*t*Bu**	**>99**
2	NiBr$_2$·diglyme	KHMDS	0
3	NiBr$_2$·diglyme	KH	7
4	Ni(cod)$_2$	KHMDS	>99
5	Ni(cod)$_2$	KH	>99

[a] Determined by ^{1}H NMR by using 1,3,5-trimethoxybenzene as an internal standard.

Table 3.9. Effect of 18-crown-6

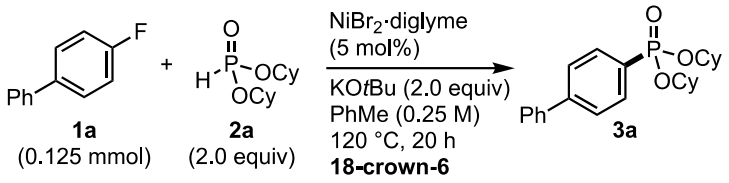

Entry	Amount of 18-crown-6	^{1}H NMR yield of **3a** [%][a]
1	0 equiv	>99
2	0.05 equiv	73
3	0.5 equiv	8
4	1.0 equiv	3
5	2.0 equiv	0

[a] Determined by ^{1}H NMR by using 1,3,5-trimethoxybenzene as an internal standard.

Table 3.10. Catalysts effects on the reaction of **1b** and **2b**

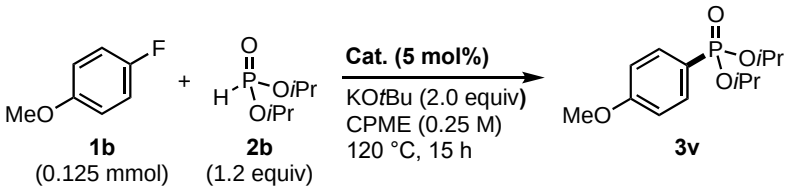

Entry	Catalyst	^{1}H NMR yield of **3v** [%][a]
1	**$NiBr_2$·diglyme**	**61**
2	$NiBr_2$·DME	42
3	$NiBr_2$	33
4	$Pd(OAc)_2$	0
5	$CuCl_2$	0
6	$ZnCl_2$	0
7	LiI	0
8	LiCl	0
9	LiF	0
10	KF	0
11	CsF	0
12	None	0

[a] Determined by ^{1}H NMR by using 1,3,5-trimethoxybenzene as an internal standard.

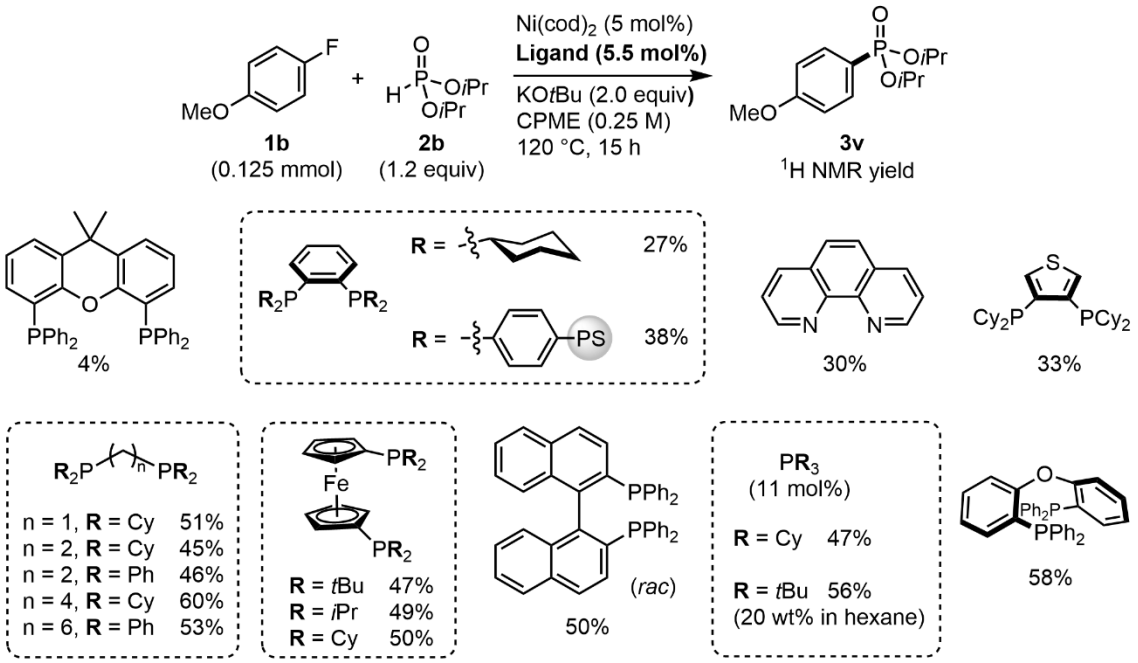

Figure 3.7. Ligand effects on the reaction of **1b** and **2b**. Yields were determined by ^{1}H NMR by using 1,3,5-trimethoxybenzene as an internal standard.

3.4.5 NMR Studies

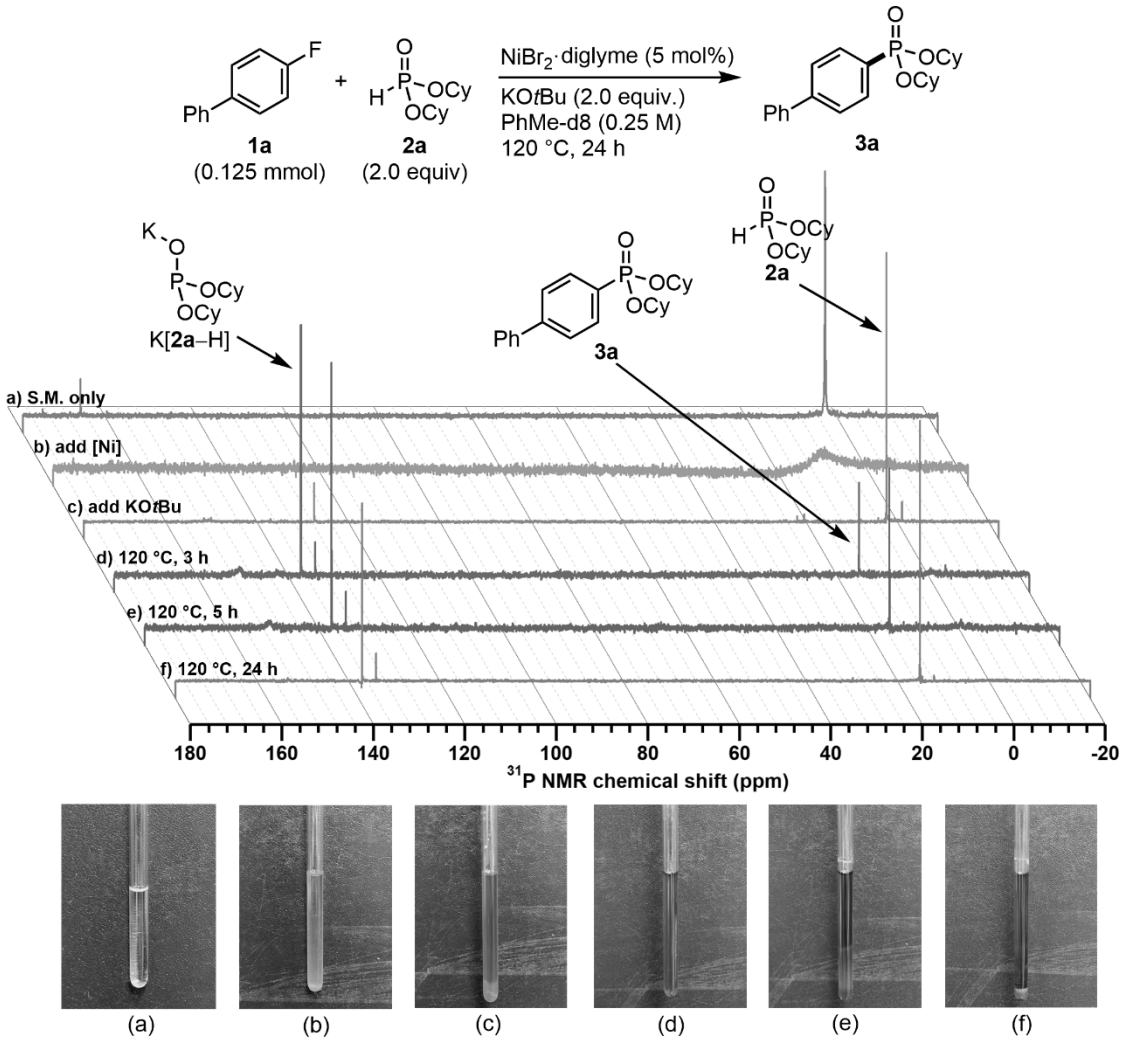

Figure 3.8. Reaction monitoring by $^{31}P\{^{1}H\}$ NMR spectroscopy.

The reaction of **1a** and **2a** with $NiBr_2$·diglyme and KO*t*Bu in PhMe-*d*$_8$ was monitored by $^{31}P\{^{1}H\}$ NMR spectroscopy (Figure 3.8). Under nitrogen atmohsphere, **2a**, **1a** and PhMe-*d*$_8$ (0.4 mL) were added to an NMR tube. $^{31}P\{^{1}H\}$ NMR analysis of the mixture showed a peak stands for **2a** (5 ppm). After addition of $NiBr_2$·diglyme and PhMe-*d*$_8$ (0.1 mL), $^{31}P\{^{1}H\}$ NMR spectrum became broad and provided no useful information about the mixture. Next, the mixture turned to orange upon the addition of KO*t*Bu and PhMe-*d*$_8$ (0.1 mL). After heating the mixture for 3 h, $^{31}P\{^{1}H\}$ NMR analysis was clearly indicative of the formation of the potassium phosphite K[**2a**–H] (139 ppm).[16] Besides, **3a** (17 ppm) was also observed on the spectrum. **3a** kept growing over the reaction time and **2a** decreasing. The experiment suggested that K[**2a**–H] might be a key intermediate in the current reaction.

3.4.6 Stepwise Reaction

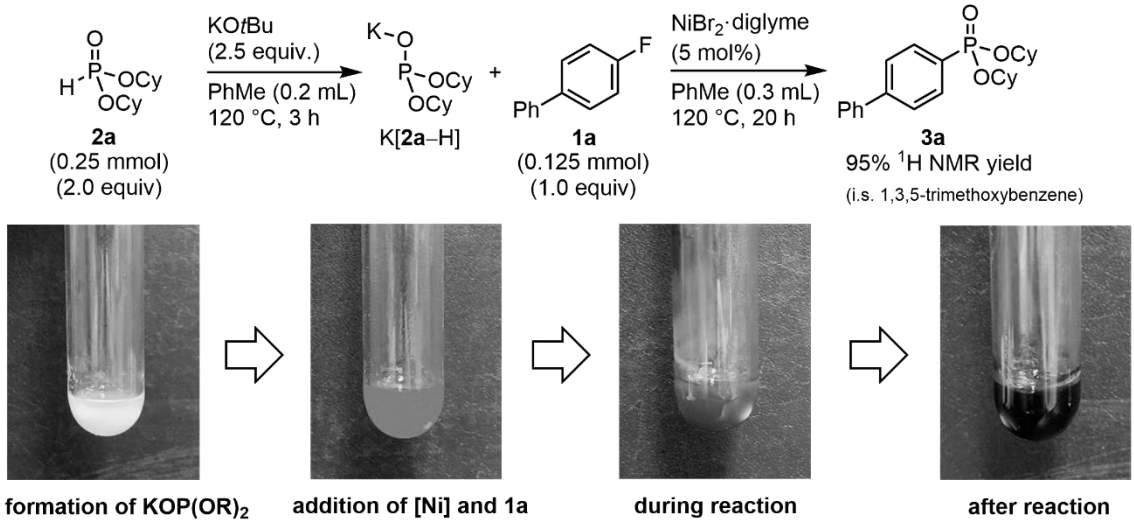

Figure 3.9. Stepwise reaction between **1a** and **2a**.

To confirm the intermediacy of potassium salt K[**2a**–H], **2a** was mixed with excess amount of KO*t*Bu and heated at 120 °C for 3 h in the absence of **1a** and $NiBr_2$·diglyme (Figure 3.9). The resulting white suspension stands for the formation of K[**2a**–H]. Next, **1a** and $NiBr_2$·diglyme was added to the suspension and the color was turned from white to orange. The mixture was heated for another 20 h. **3a** was detected in 95% ^{1}H NMR yield. The result of stepwise reaction as well as NMR experiment indicated that the present reaction is initiated by deprotonation of **2a**. Furthermore, K[**2a**–H] is the active species of the Ni-catalyzed defluorophosphonylation reaction.

3.4.7 Kinetic Experiments

Typical Procedure and General Information

Kinetic data were obtained by *in situ* IR monitoring.[17–19] A special designed glassware, which contains one stopcock valve and two round glass joint, was used in kinetic experiments (Figure 3.10). The glassware equipped with a magnetic stir bar was flame-dried and moved to a N_2-filled glove box. $Ni(cod)_2$ (3.4 mg, 0.0125 mmol, 5 mol% to Ar–F), **2a** (123.2 mg, 0.5 mmol), KO*t*Bu (56.2 mg, 0.5 mmol), and PhMe (1.0 mL) were added to the glassware and capped with a rubber septum. Next, the glassware was moved out from the glove box and connected to a vacuum/Ar manifold. Then, a ReactIR SiComp probe was pre-dried (by high vacuum) and attached to the glassware under continuous Ar flow. After acquirement of the background signal, the mixture was heated to 120 °C and stirring for 30 min, **1b** (28.3 μL, 0.25 mmol) was measured by a micro-syringe and injected through a rubber septum. IR spectra were acquired every minute over the course of the reaction. A peak around 1130 cm^{-1} appeared after the background subtraction was used for calculating the relative abundance of **3b** (peak height related to zero absorbance). Amount of **1b** or $Ni(cod)_2$ was adjusted for obtaining different kinetic data.

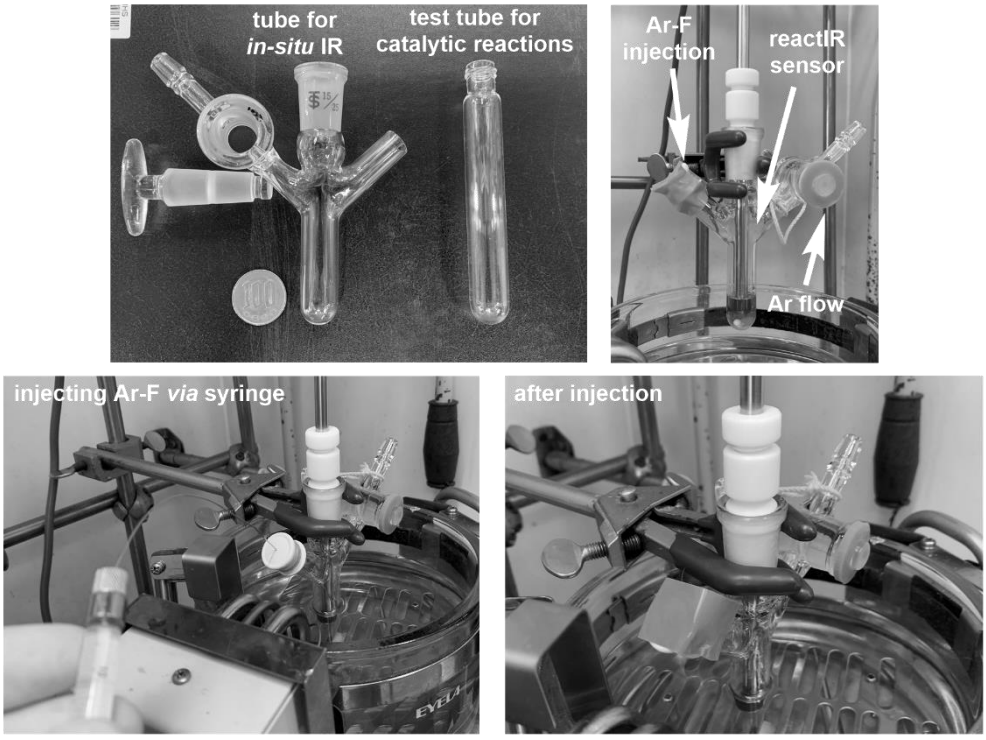

Figure 3.10. Reaction setup for kinetic experiments.

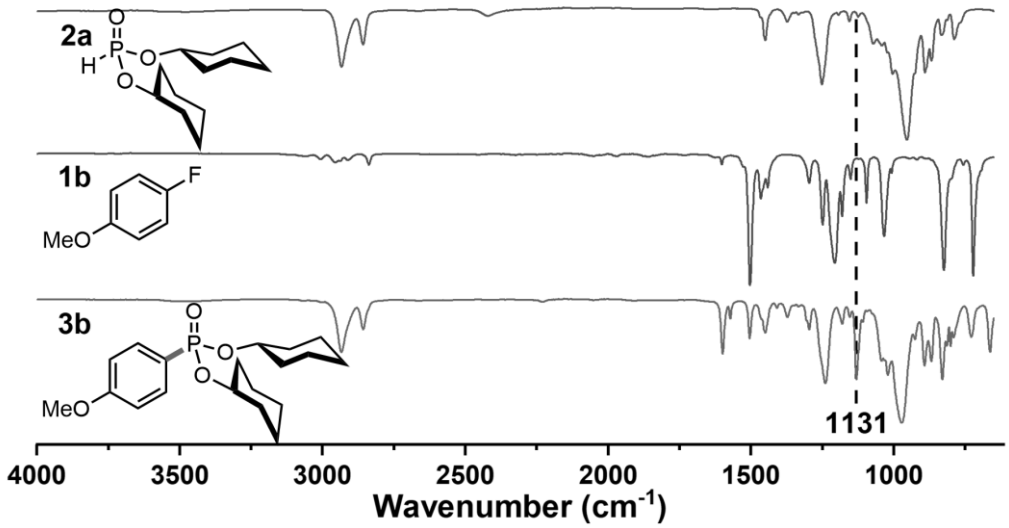

Figure 3.11. IR spectrum of **2a**, **1b** and **3b** and the peak used for ReactIR tracing.

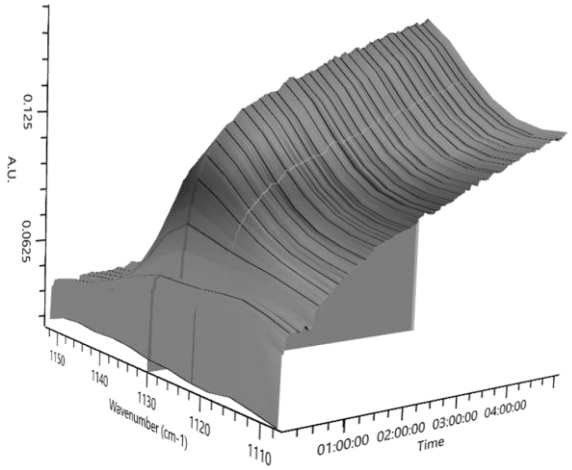

Figure 3.12. *In situ* FT-IR waterfall plots of **3b** around 1130 cm^{-1}.

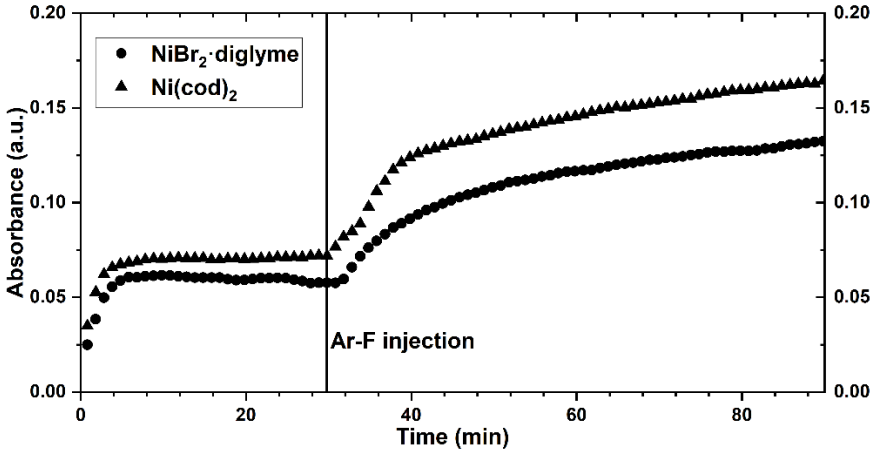

Figure 3.13. Plots of the formation of **3b** with NiBr2·diglyme and Ni(cod)2.

Kinetic Data

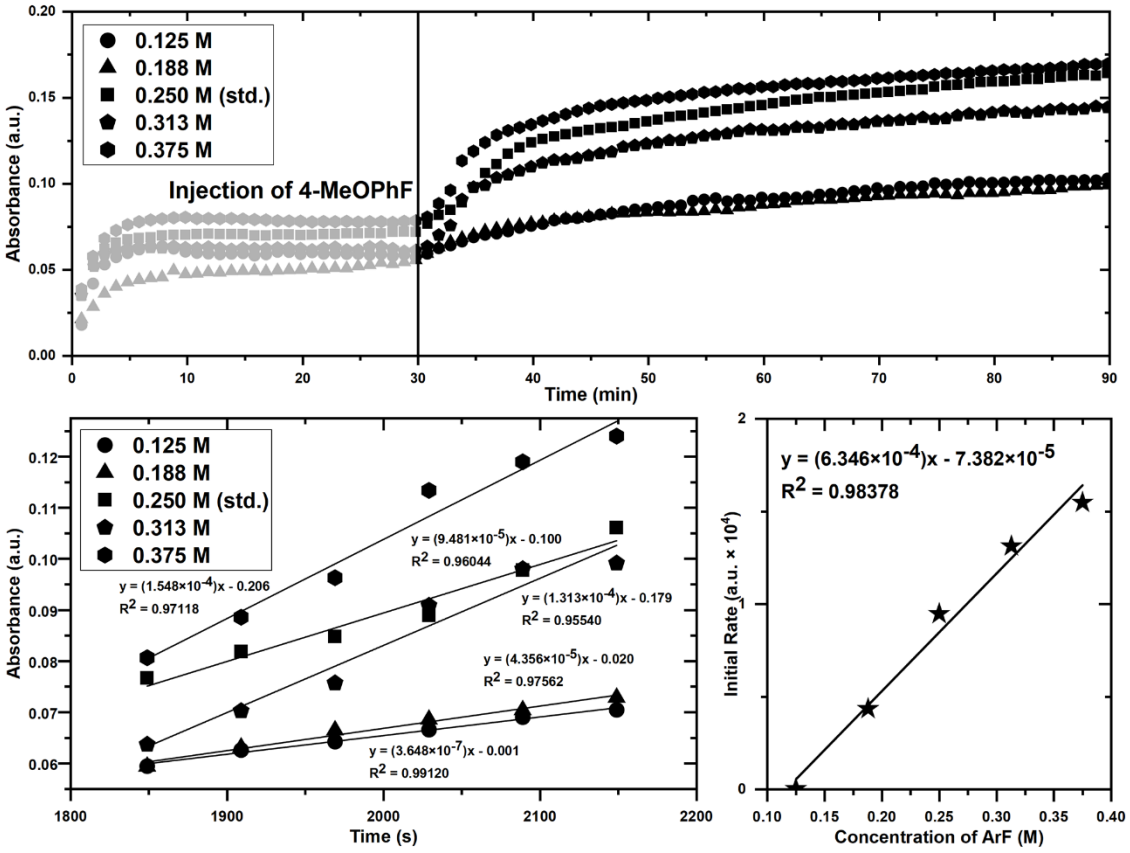

Figure 3.14. The **1b** concentration effect on the reaction kinetics.

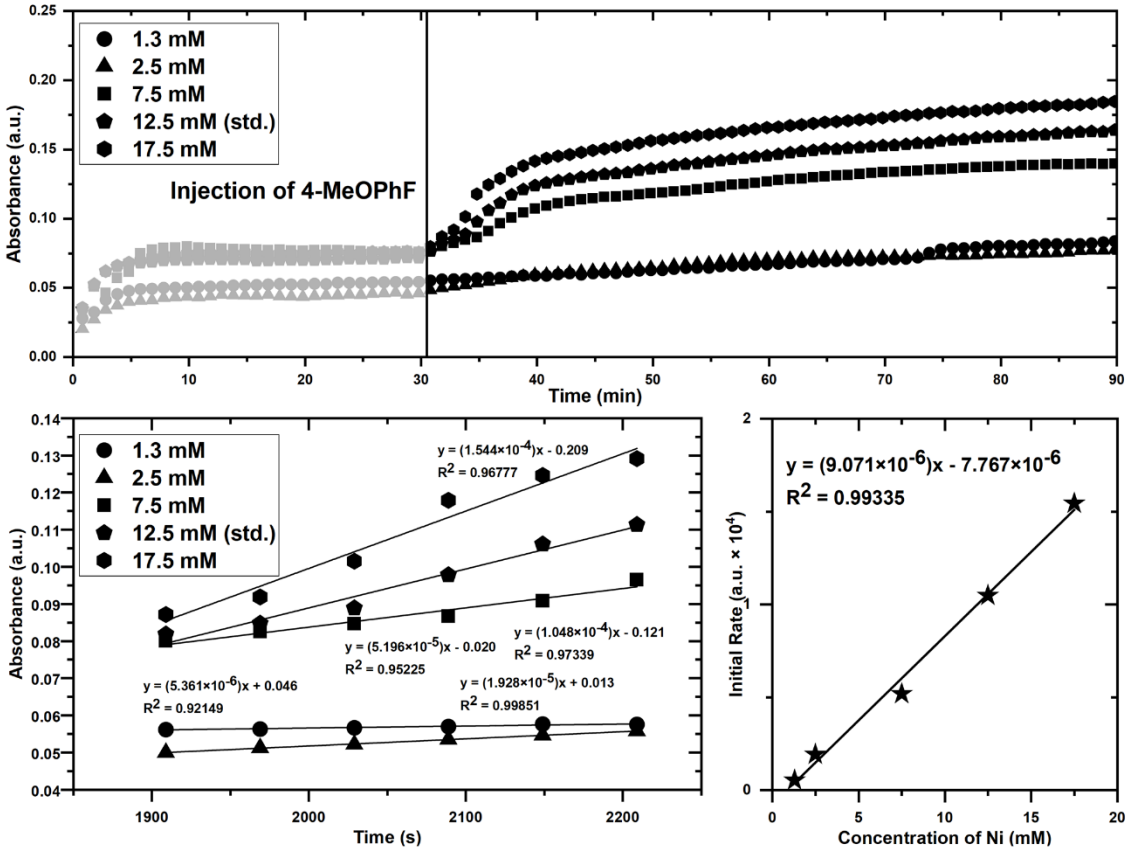

Figure 3.15. The $Ni(cod)_2$ concentration effect on the reaction kinetics.

Activation Energy Determination and Calculation

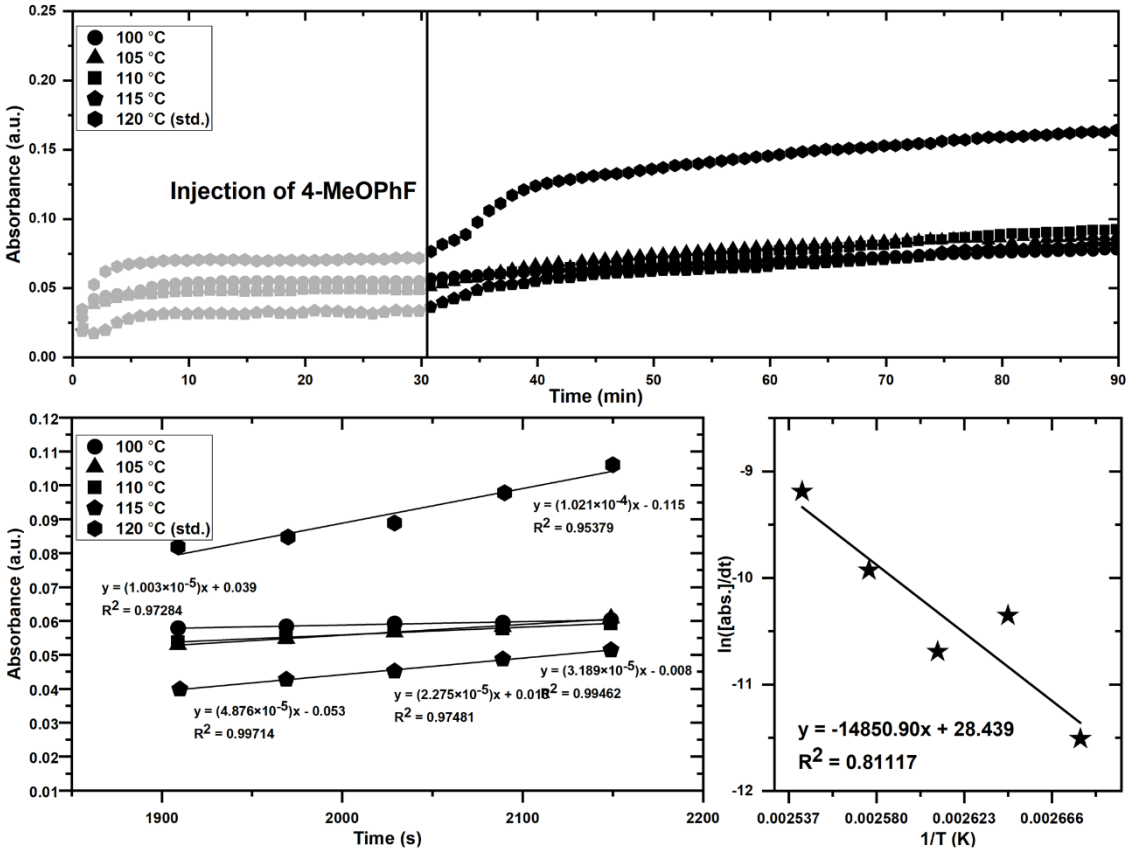

Figure 3.16. The temperature effect on the reaction kinetics.

According to the Arrhenius equation,

$$-\left(\frac{E_a}{R}\right) = -14850.90\ K$$

$$E_a = -(8.314\ J \cdot mol^{-1} \cdot K^{-1})(-14850.90\ K) = 123470\ J \cdot mol^{-1} = 29.5\ kcal \cdot mol^{-1}$$

3.4.8 Reactions with a Mixture of *H*-Phosphonates

General Procedures and Analysis of the Crude Reaction

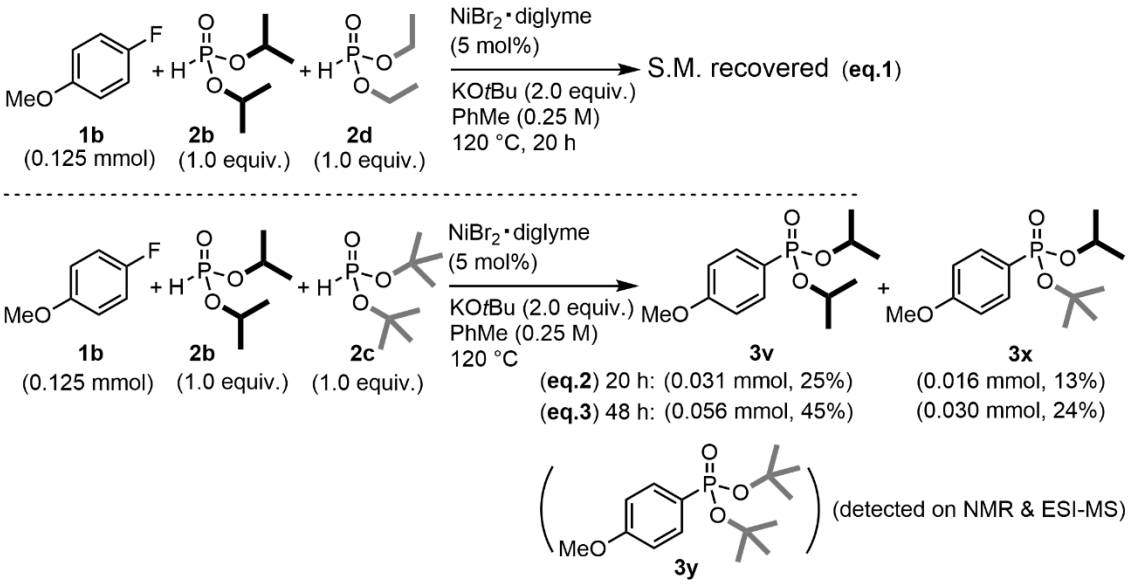

Scheme 3.6. Reaction of **1b** with a mixture of *H*-phosphonates.

In a nitrogen-filled glove box, $NiBr_2$·diglyme (2.2 mg, 0.00625 mmol, 5 mol% to Ar–F) and PhMe (0.1 mL) were placed in a flame-dried 10 mL glass tube containing a magnetic stirring bar. Next, **1b** (14.1 μL, 0.125 mmol, 1 equiv), **2b** (20.4 μL, 0.125 mmol, 1 equiv), **2c** (24.3 mg, 0.125 mmol, 1 equiv) and PhMe (0.2 mL) were added to the mixture. After stirring for 5 min, KO*t*Bu (28.1 mg, 0.25 mmol, 2 equiv.) and PhMe (0.2 mL) were added to the mixture. The glass tube was sealed with a screw cap and was removed from the glove box. The mixture was stirred at 120 °C for 20 h. After cooling to room temperature, the resulted mixture was passed through a short plug of silica gel with eluent (CH_2Cl_2/MeOH, 90:10). Volatiles were removed by evaporation under reduced pressure. 1,1,2,2-Tetrachloroethane was added as an internal standard.

In order to assign products, authentic **3y** was synthesized and its NMR spectrum was compared to the current reaction. As a result, trace amount of **3y** was found in the reaction crude. By contrast, **3v** and **3x** were found on ESI-MS analysis with a high relative abundance. Although **3y** was also detected on ESI-MS measurement, its relative abundance was too low for NMR analysis. Based on all above-mentioned experimental results, it was concluded that **3v** (0.031 mmol, 25%) and **3x** (0.016 mmol, 13%) were the major products of the reaction.

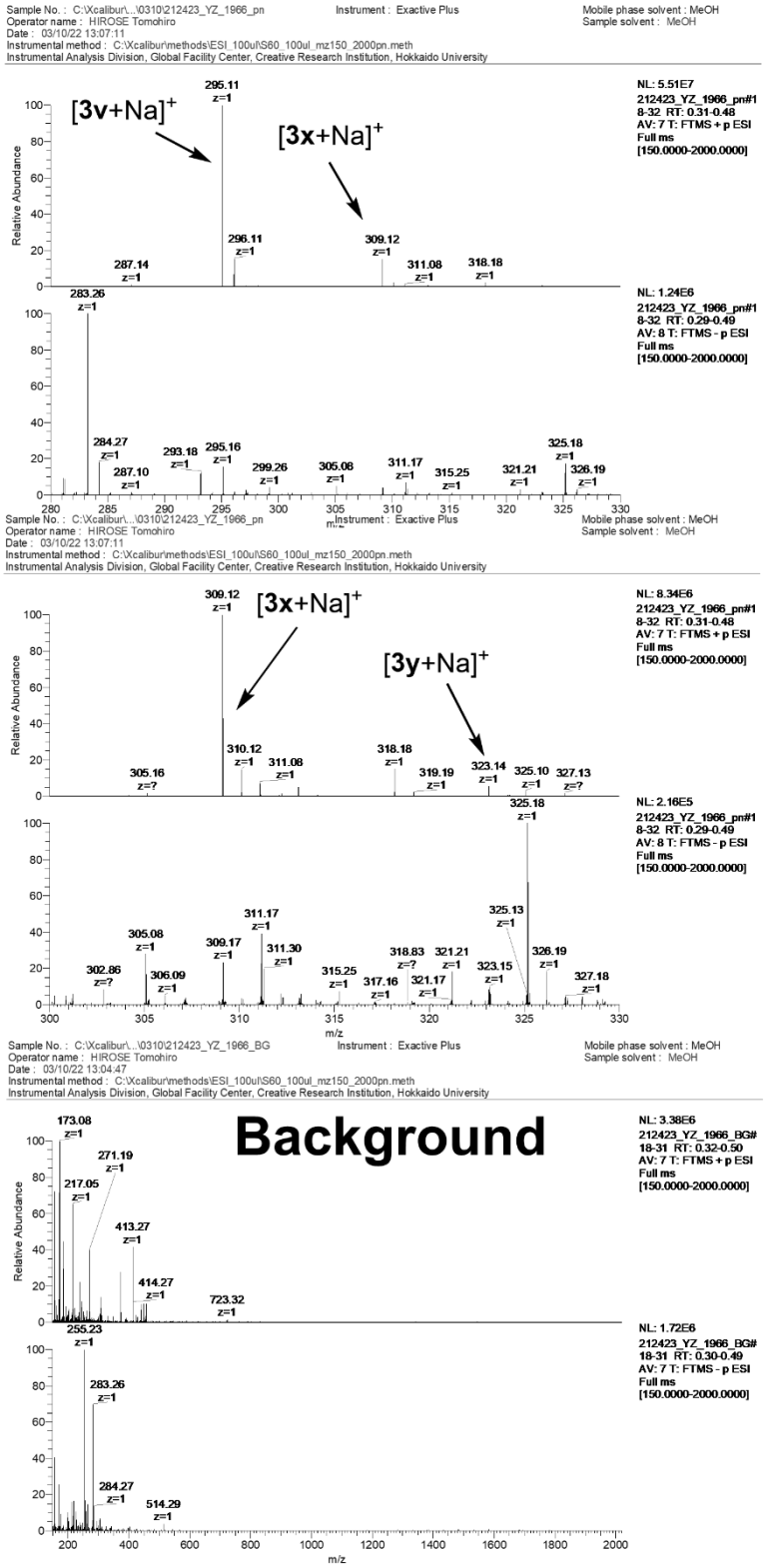

Figure 3.17. ESI-MS spectra of the reaction mixture shown in Scheme 3.6 (eq.2).

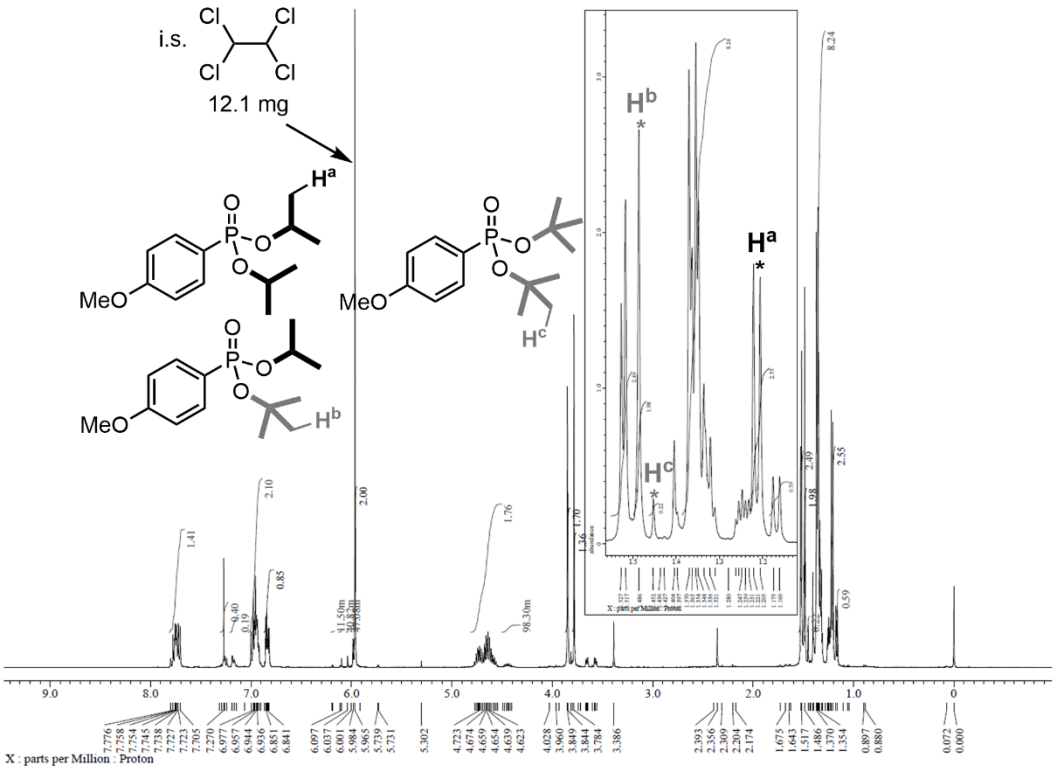

Figure 3.18. ^{1}H NMR spectrum of the crude reaction mixture in Scheme 3.6 (eq.2).

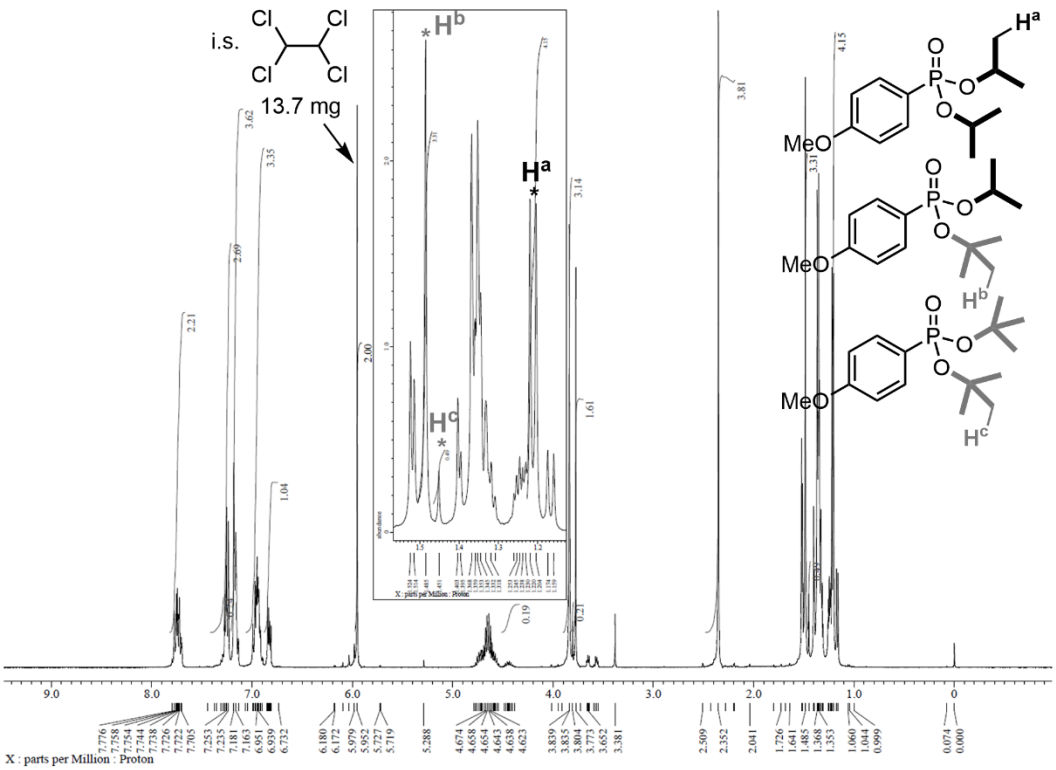

Figure 3.19. ^{1}H NMR spectrum of the crude reaction mixture in Scheme 3.6 (eq.3).

Preparation of Authentic 3y

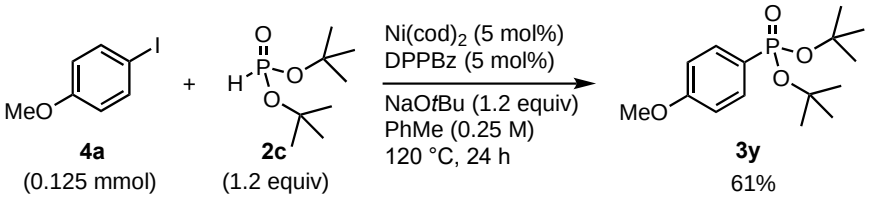

In a nitrogen-filled glove box, $Ni(cod)_2$ (1.7 mg, 0.00625 mmol, 5 mol% to Ar–I), 1,2-bis(diphenylphosphino)benzene (DPPBz, 2.8 mg, 0.00625 mmol, 5 mol%) and PhMe (0.1 mL) were placed in a flame-dried 10 mL glass tube containing a magnetic stirring bar. After stirring for 5 min, 4-iodoanisole **4a** (29.3 mg, 0.125 mmol, 1 equiv), **2c** (29.1 mg, 0.15 mmol, 1.2 equiv) and PhMe (0.2 mL) were added to the mixture. Then, NaO*t*Bu (14.4 mg, 0.15 mmol, 1.2 equiv) and PhMe (0.2 mL) were added into the mixture. The glass tube was sealed with a screw cap and was removed from the glove box. The mixture was stirred at 120 °C for 24 h. After cooling to room temperature, the reaction mixture was passed through a short plug of silica gel with eluent (CH_2Cl_2/MeOH, 90:10). Volatiles were removed by evaporation under reduced pressure. The crude product was purified by flash chromatography on silica gel with slow gradient elution (CH_2Cl_2/MeOH, 100:0-to-97:3) to give **3y** as a white powder (22.7 mg, 61% yield).

M.p.: 83.4–83.8 °C. **^{1}H NMR** (400 MHz, $CDCl_3$): δ 7.72 (dd, J = 13.2, 8.8 Hz, 2H), 6.94 (dd, J = 8.8, 3.2 Hz, 2H), 3.84 (s, 3H), 1.45 (s, 18H). **^{13}C{^{1}H} NMR** (100.5 MHz, $CDCl_3$): δ 161.9 (d, J_{C-P} = 2.8 Hz, 1C), 133.3 (d, J_{C-P} = 11.5 Hz, 2C), 125.5 (d, J_{C-P} = 199.3 Hz, 1C), 113.4 (d, J_{C-P} = 16.3 Hz, 2C), 81.8 (d, J_{C-P} = 7.7 Hz, 2C), 55.2 (s, 1C), 30.4 (s, 6C). **^{31}P{^{1}H} NMR** (161.8 MHz, $CDCl_3$): δ 11.2. **IR** (ATR): 2978, 1596, 1572, 1505, 1454, 1392, 1368, 1293, 1256, 1235, 1172, 1125, 1018, 972, 916, 844, 828, 800, 715, 701 cm^{-1}. **HRMS-ESI** (*m/z*): $[M+Na]^+$ Calcd for $C_{15}H_{25}O_4NaP$ 323.1383; found 323.1388.

3.4.9 NMR Experiments for Monitoring Complexation

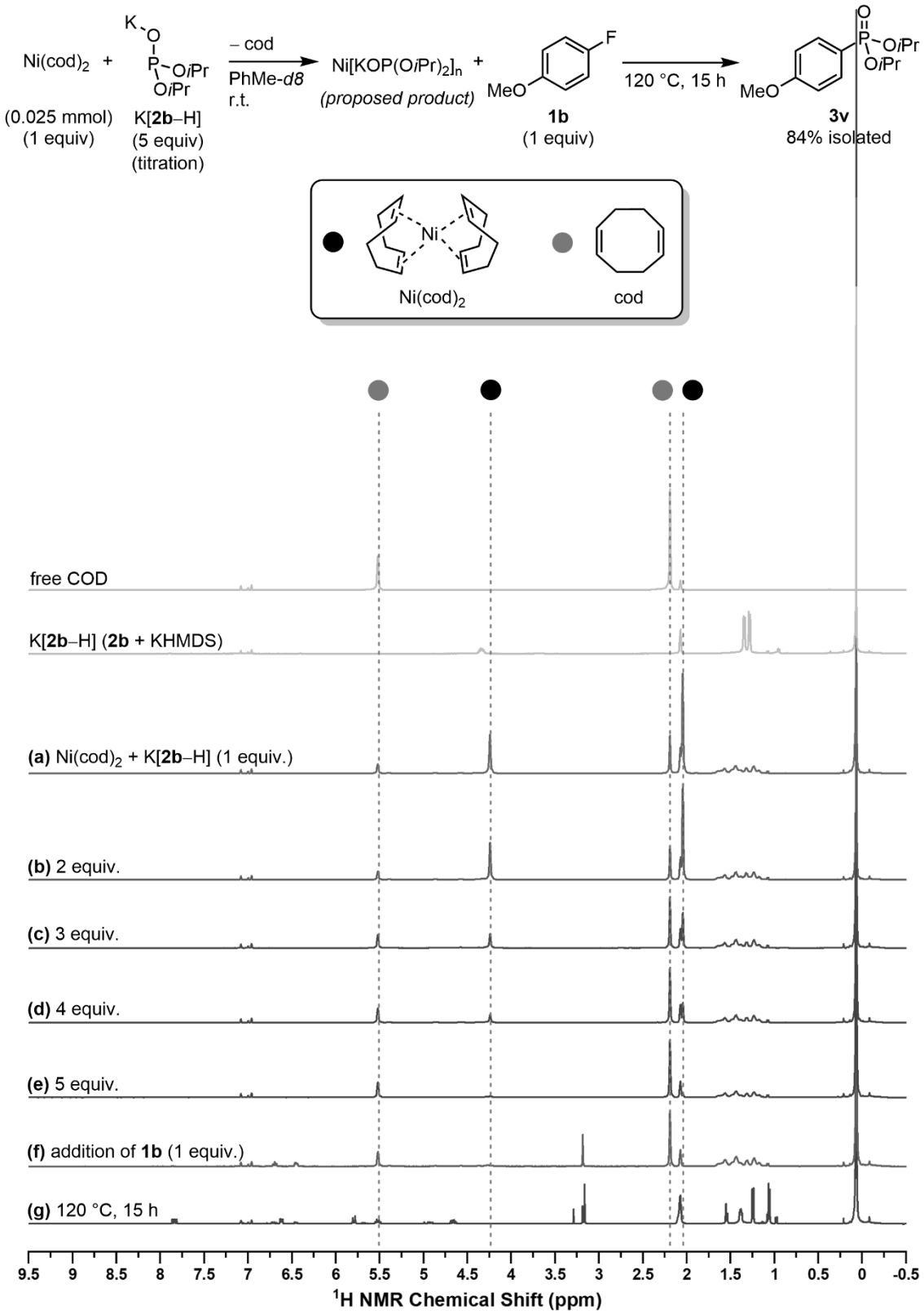

Figure 3.20. ^{1}H NMR spectra of the complexation experiment in PhMe-*d*$_8$.

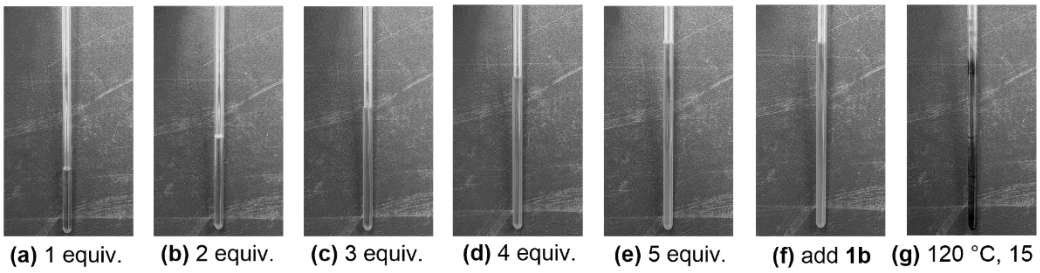

Figure 3.21. Photographic images of the complexation experiment.

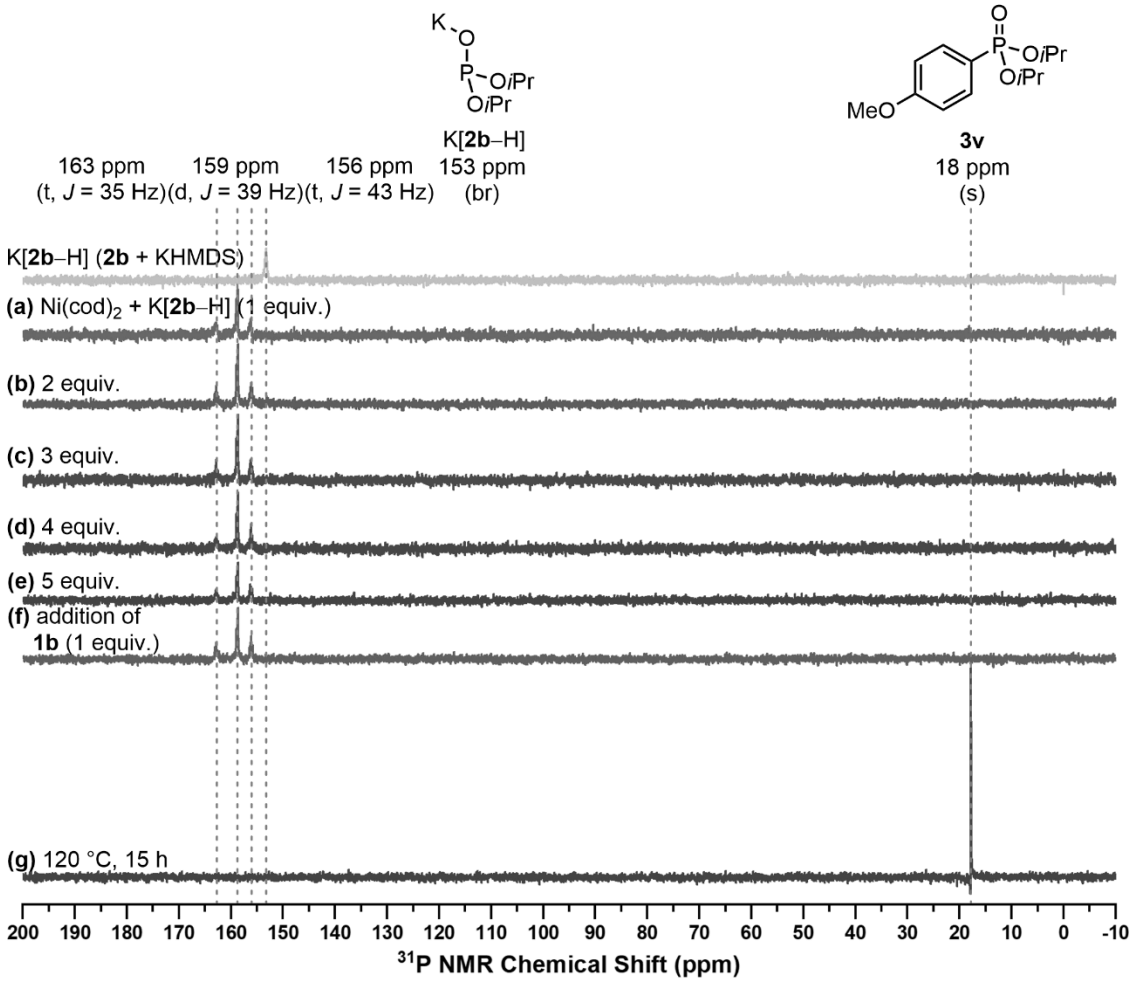

Figure 3.22. $^{31}P\{^{1}H\}$ NMR spectra of the complexation experiment in PhMe-*d*8.

The complexation of $Ni(cod)_2$ with K[**2b**–H] in PhMe-*d*8 was monitored by both ^{1}H and $^{31}P\{^{1}H\}$ NMR spectroscopy (Figure 3.20 & 3.22). Under nitrogen atmosphere, to a 10 mL vial charged with KHMDS (29.9 mg, 0.15 mmol, 6 equiv.) and PhMe-*d*8 (1.2 mL), **2b** (23.7 μL, 0.15 mmol, 6 equiv.) was added and mixed to obtain K[**2b**–H] solution. Meanwhile, $Ni(cod)_2$ (6.9 mg, 0.025 mmol, 1 equiv.) and PhMe-*d*8 (0.3 mL) were charged

into a J-Young NMR tube. 0.3 mL (1 equiv.) of K[**2b**–H] solution was added to the NMR tube and mixed by sonication. The resulted mixture was recorded by both ^{1}H and $^{31}P\{^{1}H\}$ NMR. This process was repeated until totally 5 equiv. of K[**2b**–H] had been added into the mixture. The formation of non-coordinated 1,5-cyclooctadiene (cod) was detected by ^{1}H NMR spectroscopy. However, no free K[**2b**–H] was detected on $^{31}P\{^{1}H\}$ NMR spectroscopy during the whole titration process. Besides, three new signals (163, 159, 156 ppm) were observed after the addition. These facts suggested that K[**2b**–H] coordinated to the Ni(0) center in the solution phase.

Next, 4-fluoroanisole **2b** (2.9 μL, 0.025 mmol, 1 equiv.) was added to the same J-Young NMR tube. New signals were not observed on $^{31}P\{^{1}H\}$ NMR spectroscopy. The resulted mixture was heated to 120 °C for 15 h. After returning to the room temperature, both ^{1}H and $^{31}P\{^{1}H\}$ NMR showed the formation of the corresponding aryl phosphonate product **3v** (18 ppm). Besides, signals corresponding to the Ni complex completely disappeared. The reaction crude was purified by preparative thin layer chromatography (CH_2Cl_2/MeOH 98:2) to give **3v** as a whitish oil (5.6 mg, 0.021 mmol, 84% yield).

3.4.10 Computational Studies

General Information

All geometry optimizations and single-point energy calculations were performed by Gaussian 16 package.[20] The geometry optimizations of all structures were conducted at the M06[21] functional in conjunction with the lanl2dz (for Ni)[22–25] and 6-31G(d) (for others)[26–30] basis set. Toluene molecules were introduced to all potassium cations to consider the solvation effects. Frequency analyses were performed at the same level of theory for geometry optimizations, in which the thermal free energy corrections were provided. The single imaginary frequency was confirmed for each transition states, and all the optimized structures as minima have no imaginary frequency. The transition states were traced with intrinsic reaction coordinate (IRC) analyses by using Global Reaction Route Mapping (GRRM) program[31] to confirm the connection of the reaction pathway. Further single-point energy calculations were performed at the M06 functional in conjunction with the SDD (for Ni) and 6-311+G(d,p) (for others)[32] basis set with the solvation model (SMD: toluene) to evaluate solution phase electronic energies. The solution phase Gibbs free energies (G_{sol}) at 298.15 K (25 °C) were obtained from $G_{sol} = E + G_{corr}$, wherein the solvation electronic energies (E) were given from single-point energy calculations at the M06/SDD(Ni),6-311+G(d,p)(others)/SMD level of theory and

gas-phase thermal free energy corrections (G_{corr}) were given from frequency analyses at the M06/lanl2dz(Ni),6-31G(d) (others) level of theory. For the purpose of discussion, relative Gibbs free energies (ΔG_{sol}) were calculated from $\Delta G_{sol} = \Sigma G_{sol}$ for products – ΣG_{sol} for reactants.

Alternative Reaction Pathway

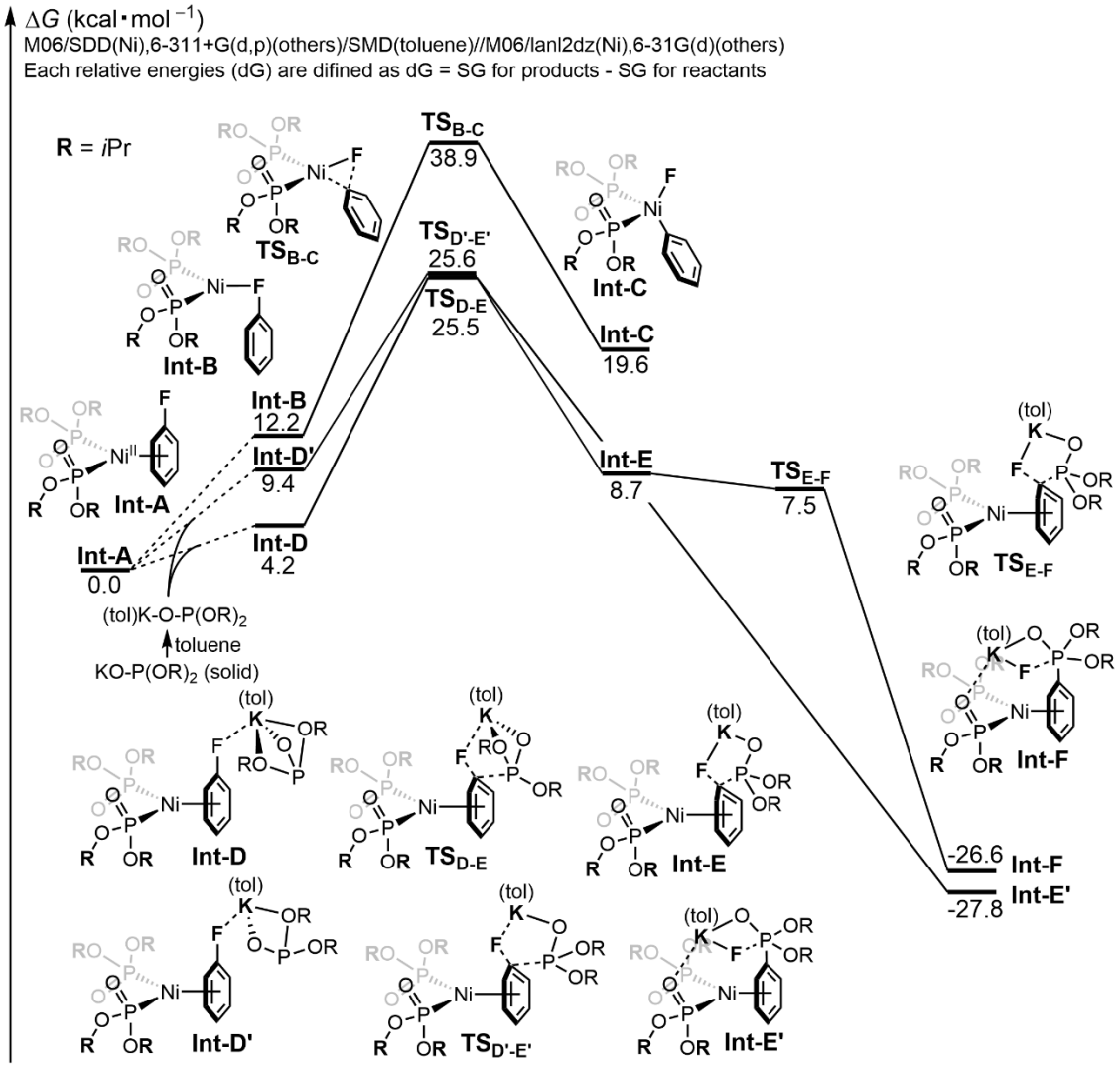

Figure 3.23. Alternative reaction pathways with Ni(II) species.

Reaction pathways for phosphonylation catalyzed by nickel(II) complexes have been investigated, as shown in Figure 3.23. Nickel(II) phosphonyl complex **Int-A** including fluorobenzene in an η^6-mannar was adopted as the initial structure for the investigations. Oxidative addition of fluorobenzene toward nickel(II) complex proceeds through $\mathbf{TS_{B\text{-}C}}$ after conformational change from **Int-A** to **Int-B**. Since the energy barrier of oxidative addition is quite high (38.9 kcal·mol^{-1}), C–F bond activation through oxidative addition to nickel(II) complex is improper pathway. Alternatively, S_NAr pathways catalyzed by nickel(II) complex as Lewis acid were examined. A fluorine atom on **Int-A** coordinates to potassium cation of toluene solvated potassium diisopropyl phosphite to afford **Int-D** or **Int-D′**. From **Int-D**, phosphonylation occurs through stepwise S_NAr pathway, in which energy barrier of $\mathbf{TS_{D\text{-}E}}$ as an apparent rate-determining step is 25.5 kcal·mol^{-1}. The concerted S_NAr reaction proceeds from **Int-D′** through $\mathbf{TS_{D'\text{-}E'}}$, which has 25.6 kcal·mol^{-1} energy barrier. Additionally, it is estimated that the actual energy barrier for $\mathbf{TS_{D\text{-}E}}$ and $\mathbf{TS_{D'\text{-}E'}}$ are higher than calculated values in Figure 3.23, since potassium diisopropyl phosphite are existed as insoluble material rather than a soluble solvated material in the reaction mixture. Thus, it is estimated that these reaction pathways requires much higher activation energies than that of oxidative addition of fluorobenzene to nickel(0) complex described in the manuscript. These results are consistent with the experimental observations using $Ni(cod)_2$ as a catalyst, indicating that participation of nickel(0) complexes to the catalytic systems.

Generation of Nickel(0) Species

In the experimental observations, the use of KO*t*Bu are crucial for forming catalytically active species from nickel(II) precursor, $NiBr_2$·diglyme. It is proposed that *tert*-butoxide anion is required for forming nickel(0) species through reductive elimination of an organophosphate from nickel(II) complexes, as described in Figure 3.24a. According to the DFT calculation results shown in Figure 3.24b, possible reductive elimination of *tert*-butyl diisopropyl phosphate from **Int-G** affords nickel(0) complex **Int-H** through $\mathbf{TS_{G\text{-}H}}$ with an energy barrier of 18.6 kcal·mol^{-1} as a 0.2 kcal·mol^{-1} exergonic process. This process possibly occurs at the reaction conditions (120 °C) in terms of energy barrier.

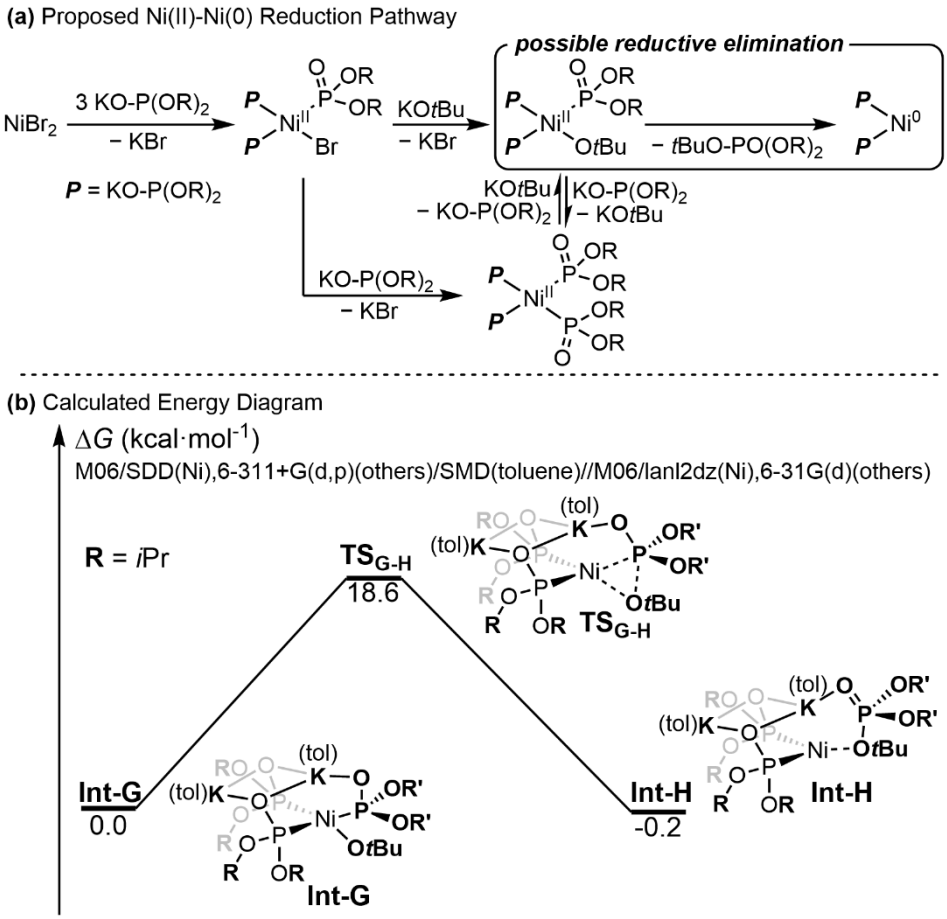

Figure 3.24. (a) Proposed Ni(II) pre-catalysts reduction pathway. (b) Energy diagram for reductive elimination.

Energies of Each Geometry

Table S9. Energies of each geometry

Geometry Name	solvation electronic energies (E) [Hartree]	thermal free energy corrections (G_{corr}) [Hartree]	solution phase Gibbs free energies (G_{sol}) [Hartree]
Int-1a	–3853.251209	0.671177	–3852.580032
TS_{1a-2a}	–3853.227258	0.669736	–3852.557522
Int-2a	–3853.270340	0.672937	–3852.597403
Int-3a	–4557.453970	0.860003	–4556.593967
TS_{3a-4a}	–4557.435069	0.858510	–4556.576559
Int-4a	–4557.466168	0.860776	–4556.605392
Int-1b	–4010.431973	0.778346	–4009.653627
TS_{1b-2b}	–4010.406463	0.778027	–4009.628436
Int-2b	–4010.451051	0.776735	–4009.674316
Int-3b	–4793.222215	1.024269	–4792.197946
TS_{3b-4b}	–4793.189928	1.023948	–4792.165980
Int-4b	–4793.233513	1.025705	–4792.207808
Int-A	–2110.400975	0.438566	–2109.962409
Int-B	–2110.378259	0.435297	–2109.942962
TS_{B-C}	–2110.333623	0.433280	–2109.900343
Int-C	–2110.366095	0.434879	–2109.931216
Int-D	–3785.829381	0.741778	–3785.087603
TS_{D-E}	–3785.799984	0.746296	–3785.053688
Int-E	–3785.825990	0.745598	–3785.080392
TS_{E-F}	–3785.826342	0.744032	–3785.082310
Int-F	–3785.885455	0.748776	–3785.136679
Int-D′	–3785.816179	0.736791	–3785.079388
$TS_{D'-E'}$	–3785.796554	0.743022	–3785.053532
Int-E′	–3785.888322	0.749701	–3785.138621
Int-G	–4558.924871	0.899325	–4558.025546
TS_{G-H}	–4558.891378	0.895417	–4557.995961
Int-H	–4558.920884	0.895018	–4558.025866
(tol)KOP(O*i*Pr)$_2$	–1675.410154	0.278253	–1675.131901

3.4.11 Compound Characterization Data

Dicyclohexyl [1,1'-Biphenyl]-4-ylphosphonate (3a)

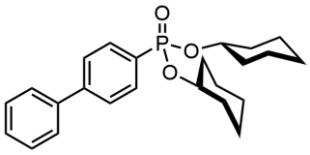

According to the procedure B, the product **3a** was isolated by flash chromatography on silica gel with slow gradient elution (CH_2Cl_2/MeOH 100:0-to-97:3) followed by preparative thin layer chromatography (CH_2Cl_2/MeOH 98:2) as a whitish oil (49.4 mg, 0.124 mmol, 99% yield). **^{1}H NMR** (400 MHz, $CDCl_3$): δ 7.89 (dd, J = 13.2, 8.4 Hz, 2H), 7.67 (dd, J = 8.4, 4.4 Hz, 2H), 7.62 (d, J = 7.6 Hz, 2H), 7.47 (dd, J = 6.8, 6.8 Hz, 2H), 7.39 (dd, J = 7.6, 7.6 Hz, 1H), 4.51–4.38 (m, 2H), 2.09–1.96 (m, 2H), 1.88–1.66 (m, 6H), 1.66–1.42 (m, 6H), 1.42–1.15 (m, 6H). **^{13}C{^{1}H} NMR** (100.5 MHz, $CDCl_3$): δ 144.6 (d, J_{C-P} = 2.9 Hz, 1C), 140.0 (s, 1C), 132.1 (d, J_{C-P} = 10.6 Hz, 2C), 128.82 (s, 2C), 128.76 (d, J_{C-P} = 190.7 Hz, 1C), 128.0 (s, 1C), 127.2 (s, 2C), 126.9 (d, J_{C-P} = 14.4 Hz, 2C), 75.5 (d, J_{C-P} = 4.8 Hz, 2C), 33.7 (d, J_{C-P} = 2.9 Hz, 2C), 33.5 (d, J_{C-P} = 4.8 Hz, 2C), 25.1 (s, 2C), 23.63 (s, 2C), 23.56 (s, 2C). **^{31}P{^{1}H} NMR** (161.8 MHz, $CDCl_3$): δ 17.4. **IR** (ATR): 2935, 2859, 2231, 1601, 1485, 1449, 1392, 1372, 1239, 1133, 1043, 977, 925, 907, 892, 868, 832, 792, 761, 726, 696, 669 cm^{-1}. **HRMS-ESI** (*m/z*): $[M+Na]^+$ Calcd for $C_{24}H_{31}O_3NaP$ 421.1903; found 421.1902.

Dicyclohexyl (4-Methoxyphenyl)phosphonate (3b)

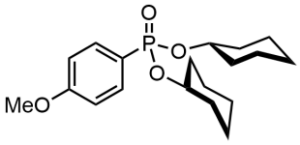

According to the procedure B, the product **3b** was isolated by flash chromatography on silica gel with slow gradient elution (CH_2Cl_2/MeOH 100:0-to-97:3) followed by preparative thin layer chromatography (CH_2Cl_2/MeOH 98:2) as a whitish oil (43.8 mg, 0.124 mmol, 99% yield). **^{1}H NMR** (400 MHz, $CDCl_3$): δ 7.75 (dd, J = 12.8, 9.2 Hz, 2H), 6.94 (dd, J = 8.8, 3.2 Hz, 2H), 4.43–4.31 (m, 2H), 3.85 (s, 3H), 2.08–1.93 (m, 2H), 1.87–1.63 (m, 6H), 1.63–1.38 (m, 6H), 1.38–1.14 (m, 6H). **^{13}C{^{1}H} NMR** (100.5 MHz, $CDCl_3$): δ 162.4 (d, J_{C-P} = 2.8 Hz, 1C), 133.6 (d, J_{C-P} = 11.5 Hz, 2C), 121.6 (d, J_{C-P} = 196.5 Hz, 1C), 113.7 (d, J_{C-P} = 15.3 Hz, 2C), 75.2 (d, J_{C-P} = 5.8 Hz, 2C), 55.2 (s, 1C), 33.7 (d, J_{C-P} = 4.5 Hz, 2C), 33.5 (d, J_{C-P} = 7.6 Hz, 2C), 25.1 (s, 2C), 23.64 (s, 2C), 23.58 (s, 2C). **^{31}P{^{1}H} NMR** (161.8 MHz, $CDCl_3$): δ 18.1. **IR** (ATR): 2934, 2858, 1599, 1572,

1505, 1450, 1409, 1372, 1296, 1239, 1180, 1154, 1131, 1043, 1021, 972, 926, 892, 868, 814, 801, 791, 771, 728, 662 cm^{-1}. **HRMS-ESI** (*m/z*): $[M+Na]^+$ Calcd for $C_{19}H_{29}O_4NaP$ 375.1696; found 375.1698.

Dicyclohexyl 4-(Dimethylamino)phenylphosphonate (3c)

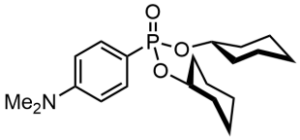

According to the procedure A, the product **3c** was isolated by flash chromatography on silica gel with slow gradient elution (CH_2Cl_2/MeOH 100:0-to-98:2) followed by preparative thin layer chromatography (CH_2Cl_2/MeOH 98:2) as a white powder (31.1 mg, 0.085 mmol, 68% yield). **M.p.**: 106.8–107.1 °C. **^{1}H NMR** (400 MHz, $CDCl_3$): δ 7.65 (dd, J = 12.4, 8.4 Hz, 2H), 6.68 (dd, J = 9.2, 3.6 Hz, 2H), 4.39–4.28 (m, 2H), 3.01 (s, 6H), 2.04–1.94 (m, 2H), 1.83–1.64 (m, 6H), 1.64–1.38 (m, 6H), 1.38–1.14 (m, 6H). **^{13}C{^{1}H} NMR** (100.5 MHz, $CDCl_3$): δ 152.4 (d, $J_{C–P}$ = 2.9 Hz, 1C), 133.2 (d, $J_{C–P}$ = 11.5 Hz, 2C), 115.0 (d, $J_{C–P}$ = 200.5 Hz, 1C), 111.0 (d, $J_{C–P}$ = 16.3 Hz, 2C), 74.8 (d, $J_{C–P}$ = 4.8 Hz, 2C), 39.9 (s, 2C), 33.8 (d, $J_{C–P}$ = 3.8 Hz, 2C), 33.5 (d, $J_{C–P}$ = 4.8 Hz, 2C), 25.2 (s, 2C), 23.71 (s, 2C), 23.65 (s, 2C). **^{31}P{^{1}H} NMR** (161.8 MHz, $CDCl_3$): δ 20.1. **IR** (ATR): 2936, 2858, 1598, 1520, 1446, 1364, 1246, 1133, 1120, 1049, 970, 839, 824, 800 cm^{-1}. **HRMS-ESI** (*m/z*): $[M+Na]^+$ Calcd for $C_{20}H_{32}O_3NNaP$ 388.2012; found 388.2011.

Dicyclohexyl 4-(Diphenylamino)phenylphosphonate (3d)

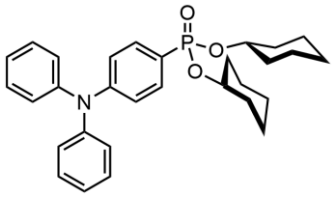

According to the procedure B, the product **3d** was isolated by flash chromatography on silica gel with slow gradient elution (CH_2Cl_2/MeOH 100:0-to-98:2) followed by preparative thin layer chromatography (CH_2Cl_2/MeOH 99:1) as a whitish oil (58.4 mg, 0.120 mmol, 96% yield). **^{1}H NMR** (400 MHz, $CDCl_3$): δ 7.60 (dd, J = 12.8, 9.2 Hz, 2H), 7.30 (dd, J = 7.2, 7.2 Hz, 4H), 7.18–7.07 (m, 6H), 7.01 (dd, J = 8.8, 3.2 Hz, 2H), 4.47–4.35 (m, 2H), 2.07–1.92 (m, 2H), 1.92–1.64 (m, 6H), 1.64–1.41 (m, 6H), 1.41–1.12 (m, 6H). **^{13}C{^{1}H} NMR** (100.5 MHz, $CDCl_3$): δ 151.0 (d, $J_{C–P}$ = 3.9 Hz, 1C), 146.7 (s, 2C), 132.7 (d, $J_{C–P}$ = 10.6 Hz, 2C), 129.5 (s, 4C), 125.7 (s, 4C), 124.2 (s, 2C), 121.3 (d, $J_{C–P}$ = 197.4 Hz, 1C), 120.2 (d, $J_{C–P}$ = 15.4 Hz, 2C), 75.2 (d, $J_{C–P}$ = 5.8 Hz, 2C), 33.8 (d, $J_{C–P}$ =

3.8 Hz, 2C), 33.6 (d, J_{C-P} = 4.8 Hz, 2C), 25.2 (s, 2C), 23.7 (s, 2C), 23.6 (s, 2C). **$^{31}P\{^{1}H\}$ NMR** (161.8 MHz, $CDCl_3$): δ 18.5. **IR** (ATR): 2934, 2857, 1586, 1490, 1450, 1372, 1331, 1317, 1267, 1191, 1154, 1130, 1043, 1021, 974, 892, 825, 792, 726, 695, 669, 622 cm^{-1}. **HRMS-ESI** (*m/z*): $[M+Na]^+$ Calcd for $C_{30}H_{36}O_3NNaP$ 512.2325; found 512.2326.

Dicyclohexyl *p*-Tolylphosphonate (3e)

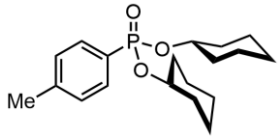

The reaction was performed according to the slightly modified procedure A. After the reaction, the crude mixture was cooled to room temperature and diluted with EtOAc. The resulting mixture was washed with deionized water and brine. The organic layer was dried over Na_2SO_4. After filtration and evaporation, the product **3e** was isolated by flash chromatography on silica gel with slow gradient elution (CH_2Cl_2/MeOH 100:0-to-97.5:1.5) followed by preparative thin layer chromatography (CH_2Cl_2/MeOH 98:2) as a colorless oil (29.4 mg, 0.088 mmol, 70% yield). **^{1}H NMR** (400 MHz, $CDCl_3$): δ 7.70 (dd, J = 13.2, 8.4 Hz, 2H), 7.24 (dd, J = 8.4, 4.4 Hz, 4H), 4.45–4.33 (m, 2H), 2.39 (s, 3H), 2.04–1.94 (m, 2H), 1.83–1.63 (m, 6H), 1.63–1.52 (m, 2H), 1.52–1.38 (m, 4H), 1.38–1.13 (m, 6H). **$^{13}C\{^{1}H\}$ NMR** (100.5 MHz, $CDCl_3$): δ 142.3 (d, J_{C-P} = 3.8 Hz, 1C), 131.7 (d, J_{C-P} = 10.6 Hz, 2C), 129.0 (d, J_{C-P} = 15.3 Hz, 2C), 127.1 (d, J_{C-P} = 190.6 Hz, 1C), 75.3 (d, J_{C-P} = 5.7 Hz, 2C), 33.8 (d, J_{C-P} = 2.8 Hz, 2C), 33.5 (d, J_{C-P} = 4.8 Hz, 2C), 25.2 (s, 2C), 23.7 (s, 2C), 23.6 (s, 2C), 21.6 (s, 1C). **$^{31}P\{^{1}H\}$ NMR** (161.8 MHz, $CDCl_3$): δ 17.9. **IR** (ATR): 2934, 2853, 1606, 1450, 1372, 1244, 1187, 1155, 1129, 1044, 974, 925, 893, 868, 832, 810, 791, 729, 713, 658, 535, 523 cm^{-1}. **HRMS-ESI** (*m/z*): $[M+Na]^+$ Calcd for $C_{19}H_{29}O_3NaP$ 359.1747; found 359.1744.

Dicyclohexyl Phenylphosphonate (3f)

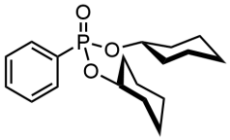

The reaction was performed according to the slightly modified procedure A. After the reaction, the crude mixture was cooled to room temperature and diluted with EtOAc. The resulting mixture was washed with deionized water and brine. The organic layer was dried over Na_2SO_4. After filtration and evaporation, the product **3f** was isolated by flash chromatography on silica gel with slow gradient elution (CH_2Cl_2/MeOH 100:0-to-98:2) as a colorless oil (36.3 mg, 0.11 mmol, 90% yield). **^{1}H NMR** (400 MHz, $CDCl_3$): δ 7.82

(dd, J = 13.2, 6.8 Hz, 2H), 7.51 (dd, J = 8.0, 8.0 Hz, 1H), 7.47–7.39 (m, 2H), 4.48–4.36 (m, 2H), 2.07–1.94 (m, 2H), 1.85–1.64 (m, 6H), 1.64–1.39 (m, 6H), 1.39–1.15 (m, 6H). **^{13}C{^{1}H} NMR** (100.5 MHz, $CDCl_3$): δ 131.9 (d, J_{C-P} = 2.9 Hz, 1C), 131.6 (d, J_{C-P} = 9.6 Hz, 2C), 130.4 (d, J_{C-P} = 188.8 Hz, 1C), 128.2 (d, J_{C-P} = 14.5 Hz, 2C), 75.5 (d, J_{C-P} = 5.7 Hz, 2C), 33.8 (d, J_{C-P} = 2.8 Hz, 2C), 33.5 (d, J_{C-P} = 4.7 Hz, 2C), 25.2 (s, 2C), 23.7 (s, 2C), 23.6 (s, 2C). **^{31}P{^{1}H} NMR** (161.8 MHz, $CDCl_3$): δ 17.2. **IR** (ATR): 2934, 2858, 1440, 1449, 1373, 1247, 1155, 1131, 1044, 975.3, 926, 868, 831, 792, 750, 718, 696 cm^{-1}. **HRMS-ESI** (*m/z*): $[M+Na]^+$ Calcd for $C_{18}H_{27}O_3NaP$ 345.1590; found 345.1594.

Dicyclohexyl 4-(4-Morpholinylcarbonyl)phenylphosphonate (3g)

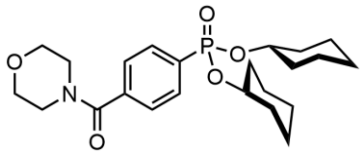

According to the procedure A, the product **3g** was isolated by flash chromatography on silica gel with slow gradient elution (CH_2Cl_2/MeOH 100:0-to-95:5) followed by preparative thin layer chromatography (CH_2Cl_2/MeOH 96.5:3.5) as a whitish oil (44.0 mg, 0.11 mmol, 86% yield). **^{1}H NMR** (400 MHz, $CDCl_3$): δ 7.88 (dd, J = 11.6, 8.4 Hz, 2H), 7.48 (dd, J = 6.8, 3.2 Hz, 2H), 4.50–4.37 (m, 2H), 3.20–4.00 (m, 8H), 2.08–1.92 (m, 2H), 1.88–1.64 (m, 6H), 1.64–1.40 (m, 6H), 1.40–1.13 (m, 6H). **^{13}C{^{1}H} NMR** (100.5 MHz, $CDCl_3$): δ 169.4 (s, 1C), 138.5 (d, J_{C-P} = 3.8 Hz, 1C), 132.1 (d, J_{C-P} = 189.7 Hz, 1C), 131.9 (d, J_{C-P} = 9.6 Hz, 2C), 126.8 (d, J_{C-P} = 14.4 Hz, 2C), 75.8 (d, J_{C-P} = 5.7 Hz, 2C), 66.7 (s, 2C), 48.0 (s, 1C), 42.4 (s, 1C), 33.7 (d, J_{C-P} = 3.8 Hz, 2C), 33.5 (d, J_{C-P} = 4.7 Hz, 2C), 25.0 (s, 2C), 23.6 (s, 2C), 23.5 (s, 2C). **^{31}P{^{1}H} NMR** (161.8 MHz, $CDCl_3$): δ 15.6. **IR** (ATR): 2936, 2858, 2234, 1635, 1557, 1499, 1450, 1431, 1390, 1371, 1278, 1242, 1115, 1043, 1026, 923, 869, 835, 792, 752, 668 cm^{-1}. **HRMS-ESI** (*m/z*): $[M+Na]^+$ Calcd for $C_{23}H_{34}O_5NNaP$ 458.2067; found 458.2068.

Dicyclohexyl 4-(Diethylcarbamoyl)phenylphosphonate (3h)

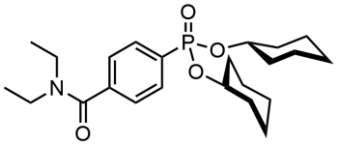

According to the procedure A, the product **3h** was isolated by flash chromatography on silica gel with slow gradient elution (CH_2Cl_2/MeOH 100:0-to-98:2) as a colorless oil (38.9 mg, 0.093 mmol, 74% yield). **^{1}H NMR** (400 MHz, $CDCl_3$): δ 7.86 (dd, J = 13.2,

8.0 Hz, 2H), 7.44 (dd, J = 8.0, 3.6 Hz, 2H), 4.49–4.37 (m, 2H), 3.56 (q, J = 6.8 Hz, 2H), 3.22 (q, J = 6.8 Hz, 2H), 2.06–1.94 (m, 2H), 1.87–1.65 (m, 6H), 1.65–1.40 (m, 6H), 1.40–1.16 (m, 9H), 1.10 (t, J = 6.8 Hz, 3H). **^{13}C{^{1}H} NMR** (100.5 MHz, $CDCl_3$): δ 170.2 (s, 1C), 140.5 (d, $J_{C–P}$ = 2.8 Hz, 1C), 131.8 (d, $J_{C–P}$ = 9.5 Hz, 2C), 131.2 (d, $J_{C–P}$ = 190.7 Hz, 1C), 126.0 (d, $J_{C–P}$ = 14.4 Hz, 2C), 75.7 (d, $J_{C–P}$ = 5.8 Hz, 2C), 43.2 (s, 1C), 39.2 (s, 1C), 33.7 (d, $J_{C–P}$ = 3.8 Hz, 2C), 33.5 (d, $J_{C–P}$ = 3.8 Hz, 2C), 25.0 (s, 2C), 23.6 (s, 2C), 23.5 (s, 2C), 14.1 (s, 1C), 12.8 (s, 1C). **^{31}P{^{1}H} NMR** (161.8 MHz, $CDCl_3$): δ 16.1. **IR** (ATR): 2935, 2859, 2233, 1631, 1500, 1449, 1427, 1374, 1316, 1288, 1244, 1132, 1091, 1043, 977, 924, 893, 868, 834, 791, 760, 727, 658 cm^{-1}. **HRMS-ESI** (*m/z*): $[M+Na]^+$ Calcd for $C_{23}H_{36}O_4NNaP$ 444.2274; found 444.2277.

Dicyclohexyl 4-(Trifluoromethyl)phenylphosphonate (3i)

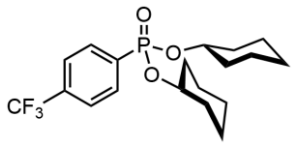

The reaction was performed according to the slightly modified procedure A. After the reaction, the crude mixture was cooled to room temperature and diluted with EtOAc. The resulting mixture was washed with deionized water and brine. The organic layer was dried over Na_2SO_4. After filtration and evaporation, the product **3i** was isolated by flash chromatography on silica gel with slow gradient elution (CH_2Cl_2/MeOH 100:0-to-96:4) as a colorless oil (7.1 mg, 0.019 mmol, 15% yield). **^{1}H NMR** (400 MHz, $CDCl_3$): δ 7.95 (dd, J = 12.8, 8.0 Hz, 2H), 7.71 (dd, J = 11.2, 3.2 Hz, 2H), 4.51–4.38 (m, 2H), 2.06–1.94 (m, 2H), 1.85–1.42 (m, 12H), 1.42–1.15 (m, 6H). **^{13}C{^{1}H} NMR** (100.5 MHz, $CDCl_3$): δ 134.7 (d, $J_{C–P}$ = 188.7 Hz, 1C), 133.6 (q, $J_{C–F}$ = 31.6 Hz, 1C), 132.1 (d, $J_{C–P}$ = 10.6 Hz, 2C), 125.1 (dq, $J_{C–P,\ C–F}$ = 15.4, 3.8 Hz, 2C), 123.6 (q, $J_{C–F}$ = 274.1 Hz, 1C), 76.1 (d, $J_{C–P}$ = 5.7 Hz, 2C), 33.7 (d, $J_{C–P}$ = 20.2 Hz, 2C), 33.6 (d, $J_{C–P}$ = 21.1 Hz, 2C), 25.1 (s, 2C), 23.6 (s, 2C), 23.5 (s, 2C). **^{31}P{^{1}H} NMR** (161.8 MHz, $CDCl_3$): δ 14.7. **IR** (ATR): 2938, 2860, 1451, 1399, 1324, 1353, 1169, 1132, 1107, 1063, 1044, 986, 894, 835, 711 cm^{-1}. **HRMS-ESI** (*m/z*): $[M+Na]^+$ Calcd for $C_{19}H_{26}O_3F_3NaP$ 413.1464; found 413.1461.

Dicyclohexyl 1-Naphthylphosphonate (3j)

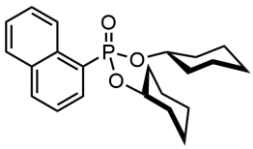

According to the procedure A, the product **3j** was isolated by flash chromatography on silica gel with slow gradient elution (CH_2Cl_2/MeOH 100:0-to-98:2) followed by preparative thin layer chromatography (CH_2Cl_2/MeOH 99:1) as a colorless oil (43.3 mg, 0.12 mmol, 93% yield). **^{1}H NMR** (400 MHz, $CDCl_3$): δ 8.55 (d, J = 8.0 Hz, 1H), 8.28 (dd, J = 16.4, 6.8 Hz, 1H), 8.01 (d, J = 8.0 Hz, 1H), 7.88 (d, J = 7.2 Hz, 1H), 7.62–7.45 (m, 3H), 4.54–4.42 (m, 2H), 2.10–1.99 (m, 2H), 1.83–1.53 (m, 8H), 1.53–1.27 (m, 6H), 1.27–1.11 (m, 4H). **^{13}C{^{1}H} NMR** (100.5 MHz, $CDCl_3$): δ 134.2 (d, $J_{C–P}$ = 9.5 Hz, 1C), 133.5 (d, $J_{C–P}$ = 12.5 Hz, 1C), 133.2 (d, $J_{C–P}$ = 2.8 Hz, 1C), 132.7 (d, $J_{C–P}$ = 10.6 Hz, 1C), 128.6 (s, 1C), 127.1 (d, $J_{C–P}$ = 3.8 Hz, 1C), 126.9 (s, 1C), 126.5 (d, $J_{C–P}$ = 183.9 Hz, 1C), 126.1 (s, 1C), 124.4 (d, $J_{C–P}$ = 16.3 Hz, 1C), 75.7 (d, $J_{C–P}$ = 5.7 Hz, 2C), 33.8 (d, $J_{C–P}$ = 3.8 Hz, 2C), 33.4 (d, $J_{C–P}$ = 4.7 Hz, 2C), 25.1 (s, 2C), 23.6 (s, 2C), 23.5 (s, 2C). **^{31}P{^{1}H} NMR** (161.8 MHz, $CDCl_3$): δ 17.4. **IR** (ATR): 2934, 2858, 2231, 1591, 1572, 1508, 1449, 1372, 1336, 1244, 1206, 1152, 1123, 1042, 1019, 970, 926, 892, 868, 802, 792, 774, 729, 676 cm^{-1}. **HRMS-ESI** (*m/z*): $[M+Na]^+$ Calcd for $C_{22}H_{29}O_3NaP$ 395.1748; found 395.1752.

Dicyclohexyl 4-(1-Naphthyl)phenylphosphonate (3k)

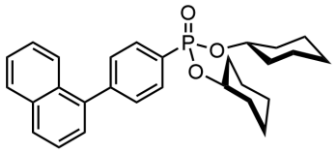

According to the procedure B, the product **3k** was isolated by flash chromatography on silica gel with slow gradient elution (CH_2Cl_2/MeOH 100:0-to-97:3) followed by preparative thin layer chromatography (CH_2Cl_2/MeOH 99:1) as a whitish oil (55.6 mg, 0.124 mmol, 99% yield). **^{1}H NMR** (400 MHz, $CDCl_3$): δ 7.99–7.80 (m, 5H), 7.62–7.37 (m, 6H), 4.58–4.45 (m, 2H), 2.12–1.98 (m, 2H), 1.98–1.69 (m, 6H), 1.69–1.46 (m, 6H), 1.46–1.11 (m, 6H). **^{13}C{^{1}H} NMR** (100.5 MHz, $CDCl_3$): δ 144.4 (d, $J_{C–P}$ = 2.9 Hz, 1C), 139.1 (s, 1C), 133.7 (s, 1C), 131.5 (d, $J_{C–P}$ = 10.5 Hz, 2C), 131.1 (s, 1C), 130.0 (s, 1C), 129.8 (s, 1C), 129.0 (d, $J_{C–P}$ = 193.6 Hz, 1C), 128.2 (d, $J_{C–P}$ = 16.3 Hz, 1C), 126.9 (s, 1C), 126.2 (s, 1C), 125.9 (s, 1C), 125.6 (s, 1C), 125.3 (s, 1C), 75.6 (d, $J_{C–P}$ = 5.7 Hz, 2C), 33.8 (d, $J_{C–P}$ = 2.9 Hz, 2C), 33.6 (d, $J_{C–P}$ = 3.8 Hz, 2C), 25.1 (s, 2C), 23.7 (s, 2C), 23.6 (s, 2C). **^{31}P{^{1}H} NMR** (161.8 MHz, $CDCl_3$): δ 17.5. **IR** (ATR): 2935, 2858, 2231, 1604, 1593,

1509, 1449, 1395, 1372, 1335, 1239, 1135, 1112, 1043, 977, 893, 868, 833, 800, 792, 777, 727, 556 cm^{-1}. **HRMS-ESI** (*m/z*): $[M+Na]^+$ Calcd for $C_{28}H_{33}O_3NaP$ 471.2060; found 471.2066.

Dicyclohexyl [1,1'-Biphenyl]-3-ylphosphonate (3l)

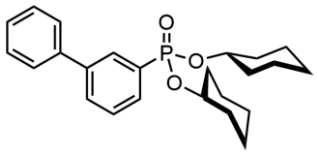

According to the procedure A, the product **3l** was isolated by flash chromatography on silica gel with slow gradient elution (CH_2Cl_2/MeOH 100:0-to-98:2) followed by preparative thin layer chromatography (CH_2Cl_2/MeOH 99:1) as a colorless oil (46.1 mg, 0.12 mmol, 93% yield). **^{1}H NMR** (400 MHz, $CDCl_3$): δ 8.05 (d, J = 14.0 Hz, 1H), 7.79 (dd, J = 12.8, 7.2 Hz, 1H), 7.74 (d, J = 7.8 Hz, 1H), 7.61 (d, J = 7.6 Hz, 2H), 7.54–7.48 (m, 1H), 7.46 (dd, J = 7.2, 7.2 Hz, 2H), 7.37 (dd, J = 7.2, 7.2 Hz, 1H), 4.53–4.39 (m, 2H), 2.08–1.96 (m, 2H), 1.87–1.55 (m, 8H), 1.55–1.42 (m, 4H), 1.42–1.12 (m, 6H). **^{13}C{^{1}H} NMR** (100.5 MHz, $CDCl_3$): δ 141.2 (d, J_{C-P} = 15.4 Hz, 1C), 140.1 (s, 1C), 131.0 (d, J_{C-P} = 188.7 Hz, 1C), 130.6 (d, J_{C-P} = 2.9 Hz, 1C), 130.4 (d, J_{C-P} = 10.6 Hz, 1C), 130.3 (d, J_{C-P} = 10.6 Hz, 1C), 128.8 (s, 2C), 128.7 (d, J_{C-P} = 15.4 Hz, 1C), 127.7 (s, 1C), 127.1 (s, 2C), 75.6 (d, J_{C-P} = 5.7 Hz, 2C), 33.8 (d, J_{C-P} = 2.8 Hz, 2C), 33.6 (d, J_{C-P} = 4.8 Hz, 2C), 25.1 (s, 2C), 23.7 (s, 2C), 23.6 (s, 2C). **^{31}P{^{1}H} NMR** (161.8 MHz, $CDCl_3$): δ 17.1. **IR** (ATR): 2934, 2858, 1596, 1473, 1449, 1402, 1373, 1244, 1192, 1129, 1042, 1021, 973, 926, 892, 869, 834, 818, 803, 791,755, 730, 700, 692, 621, 614, 599, 570, 535 cm^{-1}. **HRMS-ESI** (*m/z*): $[M+Na]^+$ Calcd for $C_{24}H_{31}O_3NaP$ 421.1903; found 421.1908.

Dicyclohexyl 3-Pyridylphosphonate (3o)

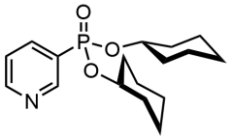

According to the procedure A, the product **3o** was isolated by flash chromatography on silica gel with slow gradient elution (CH_2Cl_2/MeOH 100:0-to-97:3) as a colorless oil (39.6 mg, 0.12 mmol, 98% yield). **^{1}H NMR** (400 MHz, $CDCl_3$): δ 8.99 (d, J = 6.4 Hz, 1H), 8.75 (d, J = 2.4 Hz, 1H), 8.17–8.03 (m, 1H), 7.43–7.33 (m, 1H), 4.54–4.37 (m, 2H), 2.07–1.87 (m, 2H), 1.87–1.41 (m, 12H), 1.41–1.11 (m, 6H). **^{13}C{^{1}H} NMR** (100.5 MHz, $CDCl_3$): δ 152.5 (s, 1C), 152.1 (d, J_{C-P} = 12.5 Hz, 1C), 139.2 (d, J_{C-P} = 7.6 Hz, 1C), 126.6 (d, J_{C-P} = 189.6 Hz, 1C), 123.1 (d, J_{C-P} = 11.5 Hz, 1C), 76.1 (d, J_{C-P} = 6.7 Hz, 2C), 33.6

(d, $J_{C–P}$ = 6.5 Hz, 2C), 33.4 (d, $J_{C–P}$ = 3.8 Hz, 2C), 25.0 (s, 2C), 23.5 (s, 2C), 23.4 (s, 2C). **^{31}P{^{1}H} NMR** (161.8 MHz, $CDCl_3$): δ 14.1. **IR** (ATR): 2934, 2853, 1580, 1566, 1450, 1405, 1373, 1329, 1251, 1194, 1143, 1121, 1044, 974, 892, 868, 829, 812, 739, 709 cm^{-1}. **HRMS-ESI** (*m/z*): $[M+Na]^+$ Calcd for $C_{17}H_{26}O_3NNaP$ 346.1543; found 346.1547.

Dicyclohexyl 4-(*9H*-Carbazol-9-yl)phenylphosphonate (3p)

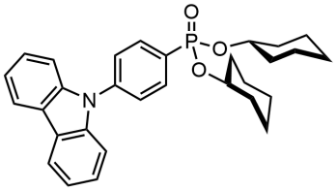

According to the procedure A, the product **3p** was isolated by flash chromatography on silica gel with slow gradient elution (CH_2Cl_2/MeOH 100:0-to-98:2) followed by preparative thin layer chromatography (CH_2Cl_2/MeOH 99:1) as a colorless oil (50.4 mg, 0.10 mmol, 83% yield). **^{1}H NMR** (400 MHz, $CDCl_3$): δ 8.14 (d, *J* = 8.0 Hz, 2H), 8.05 (dd, *J* = 13.2, 8.4 Hz, 2H), 7.68 (dd, *J* = 8.4, 3.2 Hz, 2H), 7.50–7.37 (m, 4H), 7.31 (dd, *J* = 7.6, 7.6 Hz, 2H), 4.60–4.46 (m, 2H), 2.13–1.99 (m, 2H), 1.99–1.86 (m, 2H), 1.86–1.46 (m, 10H), 1.46–1.16 (m, 6H). **^{13}C{^{1}H} NMR** (100.5 MHz, $CDCl_3$): δ 141.1 (d, $J_{C–P}$ = 2.9 Hz, 1C), 140.2 (s, 2C), 133.3 (d, $J_{C–P}$ = 10.5 Hz, 2C), 129.1 (d, $J_{C–P}$ = 192.6 Hz, 1C), 126.3 (d, $J_{C–P}$ = 15.4 Hz, 2C), 126.1 (s, 2C), 123.7 (s, 2C), 120.42 (s, 2C), 120.37 (s, 2C), 109.7 (s, 2C), 75.9 (d, $J_{C–P}$ = 6.7 Hz, 2C), 33.8 (d, $J_{C–P}$ = 2.8 Hz, 2C), 33.6 (d, $J_{C–P}$ = 3.8 Hz, 2C), 25.2 (s, 2C), 23.7 (s, 2C), 23.6 (s, 2C). **^{31}P{^{1}H} NMR** (161.8 MHz, $CDCl_3$): δ 16.3. **IR** (ATR): 2935, 2853, 1580. 1566, 1450, 1406, 1373, 1329, 1251, 1195, 1143, 1121, 1044, 974, 892, 868, 829, 826, 812, 781, 739, 709 cm^{-1}. **HRMS-ESI** (*m/z*): $[M+Na]^+$ Calcd for $C_{30}H_{34}O_3NNaP$ 510.2169; found 510.2174.

Diisopropyl [1,1'-Biphenyl]-4-ylphosphonate (3q)

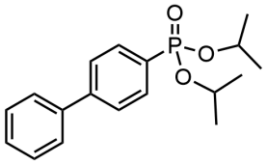

According to the procedure A, the product **3q** was isolated by flash chromatography on silica gel with slow gradient elution (CH_2Cl_2/MeOH 100:0-to-98:2) followed by preparative thin layer chromatography (CH_2Cl_2/MeOH 99:1) as a colorless oil (33.3 mg, 0.11 mmol, 84% yield). **^{1}H NMR** (400 MHz, $CDCl_3$): δ 7.89 (dd, *J* = 13.2, 6.8 Hz, 2H), 7.68 (dd, *J* = 7.2, 2.4 Hz, 2H), 7.62 (d, *J* = 8.4 Hz, 2H), 7.47 (dd, *J* = 8.4, 8.4 Hz, 2H), 7.39 (dd, *J* = 7.2, 7.2 Hz, 1H), 4.79–4.65 (m, 2H), 1.40 (d, *J* = 6.0 Hz, 6H), 1.26 (d, *J* =

5.6 Hz, 6H). **^{13}C{^{1}H} NMR** (100.5 MHz, $CDCl_3$): δ 144.7 (d, J_{C-P} = 2.8 Hz, 1C), 140.0 (s, 1C), 132.2 (d, J_{C-P} = 10.5 Hz, 2C), 128.9 (s, 2C), 128.5 (d, J_{C-P} = 189.7 Hz, 1C), 128.0 (s, 1C), 127.2 (s, 2C), 130.0 (d, J_{C-P} = 15.3 Hz, 2C), 70.7 (d, J_{C-P} = 4.8 Hz, 2C), 24.1 (d, J_{C-P} = 3.9 Hz, 2C), 23.9 (d, J_{C-P} = 4.8 Hz, 2C). **^{31}P{^{1}H} NMR** (161.8 MHz, $CDCl_3$): δ 17.4. **IR** (ATR): 2978, 2933, 1601, 1554, 1485, 1467, 1449, 1386, 1374, 1247, 1178, 1134, 1104, 1025, 1013, 972, 896, 885, 838, 760, 742, 727, 697, 667 cm^{-1}. **HRMS-ESI** (*m/z*): $[M+Na]^+$ Calcd for $C_{18}H_{23}O_3NaP$ 341.1277; found 341.1277.

Cyclohexyl (4-(Diethylcarbamoyl)phenyl)(phenyl)phosphinate (3u)

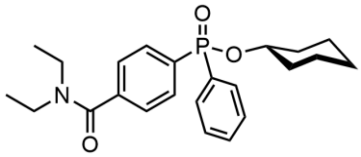

According to the procedure A, the product **3u** was isolated by flash chromatography on silica gel with slow gradient elution (CH_2Cl_2/MeOH 100:0-to-97:3) followed by preparative thin layer chromatography (CH_2Cl_2/MeOH 97:3) as a colorless oil (26.0 mg, 0.066 mmol, 53% yield). **^{1}H NMR** (400 MHz, $CDCl_3$): δ 7.91–7.78 (m, 4H), 7.56–7.49 (m, 1H), 7.48–7.40 (m, 4H), 4.49–4.36 (m, 1H), 3.54 (q, J = 6.4 Hz, 2H), 3.20 (q, J = 6.4 Hz, 2H), 1.98–1.84 (m, 2H), 1.81–1.69 (m, 2H), 1.68–1.54 (m, 2H), 1.54–1.42 (m, 2H), 1.37–1.18 (m, 5H), 1.08 (t, J = 6.8 Hz, 3H). **^{13}C{^{1}H} NMR** (100.5 MHz, $CDCl_3$): δ 170.2 (s, 1C), 140.5 (d, J_{C-P} = 2.9 Hz, 1C), 133.5 (d, J_{C-P} = 157.2 Hz, 1C), 132.1 (d, J_{C-P} = 157.1 Hz, 1C), 132.1 (d, J_{C-P} = 2.8 Hz, 1C), 131.8 (d, J_{C-P} = 10.6 Hz, 2C), 131.6 (d, J_{C-P} = 11.6 Hz, 2C), 128.4 (d, J_{C-P} = 13.5 Hz, 2C), 126.2 (d, J_{C-P} = 13.4 Hz, 2C), 75.2 (d, J_{C-P} = 5.7 Hz, 1C), 43.2 (s, 1C), 39.2 (s, 1C), 33.93 (d, J_{C-P} = 3.8 Hz, 1C), 33.86 (d, J_{C-P} = 3.8 Hz, 1C), 30.9 (d, J_{C-P} = 3.8 Hz, 1C), 25.1 (s, 1C), 23.5 (s, 1C), 14.2 (s, 1C), 12.8 (s, 1C). **^{31}P{^{1}H} NMR** (161.8 MHz, $CDCl_3$): δ 29.5. **IR** (ATR): 2935, 2859, 2227, 1629, 1555, 1499, 1438, 1427, 1382, 1348, 1316, 1288, 1224, 1129, 1113, 1090, 1070, 1036, 1009, 979, 924, 892, 872, 832, 790, 745, 727, 695, 654 cm^{-1}. **HRMS-ESI** (*m/z*): $[M+Na]^+$ Calcd for $C_{23}H_{30}O_3NNaP$ 422.1856; found 422.1855.

Diisopropyl (4-Methoxyphenyl)phosphonate (3v) (5.0 mmol scale)

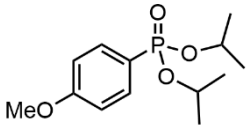

According to the procedure A, the product **3v** was isolated by flash chromatography on silica gel with slow gradient elution (CH_2Cl_2/MeOH 100:0-to-97:3) as a colorless oil

(1.14 g, 4.2 mmol, 84% yield). The isolated product was contaminated with a trace amount of **3x**. **^{1}H NMR** (400 MHz, $CDCl_3$): δ 7.75 (dd, J = 12.8, 8.8 Hz, 2H), 6.95 (dd, J = 8.8, 3.2 Hz, 2H), 4.72–4.54 (m, 2H), 3.85 (s, 3H), 1.36 (d, J = 6.0 Hz, 6H), 1.21 (d, J = 6.4 Hz, 6H). **^{13}C{^{1}H} NMR** (100.5 MHz, $CDCl_3$): δ 162.5 (d, J_{C-P} = 2.8 Hz, 1C), 133.6 (d, J_{C-P} = 11.5 Hz, 2C), 121.1 (d, J_{C-P} = 195.5 Hz, 1C), 113.7 (d, J_{C-P} = 16.3 Hz, 2C), 70.3 (d, J_{C-P} = 5.7 Hz, 2C), 55.2 (s, 1C), 24.0 (d, J_{C-P} = 3.8 Hz, 2C), 23.8 (d, J_{C-P} = 3.8 Hz, 2C). **^{31}P{^{1}H} NMR** (161.8 MHz, $CDCl_3$): δ 18.1. **IR** (ATR): 2979, 2935, 1600, 1573, 1505, 1466, 1386, 1374, 1296, 1241, 1178, 1132, 1104, 1015, 967, 896, 884, 832, 804, 771, 749, 659 cm^{-1}. **HRMS-ESI** (*m/z*): $[M+Na]^+$ Calcd for $C_{13}H_{21}O_4NaP$ 295.1070; found 295.1069.

Diisopropyl (4-((*3S*,*4R*)-3-((Benzo[d][1,3]dioxol-5-yloxy)methyl)-1-methylpiperidinyl)phenyl)phosphonate (3w)

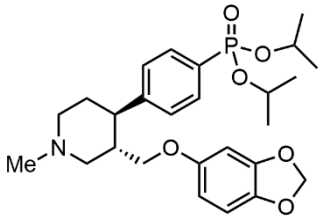

According to the procedure A, the product **3w** was isolated by flash chromatography on silica gel with slow gradient elution (CH_2Cl_2/MeOH 100:0-to-92:8) followed by preparative thin layer chromatography (CH_2Cl_2/MeOH 92:8) as a brownish oil (30.6 mg, 0.063 mmol, 50% yield). **^{1}H NMR** (400 MHz, $CDCl_3$): δ 7.73 (dd, J = 13.2, 8.4 Hz, 2H), 7.29 (dd, J = 8.8, 4.8 Hz, 2H), 6.61 (d, J = 8.4 Hz, 1H), 6.32 (d, J = 2.0 Hz, 1H), 6.10 (dd, J = 8.0, 2.0 Hz, 1H), 5.88 (s, 2H), 4.75–4.62 (m, 2H), 3.55 (dd, J = 8.8, 2.8 Hz, 1H), 3.43 (dd, J = 9.2, 7.2 Hz, 1H), 3.22 (dd, J = 11.6, 2.4 Hz, 1H), 3.01 (d, J = 11.2 Hz, 1H), 2.52 (td, J = 12.0, 4.0 Hz, 1H), 2.45–2.23 (m, 4H), 2.08 (dd, J = 20.8, 9.6 Hz, 2H), 2.01–1.79 (m, 2H), 1.36 (d, J = 6.4 Hz, 6H), 1.25–1.19 (m, 6H). **^{13}C{^{1}H} NMR** (100.5 MHz, $CDCl_3$): δ 154.2 (s, 1C), 148.3 (s, 1C), 148.1 (s, 1C), 141.5 (s, 1C), 132.0 (d, J_{C-P} = 10.6 Hz, 2C), 128.0 (d, J_{C-P} = 191.7 Hz, 1C), 127.5 (d, J_{C-P} = 15.2 Hz, 2C), 107.7 (s, 1C), 105.4 (s, 1C), 101.0 (s, 1C), 97.9 (s, 1C), 70.5 (d, J_{C-P} = 4.8 Hz, 2C), 69.3 (s, 1C), 59.3 (s, 1C), 55.9 (s, 1C), 46.3 (s, 1C), 44.2 (s, 1C), 41.6 (s, 1C), 33.8 (s, 1C), 24.0 (d, J_{C-P} = 3.8 Hz, 2C), 23.7 (d, J_{C-P} = 3.8 Hz, 2C). **^{31}P{^{1}H} NMR** (161.8 MHz, $CDCl_3$): δ 17.4. **IR** (ATR): 3676, 2977, 2935, 2733, 1632, 1605, 1503, 1488, 1468, 1406, 1384, 1242, 1181, 1132, 1103, 1077, 1065, 1038, 973, 930, 896, 885, 817, 772, 730, 706 cm^{-1}. **HRMS-ESI** (*m/z*): $[M+H]^+$ Calcd for $C_{26}H_{37}O_6NP$ 490.2353; found 490.2357.

Tetracyclohexyl 1,4-Phenylenebis(phosphonate) (5)

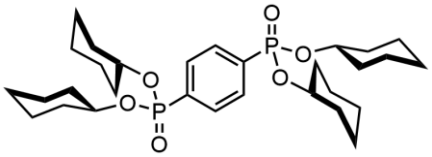

According to the modified procedure [Conditions: 1,4-difluorobenzne (**4**, 12.2 μL, 0.125 mmol, 1 equiv), **2a** (123.2 mg, 0.5 mmol, 4 equiv), $NiBr_2$·diglyme (2.2 mg, 0.00625 mmol, 5 mol%), KO*t*Bu (56.2 mg, 0.5 mmol, 4 equiv), PhMe (0.5 mL), 120 °C, 20 h], the product **5** was isolated by flash chromatography on silica gel with slow gradient elution (CH_2Cl_2/MeOH 100:0-to-97:3) followed by preparative thin layer chromatography (CH_2Cl_2/MeOH 98:2) as a whitish oil (39.5 mg, 0.079 mmol, 63% yield). **^{1}H NMR** (400 MHz, $CDCl_3$): δ 7.93–7.83 (m, 4H), 4.50–4.38 (m, 4H), 2.04–1.93 (m, 4H), 1.85–1.64 (m, 12H), 1.64–1.40 (m, 12H), 1.40–1.15 (m, 12H). **^{13}C{^{1}H} NMR** (100.5 MHz, $CDCl_3$): δ 134.2 (dd, J_{C-P} = 187.8, 2.8 Hz, 2C), 131.3 (dd, J_{C-P} = 11.5, 11.5 Hz, 4C), 75.9 (br, 4C), 33.7 (s, 4C), 33.5 (s, 4C), 25.0 (s, 4C), 23.6 (s, 4C), 23.5 (s, 4C). **^{31}P{^{1}H} NMR** (161.8 MHz, $CDCl_3$): δ 15.5. **IR** (ATR): 2934, 2858, 1450, 1373, 1242, 1141, 1041, 973, 892, 867, 826, 791, 729, 640, 607 cm^{-1}. **HRMS-ESI** (*m/z*): $[M+Na]^+$ Calcd for $C_{30}H_{48}O_6NaP_2$, 589.2818; found 589.2813.

3.5 References

[1] M. E. Falagas, E. K. Vouloumanou, G. Samonis, K. Z. Vardakas. Fosfomycin. *Clin. Microbiol. Rev.* **2016**, *29*, 321–347.

[2] K. Brücher, T. Gräwert, S. Konzuch, J. Held, C. Lienau, C. Behrendt, B. Illarionov, L. Maes, A. Bacher, S. Wittlin, B. Mordmüller, M. Fischer, T. Kurz. Prodrugs of Reverse Fosmidomycin Analogues. *J. Med. Chem.* **2015**, *58*, 2025–2035.

[3] M. Paúrová, J. Havlíčková, A. Pospíšilová, M. Vetrík, I. Císařová, H. Stephan, H.-J. Pietzsch, M. Hrubý, P. Hermann, J. Kotek. Bifunctional Cyclam-Based Ligands with Phosphorus Acid Pendant Moieties for Radiocopper Separation: Thermodynamic and Kinetic Studies. *Chem. Eur. J.* **2015**, *21*, 4671–4687.

[4] T. I. Kostelnik, H. Scheiber, R. Cappai, N. Choudhary, F. Lindheimer, M. Jaraquemada-Peláez, C. Orvig. Phosphonate Chelators for Medicinal Metal Ions. *Inorg. Chem.* **2021**, *60*, 5343–5361.

[5] S. P. Pujari, L. Scheres, A. T. M. Marcelis, H. Zuilhof. Covalent Surface Modification of Oxide Surfaces. *Angew. Chem., Int. Ed.* **2014**, *53*, 6322–6356.

[6] Y. Zhang, R. Cao, F. Yin, F.-Y. Lin, H. Wang, K. Krysiak, J.-H. No, D. Mukkamala, K. Houlihan, J. Li, C. T. Morita, E. Oldfield. Lipophilic Pyridinium Bisphosphonates: Potent γδ T Cell Stimulators. *Angew. Chem. Int. Ed.* **2010**, *49*, 1136–1138.

[7] Q. Dou, Y. Lang, H. Zeng, C.-J. Li. Photoinduced Transition-Metal and External Photosensitizer Free Phosphonation of Unactivated C(sp^2)–F Bond *via* SET Process Under Mild Conditions. *Fundam. Res.* **2021**, *1*, 742−746.

[8] J. N. H. Reek, B. Bruin, S. Pullen, T. J. Mooibroek, A. M. Kluwer, X. Caumes. Transition Metal Catalysis Controlled by Hydrogen Bonding in the Second Coordination Sphere. *Chem. Rev.* **2022**, *122*, 12308–12369.

[9] A. B. Pangborn, M. A. Giardello, R. H. Grubbs, R. K. Rosen, F. J. Timmers. Safe and Convenient Procedure for Solvent Purification. *Organometallics* **1996**, *15*, 1518–1520.

[10] J. K. Park, W. K. Shin, D. K. An. New and Efficient Synthesis of Amides from Acid Chlorides Using Diisobutyl(amino)aluminum. *Bull. Korean Chem. Soc.* **2013**, *34*, 1592–1594.

[11] X.-W. Liu, J. Echavarren, C. Zarate, R. Martin. Ni-Catalyzed Borylation of Aryl Fluorides *via* C–F Cleavage. *J. Am. Chem. Soc.* **2015**, *137*, 12470–12473.

[12] N. Santschi, A. Togni. Electrophilic Trifluoromethylation of *S*-Hydrogen Phosphorothioates. *J. Org. Chem.* **2011**, *76*, 4189–4193.

[13] G. Tran, D. G. Pardo, T. Tsuchiya, S. Hillebrand, J.-P. Vors, J. Cossy. Palladium-Catalyzed Phosphonylation: Synthesis of C3-, C4-, and C5-Phosphonylated

Pyrazoles. *Org. Lett.* **2013**, *15*, 5550–5553.

[14] B. Zheng, R. J. Fox, M. Sugiyama, A. Fritz, M. D. Eastgate. Development of Efficient Processes for the Preparation of Di-*tert*-butyl Potassium Phosphate and Di-*tert*-butyl (Chloromethyl) Phosphate. *Org. Process Res. Dev.* **2014**, *18*, 636–642.

[15] A. N. Bigley, T. Narindoshvili, D. F. Xiang, F. M. Raushel. Stereoselective Formation of Multiple Reaction Products by the Phosphotriesterase from *Sphingobium* sp. TCM1. *Biochemistry* **2020**, *59*, 1273−1288.

[16] A. J. Kendall, D. T. Seidenkranz, D. R. Tyler. Improved Synthetic Route to Heteroleptic Alkylphosphine Oxides. *Organometallics* **2017**, *36*, 2412–2417.

[17] R. Murakami, K. Sano, T. Iwai, T. Taniguchi, K. Monde, M. Sawamura. Palladium-Catalyzed Asymmetric C(sp^3)–H Allylation of 2-Alkylpyridines. *Angew. Chem. Int. Ed*. **2018**, *57*, 9465–9469; *Angew. Chem.* **2018**, *130*, 9609–9613.

[18] K. Muto, J. Yamaguchi, A. Lei, K. Itami. Isolation, Structure, and Reactivity of an Arylnickel(II) Pivalate Complex in Catalytic C–H/C–O Biaryl Coupling. *J. Am. Chem. Soc.* **2013**, *135*, 16384–16387.

[19] D. J. Darensbourg, J. C. Yarbrough, C. Ortiz, C. C. Fang. Comparative Kinetic Studies of the Copolymerization of Cyclohexene Oxide and Propylene Oxide with Carbon Dioxide in the Presence of Chromium Salen Derivatives. In Situ FTIR Measurements of Copolymer vs Cyclic Carbonate Production. *J. Am. Chem. Soc.* **2003**, *125*, 7586–7591.

[20] Gaussian16, Revision B.01. M. J. Frisch, G. W. Trucks, H. B. Schlegel, G. E. Scuseria, M. A. Robb, J. R. Cheeseman, G. Scalmani, V. Barone, G. A. Petersson, H. Nakatsuji, X. Li, M. Caricato, A. V. Marenich, J. Bloino, B. G. Janesko, R. Gomperts, B. Mennucci, H. P. Hratchian, J. V. Ortiz, A. F. Izmaylov, J. L. Sonnenberg, D. Williams-Young, F. Ding, F. Lipparini, F. Egidi, J. Goings, B. Peng, A. Petrone, T. Henderson, D. Ranasinghe, V. G. Zakrzewski, J. Gao, N. Rega, G. Zheng, W. Liang, M. Hada, M. Ehara, K. Toyota, R. Fukuda, J. Hasegawa, M. Ishida, T. Nakajima, Y. Honda, O. Kitao, H. Nakai, T. Vreven, K. Throssell, J. A. Montgomery Jr., J. E. Peralta, F. Ogliaro, M. J. Bearpark, J. J. Heyd, E. N. Brothers, K. N. Kudin, V. N. Staroverov, T. A. Keith, R. Kobayashi, J. Normand, K. Raghavachari, A. P. Rendell, J. C. Burant, S. S. Iyengar, J. Tomasi, M. Cossi, J. M. Millam, M. Klene, C. Adamo, R. Cammi, J. W. Ochterski, R. L. Martin, K. Morokuma, O. Farkas, J. B. Foresman, D.J. Fox. Gaussian, Inc., Wallingford CT, **2016**.

[21] Y. Zhao, D. G. Truhlar. The M06 Suite of Density Functionals for Main Group Thermochemistry, Thermochemical Kinetics, Noncovalent Interactions, Excited States, and Transition Elements: Two New Functionals and Systematic Testing of

Four M06-Class Functionals and 12 Other Functionals. *Theor. Chem. Acc.* **2008**, *120*, 215–241.

[22] P. J. Hay, W. R. Wadt. Ab Initio Effective Core Potentials for Molecular Calculations. Potentials for the Transition Metal Atoms Sc to Hg. *J. Chem. Phys.* **1985**, *82*, 270–283.

[23] W. R. Wadt, P. J. Hay. Ab Initio Effective Core Potentials for Molecular Calculations. Potentials for Main Group Elements Na to Bi. *J. Chem. Phys.* **1985**, *82*, 284–298.

[24] P. J. Hay, W. R. Wadt. Ab Initio Effective Core Potentials for Molecular Calculations. Potentials for K to Au Including the Outermost Core Orbitals. *J. Chem. Phys.* **1985**, *82*, 299–310.

[25] C. E. Check, T. O. Faust, J. M. Bailey, B. J. Wright, T. M. Gilbert, L. S. Sunderlin. Addition of Polarization and Diffuse Functions to the LANL2DZ Basis Set for P-Block Elements. *J. Phys. Chem. A* **2001**, *105*, 8111–8116.

[26] R. Ditchfield, W. J. Hehre, J. A. Pople. Self-Consistent Molecular-Orbital Methods. IX. An Extended Gaussian-Type Basis for Molecular-Orbital Studies of Organic Molecules. *J. Chem. Phys.* **1971**, *54*, 724–728.

[27] W. J. Hehre, R. Ditchfield, J. A. Pople. Self−Consistent Molecular Orbital Methods. XII. Further Extensions of Gaussian−Type Basis Sets for Use in Molecular Orbital Studies of Organic Molecules. *J. Chem. Phys.* **1972**, *56*, 2257–2261.

[28] W. J. Hehre, W. A. Lathan. Self-Consistent Molecular Orbital Methods. XIV. An Extended Gaussian-Type Basis for Molecular Orbital Studies of Organic Molecules. Inclusion of Second Row Elements. *J. Chem. Phys.* **1972**, *56*, 5255–5257.

[29] M. M. Francl, W. J. Pietro, W. J. Hehre, J. S. Binkley, M. S. Gordon, D. J. DeFrees, J. A. Pople. Self-Consistent Molecular Orbital Methods. XXIII. A Polarization-Type Basis Set for Second-Row Elements. *J. Chem. Phys.* **1982**, *77*, 3654–3665.

[30] A. V. Mitin, J. Baker, P. Pulay. An Improved 6-31G* Basis Set for First-Row Transition Metals. *J. Chem. Phys.* **2003**, *118*, 7775–7782.

[31] Global Reaction Route Mapping (GRRM) program, Version 17-A01. S. Maeda, Y. Harabuchi, Y. Sumiya, M. Takagi, K. Suzuki, K. Sugiyama, Y. Ono, M. Hatanaka, Y. Osada, T. Taketsugu, K. Morokuma, K. Ohno. **2017**.

[32] R. Krishnanm, J. S. Binkley, R. Seeger, J. A. Pople. Self-Consistent Molecular Orbital Methods. XX. A Basis Set for Correlated Wave Functions. *J. Chem. Phys.* **1980**, *72*, 650–654.

Publication List

Publications included in the thesis:

[1] **Zhensheng You**, Yusuke Masuda, Tomohiro Iwai, Kosuke Higashida, Masaya Sawamura. Nickel-Catalyzed Defluorophosphonylation of Aryl Fluorides. *The Journal of Organic Chemistry* **2022**, *87*, 14731−14737.

[2] **Zhensheng You**, Kosuke Higashida, Tomohiro Iwai, Masaya Sawamura. Phosphinylation of Non-Activated Aryl Fluorides through Nucleophilic Aromatic Substitution at the Boundary of Concerted and Stepwise Mechanisms. *Angewandte Chemie International Edition* **2021**, *60*, 5778−5782; *Angewandte Chemie* **2021**, *133*, 5842−5846.

Publications not included in the thesis:

[1] Tomohiro Iwai, Yuto Goto, **Zhensheng You**, Masaya Sawamura. A Hollow-Shaped Caged Triarylphosphine: Synthesis, Characterization and Applications to Gold(I)-Catalyzed 1,8-Enyne Cycloisomerization. *Chemistry Letters* **2021**, *50*, 1236−1239.

[2] **Zhensheng You**, Heng Li, Lijun Zhang, Bing Yu, Jin Zhang, Xiaoming Wu. A Host Material for Deep-Blue Electrophosphorescence Based on a Cuprous Metal−Organic Framework. *The Journal of Physical Chemistry C* **2017**, *121*, 23072−23079.

[3] Li Jun Zhang, Xiang Zhang, **Zhen Sheng You**, Heng Li, Tian Feng, Wei Li Wang. Chem-Grafted Zn-SSA as an Efficient Heterogeneous Catalyst to Synthesize 2-Pyridinones. *Catalysis Letters* **2016**, *146*, 2081−2086.

Acknowledgement

The research described in this thesis was carried out under the supervision of Prof. Dr. Masaya Sawamura at Graduate School of Chemical Sciences and Engineering (CSE), Hokkaido University from Apr. 2018 to Mar. 2023.

Z. You thanks Prof. Dr. Masaya Sawamura for kind supervision and meaningful discussions, which revealed the insight of the reaction nature and significantly improved the quality of research.

Z. You thanks Lecture Dr. Tomohiro Iwai (present address: Graduate School of Arts and Science, The University of Tokyo) and Assistant Professor Dr. Yusuke Masuda for advice, discussions and supervision during the graduate school research. The part of computational studies in this thesis was carried out in collaboration with Assistant Professor Dr. Kosuke Higashida. Z. You thanks his kind suggestions in mechanistic studies. Z. You appreciates to Associate Professor Dr. Yohei Shimizu, Associate Professor Dr. Dennis Chung-Yang Huang, and Assistant Professor Dr. Fernando Arteaga Arteaga for meaningful discussions.

Z. You is grateful to examiners of his doctoral thesis. The insightful suggestions from Prof. Dr. Takanori Suzuki, Prof. Dr. Takeshi Ohkuma, and Prof. Dr. Jun-ya Hasegawa were meaningful for improving the quality of this thesis.

Z. You thanks Program for Leading Graduate Schools (Hokkaido University "Ambitious Leader's Program (ALP)"), Japan Society for the Promotion of Science (JSPS research fellow), Hokkaido University (Special Grant Program for Self-Supported International Students), and the MEXT Doctoral program for Data-Related InnoVation Expert Hokkaido University (D-DRIVE-HU) for scholarship support.

Z. You would like to express his deep appreciation to his family, Mr. Xingfa You and Ms. Jianqin Tang for their warm support from his childhood to graduate school study, which is indispensable for continuous study in a place far away from his home.

Z. You thanks Mr. Junya Arashima for his kind support and suggestions during the initial period of the graduate school study. The other alumni and present members in Organometallic Chemistry Laboratory room 6-09 (Dr. D. Zhang, Mr. K. Tsunoda, Mr. Y. Yamazaki, Mr. R. Niizeki, Ms. M. Sato, Ms. Y. Kawamura, Mr. M. Yoshida, Mr. X. Liu, Ms. I. Qureshi, Ms. H. Mori) are acknowledged for discussions and collaborative works.

Zhensheng YOU
CSE, Hokkaido University
Mar. 2023